1. Report No. FHWA/TX-04/0-2101-2	2. Government Accession No.	3. Recipient's Catalog No.	
4. Title and Subtitle MECHANICAL PROPERTIES OF HIGH STRENGTH CONCRETE FOR PRESTRESSED CONCRETE BRIDGE GIRDERS		5. Report Date October 2003	
		6. Performing Organization Code	
7. Author(s) Mary Beth D. Hueste, Praveen Chompreda, David Trejo, Daren B. H. Cline, and Peter B. Keating		8. Performing Organization Report No. Report 0-2101-2	
9. Performing Organization Name and Address Texas Transportation Institute The Texas A&M University System College Station, Texas 77843-3135		10. Work Unit No. (TRAIS)	
		11. Contract or Grant No. Project No. 0-2101	
12. Sponsoring Agency Name and Address Texas Department of Transportation Research and Technology Implementation Office P. O. Box 5080 Austin, Texas 78763-5080		13. Type of Report and Period Covered Research: January 2000-May 2003	
		14. Sponsoring Agency Code	

16. Abstract
This is the second of four reports that document the findings of a Texas Department of Transportation sponsored research project to evaluate the allowable stresses and resistance factors for high-strength concrete (HSC) prestressed bridge girders. HSC is widely used in prestressed concrete bridges. However, current design provisions for prestressed concrete bridge structures, such as the American Association of State Highway and Transportation Officials (AASHTO) Load and Resistance Factor Design (LRFD) Specifications, were developed based on mechanical properties of normal strength concrete (NSC). As a first step toward evaluating the applicability of current AASHTO design provisions for HSC prestressed bridge members, statistical parameters for the mechanical properties of plant-produced HSC were determined. In addition, prediction equations relating mechanical properties with the compressive strength were evaluated. HSC samples were collected in the field from precasters in Texas and tested in the laboratory at different ages for compressive strength, modulus of rupture, splitting tensile strength, and modulus of elasticity. Statistical analyses were conducted to determine the probability distribution, bias factors (actual mean-to-specified design ratios), and coefficients of variation for each mechanical property. Creep and shrinkage were also monitored and evaluated.

Researchers found that for each short-term mechanical property, the mean values are not significantly different among the considered factors (precaster, age, specified strength class) or combination of these factors, regardless of the specified design compressive strength. Overall, the 28-day bias factors (mean-to-nominal ratios) decrease with an increase in specified design compressive strength due to the relative uniformity of mixture proportions provided for the specified strength range. Nevertheless, the 28-day bias factors for compressive strength are greater than those used for the calibration of the AASHTO LRFD Specifications. With few exceptions, the coefficients of variation were uniform for each mechanical property. In addition, the coefficients of variation for the compressive strength and splitting tensile strength of HSC in this project are lower than those for NSC used in the development of the AASHTO LRFD Specifications. Based on the experimental data, the creep and shrinkage of the HSC in this project are overestimated by the AASHTO equations that predict the development of creep and shrinkage with time.

17. Key Words Prestressed Concrete, High Strength Concrete, Mechanical Properties, Compressive Strength, Modulus of Elasticity, Splitting Tensile Strength, Modulus of Rupture, Creep, Shrinkage, Statistical Parameters	18. Distribution Statement No restrictions. This document is available to the public through NTIS: National Technical Information Service 5285 Port Royal Road Springfield, Virginia 22161		
19. Security Classif.(of this report) Unclassified	20. Security Classif.(of this page) Unclassified	21. No. of Pages 326	22. Price

Form DOT F 1700.7 (8-72)   **Reproduction of completed page authorized**

MECHANICAL PROPERTIES OF HIGH STRENGTH CONCRETE FOR PRESTRESSED CONCRETE BRIDGE GIRDERS

by

Mary Beth D. Hueste, P.E.
Assistant Research Engineer
Texas Transportation Institute

Praveen Chompreda
Graduate Research Assistant
Texas Transportation Institute

David Trejo, P.E.
Assistant Research Engineer
Texas Transportation Institute

Daren B. H. Cline
Professor of Statistics
Texas A&M University

and

Peter B. Keating
Associate Research Engineer
Texas Transportation Institute

Report 0-2101-2
Project Number 0-2101
Research Project Title: Allowable Stresses and Resistance Factors for High Strength Concrete

October 2003

TEXAS TRANSPORTATION INSTITUTE
The Texas A&M University System
College Station, Texas 77843-3135

DISCLAIMER

This project was performed in cooperation with the Texas Department of Transportation (TxDOT) and the Federal Highway Administration (FHWA). The contents of this report reflect the views of the authors, who are responsible for the facts and accuracy of the data presented herein. The contents do not necessarily reflect the official view or policies of TxDOT or FHWA. This report does not constitute a standard, specification, or regulation, nor is it intended for construction, bidding, or permit purposes. Trade names were used solely for information and not for product endorsement. The engineer in charge was Mary Beth D. Hueste, P.E. (TX 89660).

ACKNOWLEDGMENTS

TABLE OF CONTENTS

LIST OF FIGURES

LIST OF TABLES

xvi

1 INTRODUCTION

1.1 BACKGROUND AND PROBLEM STATEMENT

High strength concrete (HSC) has been widely used in bridges, buildings, and other structures for the past two decades. One benefit of using HSC in bridge structures is that longer span lengths can be constructed for a given girder cross-section. This can result in a substantial reduction in the number of piers in multiple span bridges. Another benefit is that the girder spacing may be increased for a given span length and cross-section. Therefore, fewer girders are needed for each span, which can result in savings in erection costs and a reduction in the size of substructures due to the reduced superstructure dead weight. Moreover, spans may use smaller and shallower girder cross-sections. This improves ground clearance and yields a more aesthetic design.

There has been a significant amount of research focusing on the mechanical properties of HSC. However, most of this research focuses on concrete made in the laboratory under carefully controlled conditions that may not properly reflect concrete in the field. Therefore, there is a need to determine the mechanical properties of plant-produced HSC made in the field by precasters.

There are limited data available in the literature quantifying the variation of concrete properties between batches, mixes, or precasters. Variations in material properties must be quantified for the development of a reliability-based design code such as the American Association of State Highway and Transportation Officials (AASHTO) Load and Resistance Factor Design (LRFD) specification (2000). Because HSC is usually produced in a plant with relatively good quality control, the variation of the material properties of HSC may be expected to be smaller than that of normal strength concrete (NSC). However, more data are needed to confirm this assumption.

1

The definition of HSC used in this project follows that used by the American Concrete Institute (ACI) Committee 363 (1997) as concrete having compressive strength greater than 6000 psi (41.4 MPa) produced without using exotic materials or techniques. HSC with compressive strengths above 6000 psi (41.4 MPa) is commonly available today and is used extensively in prestressed bridge girders. However, the current design codes such as the AASHTO standard specifications (1999) and AASHTO LRFD specification (2000) were developed based on the material properties of NSC having a compressive strength less than 6000 psi (41.4 MPa). This fact has led to concerns that the current design specifications may not be conservative enough when designers apply them to HSC members. On the other hand, the equations may be overly conservative such that the advantages of utilizing HSC members are not fully realized.

1.2 OBJECTIVES AND SCOPE

This report summarizes Phase 1 of the Texas Department of Transportation Research Project 0-2101, "Allowable Stresses and Resistance Factors for High Strength Concrete." The objective of this project was to evaluate the allowable stresses and resistance factors in the AASHTO LRFD Specification for design of HSC girders used in Texas bridges. The complete project is summarized by Hueste et al. (2003a). Phase 2 of this project focused on defining the current state of practice for design of HSC prestressed girders and identifying critical design parameters that limit the design of typical HSC prestressed bridge girders (Hueste and Cuadros 2003). Phase 3 of this project assessed the impact of different curing conditions on the compressive and flexural strength of HSC mixtures used for prestressed girders in Texas (Hueste et al. 2003b).

The portion of the research project addressed in this report (Phase 1) focused on evaluating the applicability of current prediction equations for estimation of mechanical properties of HSC and determining statistical parameters for mechanical properties of HSC produced by Texas precasters. The major objective of Phase 1 of the research project was to evaluate whether the current design provisions for prestressed concrete beams require modifications for the use of HSC. Possible revisions to the current design code can be made for service-load design through the modification of allowable stresses and for ultimate strength

2

design by modification of the resistance factors. This project provides data that can be used to direct additional research aimed at refining the current design provisions for HSC prestressed beams. New criteria for use in designing HSC prestressed members can then be developed, as appropriate, based on the results of this project.

The scope of this report is restricted to the application of HSC in precast prestressed concrete girders that are normally used in the construction of highway bridges in Texas. The HSC in this project is limited to the specified compressive strength of 10,000 psi (68.9 MPa) made using conventional materials and admixtures. It was not feasible to obtain concrete samples having a specified compressive strength greater than 10,000 psi (68.9 MPa) from precasters during the limited time frame of this project because designers rarely specified strengths in that range. In order to achieve the Phase 1 objectives, the following tasks were performed.

1.2.1   Task 1: Literature Review

The review of literature included synthesizing current knowledge regarding the mechanical properties of HSC, appropriate test methods, current practices in the design of prestressed members using HSC, current code specifications, and the reliability theory used in the development of the AASHTO LRFD Specifications (2000). The project focused on the AASHTO LRFD Specifications (2000) because they are expected to be adopted by TxDOT engineers for the design of highway bridges. The material properties under investigation included compressive strength, modulus of elasticity, splitting tensile strength, modulus of rupture, creep, and shrinkage. The effects of testing variables were also examined to evaluate the factors that may affect the test results. The literature review is summarized in Chapter 2 of this report. This section serves as background for the technical and experimental progress of this project.

1.2.2   Task 2: Experiments

The experimental program consisted of collecting and testing samples of plant-produced HSC from Texas precasters to determine relevant material properties. Concrete samples were collected from selected precasters considered to be representative of the precasters in Texas that produce prestressed bridge members. Material testing determined actual mechanical properties for comparisons with predicted values. In addition, statistical parameters of each mechanical property were determined.

1.2.3   Task 3: Analysis of Data

The data from tests were analyzed to evaluate prediction relationships and to determine the statistical parameters. Current prediction formulas that relate mechanical properties to the compressive strength were assessed to determine whether they can be used for HSC produced by Texas precasters with sufficient accuracy. This project included prediction relationships for the modulus of elasticity, splitting tensile strength, and modulus of rupture. Creep and shrinkage data were also reported and compared with prediction equations. Moreover, this task included the determination of statistical parameters, including coefficients of variation and bias factors, for each mechanical property based on test data. The results were compared with those of NSC used in the development of the AASHTO LRFD Specification (2000) to identify potential modifications to the provisions for prestressed concrete member design.

1.2.4   Task 4: Summary and Conclusion

This task consisted of drawing conclusions based on the results obtained from the experimental program. Recommendations for future research are also provided.

1.3 ORGANIZATION OF THIS REPORT

Chapter 2 of this report provides a review of previous studies on the design of prestressed concrete, the current codes and practices for the use of HSC in design, the development of reliability-based design provisions, and the mechanical properties of HSC. Chapter 3 describes the experimental programs including the selection of precasters, the collection of samples, and the material testing. The experimental data are presented in Chapter 4 along with an analysis and evaluation of these data in terms of implications for design. Ultimately, the findings from this project are summarized in Chapter 5. Recommendations for future research are also presented in this chapter. Raw test data, information on the mixture proportions of the concrete tested, and other relevant information is provided in the appendices.

2 LITERATURE REVIEW

2.1 PRESTRESSED CONCRETE

Prestressed concrete members must be designed for both service-load and ultimate-load conditions. The following sections provide background and a review of current design provisions for prestressed members. The main focus is on the AASHTO LRFD Specifications (2000) because it is widely used in the design of bridge girders.

2.1.1 Service-Load Criteria

In the service-load criteria, the flexural stresses under service loads at the top and the bottom of a prestressed member must be within the allowable tensile and compressive stress limits. In the LRFD Specifications, the Service I load combination is applied for compressive stress checks, and the Service III load combination is used for tensile stress checks. For a simply supported beam, the stresses at the bottom and top fibers of the beam are determined as:

$$f_b = -\frac{P}{A} - \frac{Pec_b}{I} + \frac{Mc_b}{I} \qquad (2.1)$$

$$f_t = -\frac{P}{A} + \frac{Pec_t}{I} - \frac{Mc_t}{I} \qquad (2.2)$$

where a tensile stress is positive; f_b and f_t are the stresses at the bottom and top fiber, respectively; P is the effective prestressing force; A is the area of the concrete cross-section; I is the moment of inertia of the concrete cross-section; e is the eccentricity of the prestressing tendons measured from the center of gravity of the concrete cross-section; c_t and c_b are the

distances from the center of gravity of the concrete cross-section to the top and bottom fiber, respectively; and M is the total moment at the beam section under consideration.

In the simplest case, the allowable stresses must be checked at the stage immediately after prestress transfer and at a long-term condition after prestress losses have taken place. For composite construction or a beam that has more than one stage of prestressing, the problem will become more complicated as various stages of construction must also be considered and different section parameters must be used in each stage. In general, the service-load criteria control the selection of a member cross-section and the number and locations of prestressing strands. The allowable stresses for pretensioned members from current standards are summarized in Table 2.1.

Table 2.1. Allowable Stresses for Prestressed Concrete Design (Pretensioned Members).

Document	Allowable Compressive Stress f_c (psi)		Allowable Tensile Stress f_t (psi)	
	Initial	Service	Initial	Service
AASHTO (1999)	$0.60f'_{ci}$	$0.40f'_c$	$7.5\sqrt{f'_{ci}}$	$6\sqrt{f'_c}$ $3\sqrt{f'_c}$ (1)
AASHTO LRFD (2000)	$0.60f'_{ci}$	$0.45f'_c$ (2) $0.40f'_c$ (3) $0.60f'_c\,\varphi_w$ (4)	$7\sqrt{f'_{ci}}$	$6\sqrt{f'_c}$ $3\sqrt{f'_c}$ (1)
ACI 318 (1999)	$0.60f'_{ci}$	$0.45f'_c$ (2) $0.60f'_c$ (5)	$3\sqrt{f'_{ci}}$ $6\sqrt{f'_{ci}}$ (6)	$6\sqrt{f'_c}$ $12\sqrt{f'_c}$ (7)

Notes:

f'_c = Compressive strength at 28 days

f'_{ci} = Initial compressive strength at transfer

(1) For corrosive exposure conditions
(2) For effective prestress plus sustained load
(3) For live load and one-half of effective prestress and sustained loads
(4) For sum of prestress, sustained loads, and transient loads and during shipping and handling.
   φ_w is the reduction factor for slenderness ratios of flange and web.
(5) For effective prestress plus total load
(6) At ends of simply supported members
(7) Where analysis based on cracked section and on bilinear moment-deflections relationships shows that immediate and long-term deflections comply with ACI definition requirements and minimum concrete cover requirements

In most instances, the allowable tensile stresses at the initial or service state control the design. These allowable tensile stress limits are imposed to prevent cracking of concrete cover that could expose the prestressing strands to corrosion. The values of the allowable tensile stresses are based on the modulus of rupture of concrete. The allowable compressive stress limits are used to ensure that the stress in concrete is within the elastic limit.

The prestressing force, P, in Equations 2.1 and 2.2 is calculated from the effective prestressing stress and the area of tendons as:

$$P = A_{ps} f_{ps} \qquad (2.3)$$

where A_{ps} is the total area of prestressing tendons and f_{ps} is the effective prestressing stress. The effective prestressing stress at any time is the difference between the initial prestressing stress and prestressing losses, determined as:

$$f_{ps} = f_{pi} - \Delta f_{pF} - \Delta f_{pA} - \Delta f_{pES} - \Delta f_{pR2} - \Delta f_{pCR} - \Delta f_{pSR} \qquad (2.4)$$

where f_{pi} is the initial prestress (in stress units), Δf_{pF} is the stress loss due to friction in the duct, Δf_{pA} is the loss of anchorage seating after transfer, Δf_{pES} is the loss from elastic shortening of the concrete member, Δf_{pR2} is the time-dependent loss due to steel relaxation after transfer, and Δf_{pCR} and Δf_{pSR} are time-dependent losses due to creep and shrinkage of concrete, respectively (AASHTO 2000).

The friction loss and the anchorage loss are only found in post-tensioned members and depend on the prestressing system (types of duct and anchorage) and tendon profile. The relaxation loss also depends on the properties of the prestressing strand and the magnitude of the prestress. Elastic shortening, creep, and shrinkage losses depend on concrete properties and will be affected by the use of HSC. The elastic shortening loss is calculated as:

$$\Delta f_{pES} = \frac{E_p}{E_{ci}} f_{cgp} \tag{2.5}$$

where E_p is the modulus of elasticity of prestressing strand, E_{ci} is the modulus of concrete at the age of transfer, and f_{cgp} is the stress in concrete due to prestressing force at transfer and the self-weight of the member at the level of the prestressing strand.

The loss due to creep (in ksi) is calculated as:

$$\Delta f_{pCR} = 12.0 f_{cgp} - 7.0 \Delta f_{cdp} \geq 0 \tag{2.6}$$

where Δf_{cdp} is the change in concrete stress at the center of gravity of prestressing steel due to additional permanent loads after prestress transfer. For pretensioned members, the loss due to shrinkage (in ksi) is calculated as:

$$\Delta f_{pSR} = (17.0 - 0.150H) \tag{2.7}$$

where H is the average annual ambient relative humidity in percent.

As part of the work of ACI-ASCE Committee 423, Zia et al. (1979) recommended the following equations for the estimation of losses due to creep and shrinkage:

$$\Delta f_{pCR} = K_{CR} \left(\frac{E_p}{E_c} \right) (f_{cgp} - f_{cdp}) \tag{2.8}$$

$$\Delta f_{pSR} = 8.2 \times 10^{-6} K_{SH} E_p \left(1 - 0.06 \frac{V}{S} \right) (100 - H) \tag{2.9}$$

where K_{CR} is equal to 2.0 for normal weight concrete, E_c is the modulus of elasticity of concrete at 28 days, K_{SH} is equal to 1.0 for pretensioned members, V/S is the volume-surface ratio in inches. Equation 2.9 is based on the ultimate shrinkage strain of 550 µε (Zia et al. 1979)

The prestress losses are influenced by many factors. Therefore, it is difficult to generalize the amount of these losses. Lin and Burns (1982) suggested representative values of average losses for average properties of concrete and steel and for average curing conditions. The values are shown in Table 2.2.

Table 2.2. Average Prestress Losses (Lin and Burns 1982).

Source of Loss	Loss of Prestress (%)	
	Pretensioned Members	Post-tensioned Members
Elastic Shortening	4	1
Creep of Concrete	6	5
Shrinkage of Concrete	7	6
Steel Relaxation	8	8
Total Loss	25	20

It is clear from Table 2.2 that losses related to concrete properties (elastic shortening, creep, and shrinkage losses) have a significant effect on the total loss of prestress, especially in pretensioned members. Therefore, inaccurate estimation of the properties of concrete, such as the modulus of elasticity, creep coefficient, and ultimate shrinkage, will result in errors in estimating prestress losses. Underestimation of prestress losses, which leads to a smaller actual effective prestress force than calculated, can result in excessive stress and deflection during service conditions. On the other hand, overestimation of prestress losses, which leads to a larger actual prestressing force than calculated, can result in excessive stress and camber after transfer.

2.1.2 Ultimate-Load Criteria

2.1.2.1 General

In the ultimate-strength design, the beam must be designed such that the reduced nominal resistance capacity is greater than the factored load effect. The ultimate-load criteria are checked for both moment and shear limit states, i.e.,

$$\phi M_n \geq M_u \tag{2.10}$$

$$\phi V_n \geq V_u \tag{2.11}$$

where M_n and V_n are the nominal moment and shear resistance capacities of the member, M_u and V_u are the factored applied moment and shear forces, and ϕ is the resistance factor. The resistance factors for prestressed members specified in the AASHTO LRFD Specifications (2000) are summarized in Table 2.3.

Table 2.3. Resistance Factors for Prestressed Concrete Member (AASHTO 2000).

Limit State	Resistance Factor
Flexure and Tension of Prestressed Concrete	1.00
Flexure with or without Tension of Partially Prestressed Components	0.90 + 0.10 (PPR)
Shear and Torsion (Normal Weight Concrete)	0.90

Notes:
Not for segmental construction
PPR = Partial prestress ratio calculated according to Section 5.5.4.2.1 of AASHTO LRFD
 Specification (2000)

The values of the resistance factors are selected such that the probability that the load is greater than the resistance is acceptably small. The theory and the development of the resistance factors are discussed in Section 2.3.

2.1.2.2 Nominal Moment Capacity

In the case of a simple rectangular section, the nominal moment capacity is calculated as (AASHTO 2000):

$$M_n = (0.85 f'_c ba)\left(d - \frac{a}{2}\right) \qquad (2.12)$$

where M_n is the nominal moment capacity of the beam, f'_c is the compressive strength of concrete, b is the width of the beam, d is the effective depth, and a is the depth of the equivalent rectangular stress block, which can be determined by solving the following equilibrium equation:

$$0.85 f'_c ba = A_{ps} f_{ps} + A_s f_y \qquad (2.13)$$

where A_{ps} is the total area of prestressing tendons, A_s is the total area of steel reinforcement resisting tension in the case of partial prestressing, f_y is the yield strength (in stress units) of steel reinforcement (assuming the steel has reached yield strength at ultimate load), and f_{ps} is the stress in the prestressing strands at ultimate load.

For bonded tendons, f_{ps} can be calculated as:

$$f_{ps} = f_{pu}\left(1 - k \frac{c}{d_p}\right) \qquad (2.14)$$

$$k = 2\left(1.04 - \frac{f_{py}}{f_{pu}}\right) \qquad (2.15)$$

where f_{py} and f_{pu} are the yield strength (in stress units) and the ultimate strength (in stress units) of prestressing tendons, respectively; c is the distance from the top fiber to the neutral axis; and d_p is the distance of the center of gravity of prestressing strands measured from the top fiber.

It can be seen that the nominal moment resistance of a prestressed concrete girder depends on the compressive strength of concrete, the geometry of the girder, the amount of prestressing strands and reinforcing bars, and the material properties of the prestressing strands and steel reinforcement. Therefore, the bias factor (mean-to-nominal ratio) of the resistance and the coefficient of variation of the resistance depend on the bias factor and the coefficient of variation of each variable. The determination of the resistance statistical parameters (bias factor and coefficient of variation) and resistance factors are discussed in Section 2.3.

2.1.2.3 Nominal Shear Capacity

The nominal shear resistance capacity of a prestressed concrete member is the smaller of the following equations (AASHTO 2000):

$$V_n = V_c + V_s + V_p \qquad (2.16)$$

$$V_n = 0.25 f'_c b_v d_v + V_p \qquad (2.17)$$

where V_c is the shear resistance of concrete, V_s is the shear resistance from transverse reinforcement, V_p is the component of the effective prestressing force in the direction of the applied shear, b_v is the effective web width, and d_v is the effective shear depth. The components V_c and V_s are determined as:

$$V_c = 0.0316\beta\sqrt{f'_c}\,b_v d_v \qquad\qquad (2.18)$$

$$V_s = \frac{A_v f_y d_v (\cot\theta + \cot\alpha)\sin\alpha}{s} \qquad\qquad (2.19)$$

where β is the factor indicating the ability of diagonally cracked concrete to transmit tension, θ is the angle of inclination of diagonal compressive stresses, α is the angle of inclination of transverse reinforcement to the longitudinal axis (usually 90°), A_v is the area of shear reinforcement within a distance s, and f_y is the yield stress of the transverse reinforcement. The value of β and θ depends on the applied shear, applied moment, applied axial force, prestressing force, modulus of elasticity of concrete, prestressing strands, longitudinal reinforcement, and section geometries. They are determined according to Section 5.8.3.4 of the AASHTO LRFD Specifications (2000).

2.2   USE OF HSC IN PRESTRESSED MEMBERS

The following sections address the current practice in designing prestressed concrete members and studies related to the application of HSC in bridge construction.

2.2.1   Current Practice

The AASHTO Standard Specifications (1999) is currently being used by TxDOT in the design of highway bridges. However, it is anticipated that TxDOT will adopt the new AASHTO LRFD Specifications (2000) for bridge design in the near future because the former specification will no longer be current. The design of precast prestressed members in the AASHTO Standard Specifications (1999) is normally based on the design compressive strength of 5000 psi (34.5 MPa). A design compressive strength of 6000 psi (41.4 MPa) or higher can also be used provided that the required strength can be obtained consistently. In the AASHTO LRFD Specifications (2000), the specified compressive strength for prestressed concrete should be greater than 4000 psi (27.6 MPa), but a specified compressive strength over 5000 psi (34.5 MPa)

can be used when it is verified that materials for such concrete are available in the area. In addition, concrete having a compressive strength exceeding 10000 psi (68.9 MPa) at 28 days can only be used when the relationships between the compressive strength and other material properties are obtained from tests.

Although the AASHTO codes allow for the use of HSC, many of the code equations are empirical and were determined based on tests of NSC specimens. As a result, engineers must rely on their own experience and judgment when using HSC. At this time, there are no national code provisions for prestressed members that have provisions specifically for the use of HSC in the United States. This lack of code limits the use of HSC because the designer and owner may feel uncomfortable using materials that are not specifically addressed by the design code.

2.2.2 Previous Studies

The benefits of using HSC for bridge applications have been studied by many investigators. Zia et al. (1989) conducted parametric studies to evaluate the structural efficiency and cost effectiveness of using HSC for bridge girders. It was found that the increase of compressive strength from 6000 to 12,000 psi (41.4 to 82.7 MPa) can increase the maximum span length of standard AASHTO and Precast/Prestressed Concrete Institute (PCI) sections by up to 30 percent. Zia et al. concluded that the compressive strength of 10000 psi (68.9 MPa) was the most effective for girder and beam sections.

Durning and Rear (1993) studied the impact of using HSC in the design of Texas Type C prestressed bridge girders. The increase of the maximum span and girder spacing with the compressive strength began to stop at a design compressive strength of 10000 psi (68.9 MPa). This behavior was due to the limitation on the number of strands that can be placed in a section. When more strands are needed, they have to be placed higher in the web, making it less effective in resisting moments. If 0.6 inch (15 mm) diameter strands had been used instead of the standard 0.5 inch (13 mm) diameter strands, the limit for the design compressive strength would be higher.

Russell (1994) studied the effect of an increase in compressive strength to the maximum span length and girder spacings of various girder types and found that the use of HSC can effectively increase the maximum span length of the girders. An increase in compressive strength from 6000 psi to 10000 psi permits an increase of the span limit from 104 ft (31.7 m) to 131 ft (39.9 m) in the case of an AASHTO Type IV girder. An increase from 98 ft (29.9 m) to 119 ft (36.3 m) was found for a Texas U54B girder when the 0.5 inch (13 mm) diameter strands are used.

The use of HSC not only allows construction of longer-span bridges, but it also results in a more economical design. Durning and Rear (1993) demonstrated that the number of girders required for a given span length was substantially reduced when 10000 psi (68.9 MPa) HSC was used instead of a 6000 psi (41.4 MPa) concrete. The reduction in the number of girders was due to the increase in the girder spacings. Although the total material cost was found to be slightly higher for HSC, the reduction in the number of girders resulted in a substantial savings in labor, transportation, and erection costs.

Because there are currently no code provisions specifically for HSC, there is concern about the applicability of the current provisions that were developed based on properties of NSC. Castrodale et al. (1988) studied the use of HSC in pretensioned composite girders. They found that the design procedures in the ACI Committee 318 code and 1983 edition of AASHTO Standard Specifications provided conservative estimates of the moment capacity. More accurate values were obtained from moment-curvature analysis. The researchers suggested that the cracking stress of $7.5\sqrt{f'_c}$ is reasonable. However, their analytical load-deflection curve departed from the initial tangent earlier than the test data from scale models. This indicated that the actual cracking stress should be greater than $7.5\sqrt{f'_c}$. The suggestion to keep this cracking stress was partly based on a recommendation from Nilson (1985) stating that, because the curing conditions of a structural member in the field are different from those in the laboratory, the modulus of rupture from specimens moist-cured in the laboratory can be higher than the cracking stress and therefore the value $7.5\sqrt{f'_c}$ appeared to be reasonable. However, no test data on field cured HSC were available to support this statement.

More recent studies in the application of high performance concrete and HSC for highway bridges have been conducted at The University of Texas at Austin (Myers and Carrasquillo 1998, Gross and Burns 2000). The studies focused on the material properties and quality control of the concrete as well as the structural behavior of highway bridges. One of the findings was that many of current design equations from the 1994 AASHTO LRFD Specifications and PCI Design Handbook (1992) cannot predict the prestress losses and deformations of the bridge very well. This is due to the inaccurate estimations of material properties of HSC, especially for the modulus of elasticity and creep.

2.3 DEVELOPMENT OF LOAD AND RESISTANCE FACTORS USING RELIABILITY THEORY

2.3.1 Reliability Theory

The concept of probability in structural design was developed because there are many uncertainties in both the applied load and the resistance that can affect the performance of a structure. Clearly, the structure must be designed such that the resistance of the structure is greater than the applied load. However, numerous sources of uncertainties in the load and resistance make it difficult to determine the exact values of load and resistance that can be expected for a structure. Therefore, it is not feasible to design a structure that is absolutely safe. The load and resistance can be treated as random variables with their own probability density function (PDF) as illustrated in Figure 2.1. The shaded area indicates failure because the load is greater than the resistance.
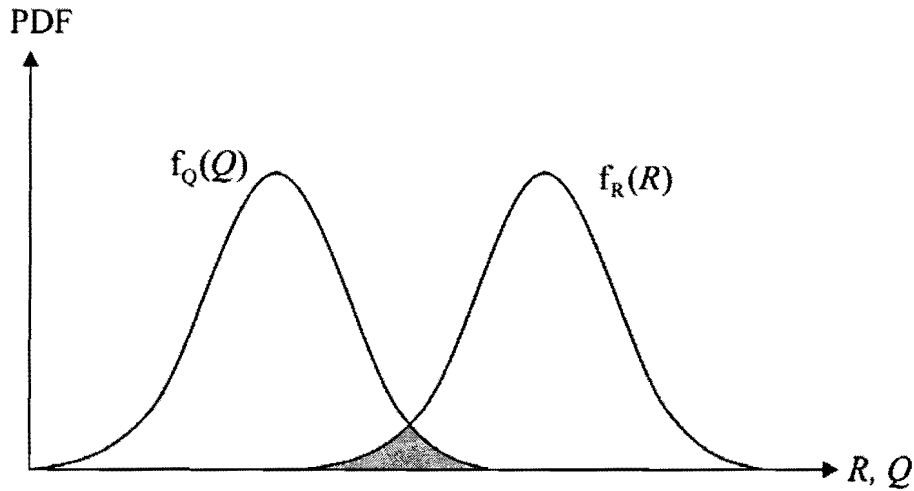
Figure 2.1. PDF of Load (*Q*) and Resistance (*R*) (Adapted from Nowak and Collins 2000).

The theories of probability and reliability are used to estimate the probability that the structure will exceed a particular limit state. A structure is said to have a satisfactory level of safety if it has an acceptably small probability of exceeding a limit state that can lead to structural failure. The limit states include the ultimate limit states, such as partial or total collapse of a structural component or structural system, and also serviceability limit states such as excessive vibration or deformation, or damage accumulation limit states such as fatigue failure (Tabsh 1992). For a case involving the resistance effect, *R*, and load effect, *Q*, the limit state can be defined using the following expression:

$$g(R,Q) = R - Q \tag{2.20}$$

The resistance effect, *R*, can be a function of many variables, such as material properties and section geometries. Similarly, the load effect, *Q*, can be a function of many load components, such as dead loads, live loads, dynamic loads, wind loads, and earthquake loads.

For limit states that can lead to failure, the probability of failure of a structure is the probability that the value of the limit state function is less than zero (resistance is less than load):

19

$$p_f = P(g < 0) = P(R < Q) \tag{2.21}$$

It can be shown that:

$$p_f = \iint\limits_{g<0} f_{R,Q}(r,q)drdq \tag{2.22}$$

where $f_{R,Q}(r,q)$ is the joint probability density function for load and resistance and the integration is performed over the failure region (where g < 0). The integration domain is the shaded area shown in Figure 2.2.
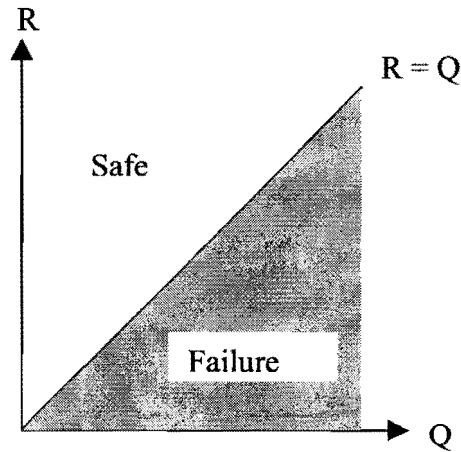
Figure 2.2. Safe and Failure Domain.

Because the load and resistance can often be assumed to be statistically independent, Equation 2.23 can be rewritten as:

$$p_f = \int_0^\infty f_R(r)dr \int_r^\infty f_Q(q)dq = \int_0^\infty f_R(r)\left[1 - F_Q(r)\right]dr \tag{2.23}$$

or

$$p_f = \int_0^{\infty} f_Q(q)dq \int_0^q f_R(r)dr = \int_0^{\infty} F_R(q)f_Q(q)dq \qquad (2.24)$$

where f_R and F_R are the PDF and cumulative density function (CDF) for the resistance, respectively; and f_Q and F_Q are the PDF and CDF for the load, respectively.

The integration in Equations 2.23 and 2.24 is often difficult to evaluate due to the complexities in the probability density functions and cumulative density functions of the loads and the resistances. In practice, the probability of failure is determined indirectly using other procedures. One such procedure was proposed by Rackwitz and Fiessler (1978), known as the first-order reliability method (FORM). This method has advantages over the first-order second-moment method (FOSM) used in the early reliability studies because it accounts for the distribution functions of the variables and it does not have the invariance problem where the reliability index changes with different formulations of mechanically equivalent limit state functions.

To avoid the invariance problem, Hasofer and Lind (1974) suggested defining the reliability index (β) as the shortest distance from the limit state to the origin in the reduced variable coordinate system. A reduced variable, or "standard form" of a variable, is defined as:

$$Z_i = \frac{X_i - \mu_{Xi}}{\sigma_{Xi}} \qquad (2.25)$$

where Z_i is the reduced variable, X_i is the variable in the original coordinates, and μ_{X_i} and σ_{X_i} are the mean and standard deviation of X_i, respectively. For the limit state where $g(R,Q) = R - Q$, it can be shown that:

$$g(\ ) = \sigma_R Z_R - \sigma_Q Z_Q + \mu_R - \mu_Q \qquad (2.26)$$

The limit state function in the reduced variable coordinate system is shown in Figure 2.3.
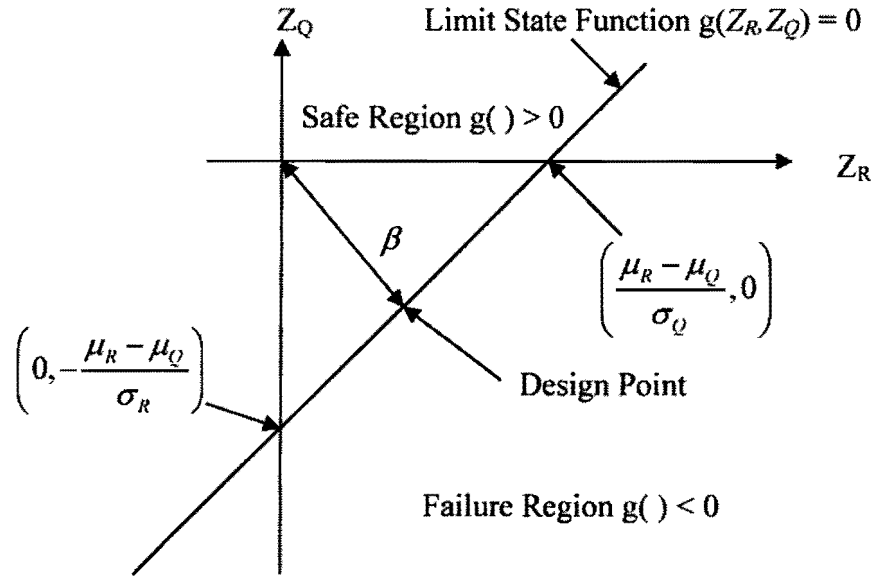
Figure 2.3. Limit State Function in Reduced Variable Coordinates (Adapted from Nowak and Collins 2000).

As stated earlier, the reliability index (β) is now defined as the shortest distance from the limit state line g( ) = 0 to the origin. From geometry, it can be shown that:

$$\beta = \frac{\mu_R - \mu_Q}{\sqrt{\sigma_R^2 + \sigma_Q^2}}$$

(2.27)

Equation 2.27 is the same as the reliability index evaluated by the FOSM method when the limit state is linear and the variables are normally distributed. The Hasofer-Lind method is invariant to nonlinear limit states because the geometric shape and the distance to the origin of the limit state is constant regardless of how the limit state is written (Haldar and Mahadevan 2000). For non-normal random variables, Rackwitz and Fiessler (1978) suggested transforming the non-normal random variables to equivalent normal variables by imposing two conditions: the CDF and the PDF of the equivalent normal variables are equal to those of actual variables at the design point. The Rackwitz-Fiessler procedure for determining the reliability index (β) is as follows (Nowak and Collins 2000):

1. Define the limit state function.

2. Assume the initial values of the design point $\{x_i^*\}$. The values for n–1 variables are assumed first; the value of the remaining variable is obtained by solving the limit state function g( ) = 0.

3. Compute the parameters of the equivalent normal standard deviation ($\sigma_{X_i}^e$) and mean ($\mu_{X_i}^e$) for each design point values x_i^* as:

$$\sigma_{X_i}^e = \frac{\phi\left\{\Phi^{-1}\left[F_{X_i}(x_i^*)\right]\right\}}{f_{X_i}(x_i^*)} \tag{2.28}$$

$$\mu_{X_i}^e = x_i^* - \Phi^{-1}\left[F_{X_i}(x_i^*)\right]\sigma_{X_i}^e \tag{2.29}$$

where $\phi(x)$ is the standard normal PDF of x and $\Phi^{-1}(x)$ is the inverse of the standard normal CDF of x.

4. Compute the reduced variates z_i^* for design point x_i^*:

$$z_i^* = \frac{x_i^* - \mu_{X_i}^e}{\sigma_{X_i}^e} \tag{2.30}$$

and define:

$$\{z^*\} = \begin{Bmatrix} z_1^* \\ z_1^* \\ \vdots \\ z_1^* \end{Bmatrix} \qquad (2.31)$$

5. Compute the partial derivative of the limit state function with respect to the reduced variates, $G_i = \partial g / \partial Z_i$ and form a matrix $\{G\}$ as:

$$\{G\} = \begin{Bmatrix} G_1 \\ G_2 \\ \vdots \\ G_n \end{Bmatrix} \qquad (2.32)$$

6. The reliability index is calculated as:

$$\beta = \frac{\{G\}^T \{z^*\}}{\sqrt{\{G\}^T \{G\}}} \qquad (2.33)$$

7. Calculate the sensitivity factor vector $\{\alpha\}$ using the following formula:

$$\{\alpha\} = \frac{\{G\}}{\sqrt{\{G\}^T \{G\}}} \qquad (2.34)$$

8. New design point values in the reduced coordinates for n–1 variables can be determined from:

$$z_i^* = \alpha_i \beta \qquad (2.35)$$

9. The new design point values in the original coordinates for n-1 variables corresponding to the values in Equation 2.35 are calculated as:

$$x_i^* = \mu_{X_i}^e + z_i^* \sigma_{X_i}^e \tag{2.36}$$

10. Solve the limit state function g( ) = 0 to find the value of the remaining random variable that was not determined in Equations 2.35 and 2.36.

11. Check the convergence of the reliability index (β) and the design points {x_i^*}. Steps 3 through 10 must be repeated until the values converge.

2.3.2 Code Calibration

Nowak (1999) provided a detailed description of the process of calibrating the first edition (1994) of the AASHTO LRFD Specifications. The purpose of code calibration is to determine the load and resistance factors for a new design code to achieve a target level of reliability. In the case of the 1994 AASHTO LRFD Specifications, the target reliability is based upon the inherent reliability of bridges designed by the 1989 edition of the AASHTO Standard Specifications that was being used at that time. It was found that the AASHTO Standard Specifications did not have a uniform level of safety, as measured by the reliability index (β), for different types of construction, span lengths, and girder spacings. Based on the reliability indices calculated for different types of bridges using the AASHTO Standard Specifications, a reliability index of 3.5 was selected as a target value for design using the AASHTO LRFD Specifications. The load and resistance factors in the LRFD code were selected such that this target reliability index (β_T) was met and was constant for all types of construction, span lengths, and girder spacings. There are many possible combinations of load factors and resistance factors that can satisfy the target reliability index requirement. However, it is preferable to have the same load factor for each load type (dead load, live load, dynamic load, etc.) and for all types of construction (steel, composite, reinforced concrete, and prestressed concrete). Therefore, the load factors were selected first to be applicable to all types of construction, and the appropriate resistance factors for each type of construction and limit state were chosen accordingly.

To determine the reliability index, the FORM method described earlier could be used. However, in practice, it is not necessary to iterate until the reliability index converges. Only one cycle is needed for the purpose of the calibration (Nowak 1999).

In the calibration of the AASHTO LRFD Specifications, the load effect Q was assumed to be a normal random variable and the resistance R was assumed as a lognormal random variable. Using one cycle of the FORM method with the limit state g( ) $= R - Q$, it can be shown that (Nowak 1999):

$$\beta = \frac{R_n\lambda_R(1-kV_R)\left[1-\ln(1-kV_R)\right]-m_Q}{\sqrt{\left[R_nV_R\lambda_R(1-kV_R)\right]^2+\sigma_Q^2}} \qquad (2.37)$$

where β is the reliability index, R_n is the nominal (design) value of resistance, λ_R is the bias factor (mean to nominal ratio) of R, V_R is the coefficient of variation of the resistance, m_Q is the mean of Q, σ_Q is the standard deviation of Q, and k is a constant (usually set equal to 2.0).

2.3.3 Determination of Resistance Parameters

It can be seen from Equation 2.37 that statistical parameters (mean and coefficient of variation) for the load and resistance are needed in order to determine the probability of failure in terms of the reliability index (β). In general, the resistance of a structural member depends on several variables, such as member geometry and material properties. It is very difficult to determine the exact mean and variance of the resistance function analytically because the resistance function is nonlinear in these variables and these variables also have different probability density functions that often cannot be written explicitly. Therefore, an estimation technique is typically utilized to determine the statistical parameters of the resistance. This technique is called Monte Carlo simulation. The procedure is as follows (Haldar and Mahadevan 2000):

1. Define the resistance in terms of geometry and material properties. A more accurate model than the usual design method in the code is needed. For instance, moment-curvature analysis was used to compute moment capacity, and the modified compression field theory (Vecchio and Collins 1986) was used to compute shear capacity when developing the AASHTO LRFD Specifications for reinforced or prestressed concrete members (Nowak et al. 1994).

2. Assign probabilistic distributions to the random variables. The appropriate distribution for each random variable may be determined based on test data, or it is sometimes assumed.

3. Generate random numbers for each random variable. Many computer software programs have a built-in random number generator that can provide uniform random numbers between zero and one. To transform the generated uniform random numbers to the random numbers of the variables with their characteristic distributions, the inverse transformation technique is used. It is done by equating the uniform random number, u_i, to the CDF of the random variable, that is:

$$u_i = F_X(x_i) \qquad (2.38)$$

Solve for x_i as:

$$x_i = F_X^{-1}(u_i) \qquad (2.39)$$

4. Evaluate the resistance deterministically for each set of random numbers for all the variables.

The mean and variance of resistance can be determined from the mean and variance of all the resistance values from the simulation. The coefficient of variation can also be determined from the ratio of the standard deviation (square root of the variance) to the mean.

In order to obtain a bias factor of the resistance (λ_R), a nominal resistance (R_n) is required. This can be determined by calculating the resistance using the design procedures

specified in the design code and using the nominal values of material properties and section geometry. The bias factor (λ_R) is then computed as the ratio of the mean resistance from the simulation to the nominal resistance (R_n) from the design code procedures.

The statistical parameters, including the mean and coefficient of variation as well as the distribution of material properties and geometry, were reported by many investigators such as Mirza et al. (1979), Ellingwood et al. (1980), and Naaman and Siriaksorn (1982). Table 2.4 provides a summary of statistical parameters for concrete compressive and splitting tensile strength used in the simulations conducted to determine resistance parameters for both reinforced and prestressed concrete members used in the calibration of the AASHTO LRFD Specifications (Tabsh and Nowak 1991, Nowak et al. 1994). These statistical parameters were taken from a study by Ellingwood et al. (1980), which in turn references the work by Mirza et al. (1979).

Table 2.4. Statistical Parameters for Concrete (Ellingwood et al. 1980).

Property	Nominal	Mean	Bias Factor	CV (%)
Concrete f'_c	3000 psi (20.7 MPa)	2760 psi (19.0 MPa)	0.920	18
Concrete f'_c	4000 psi (27.6 MPa)	3390 psi (23.4 MPa)	0.848	18
Concrete f'_c	5000 psi (34.5 MPa)	4028 psi (27.8 MPa)	0.806	15
Concrete f_t For $f'_c = 3$ ksi	-	306 (2.11 MPa)	-	18
Concrete f_t For $f'_c = 4$ ksi	-	339 (2.34 MPa)	-	18
Concrete f_t For $f'_c = 5$ ksi	-	366 (2.52 MPa)	-	18

The values of the compressive strength (f'_c) and splitting tensile strength (f_t) in Table 2.4 were calculated from relationships developed by Mirza et al. (1979) relating design compressive strength to the mean value of in-situ compressive strength. The compressive

strength of the in-situ structure ($\overline{f}_{cstrR}$) is different from that of the test cylinders because of the differences in volume and the rate of loading. Equation 2.40 relates the design compressive strength to the in-situ compressive strength for the standard load rate used in compressive strength testing of 35 psi/s (0.24 MPa/s). The effect of a nonstandard load rate on the compressive strength is accounted for in Equation 2.41.

$$\overline{f}_{cstr35} = 0.675 f'_c + 1,100 \leq 1.15 f'_c \tag{2.40}$$

$$\overline{f}_{cstrR} = \overline{f}_{cstr35} \left[0.89(1 + 0.08 \log R) \right] \tag{2.41}$$

where f'_c is the design (nominal) compressive strength in psi for minimum acceptance curing of concrete, $\overline{f}_{cstr35}$ is the mean 28-day compressive strength in psi of concrete in a structure at the standard load rate for testing, and $\overline{f}_{cstrR}$ is the mean value of the in-situ compressive strength in psi at a rate of loading R (psi/s). Ellingwood et al. (1980) suggested that the load rate of the actual structure is much lower than that applied to test cylinders. Therefore, to better estimate the strength in a structure, it was assumed that the load rate was such that the failure occurred in one hour, calculated by:

$$R = \frac{f'_c}{3600} \tag{2.42}$$

The mean in-situ tensile strength ($\overline{f}_{spstrR}$) in psi at a rate of loading R (psi/s) was computed by the following formula:

$$\overline{f}_{spstrR} = 6.4 \sqrt{\overline{f}_{cstr35}} \left[0.96(1 + 0.11 \log R) \right] \tag{2.43}$$

It should be noted that the term $6.4\sqrt{\overline{f}_{cstr35}}$ is the estimated mean value of the splitting tensile strength from the mean compressive strength. Again, the loading rate for an actual structure is assumed to be much lower than the standard test rate of 2.5 psi/s (0.017 MPa/s) for

the splitting tensile test. Therefore, the effect of loading rate has to be accounted for. The in-situ load rate (R) for the splitting tensile strength was calculated such that the failure by tension occurred in one hour (Ellingwood et al. 1980):

$$R = \frac{6.4\sqrt{\bar{f}_{cstr35}}}{3600}$$

(2.44)

The coefficients of variation for the compressive strength provided in Table 2.4 were also determined from relationships developed by Mirza et al. (1979):

$$CV_{cstrR} = \sqrt{CV_{ccyl}^2 - CV_{in-test}^2 + CV_{in-situ}^2 + CV_R^2}$$

(2.45)

where CV_{cstrR} is the coefficient of variation of the in-situ compressive strength of concrete at a given load rate, CV_{ccyl} is the coefficient of variation of test cylinders, $CV_{in-test}$ is the coefficient of variation of the test due to testing procedure, $CV_{in-situ}$ is the coefficient of variation of concrete strength in a structure with respect to the compressive strength of test cylinders, and CV_R is the coefficient of variation due to the rate of loading effect.

The in-test variation, $CV_{in-test}$, was taken by Mirza et al. (1979) as 4 percent; and the variation of concrete strength in a structure with respect to the test cylinders, $CV_{in-situ}$, was taken as 10 percent. The effect of loading rate on the variation of concrete strength was assumed to be negligible. Therefore,

$$CV_{cstrR} = \sqrt{CV_{ccyl}^2 + 0.0084}$$

(2.46)

Mirza et al. (1979) reported that the coefficient of variation of concrete cylinders was about 15 percent for "average control" for compressive strengths below 4000 psi (27.6 MPa). The standard deviation of concrete with compressive strengths above 4000 psi (27.6 MPa) was approximately constant at 600 psi (4.1 MPa) for "average control." As a result, the coefficient of

30

variation of concrete cylinders having a compressive strength of 5000 psi (34.5 MPa) was taken as 12 percent. The coefficient of variation of the in-situ compressive strength was estimated as 18 percent and 15 percent for 3000 (20.7 MPa) and 5000 psi (34.5 MPa) concrete, respectively (Ellingwood et al. 1980). The coefficient of variation for the splitting tensile strength was assumed to be 18 percent for 3000 psi (20.7 MPa) to 5000 psi (34.5 MPa) concrete. The distributions of the compressive strength and splitting tensile strength were assumed to be normal, which were determined by Mirza et al. (1979) to be reasonable assumptions based on available data.

Very limited data are available on the statistical properties of compressive strength and other material properties for HSC. Tabsh and Aswad (1995) reported statistical properties of compressive strength of the steam-cured, plant-produced HSC from producers in Pennsylvania. The results are shown in Table 2.5. The researchers found that the lognormal distribution is more appropriate for the compressive strength of HSC.

Table 2.5. Statistical Parameters for Pennsylvania HSC (Tabsh and Aswad 1995).

Parameter	Warm Season	Cold Season	Year Long	For f'_c > 7 ksi (48.3 MPa)
Bias Factor from Test	1.28	1.18	1.23	1.12
CV from Test (%)	0.15	0.08	0.13	0.07
In-situ Bias Factor	1.15	1.06	1.11	1.01
In-situ CV (%)	0.17	0.12	0.15	0.11

The in-situ bias factors in Table 2.5 were taken as 90 percent of the bias factor from the test. This is due to differences such as placing, curing conditions, bleeding of water in deep members, casting conditions, and stress contours in the member and test cylinders. The statistical parameters in Table 2.5 do not include an adjustment for load rate effects. The load rate of the in-situ compressive strength here is the same as that of the test cylinders, 35 psi/s (0.24 MPa/s). The coefficients of variation of the in-situ compressive strength were calculated using Equation 2.46, consistent with the development of the AASHTO LRFD Specifications.

Table 2.6 shows another analysis of the same data from the same authors (Tabsh and Aswad 1997).

Table 2.6. Statistical Parameters for Pennsylvania HSC by Compressive Strength Range (Tabsh and Aswad 1997).

Compressive Strength Range	Bias Factor from Test	CV from Test (%)
f'_c = 6000 psi (41.1 MPa)	1.396	0.125
6000 psi (41.4 MPa) < f'_c < 7000 psi (48.3 MPa)	1.208	0.076
f'_c > 7000 psi (48.3 MPa)	1.123	0.065

Note: Data for bridge structures only

Comparing the statistical parameters from Tabsh and Aswad (1995 and 1997) and Ellingwood et al. (1980), it can be seen that the HSC produced by precasters seems to have greater bias and a lower coefficient of variation. The lower variation of the material properties will result in lower overall variability of the resistance, and a higher bias for HSC will contribute to a higher mean resistance. Therefore, the study by Tabsh and Aswad indicates that there is a potential to increase the resistance factors used for the design of HSC members without reducing the target reliability index (β_T). However, it should be noted that Tabsh and Aswad (1995, 1997) and Ellingwood et al. (1980) reported a decrease in the bias factor with an increase in the compressive strength. Therefore, more studies may be needed to evaluate the effect of the decrease in the bias factor in the overall resistance and to determine an appropriate value for the development of a design code.

The resistance of a structural member depends not only on the uncertainties in the material and geometry, but also on the uncertainties in the analysis method used. Ellingwood et al. (1980) suggested that the resistance could be assumed in the following form:

$$R = R_n MFP \tag{2.47}$$

where R_n is the nominal resistance, M is the material factor (ratio of actual to nominal material properties), F is the fabrication factor (ratio of actual to nominal cross-sectional properties), and

32

P is the professional factor (ratio of in-situ capacity to the capacity determined using prediction models). The mean value of R (μ_R) is calculated as:

$$\mu_R = R_n \mu_M \mu_F \mu_P \qquad (2.48)$$

where μ_M, μ_F, and μ_P are the mean values of the M, F, and P factors, respectively. The coefficient of variation of R (CV_R) is calculated as:

$$CV_R = \sqrt{CV_M^2 + CV_F^2 + CV_P^2} \qquad (2.49)$$

where CV_M, CV_F, and CV_P are coefficients of variation of the M, F, and P factors, respectively.

Resistance parameters for prestressed concrete members determined by Ellingwood et al. (1980) and Nowak et al. (1994) are summarized in Table 2.7 and Table 2.8 respectively. The data from Table 2.8 were used in the calibration of the AASHTO LRFD Specifications. The resistance parameters in both tables were obtained from Monte Carlo simulations using the concrete statistical parameters in Table 2.4. Moment-curvature analysis was used for the determination of mean flexural resistance for both studies. The mean shear capacity ($\bar{R}$) for the shear resistance parameters in Table 2.7 was predicted using the equation from Zsutty (1971), while the modified compression field theory (Vecchio and Collins 1986) was used for the estimation of shear resistance ($\bar{R}$) for the calculation of parameters in Table 2.8. The nominal moment and shear strength (R_n) presented in Table 2.7 were determined using the 1977 edition of the ACI 318 design code (ACI Committee 318 1977). The nominal moment and shear resistances (R_n) in Table 2.8 were calculated using the 1989 edition of the AASHTO Standard Specifications (AASHTO 1989). The simulations were done using concrete with a compressive strength of 5000 psi (34.5 MPa) for the girders and a concrete with a compressive strength of 3000 psi (20.7 MPa) for the deck. The professional factor was included in the simulation, along with the material and fabrication factors, for the resistance parameters in Table 2.7. On the other hand, in Table 2.8, Equations 2.48 and 2.49 were used to incorporate the professional factor to

33

the resistance parameters that were determined from simulations using only material and fabrication factors.

Table 2.7. Resistance Parameters for Prestressed Concrete Members (Ellingwood et al. 1980).

Designation	Bias Factor $(\overline{R}/R_n)$	CV (%)
Flexure, Plant Precast Pretensioned Beams	1.06	8.0
Flexure, Cast-in-Place Post-tensioned Beams	1.04	9.5
Shear, Minimum Stirrups	1.00	19
Shear, Moderate Stirrups	1.09	17

Table 2.8. Resistance Parameters for Prestressed Concrete Members (Nowak et al. 1994).

Designation	Bias Factor $(\overline{R}/R_n)$	CV (%)
Moment	1.05	7.5
Shear with Steel	1.15	14

2.4 HIGH STRENGTH CONCRETE

This section provides a summary of the current literature on the microstructure, production, mechanical properties, and testing of HSC.

2.4.1 Definition

The definition of HSC has changed over the years. The strength level limit for defining HSC depends on the current practice and location. With the recent developments in concrete production technology, it is possible to produce concrete with a compressive strength of up to 20,000 psi (138 MPa) commercially using conventional materials (Burg and Ost 1992). Therefore, concrete having a maximum compressive strength of 5000 psi (34 MPa), which was

considered to be high strength in the past, is now considered NSC (ACI 363 1997). The definition of HSC for this project is that defined by ACI Committee 363 (1997), which defines HSC as concrete with a compressive strength exceeding 6000 psi (41 MPa) made without using exotic materials or techniques.

The term "HSC" is often used interchangeably with the term "high performance concrete (HPC)." Many investigators use the word high performance as a new term for HSC because, by using chemical and mineral admixtures to produce HSC, several other characteristics have also been improved consequently, such as workability and durability. On the other hand, some investigators define high performance concrete as concrete that meets some specific performance requirements such as workability, durability, or strength; it does not necessarily have a high compressive strength, although a majority of high performance concrete mixes exhibit high strength in addition to enhanced performance. ACI also defines HPC as concrete meeting special performance requirements that are not routinely met using conventional materials and normal practices (Russell 1999).

2.4.2 Microstructure of HSC

Concrete is a heterogeneous material, and its mechanical properties are influenced by the properties of its components and their interactions. Concrete can be divided into three major phases: hydrated cement paste, aggregate, and the transition zone. The mechanical properties of concrete are influenced by the microstructure features of these three phases, particularly the porosity of the hydrated cement paste and the transition zone, and the characteristics of the aggregate. Féret (1892) gave the expression that relates the volume of cement, water, and air to the strength of the hydrated cement paste as follows:

$$f'_c = k\left(\frac{c}{c+w+a}\right)^2 \tag{2.50}$$

where f'_c is the compressive strength of the hydrated cement paste; k is a constant; and $c, w,$ and a are the volume of cement, water, and air, respectively. The volume of air entrapped in the

cement paste is usually only a small percentage and can be neglected. Therefore, for cases where air content is small, this equation can be rewritten as (Aïtcin 1998):

$$f'_c = k \frac{1}{\left(1 + (w/c)\right)^2}$$ (2.51)

A reduction in the water-cement ratio increases the strength of the hydrated cement paste. The water-cement ratio affects the microstructure and strength of the hydrated cement paste. During the early stage of hydration, when there is an abundant supply of water and sufficient space between cement particles, the hydration products react outside the original boundary of the cement particles. These products of hydration, often called "outer products," are composed of large crystals of hydration products and contain a large amount of voids. As the hydration continues, the water supply in the system becomes scarce. This condition favors the formation of hydration products inside the original boundary of the cement particle. These hydration products, called "inner products," have fewer pores and are poorly crystalline which give them the higher strength. As a result, the fracture of the hydrated cement paste often passes through the outer products (Aïtcin 1998). Therefore, the strength of concrete can be increased by promoting the formation of the inner products. This can be done by reducing the water-cement ratio.

The transition zone adjacent to the coarse aggregate is usually weaker than the bulk cement paste because the bleeding water tends to accumulate around the coarse aggregate, resulting in a cement paste with a higher water-cement ratio near the aggregate. Maso (1980) reported that the structure of the transition zone is composed of ettringite and large calcium hydroxide crystals formed in oriented layers. This results in a more porous structure in the transition zone. Another cause of the reduced strength of the transition zone is the presence of microcracks in this zone. The amount of microcracks depends on the water-cement ratio, the cement content, the size and gradation of aggregate, the consolidation of fresh concrete, and the curing history (Mehta and Monteiro 1993). The reduced strength of the transition zone is often the reason why the strength of concrete is usually lower than that of the cement mortar with the same water-cement ratio and cement content.

2.4.3 Production

Because the water-cement ratio is one of the most important factors affecting the strength of concrete, the objective in proportioning HSC is to minimize the water-cement ratio as much as practicable without sacrificing other properties, such as workability and durability. In addition, the production cost must be reasonable. ACI Committee 211 (1993) provides guidelines for proportioning HSC mixes with portland cement and fly ash.

The composition of portland cement in the United States has to conform to the American Society of Testing and Materials (ASTM) standard specification C 150 (2000a). Portland cement is mainly composed of four compounds: dicalcium silicate (C_2S), tricalcium silicate, tricalcium aluminate (C_3A), and tetracalcium aluminoferrite (C_4AF). The hydration of cement paste can be taken as the combination of the hydrations of each compound under similar conditions. Typical hydration reactions of each compound are as follows (Taylor 1997):

C_2S:

$$2C_2S + 5H \rightarrow C_3S_2H_4 + CH$$
$$(C\text{-}S\text{-}H)$$

C_3S:

$$2C_3S + 7H \rightarrow C_3S_2H_4 + 3CH$$
$$(C\text{-}S\text{-}H)$$

C_3A (Without Sulphate):

$$2C_3A + 27H \rightarrow C_4AH_{19} \text{ (or } C_4AH_{13}) + C_2AH_8 \rightarrow 2C_3AH_6$$
$$\text{(Hexagonal hydrate)} \qquad \text{(Cubic hydrate)}$$

C_3A (With Sulphate):

$$C_3A + 3C\bar{S}H_2 + 26H \rightarrow C_6A\bar{S}_3H_{32}$$
$$\text{(Ettringite)}$$

$$C_6A\bar{S}_3H_{32} + 2C_3A + 4H \quad \rightarrow \quad 3C_4A\bar{S}H_{12}$$
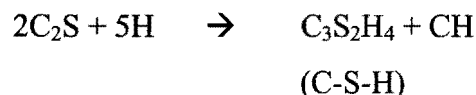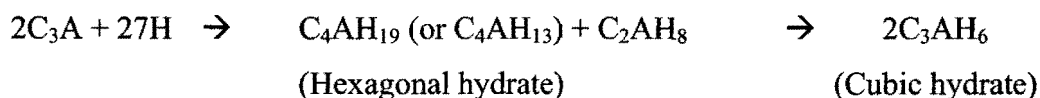
(Monosulphoaluminate hydrate)
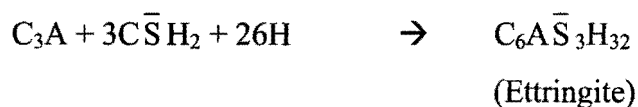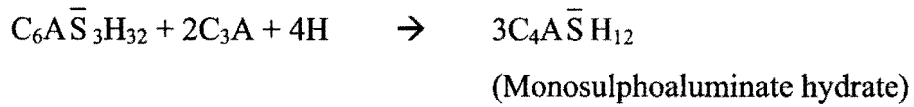
where C stands for CaO, S stands for SiO_2, A stands for Al_2O_3, F stands for Fe_2O_3, $\bar{S}$ stands for SO_3, H stands for H_2O, and CH stands for $Ca(OH)_2$.

The hydration product that contributes to strength is the calcium silicate hydrate (C-S-H) from the hydration of calcium silicates. The hydration process and the product of hydration of the C_4AF are similar to those of C_3A.

The rheological properties and strength properties of the same type of portland cements may vary considerably when they are used with a superplasticizer in a low water-cement ratio mix. Mehta and Aïtcin (1990) reported that high tricalcium aluminate (C_3A) contents in cement could result in the rapid hardening of fresh concrete by increasing the formation of ettringite. As a result, more water is needed to obtain sufficient workability and the hardened concrete may contain large voids. Such cement should be avoided for the production of HSC.

In some cases, the coarse aggregate for HSC has to be carefully selected because the hydrated cement paste can be as strong as the aggregate itself. The size of the coarse aggregate in HSC is usually smaller than that in NSC. Smaller particles of coarse aggregates are generally stronger than large particles because the size reduction eliminates internal defects in the particles (Mehta and Aïtcin 1990). Moreover, smaller aggregates have less stress concentrations around them so bond failure is not prevalent. Shapes and surface textures of both coarse and fine aggregates are also important. Crushed aggregates are more commonly used than river gravels because of their additional mechanical bond.

One aspect that distinguishes the production of HSC from NSC is the use of various admixtures. An important admixture is a high-range water-reducing admixture, commonly known as a superplasticizer. Because the amount of water needed for complete hydration is much less than the amount needed for workability, the role of the superplasticizer is to reduce the

amount of water required for a given consistency by giving cement particles negative charges. The repulsive force from electrostatic charges leads to the dispersion of cement particles. By dispersing cement particles, not only does the fresh concrete have better workability, but also the hydration process is greatly improved because more cement particles are better dispersed and are available to react with water. Consequently, the hardened concrete tends to have higher strength because of the reduced water-cement ratio and better hydration. Superplasticizers can be classified based on their chemical base as (Aïtcin 1998):

- melamine sulfonate or polycondensate of formaldehyde and melamine,
- naphthalene sulfonate or polycondensate of formaldehyde and naphthalene sulfonate,
- lignosulfonate-based, or
- polyacrylates.

The choice of the superplasticizer should not only be based on the cost, but also on the compatibility with the cement and other admixtures used. Incompatibility of the cement and superplasticizer can result in slump loss shortly after mixing. However, it is not possible at this time to determine the compatibility analytically from the properties of the cement and the superplasticizer; this has to be done experimentally.

Fly ash and silica fume are often used in HSC as a mineral admixture. The silica fume is a by-product of silicon metals or silicon alloys. The composition of these admixtures is mostly SiO_2 with a typical mean particle size similar to and much smaller than cement particles (Aïtcin 1998). The SiO_2 reacts with water and lime (CH) from the hydration of C_2S and C_3S to produce calcium silicate hydrate (C-S-H), which is the strength-contributing component. The additional reactions are as follows:

$$2C_3S + 7H \quad \rightarrow \quad C_3S_2H_4 + 3CH$$
$$(C\text{-}S\text{-}H)$$

$$2C_2S + 5H \quad \rightarrow \quad C_3S_2H_4 + 3CH$$
$$(C\text{-}S\text{-}H)$$

$$2SiO_2 + 3CH + H \quad \rightarrow \quad C_3S_2H_4$$
$$(SF) \qquad\qquad\qquad (C\text{-}S\text{-}H)$$
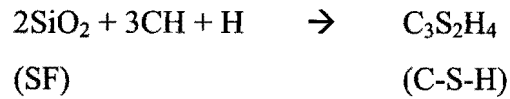
In fresh concrete, silica fume's small spherical particles help improve the workability by acting like ball bearings (Aïtcin 1998). Silica fume's high specific surface area also increases the water demand of concrete. This results in reduced bleeding and a more compact structure in the transition zone. In addition, the fine particles help fill the pores between cement particles and reduce the porosity of concrete, thus increasing the strength and reducing the permeability of concrete. Silicon fume is usually used in low quantities between 3 and 10 percent of the mass of cement (Aïtcin 1998). A higher dosage of silica fume results in a small increase of strength but requires substantially more superplasticizer to maintain the workability of fresh concrete, resulting in a smaller cost-benefit ratio.

Fly ash particles are mostly solid and spherical, but often hollow and angular-shaped particles are formed. Fly ash is categorized into two classes, class C fly ash and class F fly ash. Class C fly ash is derived from the burning of lignite or subbituminous coal, found mostly in the southern and western United States. Typically, class C fly ash contains less than 50 percent of SiO_2, Al_2O_3, and Fe_2O_3 and greater than 10 percent of CaO. Class F fly ash is obtained from burning anthracite or bituminous coal, found in the eastern United States. Class F fly ash contains less than 10 percent of CaO. Class C fly ash is more reactive than the class F fly ash. The benefit of using fly ash is to increase the workability by the ball bearing effect and to reduce bleeding. It also helps reduce the temperature of the fresh concrete, preventing cracking of concrete due to exothermic reactions, which result in high temperatures and thermal gradients. Fly ash is often used in large quantities. ACI Committee 211 (1993) recommends 15 to 25 percent replacement for class F fly ash and 20 to 35 percent replacement for class C fly ash. Other constituents such as fibers, polymers, epoxies, and specially processed aggregates may be added to produce very HSC having compressive strengths up to 80,000 psi (550 MPa) (Burg and Ost 1992). Such HSC is out of the scope of this investigation.

Curing is also critical for HSC. HSC has a very low water content, so it does not bleed as much as NSC. Therefore, without proper curing after placing, shrinkage cracks may develop on exposed surfaces (ACI Committee 363 1997). Water curing is the most common type of curing. For prestressed concrete production, where turnover time is critical, it can be advantageous to implement steam curing to accelerate the hydration process, especially in a cold climate. The rate of hydration of concrete, like any chemical reaction, is increased with increasing temperature. However, the long-term strength could be adversely affected by steam curing because the thermal expansion of air bubbles in the cement paste induces tensile stresses and causes very fine cracks (Neville 1996). These cracks actually result in a reduction of strength at all ages, but at early ages, the increase in the strength due to accelerated hydration offsets the reduction in the strength due to cracking.

2.4.4 Mechanical Properties of HSC

As a result of the low water content, the behavior of HSC may be different from low strength or NSC. Many relationships between material properties developed for NSC are not appropriate for HSC, and new relationships have been developed. Some of these relationships are described in the following subsections.

The strength of concrete is viewed as a series of links where the weakest part of the chain controls the strength. In NSC having higher water-cement ratios, the hydrated cement paste and the transition zone are usually weaker than the aggregate. Therefore, the strength of aggregate has very little influence on the strength of concrete when the failure occurs in the hydrated cement paste (HCP) and the transition zone. On the other hand, reduction of the water-cement ratio greatly improves the structure of the transition zone. The bond between the cement and aggregate is very strong. In many cases, the failure plane passes through the hydrated cement paste and the aggregate. Hence, the aggregate can be the weakest link in HSC. In addition, HSC has a denser and stronger cement paste and transition zone. The following sections review the current knowledge of the mechanical properties of HSC.

41

2.4.4.1 Stress-Strain Characteristics

Typically, the ascending part of the stress-strain curve of HSC has a greater linear portion than that of NSC. The curvature of the stress-strain curve can be attributed to the formation of microcracks. The microcracks in NSC usually form at a stress level of approximately 40 percent of the compressive strength, where the stress-strain curve departs from the linear trend. For HSC, the bond between the aggregate and mortar is stronger, resulting in fewer microcracks and a higher stress level at which the microcracks begin to form (Carrasquillo et al. 1981b). Therefore, the stress-strain curve of HSC retains its linearity up to a higher stress level than that of NSC. In addition, it was also found that the strain at the maximum stress was greater in HSC (Carrasquillo et al. 1981a). Typical stress-strain curves of NSC and HSC are shown in Figure 2.4.
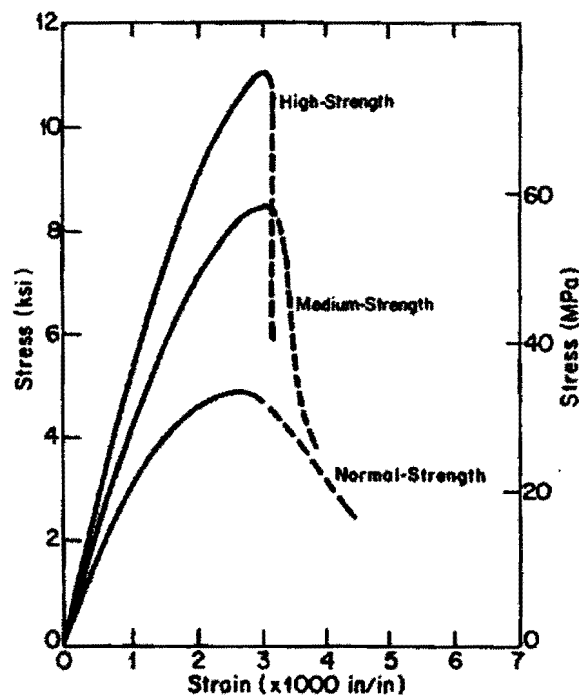
Figure 2.4. Typical Stress-Strain Curves of Concrete (Carrasquillo et al. 1981a).

2.4.4.2 Compressive Strength

Compressive strength is the most common material property used in the design of concrete structures. Its importance lies in the fact that concrete is strong in compression but weak in tension. In the ASTM C 39 standard (1999b), the compressive strength is tested using 6×12 inch (150×300 mm) or 4×8 inch (100×200 mm) cylindrical specimens. Test specimens may be made in the laboratory, cast in the field, or cored from an existing structure.

The compressive strength of concrete is influenced by several factors including time, water-cement ratio, constituent materials, curing conditions, mixture proportions, gradation of aggregates, use of admixtures, and the method of testing. The factor that is considered the most important is the water-cement ratio. HSC typically has a lower water-cement ratio when compared with NSC. A higher water-cement ratio leads to higher void content. The relationship between porosity and compressive strength of concrete is defined as (Neville 1996):

$$f_c = f_{c,0}(1-p)^n \tag{2.52}$$

where f_c is the strength of concrete with porosity p, where p is defined as a ratio of the volume of voids and the total volume of concrete, $f_{c,0}$ is the strength at zero porosity, and n is a coefficient.

The compressive strength at 28 days is the most common value specified in the design of most NSC structures. For prestressed concrete, where high early strength is usually required, the compressive strength at the time the prestressing strands are released (usually at 24 hours) is also specified. The compressive strength at 56 or 90 days is sometimes used as a long-term strength, especially when mineral admixtures are used. ACI Committee 209 (1992) uses the following equation to predict the development of compressive strength with time:

$$(f'_c)_t = \frac{t}{a + \beta t}(f'_c)_{28} \tag{2.53}$$

43

where $(f'_c)_t$ is compressive strength at time t in days, $(f'_c)_{28}$ is the compressive strength at age of 28 days, and a and β are constants. Typical values of a and β are shown in Table 2.9.

Table 2.9. Values of the Constant a and β (ACI Committee 209 1992).

Type of Curing	Moist Cured		Steam Cured	
Cement Type	Type I	Type III	Type I	Type III
a	4.0	2.3	1.0	0.70
β	0.85	0.92	0.95	0.98

The failure under uniaxial compression of HSC is somewhat different from NSC. In NSC, numerous bond microcracks at the coarse aggregate interface are connected together by the cracks through the mortar as the load increases to form complex combined cracks that eventually lead to the failure. The coarse aggregate in the NSC acts as a crack arrestor. Therefore, there are many potential failure planes formed before ultimate failure occurs. The strength of the aggregate has little or no influence on the strength of NSC, unless the aggregate is weak and very porous, because large pores and microcracks at the transition zone prevent effective stress transfer between the aggregate and hydrated cement paste (Mehta and Aïtcin 1990). In HSC, the number of bond microcracks is less because of the higher tensile bond strength and better compatibility of the elastic properties and strength of the coarse aggregate and mortar (Carrasquillo et al. 1981b). The formation of combined microcracks occurs at a higher load. The number of potential failure planes in HSC is less than in NSC because once the failure plane is developed, it grows continuously and passes through the aggregate, resulting in sudden failure. The coarse aggregate is no longer a crack arrestor (Neville 1996), and the strength of the aggregate becomes an important factor in the strength of the concrete.

2.4.4.3 Modulus of Elasticity

The modulus of elasticity is one of the most important properties for prestressed concrete applications because a significant amount of the predicted prestressing loss is due to the elastic shortening of the concrete, which depends on this property. The modulus of elasticity is typically determined from the slope of the stress-strain curve of concrete under uniaxial

compression. There are several different definitions of modulus of elasticity, namely secant modulus, tangent modulus, and initial modulus. ASTM C 469 (1994b) defines the modulus of elasticity as the secant modulus of the stress-strain curve from a strain of 50 $\mu\varepsilon$ to a stress equal to 40 percent of the compressive strength at the age of testing.

The modulus of elasticity of concrete depends on the age, water-cement ratio, the modulus of elasticity of the coarse aggregates used in the mixture, the type of cement, the load rate, the type of specimen, and the testing conditions. Many relationships have been developed to predict the modulus of elasticity from the compressive strength, which is easier to test and is usually found to verify that the specified design strength has been met. Moreover, the many factors that influence the modulus of elasticity are the same as those influencing the compressive strength. The following formula is recommended by the ACI Committee 318 (1999) and AASHTO LRFD Specifications (2000) to predict the modulus of elasticity of NSC:

$$E_c = 33 w_c^{1.5} \sqrt{f'_c} \qquad (2.54)$$

where E_c is the modulus of elasticity in psi, w_c is the unit weight of concrete in lb per ft^3 (pcf), and f'_c is the compressive strength in psi. The unit weight of concrete is included in the estimation formula because the modulus of elasticity of concrete is affected by the stiffness of the aggregate. The stiffness of aggregate is directly related to its porosity, and the unit weight of concrete is the easiest way to estimate the porosity of aggregate (Mehta and Monteiro 1993).

For HSC, ACI Committee 363 (1997) recommended the following empirical relationship, based on the work of Carrasquillo et al. (1981a):

$$E_c = (40,000\sqrt{f'_c} + 10^6)\left(\frac{w_c}{145}\right)^{1.5} \qquad (2.55)$$

where the variables have the same definition and units as in Equation 2.54. Note that this equation is the same as the equation recommended by the Canadian Code A23.3-94 (Canadian Standards Association 1994).

There are many more equations recommended by different standards and investigators that may be suitable for certain strength ranges, specific types of applications, or particular regions. The following is a list of prediction formulas in recent literature and standards:

Gardner and Zhao (1991) (in GPa):

$$E_c = 9(f'_c)^{1/3} \text{ for } f'_c > 27 \text{ MPa} \tag{2.56}$$

Norwegian Code (1992) (in GPa):

$$E_c = 9.5(f'_c)^{0.3}\left(\frac{\rho}{2400}\right)^{1.5} \text{ GPa} \tag{2.57}$$

where ρ is the unit weight of concrete in kg/m^3.

CEB-FIP Model Code 1990 (CEB 1993) (in GPa):

$$E_c = 21.5\left(\frac{f'_c}{10}\right)^{1/3} \tag{2.58}$$

where E_c in this case is defined as the tangent modulus of elasticity at the origin of the stress-strain diagram at the age of 28 days. The equation can be used to predict the modulus of elasticity from a specified compressive strength, f_{ck}, by substituting the mean compressive strength, f'_c, by ($f_{ck} + 8$) MPa.

Baalbaki (1997) (in GPa):

$$E_c = K_o + 0.2f'_c \text{ GPa} \tag{2.59}$$

where K_o is the factor depending on the type of aggregate (K_o = 9.5 GPa for sandstone aggregate, K_o = 19 GPa for granite aggregate, and K_o = 22 GPa for limestone aggregate). A comparison of these formulas is shown in Figure 2.5. Note that a unit weight of 150 pcf (2400 kg/m³) is used in the plot.
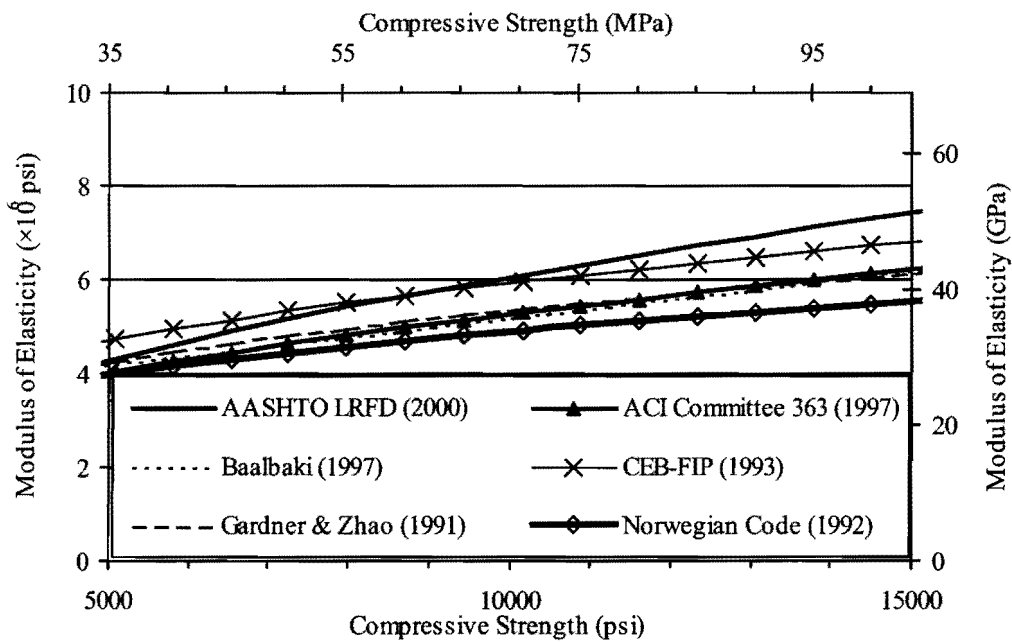
Figure 2.5. Comparison of Prediction Formulas for Modulus of Elasticity of Concrete.

Baalbaki et al. (1992a) reported that the modulus of elasticity of HSC is not controlled by the weaker hydrated cement paste as in NSC because the low water-cement ratio can cause hydrated cement paste to be as strong as, or stronger than, the aggregate. Thus, the modulus of elasticity prediction formula for NSC cannot be used for HSC. In their study, they compared the prediction formulas for modulus of elasticity of HSC and found that the ACI 363 formula performed better than the CEB-FIP Model Code 1990 (CEB 1993) and Norwegian Code

formulas. They found that the ACI 363 formula can predict the values of the moduli of elasticity of concrete made with limestone, quartzite, and granite aggregate with relatively good accuracy. However, significant error occurred when using this formula for concrete made with sandstone.

2.4.4.4 Splitting Tensile Strength

Even though concrete is not used primarily to resist tension, the tensile strength of concrete is of importance because it controls the cracking stress. Because the direct tensile test is very difficult to perform due to the difficulties in gripping and aligning test specimens in a testing machine, indirect tensile tests such as the splitting tensile test and the flexural strength test are usually performed instead. The tensile strength from the splitting tensile test is considered a close approximation of the direct tensile strength (Raphael 1984). In the CEB-FIP Model Code 1990 (CEB 1993), the splitting tensile strength is considered to be 90 percent of the direct tensile strength. The splitting tensile strength of concrete plays an important role in determining the shear resistance of prestressed concrete members. Splitting tensile strength is tested by loading a concrete cylinder on its side. The cylinder fails by induced tensile strength in the loading plane.

The splitting tensile strength is approximately 5 to 10 percent of the compressive strength of concrete and about 70 percent of the flexural tensile strength (Dewar 1964). Mokhtarzadeh and French (2000a) also reported that the ratio between the splitting tensile strength and compressive strength was between 5 and 8 percent with the average of 6 percent. ACI Committee 318 (1999) recommended the following equation for the estimation of the splitting tensile strength from the compressive strength of concrete:

$$f_t = 6.7\sqrt{f'_c} \tag{2.60}$$

where f_t is the splitting tensile strength in psi and f'_c is the compressive strength in psi. This equation is not developed specifically for HSC. For HSC, Carrasquillo et al. (1981a, 1982) and ACI 363 (1997) recommended the following formula to predict the splitting tensile strength for normal weight concrete:

$$f_t = 7.4\sqrt{f'_c} \quad \text{psi for 3000 psi} < f'_c < 12{,}000 \text{ psi} \qquad (2.61)$$

This equation is the same equation as specified by AASHTO LRFD Specifications (2000) for prediction of the splitting tensile strength of concrete.

Many investigators and standards also report recommended prediction formulas for the splitting tensile strength based on the compressive strength. Some of these are listed here:
Raphael (1984):

$$f_t = 1.7(f'_c)^{2/3} \quad \text{for } f'_c < 7000 \text{ psi} \qquad (2.62)$$

Ahmad and Shah (1985):

$$f_t = 4.34(f'_c)^{0.55} \quad \text{for } f'_c < 12{,}000 \text{ psi} \qquad (2.63)$$

Oluokun (1991):

$$f_t = 1.38(f'_c)^{0.69} \qquad (2.64)$$

Burg and Ost (1992):

$$f_t = 7.3\sqrt{f'_c} \quad \text{for moist-cured specimens} \qquad (2.65)$$

CEB (1993):

$$f_t = 1.56\left(\frac{f'_c - 8}{10}\right)^{2/3} \text{MPa} \qquad (2.66)$$

The equation can also be used to predict the splitting tensile strength from a specified compressive strength, f_{ck}, by substituting the mean compressive strength, f'_c, by $(f_{ck}+8)$ MPa.

The comparison of the above formulas is shown in Figure 2.6.

Compressive Strength (MPa)
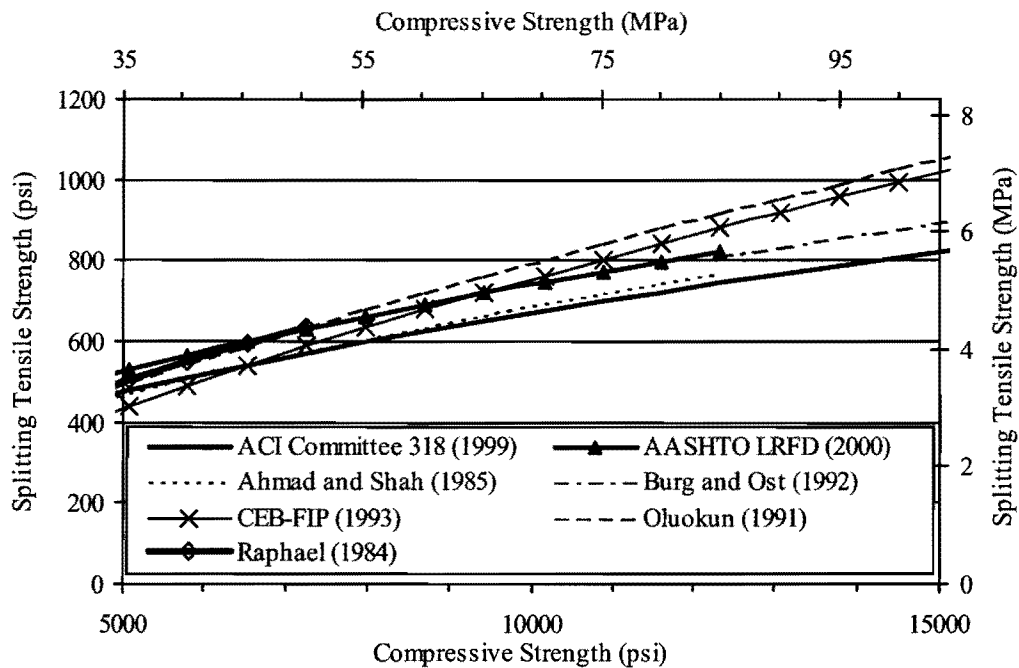
Figure 2.6. Comparison of Prediction Formulas for Splitting Tensile Strength of Concrete.

Many factors influence the relationship between compressive strength and splitting tensile strength, including the strength level, the size and type of aggregates, the water-cement ratio, the cement content, the curing conditions, and the use of air entrainment admixtures (Mirza et al. 1979).

2.4.4.5 Modulus of Rupture

In designing prestressed concrete girders, the prestressing force required and the location of prestressing tendons are usually controlled by the allowable tensile stress at the top and

50

bottom of the beam. The allowable tensile stress is based on the flexural tensile strength of the concrete measured as the modulus of rupture. It is important to limit the tensile stress at the extreme fiber because cracking can expose prestressing strands to environments that promote corrosion, which can result in the loss of prestressing force and ultimately lead to failure of the member.

The modulus of rupture is determined by loading a concrete beam at third points such that, in the middle third of the beam, there is no shear force and the bending moment is constant (ASTM 1994a). The failure will occur at the weakest area in the middle third section. Carrasquillo and Carrasquillo (1987) found that the standard deviations of the moduli of rupture tested using third-point loading were lower than those tested using center-point loading. In addition, the center-point loading yielded the modulus of rupture value approximately 14 percent higher than that of third-point loading. This behavior is because the failure section in the center-point loading is not necessarily the weakest section.

The modulus of rupture tends to overestimate the true tensile strength of concrete because it is calculated based on a linear stress distribution over the specimen depth instead of the actual parabolic distribution. However, this test is a good representation of the tensile strength of concrete in typical application, because concrete is used more in flexural tension than in direct tension.

Because the modulus of rupture test requires a relatively large specimen and the variability of the test results can be large, ACI Committee 318 (1999) and AASHTO LRFD Specifications (2000) recommend the following empirical formula to predict the modulus of rupture from the compressive strength, which can be more easily tested:

$$f_r = 7.5\sqrt{f'_c} \qquad (2.67)$$

where f_r is the modulus of rupture in psi and f'_c is the compressive strength in psi.

Carrasquillo et al. (1981a) and ACI 363 (1997) recommended that for HSC the coefficient be increased for the relationship between compressive strength and the modulus of rupture:

$$f_r = 11.7\sqrt{f'_c} \quad \text{for 3000 psi} < f'_c < 12,000 \text{ psi} \tag{2.68}$$

Other prediction formulas reported in the current literature are also listed here:
Raphael (1984) and Ahmad and Shah (1985):

$$f_r = 2.3(f'_c)^{2/3} \quad \text{for } f'_c < 12,000 \text{ psi} \tag{2.69}$$

Burg and Ost (1992):

$$f_r = 12.4\sqrt{f'_c} \quad \text{for moist-cured specimens} \tag{2.70}$$

CEB (1993) (in MPa):

$$f_r = 1.40 \frac{1 + 1.5(h_b/h_0)^{0.7}}{1.5(h_b/h_0)^{0.7}} \left(\frac{f'_c - 8}{10} \right)^{2/3} \tag{2.71}$$

where h_b is the depth of beam (mm) and h_o is equal to 100 mm. The equation can be used to predict the modulus of rupture from a specified compressive strength, f_{ck}, by substituting the mean compressive strength, f'_c, by ($f_{ck} + 8$) MPa.

Khayat et al. (1995) (in MPa):

$$f_r = 0.23 + 0.12 f'_c - 2.18 \times 10^{-4} (f'_c)^2 \tag{2.72}$$

Figure 2.7 provides a graphical comparison of these formulas.
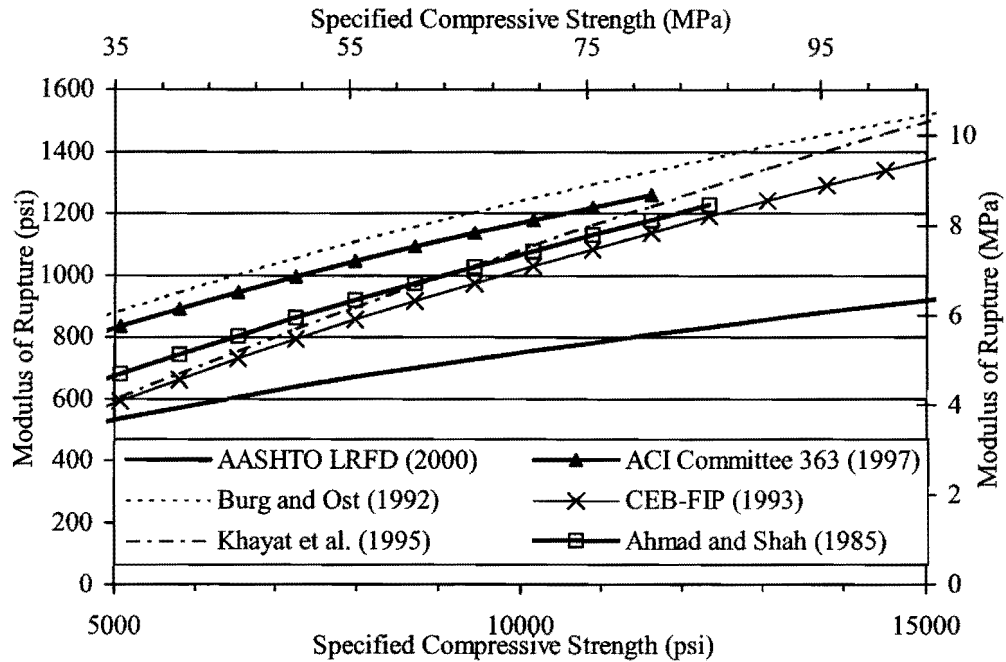
Figure 2.7. Comparison of Prediction Formulas for Modulus of Rupture of Concrete.

2.4.4.6 Creep and Shrinkage

2.4.4.6.1 General

Creep and shrinkage of concrete are both considered important factors in prestressed concrete members because they result in the loss of prestressing force. Creep is defined as the time-dependent deformation of concrete under sustained stress. Shrinkage is the time-dependent deformation of concrete from the loss of water through evaporation and chemical reactions. It is difficult to separate the effects of creep and shrinkage.

2.4.4.6.2 Shrinkage

Shrinkage can be categorized into four types:

a. Plastic shrinkage occurs from the loss of water while the concrete is still in the plastic state. The loss of water can be from the evaporation at the top surface or infiltration of water into the sub-base. When the water is removed, it creates negative capillary pressures and causes the volume of paste to contract. HSC is more susceptible to plastic shrinkage than NSC because it has less bleeding water due to the low water-cement ratio and typically more paste volume.

b. Autogenous shrinkage is the volume change that takes place after the concrete hardens by the withdrawal of water from the capillary pores by the hydration of the unhydrated cement. Concrete with very low water-cement ratios, as is the case for HSC, has been found to have greater autogenous shrinkage than NSC (Neville 1996).

c. Drying shrinkage is caused by the withdrawal of water from the concrete surface. Some part of drying shrinkage is recoverable upon rewetting. However, the large amount of drying shrinkage that occurs during the first drying is irreversible. The irreversible part of the shrinkage varies linearly with the porosity of the cement paste. As a consequence, the water-cement ratio and the degree of hydration affect the irreversible shrinkage because they influence the porosity. The irreversibility is strongly affected by the drying history of the concrete because of changes in bonding and pore size distribution.

d. Carbonation shrinkage occurs as a result of the reaction of carbon dioxide in the atmosphere and calcium silicate hydrate (C-S-H) in the hardened cement paste. The amount of carbonation shrinkage depends on the relative humidity. At very high relative humidities, carbonation shrinkage is small because the water prevents the diffusion of carbon dioxide into the paste. Carbonation shrinkage is also small at very low relative humidities (less than 25 percent) because the amount of water is insufficient for carbon dioxide to form carbonic acid that will react with the C-S-H.

The most important type of shrinkage in NSC is the drying shrinkage. The autogenous shrinkage of NSC is usually small and can be neglected. However, it was found that the autogenous shrinkage of HSC could be very significant. Aïtcin (1998) commented that the standard shrinkage testing method (ASTM C 157) was not appropriate for HSC because a large portion of autogenous shrinkage occurring at early ages (before 24 hours) is not measured.

Shrinkage of concrete is influenced by many factors. The most important factors are the following:

- Ambient conditions: Drying shrinkage is greatly affected by the relative humidity; the lower the relative humidity, the higher the rate of shrinkage. The temperature also affects the maturity of concrete, which influences the ability of concrete to resist deformation.

- Water-cement ratio: The water-cement ratio affects the shrinkage in two ways. First, as the water-cement ratio increases, the strength and the stiffness of the cement paste decrease. The decrease in the stiffness of the cement paste makes it more susceptible to deformation. Second, the increase in the water-cement ratio increases the porosity of the hardened cement paste. As a result, the shrinkage potential increases.

- Aggregate: Aggregate restrains the cement paste from shrinking. Therefore, the shrinkage of concrete is considerably less than that of cement paste. Key factors in resisting shrinkage are the modulus of elasticity and the surface textures of the aggregate; the higher the modulus of elasticity and the rougher the surface of the aggregate, the lower the shrinkage of concrete.

- Cement content: For a given water-cement ratio, an increase in cement content increases the shrinkage of concrete. This is because it reduces the amount of aggregate that can resist the shrinkage. HSC tends to have higher cement content than NSC and, therefore, can exhibit more shrinkage.

- Member size and shape: Because the magnitude of drying shrinkage depends on the amount of water loss, concrete with more exposed surface area exhibits higher rate of

55

shrinkage because water can travel to the surface at a faster rate. This factor is usually expressed in term of a volume-surface ratio.

- Age at first exposure to dry conditions: Concrete exposed at early ages to dry conditions can exhibit more shrinkage. This early shrinkage can be a result of water loss from the concrete microstructure.

- Effect of carbonation: Carbonation has a significant influence on the shrinkage in areas where carbon dioxide concentration is high.

2.4.4.6.3 Creep

Creep can also be categorized into two types:

a. Basic creep: Basic creep is the creep that occurs when there is no moisture exchange to the environment. It is measured on sealed specimens.

b. Drying creep: Drying creep is the difference between the total creep of unsealed specimens and the basic creep.

Creep is usually expressed in terms of a creep coefficient, which is the ratio of creep strain to elastic strain. The magnitude of creep is affected by the ambient conditions, water-cement ratio, cement content, aggregate quantity and type, and member geometry in the same manner as shrinkage. In addition, creep is affected by:

- Age at loading: Concrete having higher strength has greater resistance to deformations. Therefore, concrete loaded at later ages will exhibit less creep strain. HSC has been found to be more sensitive to the age of loading than normal and medium strength concrete (Khan et al. 1997), and significantly higher creep occurred when HSC was loaded at very early ages (less than 24 hours) than at later ages.

- Magnitude of stress: Creep strain is proportional to the applied stress at lower stress levels. For NSC, the limit of proportionality is between 40-60 percent of the compressive

strength. The limit is due to the extent of microcracks in concrete. However, HSC develops microcracks at a higher level of stress. Therefore, the proportionality limit of HSC is higher. Smadi et al. (1987) found that the limit was about 20 percent higher than that of NSC.

- Temperature: An increase in temperature increases the rate of creep.

2.4.4.6.4 Prediction Equations

At this time, accurately predicting creep and shrinkage is challenging because there are many factors affecting these characteristics and these factors are not independent from each other. Many investigators have proposed several prediction formulas with different levels of complexity, but none of them has been widely accepted as an accurate model. Descriptions of some of the more common models are as follows.

The AASHTO LRFD Specifications (2000) recommends the following equation for the prediction of creep:

$$\psi(t, t_j) = 3.5 k_c k_f \left(1.58 - \frac{H}{120}\right) t_j^{-0.118} \frac{(t-t_j)^{0.6}}{10.0 + (t-t_j)^{0.6}} \qquad (2.73)$$

where $\psi(t, t_j)$ is the creep coefficient defined as a ratio between the creep strain and the initial strain from the sustained load. H is the relative humidity in percent, t is maturity of concrete in days, t_j is the age of concrete in days when the prestressing force was applied, k_c is the correction factor for the effect of the volume-surface ratio, and k_f is the factor for the effect of concrete strength. The factors k_c and k_f are determined from:

$$k_c = \left(\frac{\frac{t}{26 e^{0.36(V/S)} + t}}{\frac{t}{45 + t}}\right) \left(\frac{1.80 + 1.77 e^{-0.54(V/S)}}{2.587}\right) \qquad (2.74)$$

57

$$k_f = \frac{1}{0.67 + \left(\dfrac{f_c{'}}{9}\right)} \tag{2.75}$$

where V/S is the volume-surface ratio in inches and f'_c is the specified compressive strength at 28 days (ksi).

The AASHTO LRFD Specifications (2000) provides the following relationships for estimating the shrinkage of concrete:

$$\varepsilon_{sh} = -k_s k_h \left(\frac{t}{35.0 + t}\right) 0.51 \times 10^{-3} \tag{2.76}$$

where t is the drying time in days, k_s is the size factor, and k_h is the humidity factor. The factors k_s and k_h are determined from:

$$k_s = \left(\frac{\dfrac{t}{26e^{0.36(V/S)} + t}}{\dfrac{t}{45 + t}}\right) \left(\frac{1064 - 94(V/S)}{923}\right) \tag{2.77}$$

$$k_h = \frac{140 - H}{70} \text{ for } H \le 80\% \tag{2.78}$$

$$k_h = \frac{3(100 - H)}{70} \text{ for } H \ge 80\% \tag{2.79}$$

where H is the average ambient relative humidity in percent.

The AASHTO LRFD Specifications (2000) also allows the use of other prediction formulas such as the CEB-FIP Model Code 1990 (CEB 1993) and the ACI Committee 209 (1992) formulas.

ACI Committee 209 (1992) recommends equations for the prediction of creep and shrinkage for both normal and lightweight concrete, using either steam curing or moist curing, and made with either Type I or Type III cement. Creep is predicted by the following equation:

$$v_t = \frac{t^{0.60}}{10 + t^{0.60}} v_u \qquad (2.80)$$

where v_t is the creep coefficient defined as the ratio of creep strain to initial strain, v_u is the ultimate creep coefficient, and t is the time in days after loading.

The following equation is recommended by ACI Committee 209 (1992) for the prediction of shrinkage:

$$(\varepsilon_{sh})_t = \frac{t}{35 + t}(\varepsilon_{sh})_u \qquad (2.81)$$

where t is the time in days after the end of curing, $(\varepsilon_{sh})_t$ is the shrinkage strain at time t, and $(\varepsilon_{sh})_u$ is the ultimate shrinkage strain. When the ultimate creep coefficient and the ultimate shrinkage are not available for the specific mix, they can be estimated from:

$$v_u = 2.35 \gamma_c \qquad (2.82)$$

$$(\varepsilon_{sh})_u = 780 \gamma_{sh} \times 10^{-6} \qquad (2.83)$$

where γ_c and γ_{sh} are products of correction factors for nonstandard conditions. There are correction factors for loading or drying ages, ambient relative humidity, average thickness of member, slump of fresh concrete, percentage of fine aggregate, cement content, and air content.

Mokhtarzadeh and French (2000b) found that the drying shrinkage of HSC (with 28-day compressive strengths from 8000 to 18,600 psi [55.2 to 128 MPa]) in their study was between 63

and 83 percent of values predicted by the ACI Committee 209 (1992) equations. Modifications to the ACI Committee 209 (1992) equations were suggested for the prediction of shrinkage of HSC. The researchers also recommend that the shrinkage for moist-cured HSC can be predicted as:

$$(\varepsilon_{sh})_t = \frac{t}{45+t}(\varepsilon_{sh})_u \tag{2.84}$$

where $(\varepsilon_{sh})_u = 530 \, \mu\varepsilon$. Researchers found the ACI Committee 209 (1992) equation for creep to be appropriate for HSC provided that the ultimate creep coefficient was determined from the test. The ultimate creep coefficient was found to be between 0.92 and 2.46 for HSC, as compared with the range of 1.30 to 4.15 for NSC reported by the ACI Committee 209 (1992).

In the CEB-FIP Model Code 1990 (CEB 1993), a total strain at any time is the combination of initial strain at loading, creep strain, shrinkage strain, and thermal strain. The creep strain of concrete depends on time, magnitude of sustained stress, modulus of elasticity of concrete, age of concrete at loading, compressive strength of concrete, size and shape of the member (expressed as a ratio of the cross-sectional area and the perimeter of the member in contact with the atmosphere), ambient relative humidity, and the type of cement. The shrinkage of concrete depends on time, size and shape of the member, age at the beginning of shrinkage, ambient relative humidity, compressive strength, and the type of cement. The equations for creep and shrinkage are valid for normal weight concrete having compressive strengths from 1,740 psi (12 MPa) to 11,600 psi (80 MPa). Khan et al. (1997) reported that the CEB-FIP model predicted creep results from their work reasonably well for normal, medium, and HSC with the exception of HSC loaded at very early ages.

Bažant and Panula (1984) proposed a modification to their previous models (Bažant and Panula 1978a, 1978b, 1978c, 1978d, 1979a, 1979b) for prediction of creep and shrinkage of HSC. In the model, creep is expressed in terms of a creep function. The total creep strain is the summation of strain due to initial loading, basic creep, and drying creep as:

$$J(t,t') = \frac{1}{E_0} + C_o(t,t') + C_d(t,t',t_0) - C_p(t,t',t_0) \qquad (2.85)$$

where $J(t,t')$ is the creep function defined as a strain at time t caused by a unit sustained stress applied at time t', E_0 is the modulus of elasticity of concrete, $C_0(t,t')$ is the basic creep, t_0 is the time of drying, $C_d(t,t',t_0)$ is the drying creep, and $C_p(t,t',t_0)$ is the decrease of creep from drying before loading. The variables considered in the prediction of creep are ambient relative humidity, size and shape of the member, temperature, modulus of elasticity of concrete, compressive strength, density of concrete, type of cement, and proportions of coarse aggregate, fine aggregate, cement, and water. This model makes a distinction between the development of the basic creep and the drying creep, with the intent to make the prediction more accurate.

Shrinkage strain can be predicted by using the following formula (Bažant and Panula 1978a, 1984):

$$\varepsilon_{sh}(\hat{t},t_0) = \varepsilon_{sh\infty}k_h S(\hat{t}) \qquad (2.86)$$

where $\varepsilon_{sh}(\hat{t},t_0)$ is the shrinkage strain at time t when the drying began at time t_0, $\hat{t} = t - t_0$ is the duration of drying, $\varepsilon_{sh\infty}$ is the ultimate shrinkage strain, k_h is a humidity dependence factor, and $S(\hat{t})$ is the square-root of the hyperbolic law in time. The shrinkage strain depends on ambient relative humidity, modulus of elasticity of concrete, size and shape of the member, and temperature.

Creep and shrinkage strains of HSC have been reported to be less than that of NSC because HSC usually hydrates much faster and attains a higher strength and modulus of elasticity by the age of loading. Therefore, there is a greater resistance to the deformation. In addition, the hydrated cement paste of HSC is denser and typically has smaller pores than that of NSC. The smaller pores and denser paste hinder the diffusion of water within the hydrated cement paste. As a result, deformations from creep and shrinkage of HSC are typically smaller than for NSC and take place at a much slower rate (Bažant and Panula 1984).

Smadi et al. (1987) studied the creep and shrinkage of concrete having 28 day compressive strengths ranging from 3000 to 10000 psi (20.7 to 68.9 MPa) and found that the long-term creep and shrinkage of HSC was lower than those of medium and low strength concrete. Hindy et al. (1994) reported a similar trend. The drying shrinkage of a 14,200 psi (98 MPa) concrete with a water-cement ratio of 0.22 was less than that of 11,600 psi (80 MPa) concrete with a water-cement ratio of 0.28. On the other hand, Ngab et al. (1981) found that the shrinkage of HSC is slightly greater than that of NSC. But the creep coefficient of HSC was only 50 to 75 percent of that of NSC.

De Larrard (1990) studied the creep and shrinkage of concrete having a 28-day compressive strength between 8700 and 9400 psi (60 to 65 MPa) with and without silica fume and found that the autogenous shrinkage of HSC is higher than that of NSC but the drying shrinkage is lower. As for the creep, he reported that the basic creep and drying creep was less for the HSC than those of NSC samples. In concrete with the silica fume content greater than 7 percent, the drying creep was nearly zero because the silica fume reduces the size of pores and lowers the permeability of concrete. Therefore, the creep of such concrete does not depend on the size of the member or the relative humidity. De Larrard's finding for the drying creep of silica fume concrete agrees with that of Buil and Acker (1985).

Penttala and Rautanen (1990) compared the creep and shrinkage behavior and porosity of HSC made using several types of cement. Creep and shrinkage of low heat portland cement (Type IV) with silica fume, blast furnace slag cement, and rapid hardening cement (Type III) were compared with those of NSC made using Type III portland cement. It was found that the creep and shrinkage of the HSC was significantly lower than that of the NSC. The creep and shrinkage of HSC occurred quickly during the first 40 days. Measurements of weight loss showed that the shrinkage specimens had greater weight loss than the creep specimens. Therefore, the application of stress does not increase the loss of water by squeezing the water out of the pores but instead narrows the pores such that evaporation is prevented. As a result, the change in the ambient relative humidity does not affect the creep as much as it affects the shrinkage.

2.4.5 Effects of Testing Variables

The measured mechanical properties of concrete can be affected by many variables in testing, such as specimen type, testing machines, and how the specimens are tested. These testing variables will contribute to the overall variances and biases of the material properties in the design of a structure and, consequently, the reliability of the structure. It is known that HSC is more sensitive to testing variables than NSC. Many effects that were considered insignificant for NSC can become pronounced for HSC. Therefore, the tolerance limits given in the current ASTM standards for NSC may not be sufficient to limit the variances and biases among laboratories in a satisfactory range.

The following section is the review of current research on the effect of testing variables on compressive strength and other material properties of HSC.

2.4.5.1 Specimen Size and Shape

The standard cylindrical specimen size specified in ASTM C 31 (1998a) is 6×12 inch (150×300 mm). However, a smaller specimen size such as a 4×8 inch (100×200 mm) cylindrical specimen is now widely used. The benefits of the 4×8 inch (100×200 mm) cylinder over the standard 6×12 inch (150×300 mm) cylinder are less concrete required to be cast, easier handling, easier transportation, and less storage space. In addition, when the cylinder is made of HSC, the capacity of existing testing machines may be insufficient to fail a 6×12 inch (150×300 mm) cylinder. Therefore, a smaller specimen may be needed for the test.

The influence of the size of the specimen on the measured strength can be attributed to two effects, the compaction and the probability of the weakest link. The effect of size on the compaction depends on the relative size of the coarse aggregate and the mold. When the size of aggregate is large relative to the size of the mold, the coarse aggregate prevents concrete from being compacted densely near the wall of the mold. This effect is called the "wall effect." The poorly compacted concrete near the walls results in a lower strength of the specimen. ASTM C 31 (1998a) requires that the mold size has to be at least three times the maximum size of the coarse aggregate to minimize this effect.

63

In addition, there can also be differences in the compaction of specimens having different sizes because there is no guarantee that compaction requirements specified for each size will result in the same degree of compaction. Carino et al. (1994) found that the specific gravities of 4×8 inch (100×200 mm) cylinders were greater than the companion 6×12 inch (150×300 mm) cylinders cast from the same mix.

In the weakest link theory, the failure strength of concrete is controlled by the weakest part, not the average strength. When the specimen size becomes larger, there is a higher possibility that the specimen will contain a lower strength part and result in a lower measured strength. The variability of strengths among specimens also decreases with increasing size because the lower strength part that controls the strength will be more similar in each specimen. However, the size effect due to the weakest link may become insignificant when the specimen size increases to a certain size.

The effect of specimen size on the compressive strength of concrete was found to be negligible for NSC (Gonnerman 1925, Forstie and Schnormeier 1981, Date and Schnormeier 1984). However, for HSC, French and Mokhtarzadeh (1993) investigated the effect of cylinder size on the compressive strength and concluded that the 4×8 inch (100×200 mm) cylinders tested 6 percent higher than the companion 6×12 inch (150×300 mm) cylinders. Similarly, Lessard et al. (1993) reported that the compressive strengths of 4×8 inch (100×200 mm) cylinders are 5 percent higher than those tested using 6×12 inch (150×300 mm) cylinders for the compressive strength between 10,400 psi to 18,300 psi (72 to 126 MPa). However, Pistilli and Willems (1993) reported that there was no significant difference at 95 percent confidence between compressive strengths tested using 4×8 inch (100×200 mm) and 6×12 inch (150×300 mm) cylinders in the range of 4000 to 15,000 psi (27.5 to 103.4 MPa) when the cylinders were capped with sulfur mortar. For cylinder tests using polymer pads, the researchers found the difference was insignificant in the range of 4000 to 9000 psi (27.5 to 62.1 MPa). From 9000 to 16,000 psi (62.1 to 110.3 MPa), the 4×8 inch (100×200 mm) cylinders yielded higher strengths. Based on test data from various investigators, Carino et al. (1994) concluded that the compressive strength of 4×8 inch (100×200 mm) cylinders was expected to be about 4 percent greater than that of 6×12 inch (150×300 mm) cylinders, and this difference was independent of compressive

strength. Kim et al. (1999) used nonlinear fracture mechanics to explain the strength difference between cylinders of various sizes and height-diameter ratios. They found that the effect of compressive strength and maximum aggregate size was negligible within practical ranges. Using their proposed equation, the compressive strength of a 4×8 inch (100×200 mm) cylinder would be 3 percent higher than the companion 6×12 inch (150×300 mm) cylinder.

The variation of the compressive strength results has also been investigated. Malhotra (1976) reported that 4×8 inch (100×200 mm) cylinders produce higher variability in the compressive strength than the 6×12 inch (150×300 mm) cylinders. Therefore, more specimens are required for 4×8 inch (100×200 mm) cylinders to achieve the same precision as 6×12 inch (150×300 mm) cylinders. In contrast, a more recent study from Pistilli and Willems (1993) showed that the variances of 6×12 inch (150×300 mm) cylinders and 4×8 inch (100×200 mm) cylinders are not significantly different for compressive strengths from 2000 to 15,000 psi (13.8 to 103.4 MPa) and 2000 to 13,000 psi (13.8 to 89.6 MPa) when tested with sulfur caps and polymer pads, respectively. From 13,000 psi to 17,000 psi (89.6 to 117.2 MPa), 4×8 inch (100×200 mm) cylinders show lower variances than 6×12 inch (150×300 mm) cylinders when tested with polymer pads.

The size of test cylinders can also affect the failure mode of HSC. Senor (1997) reported that the failure of larger specimens tends to be more brittle than that of smaller specimens.

Very little data are available for the effect of size on the modulus of elasticity test of HSC. Baalbaki et al. (1992b) reported that the modulus of elasticity found using a 6×12 inch (150×300 mm) cylinder is approximately 5 percent higher than that found using a 4×8 inch (100×200 mm) cylinder. However, the consolidation method used in their study for 4×8 inch (100×200 mm) cylinders did not follow ASTM standard C 31 (1998a) or C 192 (1998c). Therefore, their results cannot be directly compared to others. Nevertheless, the researchers suggested that the difference in the modulus of elasticity might be attributed to the compaction in specimens of different sizes and the friction on the bearing plates of the testing machine. In contrast, Mokhtarzadeh and French (2000a) reported that the modulus of elasticity values of HSC tested using 4×8 inch (100×200 mm) cylindrical specimens were 620,000 psi (4.3 GPa)

65

higher than those tested using 6×12 inch (150×300 mm) cylindrical specimens for compressive strength between 8000 to 18,600 psi (55.2 to 128 MPa).

Indirect tensile test results are also influenced by the size effect of the specimen. In general, the larger the specimen, the lower the strength. Malhotra (1970) found that for all three tensile strength tests (direct-tension test, ring-tension test, and splitting-tension test), the tensile strength values decreased with an increase in the size of the specimens. For the splitting-tension test, the measured strength tested by using 4×8 inch (100×200 mm) cylinders was approximately 7 percent higher than the results from tests of 6×12 inch (150×300 mm) cylinders.

For creep and shrinkage tests, the size and shape of the test specimen affects the distance the water needs to travel to the surface. Therefore, the creep and shrinkage strains in test specimens are typically much higher than that of the structural member. To predict the creep and shrinkage in the actual structure from the test specimens, ACI Committee 209 (1992) uses an average thickness and a volume-surface ratio to account for the size and shape differences, respectively. The AASHTO LRFD Specifications (2000) uses only a volume-surface ratio in the prediction of creep and shrinkage. Bažant and Panula (1978a, 1979a, 1980) included the effect of size and shape in terms of a volume-surface ratio and shape factors for their prediction models.

2.4.5.2   End Preparation

For the compressive strength and modulus of elasticity tests, it is important that the ends of the concrete cylinder specimen are perpendicular to the longitudinal axis and sufficiently smooth such that the load from the testing machine can be applied to the specimen without resulting in stress concentrations that can reduce the apparent strength. To achieve this level of smoothness, additional end surface preparation is required. For NSC, end preparation is usually done by capping with sulfur capping compound. For HSC, specimen end capping with sulfur capping compound can result in lower strength values if the compressive strength of the capping is lower than that of the concrete. However, due to the confinement effect, it may be possible to

use a capping compound with a lower cube strength than the cylinder strength of concrete to cap the ends of the specimen, provided that the cap thickness is small enough.

In the past decade, polymer pads became an alternative way to cap the ends of a concrete cylinder specimen. The polymer pad (usually made with neoprene) is placed snugly in a metal retaining ring. The neoprene will deform to the contour of the ends of the specimen to prevent high localized stresses and will result in better load distribution. The retaining ring is used to prevent the pad from expanding laterally and prevents induced tensile stresses (Carino et al. 1994). This method has several benefits over sulfur capping. First, it can be done immediately before the test, reducing the time required for specimen preparation. Second, the pads are reusable so the test is very economical. Lastly, it is safer to use when compared with the use of sulfur compound, which has risks associated with toxic fumes and handling of hot liquid.

In the case of NSC, neoprene pads have been shown to produce results comparable to those obtained using sulfur caps (Ozyildirim 1985). However, at higher strength levels, the pads tend to flow out of the restraining ring, resulting in higher compressive strengths due to end confinement. Therefore, it is important to select an appropriate hardness of pads for the level of the strength of concrete tested. Neoprene pads with a shore A durometer hardness of 70 are specified in ASTM C 1231 (2000b) for use with concrete having compressive strengths from 7000 to 12,000 psi (48.3 to 82.7 MPa).

Carrasquillo and Carrasquillo (1988b) compared the compressive strength of cylinders capped with sulfur compound and two different polymer cap systems. For polyurethane caps having durometer hardness values of 40 and 50, the compressive strength was within 5 percent of the results from sulfur caps in the range of 4000 to 10000 psi. The compressive strengths up to 11,000 psi (75.8 MPa) of cylinders tested using neoprene caps with durometer hardness values of 70 were within 3 percent of the compressive strength values obtained from sulfur caps. At strengths higher than 10000 psi (68.9 MPa) for polyurethane caps and 11,000 psi (75.8 MPa) for neoprene caps, the pads produced higher strength results. This could be because of the inadequacy of sulfur capping for higher strengths of concrete, either material or capping procedure, or the confinement effect at the ends of the cylinders when polymer pads were used.

The researchers also investigated the effect of the size of the rings on the measured compressive strength and found that the compressive strength was independent of the ring dimensions. The dimensions of the rings only affected the damage of the polymer inserts.

Another alternative to capping is grinding the ends of the specimen. Grinding is considered the best method of end preparation for HSC. Because there is no effect of capping, this method is considered to give the true compressive strength of concrete. However, it is very time consuming and expensive. Therefore, it is usually only used in research. The compressive strength from ground cylinders was found to be, on average, 2.1 percent higher than the compressive strength from sulfur-capped cylinders (Carino et al. 1994).

French and Mokhtarzadeh (1993) reported that the compressive strength values of HSC (9000 to 15,000 psi [62.0 to 103.4 MPa]) tested using unbonded neoprene caps is similar to results obtained from samples with ground ends and about 1 percent higher than compressive strength values of cylinders capped with high strength capping compound. Similar results were obtained from Pistilli and Willems (1993). It was concluded that, for 4×8 inch (100×200 mm) cylinders, there is no significant difference between compressive strength values when using sulfur caps and polymer pads with cylindrical test specimens with a compressive strength below 13,000 psi (89.6 MPa).

The effects of neoprene capping pads on the variation of compressive strength have been reported extensively in the literature. According to the data from Ozyildirim (1985), the use of these pads was found to be not statistically different from samples tested with sulfur capping for concretes having compressive strengths up to approximately 5500 psi (37.9 MPa). This result agrees with the data from a more recent study of Pistilli and Willems (1993). It was found that the test variability is not statistically different between sulfur capping and neoprene capping in the compressive strength range of 2000 to 7000 psi (13.8 to 48.3 MPa) for 6×12 inch (150×300 mm) cylinders and 2000 to 10000 psi (13.8 to 68.9 MPa) for 4×8 inch (100×200 mm) cylinders. Above these ranges, the sulfur capping had greater variability at 95 percent confidence level. The possible reason is that the strength of sulfur becomes lower than that of concrete. Carrasquillo and Carrasquillo (1988b) also found that the compressive strength from

both polyurethane and neoprene pads were more uniform than the compressive strength from sulfur caps. Richardson (1990) investigated the effects of testing variables on the compressive strength tested with neoprene caps and sulfur caps. It was found that many testing variables, while affecting the compressive strength tested using sulfur caps, did not cause the compressive strengths to be statistically different from those of standard specimens when tested using neoprene caps.

2.4.5.3 Other Considerations

In addition to the size and end preparations of the specimen, there are many other factors that can affect the test results of HSC. These factors are discussed in this section.

Several investigators reported slightly lower compressive strengths for specimens cast in single use plastic molds than that of cylinders cast in reusable steel molds. French and Mokhtarzadeh (1993) found that compressive strengths from specimens cast in steel molds were 2.5 percent higher than those cast in plastic molds. Hester (1980) explained that the strength difference came from the difference in the degree of compaction. The consolidation is more effective with rigidly constructed molds. Carino et al. (1994) observed that the density of the concrete cylinders cast in single-use plastic molds were lower than the same concrete cast in heavy gage steel molds, confirming the conclusion from Hester (1980). However, Carrasquillo and Carrasquillo (1988a) reported no strength difference between 4×8 inch (100×200 mm) cylinders cast in rigid steel, plastic, or cardboard molds, but the steel molds resulted in compressive strengths about 5 percent higher than those using plastic molds for 6×12 inch (150×300 mm) cylinders. Another possible explanation for the strength difference may be the ability to retain the shape of the plastic cylinders. Plastic cylinders can deform slightly and produce an out-of-round specimen. Richardson (1990) found that, for specimens that are only 2 percent out-of-round, significantly different compressive strengths could occur for concrete having compressive strengths between 2700 to 16,000 psi (18.6 to 110.3 MPa).

The stiffness of the testing machine has been reported to affect the compressive strength test. A longitudinally stiff machine is generally preferred to avoid the explosive failure mode. A

laterally stiff testing machine is also preferred in order to obtain a uniform rate of loading when the specimen is eccentrically loaded (Carino et al. 1994). However, Carino et al. (1994) reported that there are conflicting data regarding the effect of the testing machine stiffness on the compressive strength value.

The rate of loading can also affect the compressive strength. It is generally known that the faster the rate of loading, the higher the measured strength. It is important to use the standard load rate in testing so that the test result is comparable with others. However, Carrasquillo et al. (1981a) reported that HSC was not affected as much as NSC by different load rates.

3 EXPERIMENTAL PROGRAM

The objective of the experimental project is to evaluate several important material properties for the design of prestressed concrete and their relationships to each other, as well as statistical parameters such as the bias factor and coefficient of variation of each property. This project consists of collecting samples from prestressed concrete manufacturers (precasters) and then testing the material properties in the laboratory.

3.1 COLLECTION OF SAMPLES

To evaluate the material properties of HSC for the design of prestressed concrete members, the concrete used in this project must be the same materials and mixture proportions as those used to cast the actual members so that the variability in the materials and mixing procedures can be captured. HSC samples were collected from several precasters in Texas to identify variability in HSC produced in the state. Because the properties of HSC can be influenced by many factors, the precasters to be used in the project were selected to provide a good representation of the precasters in the state who produce prestressed concrete bridge girders. The following sections address the selection of the precasters and the collection plan.

3.1.1 Selection of Precasters

TxDOT identified a total of eight precasters as suppliers of prestressed bridge girders for TxDOT projects. Each of the eight precasters was contacted to gather information on plant production practices and product details. Three of the eight precasters were selected as representative plants from which samples would be collected for the material testing program.

71

The main selection criteria used include the following:

- Geographical location: It is desirable to choose plants that are in different parts of the state because the climate and materials source influence the design of concrete mixture proportions. Nevertheless, due to the limitation in the ASTM standard C 31 (1998a) that the transportation time to the laboratory should not exceed four hours, some precast plants that required significantly more travel time were not selected.

- Production capacity: Production capacity of a plant is determined by the volume of concrete produced annually. It is important to include plants with different production capacities because of possible differences in the number of mixes used, quality control, and other production practices.

- Member types produced: This project focuses on girders used in longer span Texas highway bridges, particularly AASHTO Type IV girders and Texas U beams.

- Ability to produce HSC: The plant must be able to produce HSC.

- The frequency of HSC work: It is desirable to determine the variability in HSC that is produced on a routine basis versus HSC produced infrequently at a plant.

- Willingness to participate in the research project.

Table 3.1 provides a summary of information obtained through interviews with the eight precasters. Information relevant to the eight precasters as a group is given, along with specific information for each of the three selected precasters.

Table 3.1. Summary of Precaster Questionnaires.

Description Parameter		All Precasters	Precaster A	Precaster B	Precaster C
Location			South Texas	Central Texas	Central Texas
Section Types Provided		Mostly A, B, C, and AASHTO Type IV. Some Produce U Beams and Box Sections	TxDOT Type A, B, C, and U, AASHTO Type IV	TxDOT Type A, B, C, and U, AASHTO Type IV, and Various Box Sections	TxDOT Type A, B, and C, AASHTO Type IV, 54, 72, VIM
Annual Production (ft/year)		Range from 56000 - 890,000	280,000 (2)	166,000 (1)	225,000
Standard Strength Supplied (psi)	Release	Range from 4000 - 8000	8000	4000-6500	-
	Design	Range from 5000-11000	4000-9000 (3)	5000-8000	4000-10000
HSC Definition		6250-8000 Release 7000-9000 Design	8000 Release 9000 Design	6250-8000 Release 7000-9000 Design	> 9000 psi
HSC Production Frequency		Rarely-Everyday	Everyday for 6000-8000 psi	4-5 Projects/ Year (30,000 ft/year)	Regularly
Ability to Provide Strengths Other than Standard Strengths		Yes for 6 out of 8 Precasters	Yes	Yes	No
Ability to Supply 0.6 inch (15 mm) Diameter Strands		Yes for 2 out of 8 precasters	Yes	Yes (U Beams only)	No
Test Performed to Obtain Concrete Properties		Compression, Modulus of Rupture (If Requested)	Compression, Modulus of Rupture (If Requested)	Compression	Compression
Specimens Used for Testing of Compressive Strengths		4×8 inch (100×200 mm) or 6×12 inch (150×300 mm) Cylinder	4×8 inch (100×200 mm) Cylinder	4×8 inch (100×200 mm) Cylinder	4×8 inch (100×200 mm) Cylinder

Table 3.1. Summary of Precaster Questionnaires (Continued).

Description Parameter		All Precasters	Precaster A	Precaster B	Precaster C
Curing Conditions	First 24 Hours	Wet Mat and Tarps, Steam Curing, Water Pond	May-Oct: Wet Mats and Tarps Nov-Apr: Steam Curing	Wet Mat and Tarps in Warm Weather, Steam Curing in Cold Weather	Wet Mats and Tarps, Steam Curing May Be Used If Necessary
	After 24 Hours	No Curing, Cure until the Release Strength is Reached	Cure until the Release Strength is Reached	No Curing	Cure until the Release Strength is Reached
Limitations in Producing HSC		Cost of Production, Heat of Hydration, Release Strength Not Met in One Day, Availability of Materials	Availability of Local Materials	Problems with the Heat of Hydration, Release Strength not Met in One Day	Uneconomical for design strength Greater than 9000 psi
Seasonal Variations in Mixture Proportions		Mostly Yes	8-10 Mixture Proportions Depending on Time, Weather, Temperature, and Strength	More Cement and Admixtures During Winter	Yes
Limits on the Ambient Temperature during Casting		Most Cannot Cast in Very Low Temperature	No	Use TxDOT Specification	Cannot Cast Below 40 °F (4.4 °C)
Plant Certification		Some Do Not Have, Some Have TxDOT, OK DOT or PCI	PCI	PCI	PCI

Notes:
  (1) Calculated by LF = 100 ft/beam × no. of beams produced
  (2) Calculated by LF = 50,000 cyd/ (0.18 cyd/ft)
  (3) Compressive strength up to 14,000 psi has been produced

3.1.2 Sample Collection Schedule

The collections of concrete samples were categorized into several compressive strength ranges so that the effect of strength level on the relationships of material properties and their statistical parameters could be evaluated. Because many precasters did not design a specific mixture proportion for each project, it was not possible to obtain several mixture proportions having different mixture design compressive strengths to complete the entire experimental plan. In addition, the required nominal design compressive strength was deemed to be the critical selection criterion for the reliability study. Therefore, the selection of samples to be collected was based on the required 28-day compressive strength specified by the designer, rather than the mixture design compressive strength of the concrete mix. The plan was to collect the samples in the following compressive strength classes:

- 6000 ± 1000 psi (41.1 ± 6.8 MPa)
- 8000 ± 1000 psi (55.2 ± 6.8 MPa)
- 10000 ± 1000 psi (68.9 ± 6.8 MPa)

Although it would be desirable to test mixes for compressive strengths greater than 10000 psi (68.9 MPa), these higher strengths were not available from the selected precasters during the testing program.

It was initially expected that there would be a variation between concrete mixture proportions and curing methods during the summer and winter based on initial interviews with the precasters. Therefore, two collections, a summer collection and a winter collection, of each compressive strength class were required from each precaster to account for this variability. However, it was later found that two of the three selected precasters do not have different mixtures for different seasons and use the same mixture for both summer and winter. For the precaster that has different mixtures, it was found that the time of casting is often more significant in the selection of the mixture proportions than the ambient temperature. Therefore, the seasonal effect was not considered in later collections. Nevertheless, two collections of the same strength range were still collected from each precaster to account for possible variations of

the mix. For each collection day, two sets of concrete specimens were collected from two different batches of the same mixture proportion. The purpose of having two sets was to determine the variation of concrete properties between batches with the same mixture proportions. This reflects the quality and consistency of the batching and mixing of concrete. Table 3.2 shows the sample collection plan for each precaster. A minimum of six visits to each precaster were required (two for each of the three strength classes), for a total of 18 sample collections (36 batches).

Table 3.2. Sample Collection Plan per Precaster.

Compressive Strength Range	Set 1		Set 2	
	Batch 1	Batch 2	Batch 1	Batch 2
6000 ± 1000 psi (41.1 ± 6.8 MPa)	✓	✓	✓	✓
8000 ± 1000 psi (55.2 ± 6.8 MPa)	✓	✓	✓	✓
10000 ± 1000 psi (68.9 ± 6.8 MPa)	✓	✓	✓	✓

It should be noted that there were three collections where the required compressive strengths were not based on the actual specified compressive strength of a girder in production, but rather the specified strength given by the research team. This was because these strength requirements were not available during the testing program. Precasters were asked to provide mixtures that they would use for an actual structure for the given specified strength. Details on the compressive strength requirements and mixture proportions for each set of samples collected are provided in Appendix A.

3.1.3 Collection Protocol

The following sections discuss the selection of specimens, the casting of specimens, and the curing of specimens.

3.1.3.1 Selection of Specimens

Four inch (100 mm) by eight inch (200 mm) cylindrical specimens were used to evaluate the compressive strength, modulus of elasticity, splitting tensile strength, and creep. These specimens were used for the following reasons:

- To prevent the wall effect on the compaction, the smallest dimension of the specimen must be at least three times the maximum size of the aggregate. For the precasters used in this research, the maximum size of aggregate was less than 1 inch (25 mm). Therefore, the use of 4×8 inch (100×200 mm) cylinders was deemed adequate.

- Only one truck was required to transport the specimens back to the laboratory when using the smaller 4×8 inch (100×200 mm) specimens.

- The capacity of the testing machine limits the maximum compressive strength that can be tested safely using standard 6×12 inch (150×300 mm) specimens.

- Based on the current literature, the difference in the strengths between the 6×12 inch (150×300 mm) and 4×8 inch (100×200 mm) cylindrical specimens is expected to be small (on the order of 3 to 5 percent).

- The 4×8 inch (100×200 mm) specimens were used for the compressive strength tests conducted at each of the precast plants that participated in the project. Therefore, using the same specimen size allows a more direct comparison between the strength from the laboratory and the strengths determined by the precasters.

- The 4×8 inch (100×200 mm) specimens were used in the development of many of the ACI Committee 363 (1997) formulas for determining properties of HSC. Again, direct comparison could be done if the same specimen size was used.

- Past research in Texas on HSC (Gross and Burns 2000, Myers and Carrasquillo 1998) used 4×8 inch (100×200 mm) cylinders.

The compressive strength and the splitting tensile test required three specimens per batch for each test. Two specimens per batch were required for each test of the modulus of elasticity.

The beam specimens for the flexural strength (modulus of rupture) test were 6×6×20 inches (150×150×500 mm), the smallest size allowed to be cast in the field by the ASTM C 31 (1998a). The span length used in the test was 18 inches (450 mm), resulting in a 1 inch (25 mm) overhang on each side of the support. Three beam specimens were required from each batch for the modulus of rupture test.

The test specimen size for the shrinkage tests was selected based on the maximum aggregate size used by the precasters. A prism of 4×4×11.25 inches (100×100×285 mm) was used because this is adequate when all the aggregates pass a 2 inch (50 mm) sieve. Two to three specimens were cast for each batch.

The specimens were tested at the age of 7, 28, and 56 days. The total numbers of specimens required per trip were 72 cylinders, 18 beams, and four to six prisms. Additional specimens were added to these numbers to allow for damage to specimens that could occur during the transportation or during preparation for testing. The specimen types and sizes and the number of specimens required for each test are summarized in Table 3.3.

Table 3.3. Summary of Specimen Types and Number of Specimens Required for Each Batch.

Standard Test Method	Specimen Type and Size	Number of Specimens Required	
		Per Age Tested	Total
Compressive Strength	Cylinder, 4×8 inch (100×200 mm)	3	9
Modulus of Elasticity	Cylinder, 4×8 inch (100×200 mm)	2	6
Splitting Tensile Strength	Cylinder, 4×8 inch (100×200 mm)	3	9
Flexural Strength	Beam, 6×6×20 inch (150×150×500 mm)	3	9
Creep	Cylinder, 4×8 inch (100×200 mm)	-	3
Shrinkage	Prism, 4×4×11 ¼ inch (100×100×285 mm)	-	2-3

3.1.3.2 Field Casting of Specimens

For most collections, test specimens were cast at the same time the precasters were casting girders. The fresh concrete used in the casting was sampled directly from the concrete used for the girders. Two sets of specimens were made for each collection: one was collected near the beginning of the pour, and the other was collected near the end. Approximately 7.0 ft^3 (0.18 m^3) of concrete was needed for each set of specimens.

The specimens were cast according to ASTM C 31/C 31M (1998a). All cylinders except the creep specimens were cast in single-use plastic molds. Cylindrical specimens used in the creep test were cast in reusable steel molds. The reason for this is that the steel molds have better dimension stability than the plastic molds. It is considered important for the creep test because the specimens have to be capped with sulfur and stacked one on top of the other in a creep frame. If the side of the specimen is not perpendicular to the base, it will become difficult to obtain a perfectly level cap. Small inclinations of the caps of each specimen can produce a large inclination at the top when they are stacked together. It was observed that the plastic molds are approximately 1/16 to 1/8 inches (1.6 to 3.2 mm) larger in diameter at the top of the cylinder than at the bottom. Although this difference is still within the allowable limit specified in ASTM

C 470 (1998d), the steel molds were used to minimize error in the creep test. The beam molds for the modulus of rupture test and the prism molds for the shrinkage test were also reusable steel molds. A thin layer of hydraulic oil was used to coat the steel molds to prevent concrete from bonding with the molds. It was unnecessary to coat the single-use plastic molds.

All the specimens were compacted by means of manual tamping. The dimensions of the tamping rods were governed by the dimension of the molds according to ASTM C 31 (1998a). Table 3.4 provides a summary of the compaction requirements for each specimen type.

After compaction, the top surface of each specimen was finished using a trowel. The total casting time for each batch was approximately 45 minutes. The casting environment was not controlled, but the ambient temperature and humidity at the time of casting were recorded. The temperature at the time of casting ranged from 60 to 125 °F (16 to 52 °C), and the relative humidity ranged from 40 percent to more than 98 percent.

Table 3.4. Compaction Requirements for Each Specimen Type.

Specimen Type and Size	Number of Layers	Number of Roddings per Layer
Cylinder, 4×8 inch (100×200 mm)	3	25
Prism, 4×4×11 ¼ inch (100×100×285 mm)	2	45
Beam, 6×6×20 inch (150×150×500 mm)	2	60

3.1.3.3 Curing and Sample Preparation

After finishing the casting, all cylinders in plastic molds were covered with plastic lids. All other specimens were covered with plastic sheets to prevent moisture loss from evaporation. All specimens were then covered with wet burlap and plastic tarps to retard the evaporation. Figure 3.1 shows specimens in the field after finishing, before being covered with wet burlap and plastic tarps. Specimens were cured overnight at the precast plant. On the next day, all

specimens were loaded on a truck and transported back to the laboratory. The transportation time ranged from 2 to 3 hours. During that time, moisture loss was prevented by means of wet burlap covers and plastic tarps. Immediately upon arrival at the laboratory, specimens were unloaded and removed from the molds, labeled, and stored in a moist room for final curing. The temperature and humidity in the moist room were controlled at 73 ± 3 °F (23 ± 2 °C) and greater than 98 percent, respectively.

Figure 3.1. Specimens after Finishing.

ASTM C 157 (1999c) requires that an initial reading of shrinkage specimens must be taken at $24 \pm \frac{1}{2}$ hours after casting. As a result of this requirement, the specimens cast in the morning were removed from the molds at the precast plant on the next morning and submerged in a lime solution at 73 °F (23 °C) for 30 minutes before the initial reading was taken. After that, they were transported to the laboratory. During the transportation, the shrinkage specimens were stored in the lime solution. Upon arrival at the laboratory, they were transferred to another lime solution container in the moist room with a temperature-controlled environment until the second reading at the age of 28 days. For specimens cast in the afternoon, sufficient time was available to transport the specimens back to the laboratory before they reached the age of $24 \pm \frac{1}{2}$ hours. Therefore, the initial reading was taken at the laboratory. These specimens were then cured in the same manner as the morning cast shrinkage specimens until the second reading.

One day before testing, specimens were randomly selected for preparation for the tests. The specimens for the compressive strength test and the modulus of elasticity test were labeled, measured, and, when necessary, capped with sulfur compound according to ASTM C 617 (1994c). Splitting tensile strength test specimens were labeled and measured. Creep specimens were capped with sulfur mortar, and strain gages were glued on the surfaces according to the recommended procedures from the strain gage manufacturer. Plastic sheets and a water sprayer were used to keep the specimens moist when they were not being prepared. After the sample preparation was finished, the specimens were taken back to the moist room until testing.

The beam specimens for the modulus of rupture test were placed in water saturated with calcium hydroxide one day before the test. The temperature of the bath was the same as the laboratory temperature, which varied between approximately 70 and 75 °F (21 and 24 °C).

On the testing day, all cylindrical specimens were placed on a cart and transported from the moisture room to the testing laboratory. Before being tested, the specimens were covered with plastic sheets to prevent moisture loss. A water sprayer was also used when needed to keep the specimen surfaces moist.

The shrinkage specimens were stored in the lime-saturated water under a controlled temperature of 73 ± 3 °F (23 ± 2 °C) for 28 days before recording a second reading. ASTM C 157 (1999c) requires that specimens be moved to a drying room with a temperature of 73 ± 3 °F (23 ± 2 °C) and a relative humidity of 50 percent for air drying. However, due to the unavailability of a humidity-controlled room, the specimens were stored in a laboratory. The temperature and relative humidity in the laboratory were recorded at the time of shrinkage reading. The temperature of the laboratory room was approximately 70 to 75 °F (21 to 24 °C), and the relative humidity was between 40 to 50 percent. The specimens were placed on metal racks with a clearance of at least 1 inch on each side as required by ASTM C 157 (1999c).

3.2 TEST APPARATUS

3.2.1 Testing Machines

Three testing machines were used in the material testing program. These machines are all servo-controlled closed-loop hydraulically operated machines that can be programmed to run in a displacement-controlled or load-controlled mode. The three machines were manufactured by MTS with loading capacities of 20 kips (89 kN), 100 kips (445 kN), and 500 kips (2224 kN). They are located in the Texas Engineering Experiment Station (TEES) Testing, Machining, and Repair Facility (TMRF) on the Texas A&M University (TAMU) campus.

The 500 kip (89 kN) MTS machine was used for all compressive strength tests, modulus of elasticity tests, and all splitting tensile strength tests. Some of the modulus of ruptures tests were done on this machine by changing the support and loading head. The time, displacement of the hydraulic piston, load magnitude, and strain readings from Linear Variable Displacement Transducers (LVDTs) (if used) were recorded with a computerized data acquisition system.

The 20 and 100 kip (445 and 2224 kN) MTS machines were used for the flexural strength test of concrete beams. The time, displacement of the hydraulic piston, and load magnitude were recorded with a computerized data acquisition system.

3.2.2 Neoprene Pads

Commercially available neoprene pads and steel retaining rings were used for the compressive strength test and the modulus of elasticity test (see Figure 3.2). The neoprene pads had a durometer hardness of 70, determined according to ASTM D 2240 (2000c). This is required by ASTM C 1231 (2000b) for HSC having compressive strength from 4000 to 12,000 psi (27.6 to 82.7 MPa). Neoprene pads were changed frequently when damage occurred from testing or when the pads became worn. Usually they were replaced before 30 reuses.
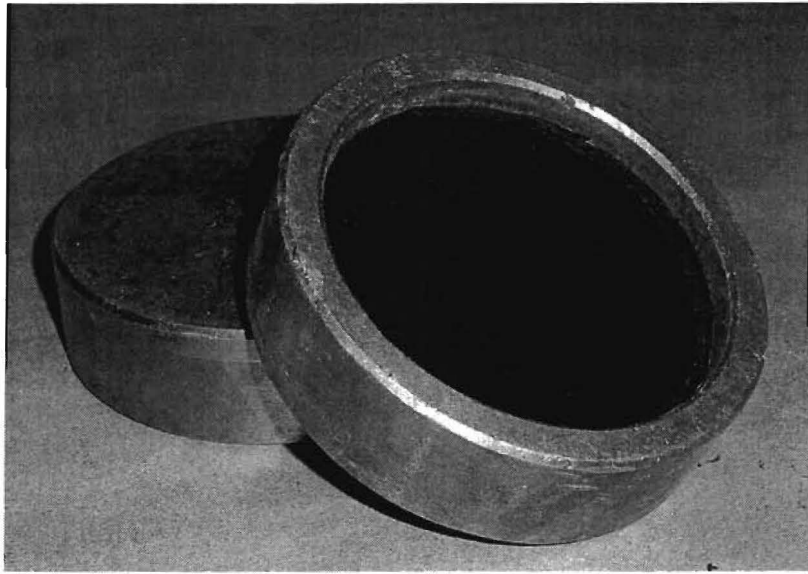
Figure 3.2. Neoprene Pads in Steel Retaining Rings.

3.2.3 Compressometer

The compressometer shown in Figure 3.3 was used for the modulus of elasticity test. It is composed of two aluminum yokes. These yokes were attached to the cylindrical specimen by means of three screws on the perimeter spaced at 120 degrees from each other. The vertical distance between the yokes was 4.0 inches (100 mm). Two temporary support legs were used to keep the yokes at 4.0 inches (100 mm) apart during the installation and were removed before the test. Two LVDTs were installed 180 degrees from each other to measure the strain in the concrete. The LVDTs were connected to the computer that controls the testing machine so that the load and strain could be recorded simultaneously.
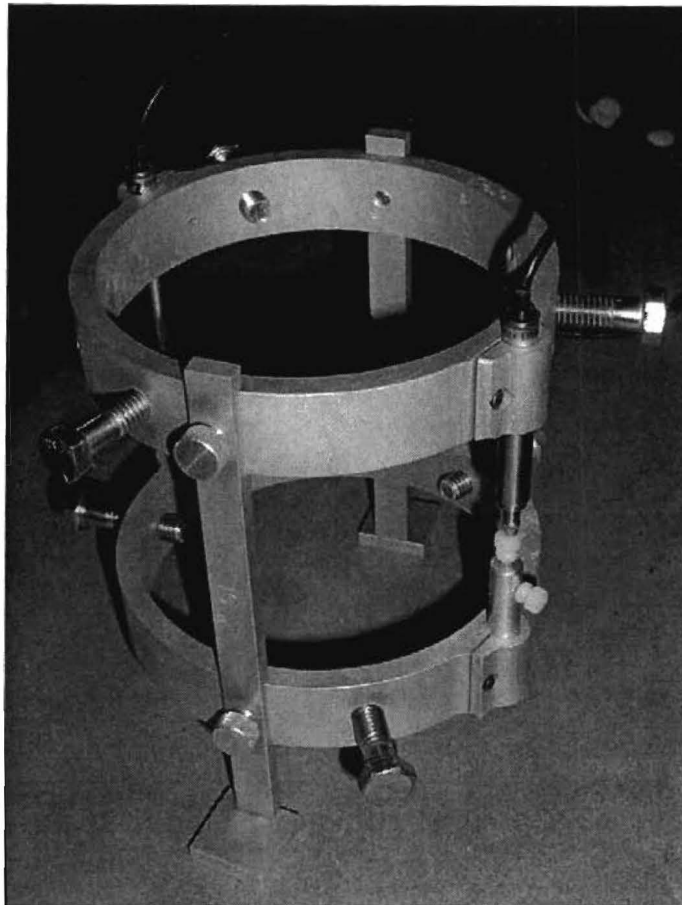
Figure 3.3. Compressometer.

3.2.4 Aligning Jig

An aligning jig, shown in Figure 3.4, was used to facilitate the splitting tensile tests by holding the plywood bearing strips and bearing bar in place. The jig was similar to that specified in ASTM C 496 (1996) but was scaled down for 4×8 inch (100×200 mm) cylindrical specimens.
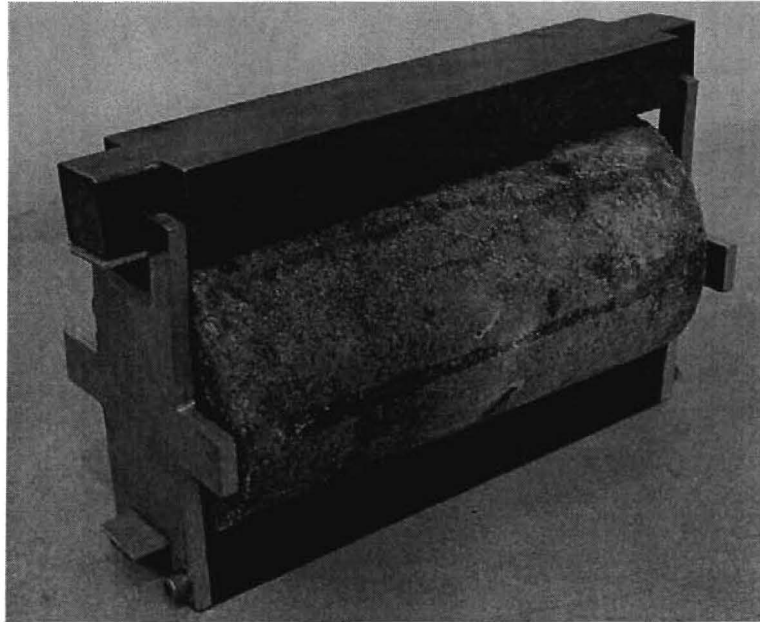
Figure 3.4. Aligning Jig for Splitting Tensile Test.

3.2.5 Creep Frame

Creep was tested using creep frames as shown in Figure 3.5. The frame was primarily composed of two springs, four threaded rods, and three metal plates. The springs were used to maintain constant load on the specimens. A circular steel plate and a steel ball were used at each end to adjust to the ends of specimens. The creep frame was loaded in the 500 kip (2224 kN) MTS testing machine to the desired load, compressing the springs. The nuts over the top plate were then tightened, and the load from the testing machine was released. Some elastic elongation in the rods occurred after the release of the load, resulting in a load loss. The amount of the elongation could be determined by measuring the change in the spring length before and after releasing the load. The load lost is equal to the product of the change in the spring length and the average stiffness of the springs. It was assumed that the deformation of the plates was negligible. Four smaller threaded rods were then placed adjacent to the specimens to help hold the cylinders in place during assembly and for safety purposes. Each frame accommodated four 4×8 inch (100×200 mm) cylinders and two 4×4 inch (100×100 mm) concrete plugs.
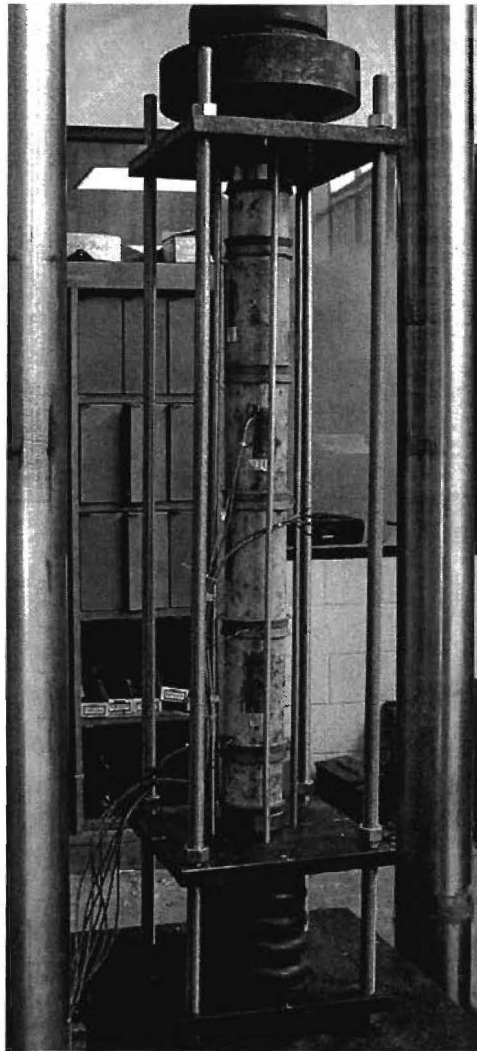
Figure 3.5. Creep Frame at Loading.

3.2.6 Length Comparator

The change in length of the shrinkage prisms was measured with the length comparator shown in Figure 3.6. It was composed of a frame with an elevating screw and an anvil support for a contact point at the base and a digital gage at the top. An invar rod was used as a standard length to calibrate the digital gage before each reading. The difference in the lengths of the specimen and the invar rod can be read from the electronic display. The gage had a precision of 0.0001 inch (0.0025 mm).
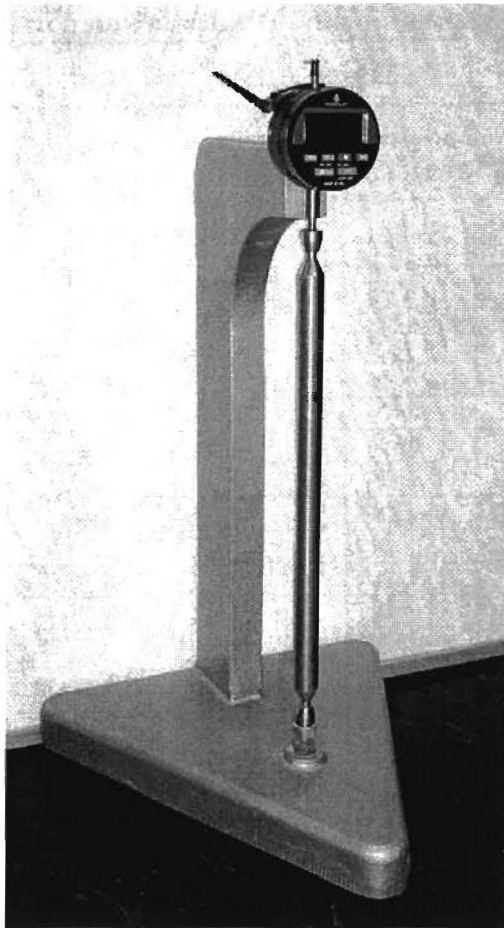
Figure 3.6. Length Comparator.

3.3 MATERIAL TESTING

All the material properties reported were obtained from the tests conducted at TAMU, except the 1-day compressive strength data, which were obtained from testing performed by the precasters. A summary of data obtained in this project is shown in Table 3.5. The following section describes the test methods and procedures for each test conducted at TAMU. The testing notes provided in Appendix F describe any modifications that occurred during a test.

Table 3.5. Summary of Data Included in the Project.

Precaster and Sample Set	Design f'_c* Category (psi)	Collection Date	Compressive Strength			Modulus of Elasticity			Splitting Tensile Strength			Modulus of Rupture			Creep (days)	Shrinkage (weeks)
			7	28	56	7	28	56	7	28	56	7	28	56		
A Set 1	6000	06/20/01	X	X	X	X	X	X	X	X	X	X	X	X	NT	NT
	8000	09/15/00	X	X	X	NR	NR	NR	X	X	X	X	X	X	NT	NT
		06/18/01	X	X	X	X	X	X	NT	NT	NT	NT	NT	NT	NT	NT
	10000	06/25/01	X	X	X	X	X	X	X	X	X	X	X	X	NT	64
A Set 2	6000	03/19/01	X	X	X	X	X	X	X	X	X	X	X	X	670	64
	8000	04/02/01	X	X	X	X	X	X	X	X	X	X	X	X	650	64
	10000	05/23/01	X	X	X	X	X	X	X	X	X	X	X	X	600	64
B Set 1	6000	09/20/00	X	X	X	NR	NR	NR	X	X	X	X	X	X	NT	NT
		06/21/01	X	X	X	X	X	X	NT	NT	NT	NT	NT	NT	NT	64
	8000	09/04/01	X	X	X	X	X	X	X	X	X	X	X	X	NT	64
	10000	06/07/01	X	X	X	X	X	X	X	X	X	X	X	X	NT	64
B Set 2	6000	06/14/01	X	X	X	X	X	X	X	X	X	X	X	X	580	64
	8000	08/27/01	X	X	X	X	X	X	X	X	X	X	X	X	510	64
	10000	06/04/01	X	X	X	X	X	X	X	X	X	X	X	X	590	64
C Set 1	6000	07/18/01	X	X	X	X	X	X	X	X	X	X	X	X	NT	64
	8000	09/25/00	X	X	X	NR	NR	NR	X	X	X	X	X	X	NT	NT
		06/13/01	X	X	X	X	X	X	NT	NT	NT	NT	NT	NT	NT	NT
	10000	09/07/01	X	X	X	X	X	X	X	X	X	X	X	X	NT	64
C Set 2	6000	04/04/01	X	X	X	X	X	X	X	X	X	X	X	X	650	64
	8000	04/26/01	X	X	X	X	X	X	X	X	X	X	X	X	630	64
	10000	04/24/01	X	X	X	X	X	X	X	X	X	X	X	X	630	64

Notes:
* = Nominal range
X = Tested
NT = Not tested
NR = Not reported (insufficient data)

3.3.1 Test Standards

In this project, all tests are performed according to the appropriate TxDOT or ASTM standards. Precasters in Texas use the TxDOT standards. It was found that there is no significant difference between the procedures specified by the TxDOT standards and ASTM standards for all the tests conducted in this project. Therefore, the ASTM standards were followed for all the tests. The test methods and corresponding standards are summarized in Table 3.6.

Table 3.6. Summary of Test Standards.

Test Method	ASTM Standards	TxDOT Standards
Compressive Strength	C 39/C 39M-99	Tex-418-A
Modulus of Elasticity	C 469-94	-
Splitting Tensile Strength	C 496-96	Tex-421-A
Flexural Strength	C 78-94	Tex-448-A
Creep	C 512-87	-
Shrinkage	C 157-99	-

3.3.2 Compressive Strength Test (ASTM C 39/C 39M-99)

Compressive strength was determined according to the standard ASTM C 39/C 39M (1999b) test method at the age of 7, 28, and 56 days. For each test date, three 4×8 inch (100 x 200 mm) cylinders from each batch were randomly selected for testing. The specimens were loaded at a constant stress rate of 35 psi/s (0.24 MPa/s) until failure. The specimens were tested using neoprene caps because it was determined from early tests that specimens tested using sulfur caps did not provide consistent results. It is believed that this was due to the effect of the cap thickness and the shape of the specimen. It was found that when the cap was thick (as in the case when the ends of the cylinder are not perpendicular to its longitudinal axis), a low strength result can occur. It was also found that lower strength can result when the specimens are out-of-round. The plastic molds were not sufficiently stiff to retain their cylindrical shape, especially on hotter days. Moreover, neoprene capping was used for verification of compressive strength by all precasters participating in the project. Using the same capping system eliminates an additional variable that could affect the results.

3.3.3 Modulus of Elasticity Test (ASTM C 469-94)

According to ASTM C 469 (1994b), the modulus of elasticity of concrete is defined as a secant modulus between the strain of 50 $\mu\varepsilon$ to the stress of 40 percent of the compressive strength at the age of testing. The modulus of elasticity (E) is calculated as:

$$E = \frac{S_2 - S_1}{\varepsilon_2 - \varepsilon_1}$$

(3.1)

where S_2 is the stress corresponding to 40 percent of the ultimate load; S_1 is the stress corresponding to the longitudinal strain ε_1, which is approximately 50 $\mu\varepsilon$; and ε_2 is the longitudinal strain at stress S_2.

Two 4×8 inch cylinders from each batch were used for each test date for determining the modulus of elasticity. Both specimens were capped with neoprene pads. Another study was conducted to compare the effect of capping on the modulus of elasticity, and it was found that the result from sulfur mortar capping and neoprene capping were not statistically different (see Appendix C). A compressometer (Section 3.2.3) was used to measure the longitudinal strain. Cylindrical specimens were tested at a constant stress rate of 35 psi/s (0.24 MPa/s) up to approximately 40 percent of the average compressive strength. Each specimen was loaded at least three cycles as required by ASTM C 469 (1994b). Only the stress-strain relationships from the last two cycles were used for the calculation of the modulus of elasticity. Figure 3.7 shows the test setup.
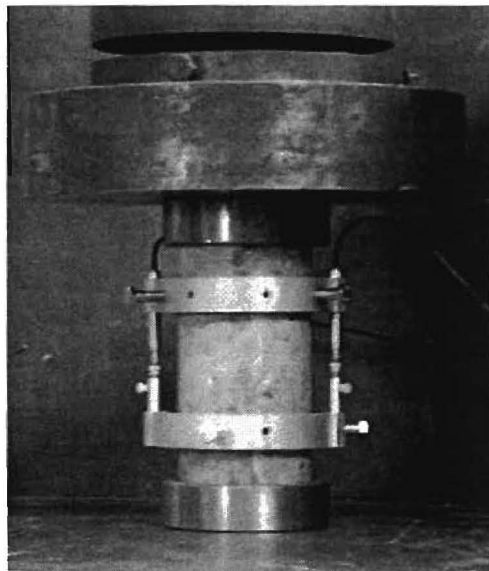
Figure 3.7. Modulus of Elasticity Test.

91

3.3.4 Splitting Tensile Strength Test (ASTM 496-96)

Splitting tensile strength tests were performed by placing a 4×8 inch (100×200 mm) cylinder on its side between the upper and lower bearing blocks of the testing machine. An aligning jig (Section 3.2.4) was used for the majority of the splitting tensile tests to assist in aligning the cylinder, as shown in Figure 3.8. Two plywood strips, ⅛ inch (3 mm) thick by 1 inch (25 mm) wide were placed between the specimen and the bearing blocks to help distribute the load uniformly to the specimen. Three specimens from each batch were used for the test. The standard rate of loading was 150 psi/min (1.03 MPa/min) of tensile stress, or the equivalent of the load rate of 7.5 kips/min (33.4 kN/min) for the 4×8 inch (100×200 mm) cylinders.
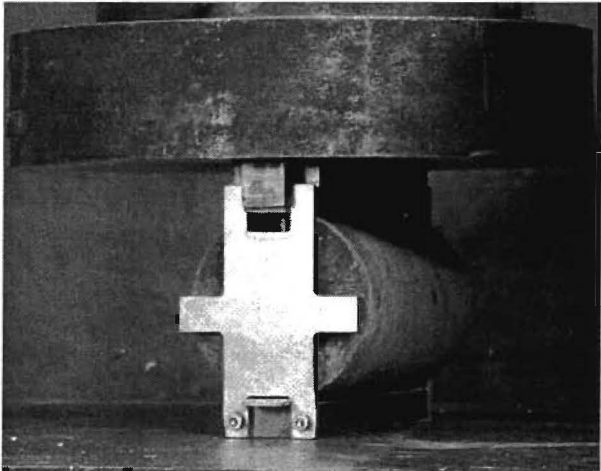
Figure 3.8. Splitting Tensile Test.

The splitting tensile strength was calculated as follows:

$$T = \frac{2P}{\pi l d} \tag{3.2}$$

where T is the splitting tensile strength (in stress units), P is the maximum applied load, l is the average length of cylinder, and d is the average diameter of the cylinder.

3.3.5 Flexural Strength Test (ASTM C 78-94)

Three 6×6×20 inch (150×150×500 mm) concrete beams from each batch were used to test the modulus of rupture. The test setup is shown in Figure 3.9. The span length of the support was 18 inches (450 mm). The load was applied at the third points at the rate of 150 psi/min (1.03 MPa/min) of the tensile stress at the bottom fiber until the failure occurred. After failure, the width and depth at three locations and the location of failure of the beam were measured for the calculation of the modulus of rupture.
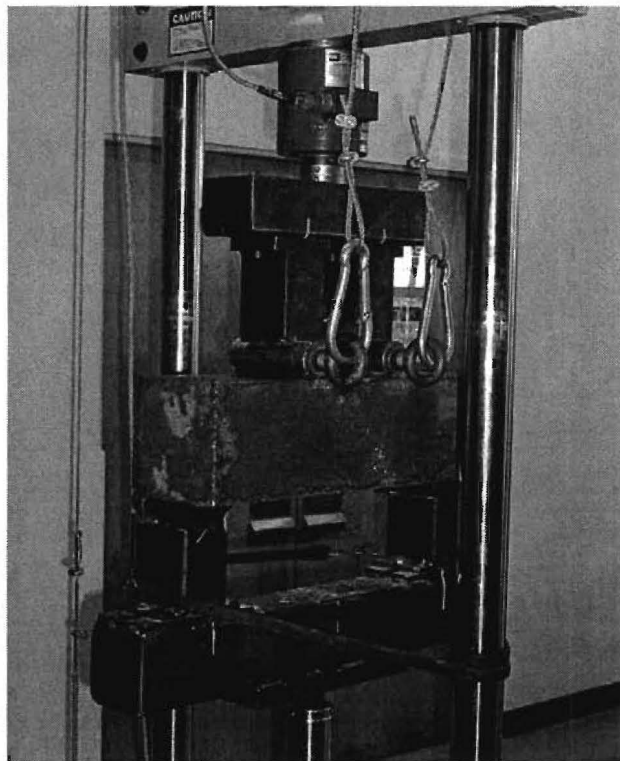
Figure 3.9. Modulus of Rupture Test on 20 kip MTS Machine.

The modulus of rupture, when the failure occurs between the loading points (all specimens tested failed in this mode), is calculated as:

$$R = \frac{PL}{bd^2} \tag{3.3}$$

where R is the modulus of rupture (in stress units), P is the maximum load, L is the span length of the beam specimen, b is the average width of the specimen, and d is the average depth of the specimen.

3.3.6   Creep Test (ASTM C 512-87)

Dimensional changes in the concrete cylinder result from movement of moisture, thermal changes, and creep. To evaluate the creep, the dimensional change resulting from moisture movement and temperature variation need to be determined and subtracted from the overall dimensional change. Three cylinders from each batch of a mixture were used for the creep tests. Two cylinders from a batch were loaded in the creep frame with another two cylinders from the second batch of the same mixture proportion collected on the same day. In addition, one cylinder from each batch was used as a control specimen to determine the drying shrinkage. Two strain gages were glued longitudinally on opposite sides of a specimen to measure the longitudinal strain. Another two strain gages were placed on a steel block. The strain gages used had a gage length of 2 inches (50 mm). Because concrete is not a homogeneous material, a long gage length is needed to obtain a more accurate measurement. Some strain gages used on the steel blocks had a gage length of 0.125 inches (3.18 mm). A longer gage length is not necessary because steel is more homogeneous than concrete.

The strain gages were connected in a Wheatstone bridge circuit to increase the sensitivity of the measurement and to reduce the number of channels required to record the data. In addition, the purpose of having strain gages on the steel block is to compensate for the temperature strains. Because the coefficient of thermal expansion of steel is similar to that of concrete, most of the thermal expansion in concrete can be canceled out by thermal strain measured from the steel. It is not possible to place the strain gages for thermal expansion on concrete because this would include the effect of shrinkage resulting from moisture loss. The strain gage configuration on the concrete specimen and the steel block are shown in Figure 3.10. Appendix D provides more details on the strain gage circuit.

The creep frames were loaded at the age of 7 days to a load of approximately 30 percent of the concrete compressive strength at that age using the 500 kip (2224 kN) MTS testing machine. The load in the creep frame was monitored over time by measuring the change in length of the spring. According to ASTM C 512 (1992), if the load changed by more than 2 percent of the original load, it was necessary to readjust the load. Figure 3.11 shows the creep test frames.

| (a) Concrete Specimen | (b) Steel Block (2 inch Gage Length) | (c) Steel Block (0.125 inch Gage Length) |
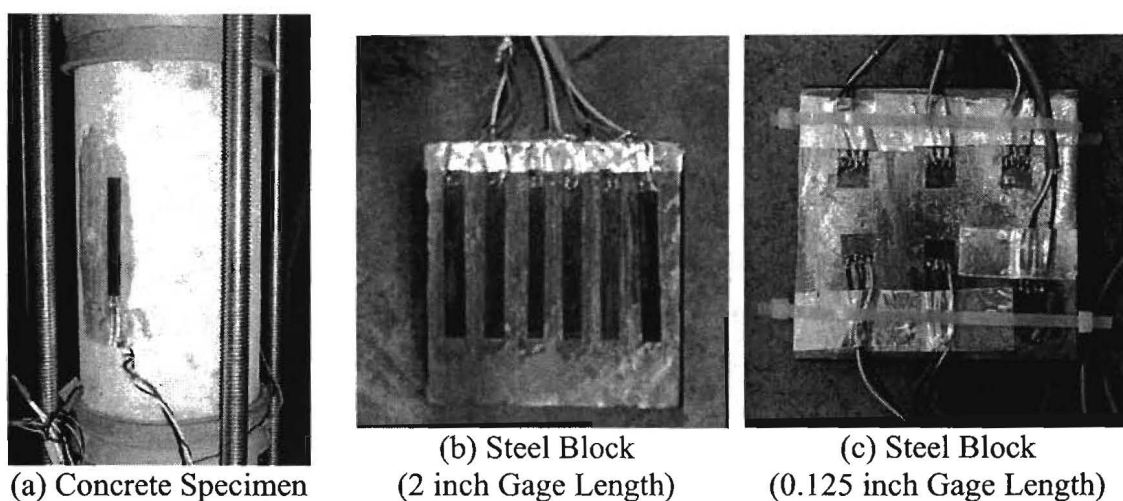
Figure 3.10. Strain Gage Configuration.
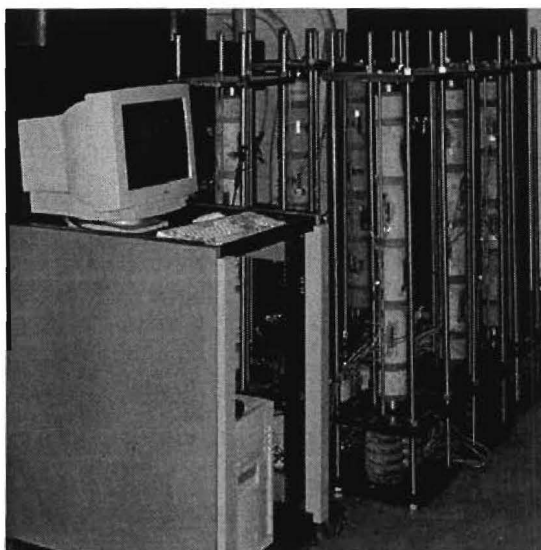
Figure 3.11. Creep Test Setup.

3.3.7 Shrinkage Test (ASTM C 157/C 157M-99)

The shrinkage tests were performed according to ASTM C 157 (1999c). Two to three specimens of the same batch were used for the test. The change in length (shrinkage) was determined by comparing the length of a 4×4×11 ¼ inch (100×100×285 mm) concrete prism to the length of the reference invar rod using the length comparator. Before each reading, the comparator gage was calibrated by placing the reference rod in the comparator and resetting the gage reading to zero. The readings were taken at 1 day after casting (initial reading); at 28 days (second reading); at 4, 7, 14, and 28 days after the second reading; and at 8, 16, and 32 weeks after the second reading. The ambient temperature and relative humidity were also recorded at each reading. The change in length is calculated as:

$$\Delta L_x = \frac{CRD - \text{initial } CRD}{G} \times 100 \tag{3.4}$$

where ΔL_x is the change in length of the specimen in percent, CRD is the difference between the comparator reading of the specimen and the reference rod, and G is the gage length of 10 inches (250 mm).

4 EXPERIMENTAL RESULTS AND EVALUATION

In this chapter, the methodology for the data analysis and a summary of the experimental results are presented. The experimental results include compressive strength, modulus of elasticity, splitting tensile strength, modulus of rupture, creep, and shrinkage data. Statistical analyses determined the mean, standard deviation, and bias factor for the compressive strength, modulus of elasticity, splitting tensile strength, and modulus of rupture. The effects of precaster, age of concrete, and specified strength level on the mechanical properties are investigated. An evaluation of prediction formulas for modulus of elasticity, splitting tensile strength, modulus of rupture, creep, and shrinkage is also presented. Test results and measurements of each specimen can be found in Appendix B.

4.1 ANALYSIS OF DATA

The data analysis is discussed in this section. The methodologies for determining the statistical parameters are described in Sections 4.1.1, 4.1.2, and 4.1.3 for mean, bias factor, and coefficient of variation, respectively. Section 4.1.4 outlines the methodology for determining the probability distribution of the data. Analysis of variances is discussed in Section 4.1.5. Section 4.1.6 describes the evaluation of the goodness of fit for prediction formulas.

4.1.1 Mean

In general, the mean ($\overline{X}$) of a set of n data points, $X_1, X_2, ..., X_n$, is calculated as:

$$\overline{X} = \frac{\sum_{i=1}^{n} X_i}{n} \tag{4.1}$$

In the analysis, three types of mean (or average) value are calculated, namely batch average, mixture average, and average of mixture averages.

4.1.1.1 Batch Average

The batch average is the average of the test results from the specimens within the same batch. Test results from three specimens are used to calculate the batch average for compressive strength, splitting tensile strength, and modulus of rupture. For the modulus of elasticity test, results from only two specimens are used. The batch average is considered to be the primary response variable because the material properties are usually obtained or verified from tests of samples within the same concrete batch. Batch averages are used in the calculation of the coefficient of variation within a mixture, as will be discussed later.

4.1.1.2 Mixture Average

The mixture average is calculated by averaging two batch averages from the same collection day. These two batches that are averaged have the same mixture proportion and specified (nominal) compressive strength. This mixture average value can be taken as an average strength of a prestressed beam because several batches are required to cast a beam. Mixture averages are used in the calculation of the coefficient of variation of mixture averages.

4.1.1.3 Average of Mixture Averages

The average value of mixture averages across various categories such as precaster, age, or strength categories (based on nominal strength) represents the strength characteristic in a particular group; for instance, compressive strength for concrete from Precaster A at the age of 28 days.

4.1.2 Bias Factor

The bias factor is defined as the ratio of the mean value to the nominal (specified) value as:

$$\lambda = \frac{\mu_R}{R_n} \qquad (4.2)$$

where μ_R is the mean value that can be approximated by the sample mean $\overline{X}$ and R_n is the nominal value (specified value). The mean value is obtained from material testing, and the nominal value is specified by the designer.

Bias factors are calculated for concrete at the age of 1 and 28 days. The 1-day bias factor is the ratio of the batch average of release strength (obtained from the precasters) to the specified release strength. The 28-day bias factor is calculated as the ratio of the batch average of the 28-day compressive strength to the specified design strength.

The bias factor value indicates the amount of additional strength provided in practice. A bias factor greater than one is desirable for design because the corresponding mean actual strength is greater than the design strength for this case. However, a bias factor much greater than one may not be economical.

4.1.3 Coefficient of Variation

Coefficient of variation (CV) is defined as the ratio of the standard deviation to the mean. It measures the variability of the data from the mean value with respect to the mean. CV is often expressed in percent as:

$$CV = \frac{S}{\overline{X}} \times 100\% \qquad (4.3)$$

where S is the standard deviation calculated by the following equation:

$$S = \sqrt{\frac{n\sum_{i=1}^{n} X_i^2 - \left(\sum_{i=1}^{n} X_i\right)^2}{n(n-1)}} \qquad (4.4)$$

99

For this project, four types of *CVs* are calculated. These *CVs* are described in the following sections.

4.1.3.1 Coefficient of Variation within a Batch

The coefficient of variation within a batch (CV_{Batch}) is calculated from the test values from specimens of the same batch at the same age. For the compressive strength, splitting tensile strength, and modulus of rupture, the mean and the standard deviation of three specimens are used for the calculation of CV_{Batch}. For modulus of elasticity, values from only two specimens are used. This coefficient of variation captures the variation of the concrete properties in a batch and any variation in the test procedures.

4.1.3.2 Coefficient of Variation within a Mixture

The coefficient of variation within a mixture (CV_{Mix}) is calculated from two batch average values from the same mixture. This coefficient of variation captures the variation of the concrete between the two batches. Therefore, it indicates the consistency of the proportioning and mixing processes.

4.1.3.3 Coefficient of Variation of Mixture Averages

The coefficient of variation of mixture averages (CV_{MixAvg}) is calculated from several mixture average values for a particular material property. This coefficient of variation captures the variation of a mechanical property within a group, such as the variation among precasters.

4.1.3.4 Coefficient of Variation of Batch Averages

The coefficient of variation of batch averages ($CV_{BatchAvg}$) provides a measure of the relative variation in batch average values. Because the batch average value is considered to be the primary response variable of the analysis, this coefficient of variation is the value that will be

used in the determination of the resistance parameters. The variation of the batch average is a combination of the variation of mixture averages and the variation within a mixture. $CV_{BatchAvg}$ is calculated from CV_{Mix} and CV_{MixAvg} as:

$$CV_{BatchAvg} = \sqrt{CV^2_{within\ Mix} + CV^2_{MixAvg}} \qquad (4.5)$$

4.1.4 Determination of Probability Distribution

In addition to the statistical parameters (mean and coefficient of variation), the distribution of a mechanical property is important for the development of a probability-based design code. The statistical parameters of mechanical properties and their distribution are required for simulations of resistance parameters (Section 2.3.3). This section outlines the methodology for evaluating the distribution of mechanical properties based on the observed data.

There are several ways to determine the distribution of the data. One is to plot the arranged data with the quantile of a distribution. If the data follow the distribution, the points in the plot should lie approximately on a straight line. This plot is called a quantile plot or probability paper plot. To determine normal distribution, the quantile can be calculated as:

$$Q_i = \Phi^{-1}\left(\frac{R_i - \frac{1}{2}}{n}\right) \qquad (4.6)$$

where $\Phi^{-1}(x)$ is the inverse of the cumulative distribution function (CDF) of the standard normal distribution of x, $R_i = rank(x_i)$, and $x_i = x_1, x_2, ..., x_n$ are random samples of continuous data. If the data are normally distributed with mean μ and standard deviation σ, then:

$$x_i = \mu + \sigma z_i = \mu + \sigma Q_i \qquad (4.7)$$

101

where z_i is the standard variate of x_i. It can be seen that by plotting x_i and Q_i, the plot should look approximately linear with slope σ and intercept μ.

In fact, one could test the distribution of the data against any distribution function by changing the inverse CDF of the standard normal distribution in Equation 4.6 to an appropriate inverse of the distribution function to be tested. There may be a number of standard distribution functions that provide an appropriate description of this data. In this project, only the normal and lognormal distribution functions are evaluated. As will be seen later, these standard distribution functions provide a reasonable fit to the data.

Because the concrete samples collected in this project are not based on the same mixture proportion, the actual values of the mechanical property cannot be used directly. Instead, differences between an individual measurement of the specimen within a batch and the batch average (called residual) are used for the plot. If the data follow the normal distribution, the average will also follow the normal distribution. In addition, linear combinations (adding or subtracting) of normal variables are also normal. As a result, the residual will follow the normal distribution. Similarly, if the data follow the lognormal distribution, the logarithm of the data will be normal. Hence, the mean of the logarithm of the data and the residual of the logarithm will follow the normal distribution. Therefore, by plotting the residuals of the data (denoted as E in the plots) or the residuals of the logarithm of the data (denoted as EL in the plots) with their corresponding normal quantiles, one can test the distribution of the data with the normal distribution or lognormal distribution, respectively. In this project, the quantile plots are performed using SAS statistical analysis software (SAS Institute Inc. 1999). The vertical axis of the plot is the value of the variable, either the residual or the residual of the logarithm. The horizontal axis is the quantile of the normal distribution. The label N_*variable name* is used by the software to indicate that the normal quantile is plotted.

4.1.5 Analysis of Variances

In this section, the methodology for the analysis of variances is outlined. Details of this procedure can be found in many statistics textbooks, such as that by Milton and Arnold (1995).

The objective of this analysis is to determine the effect of several factors on the measured response. The measured responses that will be investigated include the mean and coefficient of variation within a batch, coefficient of variation within a mix, and the mean of the logarithm of batch averages. There are three factors of interest: precasters, design compressive strength range, and age of concrete. The model for three-factor factorial design with interactions is:

$$Y_{ijkl} = \mu_{ijk} + \varepsilon_{ijkl} \tag{4.8}$$

where Y_{ijkl} is the lth observation from group $A_iB_jC_k$, μ_{ijk} is the average response Y for group $A_iB_jC_k$, and ε_{ijkl} is the random difference between the observation Y_{ijkl} and the mean of the group $A_iB_jC_k$. The model can be also expressed as an "effects" model as:

$$Y_{ijkl} = \mu... + \alpha_i + \beta_j + \gamma_k + (\alpha\beta)_{ij} + (\alpha\gamma)_{ik} + (\beta\gamma)_{jk} + (\alpha\beta\gamma)_{ijk} + \varepsilon_{ijkl} \tag{4.9}$$

where $\mu...$ is the overall average, α_i is the effect of A irrespective of B and C; β_j is the effect of B irrespective of A and C; γ_k is the effect of C irrespective of A and B; $(\alpha\beta)_{ij}$, $(\alpha\gamma)_{ik}$, and $(\beta\gamma)_{jk}$ are the effects of interaction between two factors; and $(\alpha\beta\gamma)_{ijk}$ is the three-way interaction term. Parameters α_i, β_j, and γ_k measure the main effect of factor A, B, and C, respectively. The two-way interaction effects indicate the non-additivity of the combined effect (i.e., the change in slope of the response with respect to one factor when the other factor changes value). The three-way interaction effect indicates the effect of one factor to the non-additivity of the interaction of the other two factors.

To determine whether the effects are significant on the mean value of the variable, hypothesis tests are performed. The hypotheses include null hypothesis (H_0), which is the model to be tested; and the alternative hypothesis (H_1), which will be accepted if H_0 is rejected. The first hypothesis to be tested is the null hypothesis of the three-way interaction term:

H_0: $(\alpha\beta\gamma)_{ijk} = 0$ for all i, j, k

H_1: some $(\alpha\beta\gamma)_{ijk} \neq 0$

Then, the following are tested:

H_0: $(\alpha\beta)_{ij} = 0$ for all i, j

H_1: some $(\alpha\beta)_{ij} \neq 0$

H_0: $(\alpha\gamma)_{ik} = 0$ for all i, k

H_1: some $(\alpha\gamma)_{ik} \neq 0$

H_0: $(\beta\gamma)_{jk} = 0$ for all j, k

H_1: some $(\beta\gamma)_{jk} \neq 0$

If no interaction is present, the main effect will then be tested, as follows:

H_0: $\alpha_i = 0$ for all i

H_1: some $\alpha_i \neq 0$

H_0: $\beta_j = 0$ for all j

H_1: some $\beta_j \neq 0$

H_0: $\gamma_k = 0$ for all k

H_1: some $\gamma_k \neq 0$

The appropriate test statistic is:

$$F_{Effect} = \frac{MS_{Effect}}{MS_{Error}} \qquad (4.10)$$

where F_{Effect} is the test statistic, MS_{Effect} is the mean square of the effect (main effects or interactions), and MS_{Error} is the mean square of errors.

When the null hypothesis H_0 is true, this F_{Effect} ratio has an F distribution with the degree of freedom of the effect and error. A large value of F_{Effect} indicates that the influence of the effect (expressed as MS_{Effect}) is large relative to the variation of the sample (expressed as MS_{Error}); in other words, the effect is too large to occur by chance and will result in the rejection of H_0. The criterion that is used to judge the significance is the p-value, which is defined as the probability of having equal or greater evidence in favor of H_1 than the current sample. The p-value is the area on the right of F_{Effect} in Figure 4.1. A small p-value indicates that the effect is significant. In this project, a p-value less than 0.05 is considered significant.
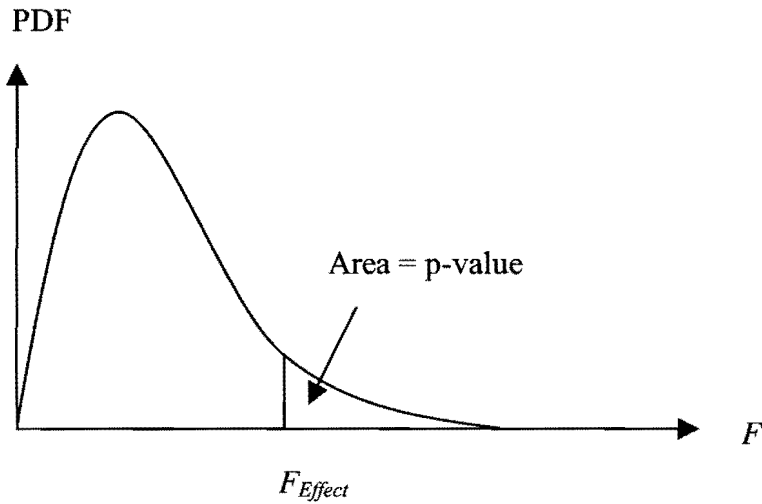
Figure 4.1. F-Probability Density Function.

The result of the analysis is usually summarized in a table format called an analysis of variance (ANOVA) table. For this project, the analysis of variance was performed using SAS statistical analysis software (SAS Institute Inc. 1999). A typical ANOVA table generated by the software is shown in Table 4.1.

Table 4.1. Example of an ANOVA Table.

(1) Dependent Variable: CVBatch						
(2)	Source	DF	Sum of Squares	Mean Square	F Value	Pr > F
(3)	Model	26	0.07376835	0.00283724	1.11	0.3481
(4)	Error	81	0.20657570	0.00255032		
(5)	Corrected Total	107	0.28034405			
(6)		R-Square	Coeff Var	Root MSE	CVBatch Mean	
(7)		0.263135	59.04048	0.050501	0.085536	
(8)	Source	DF	Type I SS	Mean Square	F Value	Pr > F
(9)	Precaster	2	0.02989685	0.01494843	5.86	0.0042
(10)	Age	2	0.00419556	0.00209778	0.82	0.4429
(11)	Precaster*Age	4	0.01344105	0.00336026	1.32	0.2705
(12)	Class	2	0.00705763	0.00352882	1.38	0.2565
(13)	Precaster*Class	4	0.00062223	0.00015556	0.06	0.9930
(14)	Age*Class	4	0.00883789	0.00220947	0.87	0.4879
(15)	Precaster*Age*Class	8	0.00971713	0.00121464	0.48	0.8696

106

The first line of the table indicates the name of the variable being tested. The next part (lines 2 to 5) is called a utility F-test. This part is the test to determine whether there is any difference among the means of various groups (for this case, 3^3 combinations of three compressive strength groups, three precasters, and three ages). The F statistic and its corresponding p-value (denoted as "Pr>F") is given in the last two columns. The R-Square value given in line 7 indicates the proportion of the total variability in the data that is explained by the linear model containing 3^3 variables (group means). Root MSE value is the square root of the mean square of error given in line 4. Coefficient of variation is the ratio of the Root MSE to the variable mean. This coefficient of variation is not meaningful for the analysis and should be neglected. Lines 8 to 15 are hypothesis tests of the group means for each design strength group, age, precaster, and interactions of these variables. The DF column is the degree of freedom. It is equal to (n_i -1), (n_i-1)(n_j-1), and (n_i-1)(n_j-1)(n_k-1) for main effect, two-way interaction, and three-way interaction, respectively; where n_i, n_k, and n_k are the number of groups for the variable i, j, and k, respectively. The F statistics and the corresponding p-values are given in the last two columns. The test in this part is more informative than the utility F-test as it indicates which group has different means.

4.1.6   Evaluation of Goodness of Fit

In this analysis, the goodness of fit of the prediction formulas is evaluated. Evaluations are made when the formulas are calculated using both the actual compressive strength from tests and specified compressive strength. Batch averages are used in the calculation.

The evaluations are made visually by plotting the test data with the predicted values and analytically by using an appropriate criterion. There are several ways to evaluate the goodness of fit analytically. For this project, the goodness of fit is evaluated using a relative prediction error as:

$$RPE = \frac{1}{n}\sum_{i=1}^{n}\left(\frac{f'}{f}-1\right)^2 \qquad (4.11)$$

where f is the value of material property (tensile strength, modulus of elasticity, etc.) from the test and f' is the predicted value from the corresponding compressive strengths. A large value of the relative prediction error indicates that the error in the prediction is large. Therefore, the best prediction formula is the one that yields the smallest relative prediction error. The coefficient of determination (R^2) is not appropriate for this analysis because the equations are not linear.

The goodness of fit of a prediction formula can vary for different ages of testing because many formulas were developed using test data only at the age of 28 days. Therefore, calculation of the relative prediction errors and plots of relationships are made separately for each age.

Relationships of mechanical properties with compressive strength at early ages are important for the design of prestressed concrete members. For example, the modulus of elasticity of concrete at transfer is used to calculate the prestress loss due to elastic shortening, and the modulus of rupture at transfer is used to determine whether the concrete will crack in tension.

In addition, the effect of precaster is investigated because the relationships between material properties and compressive strengths of concrete from different precasters may vary because of the differences in materials and mixture proportions.

4.2   ANALYSIS RESULTS

In this section, the analyses for the mean, coefficient of variation, and bias factor of the compressive strength, modulus of elasticity, splitting tensile strength, and modulus of rupture are presented. In addition, the creep and shrinkage measurements are documented. For all properties, except the compressive strength, comparisons are made to existing prediction relationships. The SAS source code used for the statistical analysis is provided in Appendix E.

108

4.2.1 Compressive Strength

Table 4.2 provides a summary of samples included in the analysis for compressive strength. Results from 325 specimens were included in this analysis.

Table 4.2. Summary of Data Used in the Analysis for Compressive Strength.

Precaster	Design f'_c Classification* (psi)	Batch No.	Test Ages		
			7 Days	28 Days	56 Days
Precaster A	6000	A15-A16	X	X	X
	8000	A5-A6	NI	NI	NI
Set 1		A13-A14	X	X	X
	10000	A17-A18	X	X	X
Precaster A	6000	A7-A8	X	X	X
	8000	A9-A10	X	X	X
Set 2	10000	A11-A12	X	X	X
Precaster B	6000	B3-B4	NI	NI	NI
		B11-B12	X	X	X
Set 1	8000	B15-B16	X	X	X
	10000	B7-B8	X	X	X
Precaster B	6000	B9-B10	X	X	X
	8000	B13-B14	X	X	X
Set 2	10000	B5-B6	X	X	X
Precaster C	6000	C15-C16	X	X	X
	8000	C3-C4	NI	NI	NI
Set 1		C13-C14	X	X	X
	10000	C17-C18	X	X	X
Precaster C	6000	C7-C8	X	X	X
	8000	C11-C12	X	X	X
Set 2	10000	C9-C10	X	X	X

Notes:
* = Nominal range
X = Tested
NI = Not included in this analysis

Specimens were tested using neoprene caps and loaded using a constant stress rate of 35 psi/s (0.24 MPa/s). Due to the release of the energy stored in the neoprene pads, the specimens typically fail into small pieces. The specimens under compression fail in a brittle, explosive manner. Figure 4.2 shows a typical failure of a specimen tested using neoprene pads.

Figure 4.2. Failure of Compressive Strength Specimen.

4.2.1.1 Development of Compressive Strength with Time

Table 4.3 provides a summary of the mean ratio of batch average to the 28-day batch average for each precaster. Individual values for each batch are provided in Appendix B. It can be seen (Table 4.3) that the increases in the compressive strength before 28 days are substantial. The compressive strength at release is approximately 69 percent of the compressive strength at 28 days, and the compressive strength at 7 days is about 88 percent of the compressive strength. On the other hand, the increase in the compressive strength from 28 days to 56 days was found to be relatively small with about a 4 percent increase. In fact, some batches have smaller 56-day compressive strength than the 28-day value, indicating that the increase in the compressive strength between 28 days and 56 days is small and can be overcome by the randomness of the strength among specimens or by variations associated with the test. The ratios of compressive strength at different ages appear to be similar for all precasters.

Comparison of the data with the predicted value from the equation recommended by the ACI Committee 209 (1992) (Section 2.4.4.2) using parameters for moist-cured concrete and portland cement Type III are also provided in Table 4.3. The time of 1 day was used for the

prediction of compressive strength at release. It can be seen that the actual compressive strength at 7 days and at release (expressed as ratios of the 28-day compressive strength) from the tests are higher than the predicted value, especially for the release strength. The possible explanation is that the use of superplasticizer allows the cement particles to be better dispersed, which could result in a faster and more complete hydration. Another possible explanation is that the properties of cement can vary significantly among different suppliers even though they are all the same type. The behavior of the cement used in the mixtures of concrete in this project may not be predicted well by this model.

Table 4.3. Ratio of Batch Average to 28-Day Batch Average for Compressive Strength.

Precaster	Ratio to 28-Day Average			
	Release	7 Days	28 Days	56 Days
Precaster A	0.64	0.87	1.00	1.05
Precaster B	0.68	0.87	1.00	1.05
Precaster C	0.75	0.90	1.00	1.03
Overall	0.69	0.88	1.00	1.04
ACI Committee 209 (1992)	0.31	0.80	1.00	1.04

4.2.1.2 Probability Distribution

Quantile plots for the compressive strength data are shown in Figure 4.3. It can be seen that the quantile plots based on the assumption of normal and lognormal distribution of compressive strength appear to be reasonably linear. Therefore, it is appropriate to analyze the data based on the assumption of either a normal or lognormal distribution of the compressive strength. A constant CV is a characteristic of lognormally distributed data, whereas normally distributed data has a constant standard deviation or variance. The use of CV in the analysis based on the assumption of a lognormal distribution is convenient because it provides more information about the relative variation of the data than the use of standard deviation or variance. Therefore, a lognormal distribution was assumed in this project.
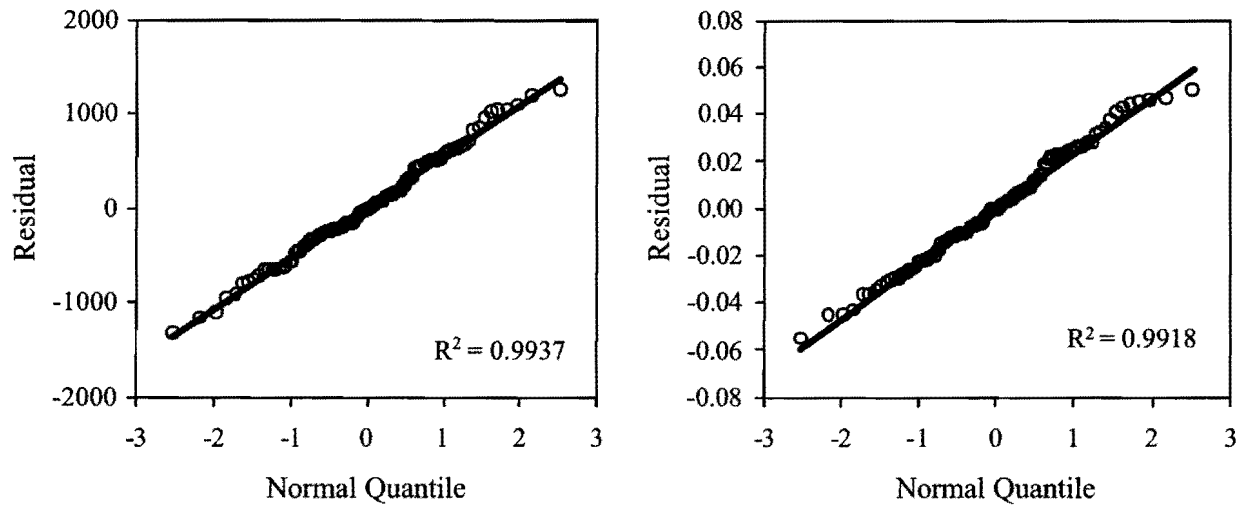
(a) Normal Distribution   (b) Lognormal Distribution

Figure 4.3. Quantile Plots for Compressive Strength.

4.2.1.3 Mean and Coefficient of Variation

The CV_{Batch} and batch average values are plotted with the design strengths, ages, and precasters in Figure 4.4. The results from the ANOVA of the CV_{Batch} are summarized in Table 4.4. It can be seen from Figure 4.4 that the CV_{Batch} appears to have a constant mean for all ranges of design strength, ages, and precasters. The analysis of variance also shows large p-values (denoted in Table 4.4 as "Pr > F") for precaster, age, strength classification, and interaction of these factors, which confirm the observation that the CV_{Batch} is not dependent on a group. Therefore, it can be concluded that the CV_{Batch} has the same mean for all groups. The mean value of the CV_{Batch} can be determined by averaging all the CV_{Batch} values and was found to be 2.4 percent.
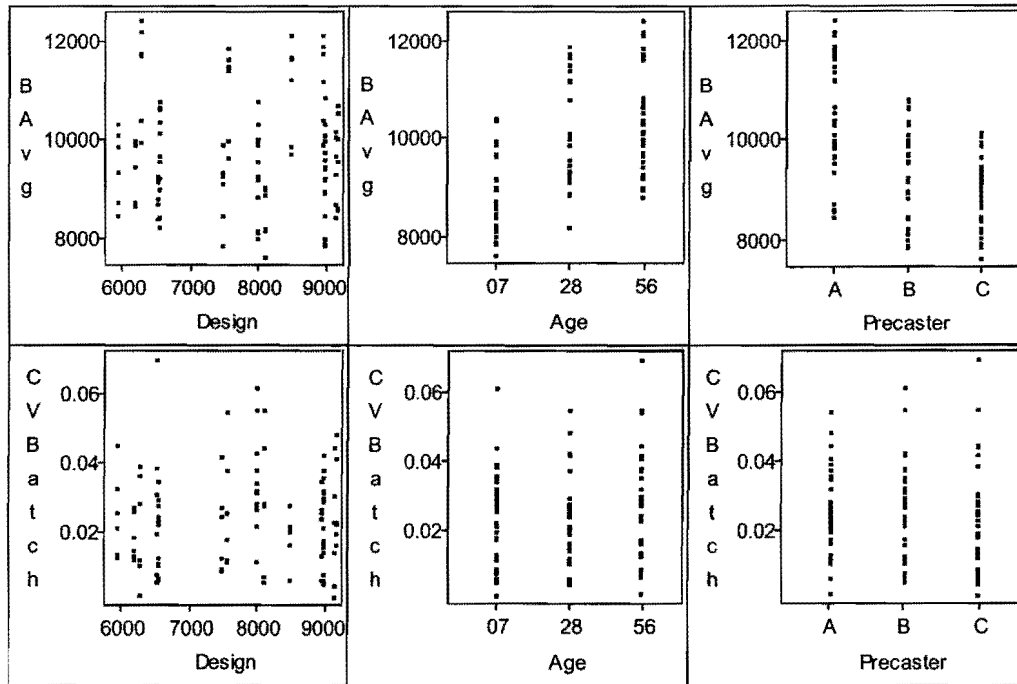
Figure 4.4. Scatter Plots of Batch Average and Coefficient of Variation within a Batch for Compressive Strength.

Table 4.4. ANOVA Table of Coefficient of Variation within a Batch for Compressive Strength.

```
Dependent Variable: CVBatch

                                 Sum of
Source                  DF       Squares     Mean Square   F Value   Pr > F

Model                   26    0.00537080     0.00020657      1.06    0.4077

Error                   81    0.01580585     0.00019513

Corrected Total        107    0.02117665


           R-Square    Coeff Var    Root MSE    CVBatch Mean

           0.253619    57.69156     0.013969       0.024213


Source                  DF    Type I SS     Mean Square   F Value   Pr > F

Precaster               2    0.00050695     0.00025348      1.30    0.2784
Age                     2    0.00077098     0.00038549      1.98    0.1453
Precaster*Age           4    0.00021095     0.00005274      0.27    0.8963
Class                   2    0.00068454     0.00034227      1.75    0.1796
Precaster*Class         4    0.00143565     0.00035891      1.84    0.1293
Age*Class               4    0.00044051     0.00011013      0.56    0.6892
Precaster*Age*Class     8    0.00132121     0.00016515      0.85    0.5650
```

113

Next, the CV_{Mix} is investigated. The scatter plots of the CV_{Mix} are provided in Figure 4.5, and its ANOVA is summarized in Table 4.5. From Figure 4.5, the CV_{Mix} appears to have a constant mean across all design strengths (both actual design strengths and design strength classifications), ages, and precasters. Table 4.5 also shows large p-values for all of the groups, which confirm the observation of Figure 4.5. Therefore, the CV_{Mix} can be assumed to be constant. A constant CV is the assumption for the lognormal distribution of data (batch average). Therefore, the assumption of the lognormal distribution appears to be valid. The mean of the CV_{Mix} is determined by averaging all the CV_{Mix} values. It was determined to be 2.4 percent.

If the batch average follows a normal distribution, the mean of the batch averages (mixture average) will be of interest. However, because the batch average is found to follow a lognormal distribution, the mean value of the log of the batch average is of interest instead. Scatter plots of mixture average values for different categories are shown in Figure 4.5. The ANOVA table of the log of batch average values is shown in Table 4.6.
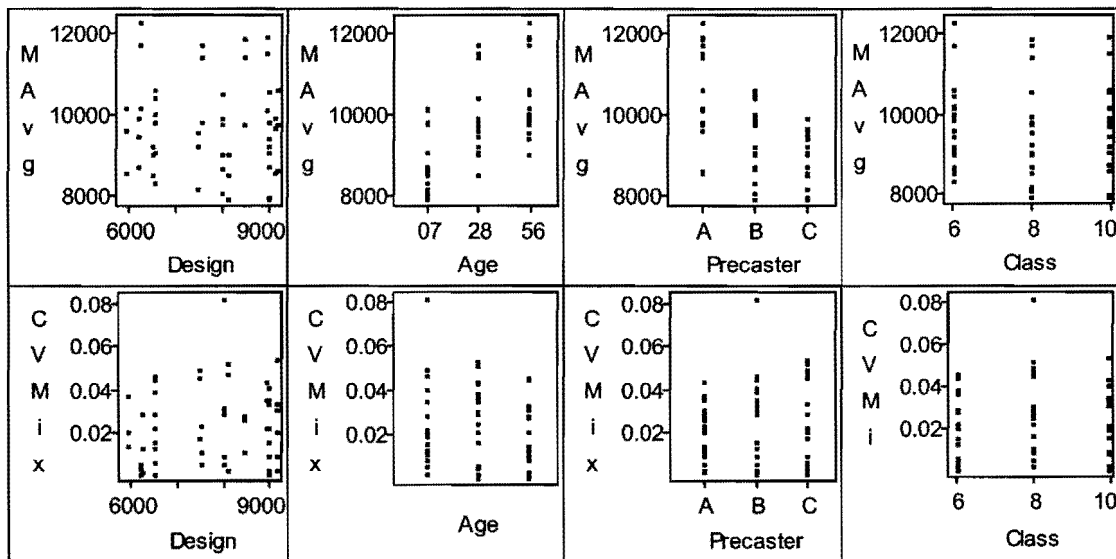
Figure 4.5. Scatter Plots of Mixture Average and Coefficient of Variation within a Mixture for Compressive Strength.

114

Table 4.5. ANOVA Table of Coefficient of Variation within a Mixture for Compressive Strength.

```
Dependent Variable: CVMix

                                  Sum of
         Source            DF     Squares      Mean Square    F Value    Pr > F

         Model             26   0.00649338     0.00024975       0.63     0.8766

         Error             27   0.01065819     0.00039475

         Corrected Total   53   0.01715158


                R-Square      Coeff Var      Root MSE      CVMix Mean

                0.378588      81.95266       0.019868       0.024244


         Source              DF     Type I SS     Mean Square    F Value    Pr > F

         Precaster            2   0.00038031     0.00019016       0.48     0.6229
         Age                  2   0.00025647     0.00012823       0.32     0.7254
         Precaster*Age        4   0.00014772     0.00003693       0.09     0.9837
         Class                2   0.00077649     0.00038824       0.98     0.3870
         Precaster*Class      4   0.00149978     0.00037495       0.95     0.4507
         Age*Class            4   0.00123905     0.00030976       0.78     0.5451
         Precaster*Age*Class  8   0.00219356     0.00027419       0.69     0.6930
```

Table 4.6. ANOVA Table of the Mean of the Logarithm of Batch Average Values for Compressive Strength.

```
Dependent Variable: MLogBAvg

                                  Sum of
         Source            DF     Squares      Mean Square    F Value    Pr > F

         Model             17   0.10395570     0.00611504       7.66     <.0001

         Error             36   0.02874689     0.00079852

         Corrected Total   53   0.13270259


                R-Square      Coeff Var      Root MSE      MLogBAvg Mean

                0.783374      0.708938       0.028258         3.985987


         Source                 DF     Type III SS    Mean Square    F Value    Pr > F

         Design                  1   0.00045607     0.00045607       0.57     0.4547
         Precaster               2   0.00069043     0.00034522       0.43     0.6523
         Age                     2   0.00037159     0.00018579       0.23     0.7936
         Precaster*Age           4   0.00040482     0.00010120       0.13     0.9718
         Design*Precaster        2   0.00116712     0.00058356       0.73     0.4885
         Design*Age              2   0.00036699     0.00018350       0.23     0.7959
         Design*Precaster*Age    4   0.00029322     0.00007330       0.09     0.9844
```

115

It can be seen from Table 4.6 that the means of the log of batch average are not significantly different among design strength categories, precasters, ages, and interaction of these groups. Although the hypothesis test shows that the mean of the log of the batch average is not significantly different among concrete ages, it contradicts the fact that concrete typically gains strength with time. Therefore, it will be assumed that the mean is different among ages, and analyses will be performed separately for each age. The possible explanation of the insignificant difference among ages is that all of the samples are made with Type III portland cement. The majority of the long-term strength of concrete made with Type III portland cement occurs within a few days after casting. As a result, the strength differences between 7 and 56 days are not substantial and can be overcome in the statistical analysis by the variations in the mixture proportions and testing variables.

The reason for the constant mean of the log of batch average across all the design strength ranges is because two of the three precasters do not design specific mixture proportions for different design strength requirements, but simply use only one mixture proportion for all of the required design strengths, as long as the required strength does not exceed the actual strength of the mixture proportion. As a result, the same mixture proportion may be used, for example, from the required strength of 6000 psi (41.4 MPa) to 10000 psi (68.9 MPa). For that reason, it can be expected that all the concrete samples collected from these precasters will yield very close compressive strengths. The differences in the compressive strengths at different strength requirements of concrete from these precasters can only be attributed to variations in proportioning, mixing, curing conditions, and testing.

Although one of the precasters uses different mixture proportions for different strength requirements, several other factors, such as time of casting, temperature, and required release strength appear to be as least as important in the selection of the mixture proportion as the design compressive strength. In fact, the mixture proportion is selected so that the prestressing strands can be released as soon as possible on the next day. The longer the girder has to sit on the casting bed, the lower the productivity and, hence, less profits. Therefore, the same mixture

proportion could have been used for either a higher release strength girder cast in the morning or a lower release strength beam cast in the afternoon. As a result, the increase in the actual compressive strength with the required compressive strength becomes unclear.

Because the design compressive strength does not appear to significantly affect the average compressive strength (in terms of the batch average and the mean of the log of the batch average), this effect will not be considered in the following analysis. Although the precasters do not appear to have a significant effect on the mean of the log of batch average, the analyses will be carried out separately for each precaster because the precasters were not randomly selected. Conservative statistical parameters among the precasters will be used.

The mean of mix averages (denoted as "Mean") and CV_{MixAvg} (denoted as "Coeff of Variation") are summarized in Table 4.7. The lowest mean of the 28-day mixture average is 9240 psi (63.7 MPa) for Precaster C. The largest coefficient of variation is 8.8 percent for Precaster A. Note that the CV_{MixAvg} is smaller for Precasters B and C than for Precaster A because Precasters B and C typically use only one mixture proportion per precaster for this strength range, whereas several mixture proportions are used by Precaster A. As a result, the variation of the compressive strengths for samples collected from Precasters B and C can be expected to be small. Using Equation 4.5, the $CV_{BatchAvg}$ is estimated to be 9.1 percent.

If the mean values for the CV_{MixAvg} and the mixture averages of all precasters are considered instead of the more conservative values provided above, the mean mixture average at 28 days is determined by averaging the mean of the three precasters and is found to be 10000 psi (68.9 MPa). The mean CV_{MixAvg} ($CV_{MixAvg,Mean}$) for 28-day compressive strengths is determined by the following equation:

$$CV_{MixAvg,Mean} = \sqrt{\frac{CV_{MixAvg,A}^2 + CV_{MixAvg,B}^2 + CV_{MixAvg,C}^2}{3}} \tag{4.12}$$

where $CV_{MixAvg,A}$, $CV_{MixAvg,B}$, and $CV_{MixAvg,C}$ are the values of CV_{MixAvg} for Precasters A, B, and C, respectively. The $CV_{MixAvg,Mean}$ is found to be 6.4 percent. Using Equation 4.5, the $CV_{BatchAvg}$ is estimated to be 6.9 percent.

Table 4.7. Summary of the Mean and Coefficient of Variation of Mixture Averages for Compressive Strength.

Precaster	Age	N Obs	N	Mean	Coeff of Variation
A	07	7	6	9563.43	7.6979418
	28	7	6	10983.58	8.7951669
	56	7	6	11513.02	7.3388738
B	07	7	6	8503.69	5.2754406
	28	7	6	9772.89	5.2916986
	56	7	6	10286.17	3.8755338
C	07	7	6	8348.67	4.0998105
	28	7	6	9242.12	4.2312474
	56	7	6	9523.30	4.3900905

The comparisons of the coefficients of variation for compressive strength are provided in Table 4.8. The coefficient of variation developed from this project is smaller than those reported by Ellingwood et al. (1980), which were used in the development of the AASHTO LRFD Specifications (2000). The reason is probably because the data from Ellingwood et al. (1980) were not specifically developed for precast bridge girders. Larger variations can be expected for cast-in-place concrete, especially when the concrete is mixed at the construction site. In addition, improvements in manufacturing of materials and quality control of productions in recent years can contribute to lower variations for the concrete in this project. Note that the non-in-situ value for the Ellingwood et al. (1980) data were calculated using the equation proposed by Mirza et al. (1979), which Ellingwood et al. used to relate the coefficient of variation of the test to the in-situ coefficient of variation. The result from this research appears to lie between the maximum and minimum values reported by Tabsh and Aswad (1997), which are based on data obtained from precasters in Pennsylvania. However, the study from Tabsh and Aswad (1997) did not include the variation of the concrete between batches in the study. Therefore, the

coefficients of variation from their analyses would be larger had the batch variation been accounted for.

Table 4.8. Comparison of Coefficients of Variation of Compressive Strength.

Source	Specified Compressive Strength Level	Coefficient of Variation (%)
This Study	5900 - 9200 psi (40.7 - 63.4 MPa)	9.1 (6.9[+])
Ellingwood et al. (1980)	3000 psi (20.7 MPa)	15.5 (18*)
	4000 psi (27.6 MPa)	15.5 (18*)
	5000 psi (34.5 MPa)	11.9 (15*)
Tabsh and Aswad (1997)	< 6000 psi (41.4 MPa)	12.5
	6000 - 7000 psi (41.4 - 48.3 MPa)	7.6
	> 7000 psi (48.3 MPa)	6.5

Notes:
[+] = Value based on the mean values of all precasters
* = Values for in-situ condition (originally reported), calculated using Equation 2.46

4.2.1.4 Bias Factors

Bias factor is defined as the ratio of the mean value to the nominal value (see Section 4.1.2). The analysis of the mixture averages in Section 4.2.1.1 indicates that all the concrete samples appear to have a constant mean regardless of the design compressive strength due to the fact that precasters do not use the design compressive strength as a main selection criterion in choosing a mixture proportion, but rather the release strength. The resulting bias factors were calculated for the purpose of comparison with bias factors from previously reported data.

The bias factors are plotted with the compressive strengths in Figure 4.6. It can be seen from the Figure 4.6 (a) that the 28-day bias factor (ratio of the batch average of the 28-day compressive strength to the specified design strength) decreases with an increase in the specified design strength. On the other hand, from Figure 4.6 (c), the 1-day bias factors are close to 1.0 above the release strength of 6000 psi (41.4 MPa). The mean of the 1-day bias factor appears to be constant regardless of the specified compressive strength or the bias factor at 28 days as shown in Figure 4.6 (b) and (d). It must be noted that the 1-day compressive strengths obtained

from precasters are not necessarily at 24 hours, nor do they reflect the same curing time. Precasters usually conduct compressive strength testing to verify the release strength early in the morning. If the release strength is not achieved, then additional tests are conducted later in the day until the strength is met. At that point, the prestressing strands are released, and the prestress force is transferred to the girder. Therefore, a bias factor close to 1.0 is expected for 1-day data.

(a) 28-Day Bias Factor vs. Specified f_c

(b) 1-Day Bias Factor vs. Specified f_c

(c) 1-Day Bias Factor vs. Specified f_{ci}

(d) 28-Day Bias Factor vs. 1-Day Bias Factor
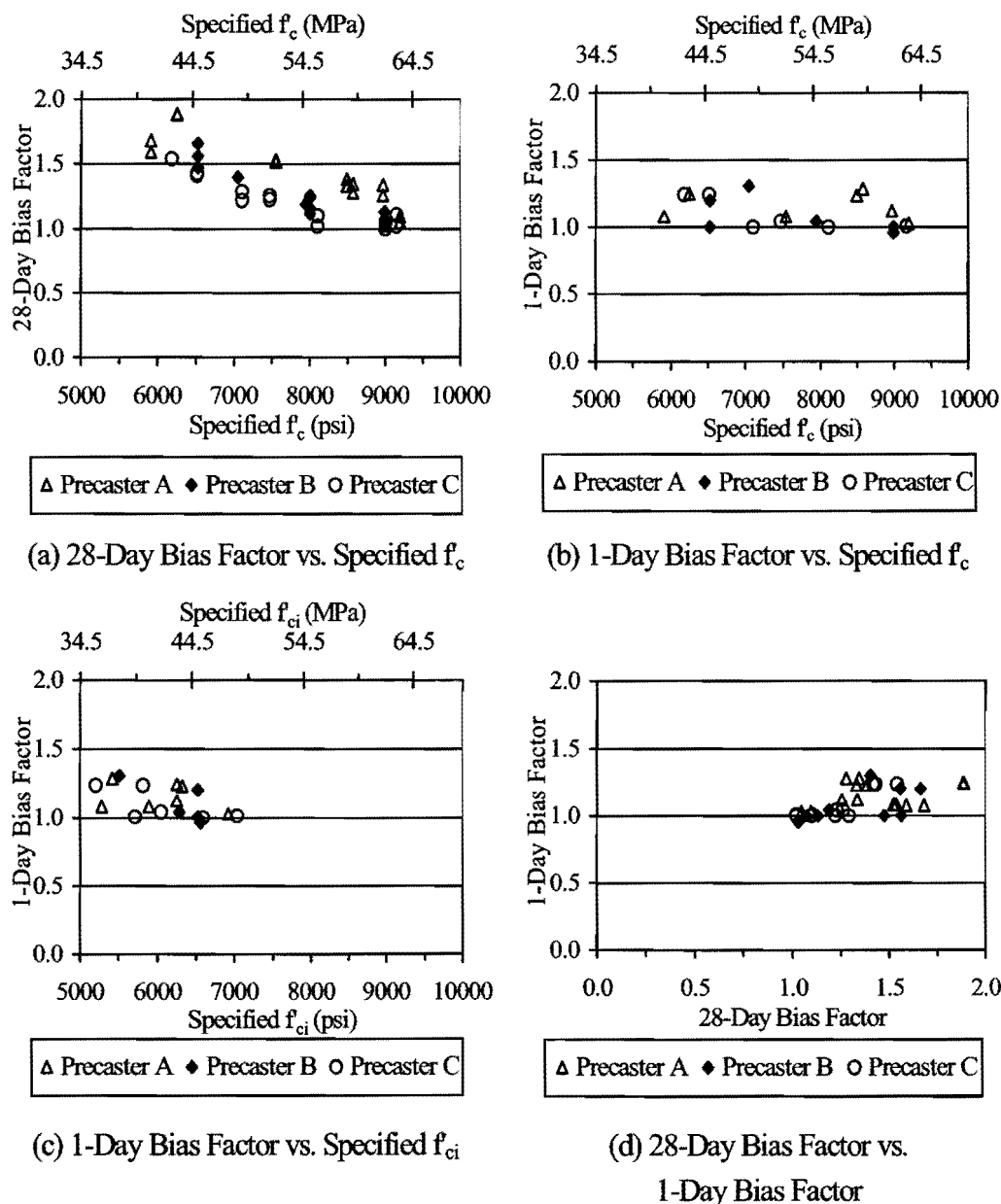
Figure 4.6. Bias Factors for Compressive Strength.

120

The decrease of the 28-day bias factor with the increase in the specified compressive strength of the samples from Precasters B and C is clearly because one mixture proportion was used by these two precasters for all the strength requirements sampled in this project (although Precaster B did change the coarse aggregate type during the project). The 28-day bias factors for the samples from Precaster A also decrease with the increase in the specified compressive strength despite the fact that several different mixture proportions were used by this precaster. This is because the increase in the 28-day compressive strength did not match the corresponding increase in the specified compressive strength, or because other factors also considered in the selection of the mixture proportion masked the effect of the design compressive strength.

Although the extrapolation of the data in the Figure 4.6 (a) and (b) suggests that the bias factor may be less than 1.0 for the compressive strength values greater than 10000 psi, this is not realistic. Precasters must verify that the 28-day compressive strength is achieved before a girder can be put into service. If the 28-day compressive strength is less than the required strength, then the girder must be replaced or retrofitted. Therefore, it is not possible to have a bias factor less than 1.0 for a prestressed concrete application as long as these requirements are met.

The bias factors for the 28-day compressive strength data within a batch (without any adjustments) range from 0.99 to 1.89. When the compressive strength within a mixture is considered, the 28-day bias factors range from 1.01 to 1.89. A summary of bias factors for each batch is provided in Appendix B.

Mirza et al. (1979) suggested a reduction in the compressive strength due to the effect of loading in the actual structure being at a much slower rate than the standard rate of loading used in compression tests of cylindrical specimens. Ellingwood et al. (1980) utilized this relationship in developing statistical data for normal strength concrete, assuming a load rate of one hour to reach the specified compressive strength in a structure. The use of this relationship does not seem appropriate for prestressed bridge structures because the load that would cause failure in a bridge is dynamic and closer to an impact load than a static load.

Limited data are available for the difference between the compressive strength of concrete in a structure (in-situ strength) and the compressive strength of the companion test specimens for HSC. For NSC, Mirza et al. (1979) suggested that the compressive strength of concrete in a structure could be taken as 90 percent of the compressive strength from the test cylinders. Assuming that this is applicable to HSC, the modified bias factor will range between 0.91 and 1.70. Even when adjusted for the concrete in a structure, the bias factor for HSC is still greater than those for NSC reported by Ellingwood et al. (1980) and used for the calibration of the AASHTO LRFD Specifications (Nowak 1999).

Table 4.9 provides comparisons of the bias factors reported by other researchers and from this project. All of the data show that the bias factor decreases with an increase in the compressive strength regardless of the design strength considered.

Table 4.9. Bias Factor for Compressive Strength.

Source	Specified Compressive Strength Level	Bias Factor
This Study	5900 - 9200 psi (40.7 - 63.4 MPa)	1.01-1.89**
	6000 ± 1000 psi (41.4 ± 6.9 MPa)	1.59
	8000 ± 1000 psi (55.2 ± 6.9 MPa)	1.24
	10000 ± 1000 psi (68.9 ± 6.9 MPa)	1.10
Ellingwood et al. (1980)	3000 psi (20.7 MPa)	0.92*
	4000 psi (27.6 MPa)	0.85*
	5000 psi (34.5 MPa)	0.81*
Tabsh and Aswad (1997)	< 6000 psi (41.4 MPa)	1.4
	6000 - 7000 psi (41.4 - 48.3 MPa)	1.2
	> 7000 psi (48.3 MPa)	1.1

Notes: * Values for in-situ condition
** Bias factor decreases with an increase in compressive strength

4.2.1.5 Discussion of Implications for Design Provisions

Compressive strength is used in the design of prestressed concrete members in the calculation of moment resistance and in estimations of other material properties for the calculation of shear resistance and prestress losses. In addition, compressive strength is used as a criterion in specifying concrete for construction. Therefore, the bias and variation in the compressive strength can affect various aspects of prestressed concrete members. A smaller coefficient of variation of the compressive strength could lead to a smaller coefficient of variation of the moment resistance, resulting in a greater reliability index for a member in flexure. A larger bias factor of the compressive strength could also result in a greater reliability index for a member in flexure. However, a bias factor considerably larger or smaller than 1.0, indicating that the design compressive strength is substantially different from the actual compressive strength, could influence the accuracy in the prediction of material properties because the prediction formulas are often developed based on actual compressive strength, not the design compressive strength.

The compressive strength data in this project have a smaller coefficient of variation and larger bias factor than those used in the determination of the resistance parameters for the calibration of the AASHTO LRFD Specifications. The difference will be even larger if the effect of size of the test specimen on the coefficient of variation is considered. The coefficient of variation of compressive strength tested using a 4×8 inch (100×200 mm) specimen, which is used in this project, has been reported to be larger than that tested using a standard 6×12 (150×300 mm) specimen, which was used in the past. The coefficient of variation in this study can be taken as a conservative estimation of the coefficient of variation tested using 6×12 (150×300 mm). Therefore, there is a potential that the design provisions in the AASHTO LRFD Specifications related to the compressive strength can be modified for HSC. However, it should be noted that the bias factor and coefficient of variation for the compressive strength in this project are applicable only to the portion of resistance provided by the precast girder section.

Where the deck provides a portion of the resistance, such as in positive bending, the bias factor (or mean) and coefficient of variation of the deck concrete should also be considered.

4.2.2 Modulus of Elasticity

In this section, the experimental data and analyses for modulus of elasticity are presented. The summary of samples included in the analysis is provided in Table 4.10. For each test age, two 4×8 inch (100×200 mm) cylindrical specimens per batch were used to determine the modulus of elasticity. Results from 216 specimens are included in this analysis.

Table 4.10. Summary of Data Used in the Analysis for Modulus of Elasticity.

Precaster	Design f'_c Classification* (psi)	Batch No.	Test Ages		
			7 Days	28 Days	56 Days
Precaster A Set 1	6000	A15-A16	X	X	X
	8000	A5-A6	NR	NR	NR
		A13-A14	X	X	X
	10000	A17-A18	X	X	X
Precaster A Set 2	6000	A7-A8	X	X	X
	8000	A9-A10	X	X	X
	10000	A11-A12	X	X	X
Precaster B Set 1	6000	B3-B4	NR	NR	NR
		B11-B12	X	X	X
	8000	B15-B16	X	X	X
	10000	B7-B8	X	X	X
Precaster B Set 2	6000	B9-B10	X	X	X
	8000	B13-B14	X	X	X
	10000	B5-B6	X	X	X
Precaster C Set 1	6000	C15-C16	X	X	X
	8000	C3-C4	NR	NR	NR
		C13-C14	X	X	X
	10000	C17-C18	X	X	X
Precaster C Set 2	6000	C7-C8	X	X	X
	8000	C11-C12	X	X	X
	10000	C9-C10	X	X	X

Notes:
*   = Nominal range
X   = Tested
NR = Not reported (insufficient data)

124

A typical stress-strain plot for the determination of the modulus of elasticity is shown in Figure 4.7. This plot is obtained by averaging strains measured by two LVDTs mounted 180 degrees apart on a compressometer (Section 3.2.3). Figure 4.7 shows that the relationship between the stress and strain is linear. According to ASTM C 469 (1994b), modulus of elasticity is defined as a secant modulus between a strain of 50 $\mu\varepsilon$ and a stress of 40 percent of the compressive strength at the same age (determined from the compression test of the specimens within the same batch). Modulus of elasticity values for each specimen and stress-strain plots are provided in Appendix B.
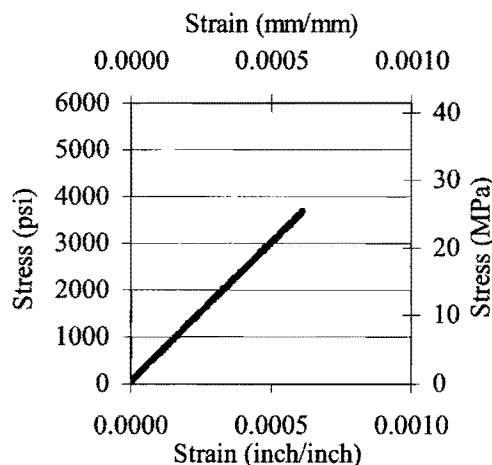
Figure 4.7. Typical Stress-Strain Plot for Determination of Modulus of Elasticity.

4.2.2.1   Development of Modulus of Elasticity with Time

The ratio of batch average to the 28-day batch average is provided in Table 4.11. Individual values for each batch are provided in Appendix B. Comparing the values in Table 4.11 with those in Table 4.3, it can be seen that the modulus of elasticity does not change much with age compared with the compressive strength. An increase of 4 percent is found between 7 and 28 days. Only about a 2 percent increase is found between 28 and 56 days. Because the increase of the modulus of elasticity with time is small, it can be overcome by the effect of

variations in the modulus of elasticity due to random sampling of the test specimens and various testing variables. This helps explain why some batches have larger 7-day average modulus of elasticity or smaller 56-day average modulus of elasticity than the average at 28 days (see Appendix B).

Table 4.11. Ratio of Batch Average to 28-Day Batch Average for Modulus of Elasticity.

Precaster	Ratio to 28-Day Average		
	7 Days	28 Days	56 Days
Precaster A	0.97	1.00	1.03
Precaster B	0.95	1.00	1.02
Precaster C	0.95	1.00	1.02
Overall	0.96	1.00	1.02

4.2.2.2   Probability Distribution

Quantile plots for modulus of elasticity are shown in Figure 4.8. Figure 4.8 shows that either normal or lognormal distribution can be reasonably assumed. A lognormal distribution was assumed in the statistical analyses of modulus of elasticity, because of the convenience of using the CV in the analysis.

126
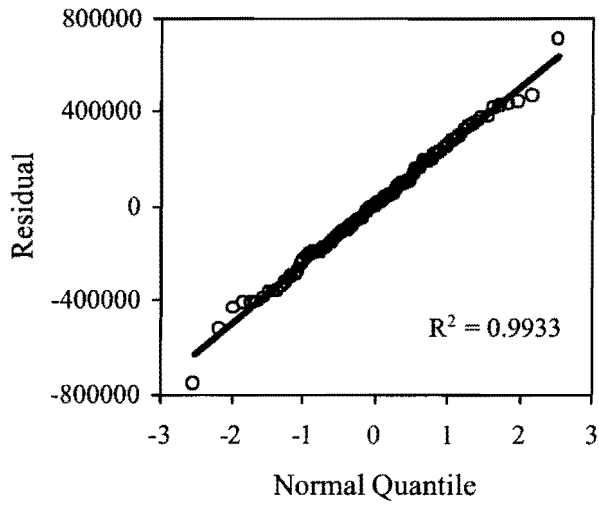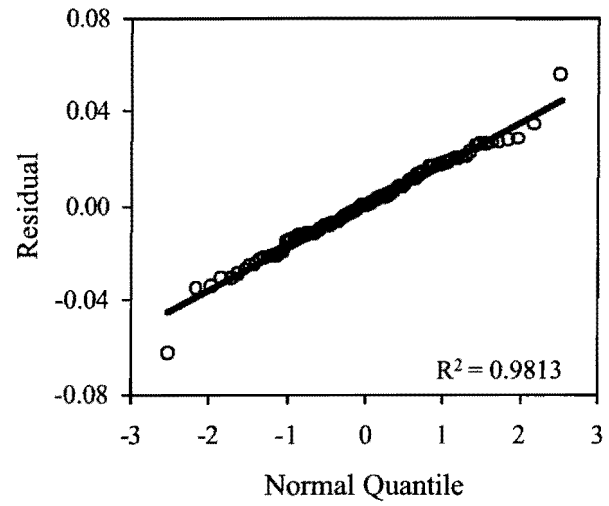
(a) Normal Distribution   (b) Lognormal Distribution

Figure 4.8. Quantile Plot for Modulus of Elasticity.

4.2.2.3 Mean and Coefficient of Variation

Scatter plots of the batch average and CV_{Batch} for the modulus of elasticity versus specified design strength, age, and precaster are shown in Figure 4.9. ANOVA of CV_{Batch} for the modulus of elasticity is provided in Table 4.12. From Figure 4.9, the batch average does not seem to increase with the design strength and only increases slightly with age. However, the batch average appears to be different among precasters with a higher value for Precaster A than for Precasters B and C. The CV_{Batch} seems to have a constant mean for all design strengths but seems to be different among ages and precasters. The hypothesis tests of the mean of the CV_{Batch} in Table 4.12 show that the mean of the CV_{Batch} is significantly different at a 0.05 level among ages.
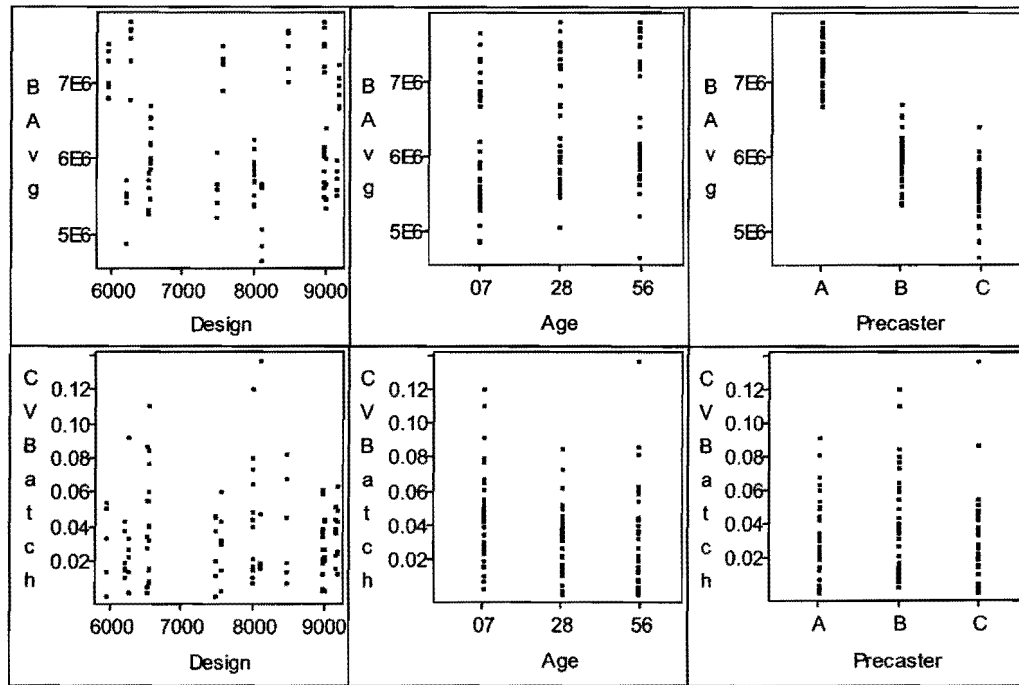
Figure 4.9. Scatter Plots of Batch Average and Coefficient of Variation within a Batch for Modulus of Elasticity.

Table 4.12. ANOVA Table of Coefficient of Variation within a Batch for Modulus of Elasticity.

```
Dependent Variable: CVBatch

                                     Sum of
Source                    DF         Squares      Mean Square    F Value    Pr > F

Model                     26       0.02424574      0.00093253      1.44     0.1083

Error                     81       0.05230716      0.00064577

Corrected Total          107       0.07655290


              R-Square      Coeff Var      Root MSE      CVBatch Mean

              0.316719      70.08276       0.025412         0.036260


Source                    DF       Type I SS      Mean Square    F Value    Pr > F

Precaster                  2       0.00284687      0.00142343      2.20     0.1169
Age                        2       0.00404304      0.00202152      3.13     0.0490
Precaster*Age              4       0.00430476      0.00107619      1.67     0.1658
Class                      2       0.00088612      0.00044306      0.69     0.5064
Precaster*Class            4       0.00061493      0.00015373      0.24     0.9161
Age*Class                  4       0.00436897      0.00109224      1.69     0.1600
Precaster*Age*Class        8       0.00718106      0.00089763      1.39     0.2134
```

128

The mixture average and CV_{Mix} for the modulus of elasticity are plotted in Figure 4.10. Table 4.13 provides ANOVA of the CV_{Mix}. According to Table 4.13, the mean of the CV_{Mix} is significantly different at 0.05 level among precaster-age interaction, strength classification, precaster-strength classification, and age-strength classification interaction groups. This appears to be due to high CV_{Mix} values from two sample sets for Precaster C at 8000 psi (55.2 MPa) strength category and tested at 56 days. However, these two outliers appear to be only a coincidence because the mixture proportions are all the same for Precaster C regardless of the design strength. Therefore, it is not expected that the mixture at 8000 psi (55.2 MPa) will exhibit different properties from the others. In addition, other material properties from these two sets at the same age and the modulus of elasticity from these two sets at early ages do not have high CV_{Mix} values. When these two sets of samples were excluded in the analysis, it was found that the CV_{Mix} was not significantly different among any groups. As a result, the modulus of elasticity will be analyzed as if the CV_{Mix} is not different among groups. The mean of the CV_{Mix} calculated by averaging all the CV_{Mix} values can be taken as 3.3 percent.
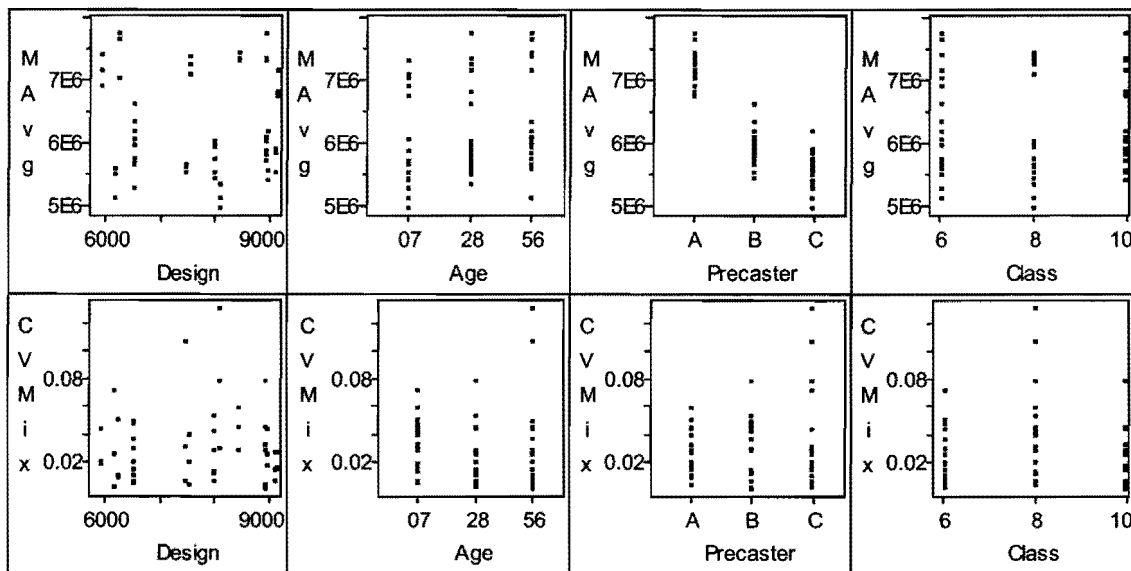
Figure 4.10. Scatter Plots of Mixture Average and Coefficient of Variation within a Mixture for Modulus of Elasticity.

Table 4.13. ANOVA Table of Coefficient of Variation within a Mixture for Modulus of Elasticity.

```
Dependent Variable: CVMix
```

Source	DF	Sum of Squares	Mean Square	F Value	Pr > F
Model	26	0.02676111	0.00102927	2.67	0.0069
Error	27	0.01042755	0.00038621		
Corrected Total	53	0.03718866			

R-Square	Coeff Var	Root MSE	CVMix Mean
0.719604	60.18189	0.019652	0.032655

Source	DF	Type I SS	Mean Square	F Value	Pr > F
Precaster	2	0.00096672	0.00048336	1.25	0.3021
Age	2	0.00025721	0.00012861	0.33	0.7197
Precaster*Age	4	0.00574340	0.00143585	3.72	0.0155
Class	2	0.00285077	0.00142538	3.69	0.0383
Precaster*Class	4	0.00485445	0.00121361	3.14	0.0304
Age*Class	4	0.00479127	0.00119782	3.10	0.0319
Precaster*Age*Class	8	0.00729729	0.00091216	2.36	0.0453

Because the data (batch averages) follow the lognormal distribution, the mean of the logarithm of the batch average should be used in hypothesis tests instead of the mixture average. Table 4.14 shows that the mean of the logarithm of the batch average appears to be significantly different among precasters. This is because the moduli of elasticity of samples from Precaster A are higher than those from Precasters B and C. A possible reason is the different type of coarse aggregate used by Precaster A, as compared to Precaster C and most Precaster B samples. This topic will be discussed in the following section.

Table 4.15 provides the summary of the mean and the CV_{MixAvg} for the modulus of elasticity by precaster and age. Because precasters were not selected in a completely random manner, the CV_{MixAvg} can be conservatively taken as the highest of these values, which is 5.2 percent. The corresponding $CV_{BatchAvg}$ is calculated according to Equation 4.5 and was found to be 6.1 percent. If the mean value CV_{MixAvg} and the mean mixture average are considered, the mean mixture average of the modulus of elasticity at 28 days was determined to be 6,360,000 psi (43.9 GPa), and the CV_{MixAvg} was 4.3 percent. Using Equation 4.5, the $CV_{BatchAvg}$ can be estimated as 5.4 percent.

130

Table 4.14. ANOVA Table of the Mean of the Logarithm of Batch Averages for Modulus of Elasticity.

Dependent Variable: MLogBAvg

Source	DF	Sum of Squares	Mean Square	F Value	Pr > F
Model	17	0.14505732	0.00853278	25.33	<.0001
Error	36	0.01212921	0.00033692		
Corrected Total	53	0.15718654			

R-Square	Coeff Var	Root MSE	MLogBAvg Mean
0.922836	0.270075	0.018355	6.796429

Source	DF	Type III SS	Mean Square	F Value	Pr > F
Design	1	0.00013094	0.00013094	0.39	0.5369
Precaster	2	0.00648750	0.00324375	9.63	0.0004
Age	2	0.00105984	0.00052992	1.57	0.2214
Precaster*Age	4	0.00009398	0.00002349	0.07	0.9907
Design*Precaster	2	0.00169009	0.00084504	2.51	0.0956
Design*Age	2	0.00063528	0.00031764	0.94	0.3990
Design*Precaster*Age	4	0.00011638	0.00002909	0.09	0.9861

Table 4.15. Summary of the Mean and Coefficient of Variation of Mixture Averages for Modulus of Elasticity.

Precaster	Age	N Obs	N	Mean	Coeff of Variation
A	07	7	6	7128755.29	3.2122695
	28	7	6	7348146.42	4.1076421
	56	7	6	7527249.06	2.9308168
B	07	7	6	5773167.83	4.0336634
	28	7	6	6069332.19	5.2092584
	56	7	6	6157808.07	2.5011094
C	07	7	6	5363982.61	4.3626726
	28	7	6	5663300.40	3.2690910
	56	7	6	5754257.97	6.2074934

4.2.2.4   Bias Factors

The bias factors for the modulus of elasticity are shown in Figure 4.11. The plot is based on the nominal value calculated by AASHTO LRFD Specifications (2000) using the specified compressive strength for design.
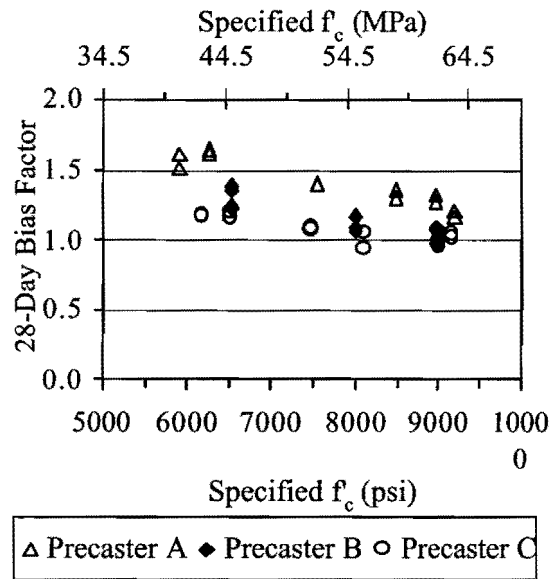
Figure 4.11. Bias Factor for Modulus of Elasticity (Using AASHTO Equation).

It can be seen from Figure 4.11 that the bias factor decreases slightly with the increase in the specified compressive strength. This is because the actual modulus of elasticity does not increase with the specified compressive strength, while the predicted value increases with the specified compressive strength. As a result, the bias decreases with an increase in the specified compressive strength. When the AASHTO LRFD Specifications (2000) equation is used, the bias factors range from 0.94 to 1.64 for modulus of elasticity within a batch. For modulus of elasticity within a mixture, the bias factors range from 0.98 to 1.63. Table 4.16 provides a summary of the bias factors for modulus of elasticity calculated using AASHTO LRFD Specifications (2000) equation.

Table 4.16. Bias Factors for Modulus of Elasticity (Using AASHTO Equation).

Specified Compressive Strength Level	Bias Factor
6000 ± 1000 psi (41.4 ± 6.9 MPa)	1.31
8000 ± 1000 psi (55.2 ± 6.9 MPa)	1.13
10000 ± 1000 psi (68.9 ± 6.9 MPa)	1.09

4.2.2.5 Prediction Formulas

In this section, prediction formulas that relate the modulus of elasticity to the compressive strength are investigated to determine the goodness of fit for the experimental data collected in this project. The equations are summarized in Table 4.17. A description of terms for these equations is provided in Section 2.4.4.

Table 4.17. Equations for Determining the Modulus of Elasticity (MOE) from the Compressive Strength of Concrete.

Author(s)	Equation	Units of MOE
ACI Committee 318 (1999) AASHTO LRFD Specifications (2000)	$33(w_c)^{1.5}\sqrt{f_c'}$	psi
Carrasquillo et al. (1981) Canadian Code (CSA 1994) ACI Committee 363 (1997)	$\left(40{,}000\cdot\left(\sqrt{f_c'}\right)+10^6\right)\left(\dfrac{w_c}{145}\right)^{1.5}$	psi
CEB-FIP Model Code 1990 (CEB 1993)	$21.5\cdot\left(\dfrac{f_c'}{10}\right)^{\frac{1}{3}}$	GPa
Gardner and Zao (1991)	$9\cdot(f_c')^{\frac{1}{3}}$ for $f_c' > 27$ MPa	GPa
Norwegian Code (1992)	$9.5\cdot(f_c')^{0.3}\left(\dfrac{\rho}{2400}\right)^{1.5}$	GPa
Baalbaki (1997)	$K_o + 0.2\cdot f_c'$	GPa

Note:
w_c is the unit weight of the concrete (lb/ft^3)
ρ is the unit weight of concrete (kg/m^3)
K_o is a factor dependent on aggregate type

The modulus of elasticity values are plotted with corresponding compressive strength values in Figure 4.12. Each data point is obtained from the average of the modulus of elasticity values determined for two specimens and the average of the compressive strengths determined for three specimens, all within the same batch and at the same test age. Overall, it can be seen that all of the prediction formulas presented here underestimate the modulus of elasticity of the sampled HSC. From observations, the AASHTO LRFD Specifications (2000) equation and the CEB-FIP Model Code 1990 (CEB 1993) equation appear to be the best prediction formulas mainly because they give relatively higher prediction values than the rest of the formulas.
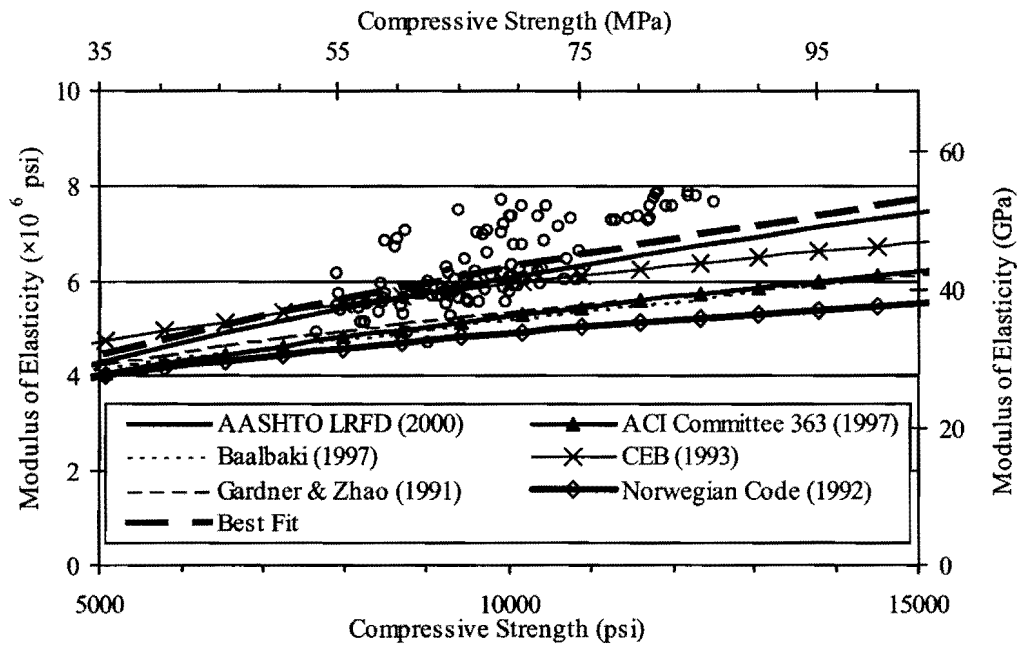
Figure 4.12. Modulus of Elasticity versus Compressive Strength.

Table 4.18 summarizes the relative prediction errors (see Section 4.1.6 for determination of relative prediction error) for each formula and for each test age. A small value of the relative prediction error indicates that the error in the prediction is small and, therefore, the equation fits the data well. From this table, the equation from AASHTO LRFD Specifications (2000) is the

134

best prediction formula presented here. The equation recommended by the ACI Committee 363 (1997) for HSC does not give a good prediction for the data in this project as it underestimates the modulus of elasticity. From Table 4.18, the age of testing does not seem to have an effect on the relative goodness of fit of the prediction formulas because the ranks of the formulas are the same for each age and for the overall data (all ages). However, for each formula, the relative prediction error tends to be smaller at 28 days than at 7 or 56 days. This may be because these prediction formulas were developed for 28-day data.

Table 4.18. Relative Prediction Errors of Prediction Formulas for Modulus of Elasticity When Using Compressive Strength Values from Tests.

Equation	Age of Concrete			
	7 Days	28 Days	56 Days	Overall
AASHTO LFRD Specifications (2000)	0.0072	0.0048	0.0061	0.0088
ACI Committee 363 (1997)	0.0242	0.0229	0.0249	0.0358
Baalbaki (1997)	0.0249	0.0239	0.0261	0.0373
CEB-FIP Model Code 1990 (CEB 1993)	0.0087	0.0073	0.0091	0.0124
Gardner and Zhao (1991)	0.0192	0.0189	0.0214	0.0298
Norwegian Code (1992)	0.0357	0.0372	0.0405	0.0565
Best Fit	0.0068	0.0048	0.0062	0.0084

The best fit curve shown in Figure 4.12 is determined using the following equation:

$$E_c = 63,000\sqrt{f'_c}$$

(4.13)

where E_c is the modulus of elasticity in psi and f'_c is the compressive strength in psi. This equation was determined by finding a coefficient to be multiplied by the square root of compressive strength such that the relative prediction error values in Table 4.17 are minimized. Because the data in this project cover a relatively small range of compressive strength and there are considerable variations in the data, the square root model used by ACI Committee 318 (1999) and AASHTO LRFD Specifications (2000) was chosen for consistency with current accepted

135

relationships. In addition, no substantial improvement in the prediction error would be achieved with a more complex equation.

It can be seen from Figure 4.12 that the best fit equation gives slightly higher predicted values than the AASHTO LRFD Specifications (2000) equation and has lower relative prediction error values in Table 4.18. Nevertheless, considering the variation in the data, the AASHTO LRFD Specifications (2000) may be acceptable for the prediction of modulus of elasticity.

The above comparisons use the actual compressive strength data. In the design process, however, it is the design compressive strength that is used for estimation of other material properties. Therefore, it is useful to evaluate how well the prediction formulas estimate the modulus of elasticity when the design strength is used. Figure 4.13 shows the plot of the modulus of elasticity and the design compressive strength. Only the batch averages at 28 days are plotted. It can be seen that all the prediction formulas underestimate the modulus of elasticity values from the tests even more than when the actual compressive strengths were used. This is expected because the actual compressive strengths from the tests are greater than the specified compressive strength (at 28 days) for all the batches in this project. Table 4.19 is the summary of the relative prediction values when the design compressive strength is used. In this case, the CEB-FIP Model Code 1990 equation (CEB 1993) gives the closest predictions overall, followed by the AASHTO LRFD Specifications (2000) equation.

The effect of age of testing and the effect of precasters were further investigated. Figure 4.14 shows plots of modulus of elasticity and compressive strength (both actual and design) at different test ages and with different symbols for each precaster. Note that the specified compressive strengths used in the plots shown in Figure 4.14 (b), (d), and (f) are the same at all ages because the compressive strength is specified for 28 days only. The actual compressive strength values (Figure 4.14 [a], [c], and [e]) are the average measured values for each age tested. From Figure 4.14 (b), (d), and (f); it can be seen that the modulus of elasticity from each precaster does not appear to increase with the specified design compressive strength. For

136

Precasters B and C, the reason is that only one mixture proportion was used in the proportioning of the concrete used for all the samples in this project even though the design compressive strength varied.
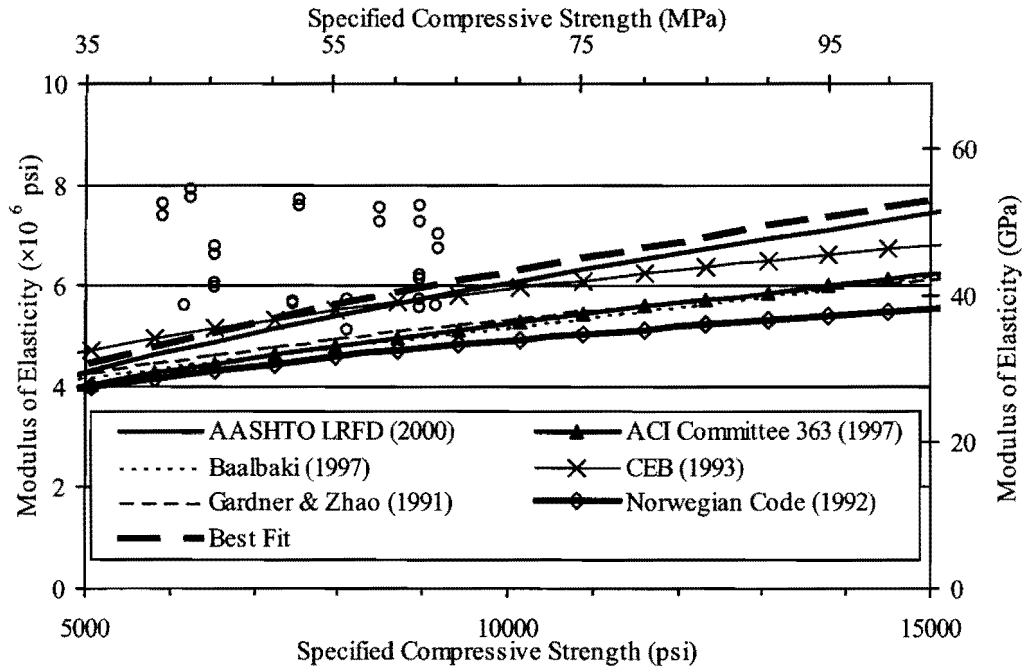
Figure 4.13. Modulus of Elasticity versus Specified Compressive Strength.

Table 4.19. Relative Prediction Errors of Prediction Formulas for Modulus of Elasticity When Using Specified Compressive Strength.

Equation	28 Days
AASHTO LFRD Specifications (2000)	0.0385
ACI Committee 363 (1997)	0.0717
Baalbaki (1997)	0.0688
CEB-FIP Model Code 1990 (CEB 1993)	0.0218
Gardner and Zhao (1991)	0.0576
Norwegian Code (1992)	0.0875
Best Fit	0.0299
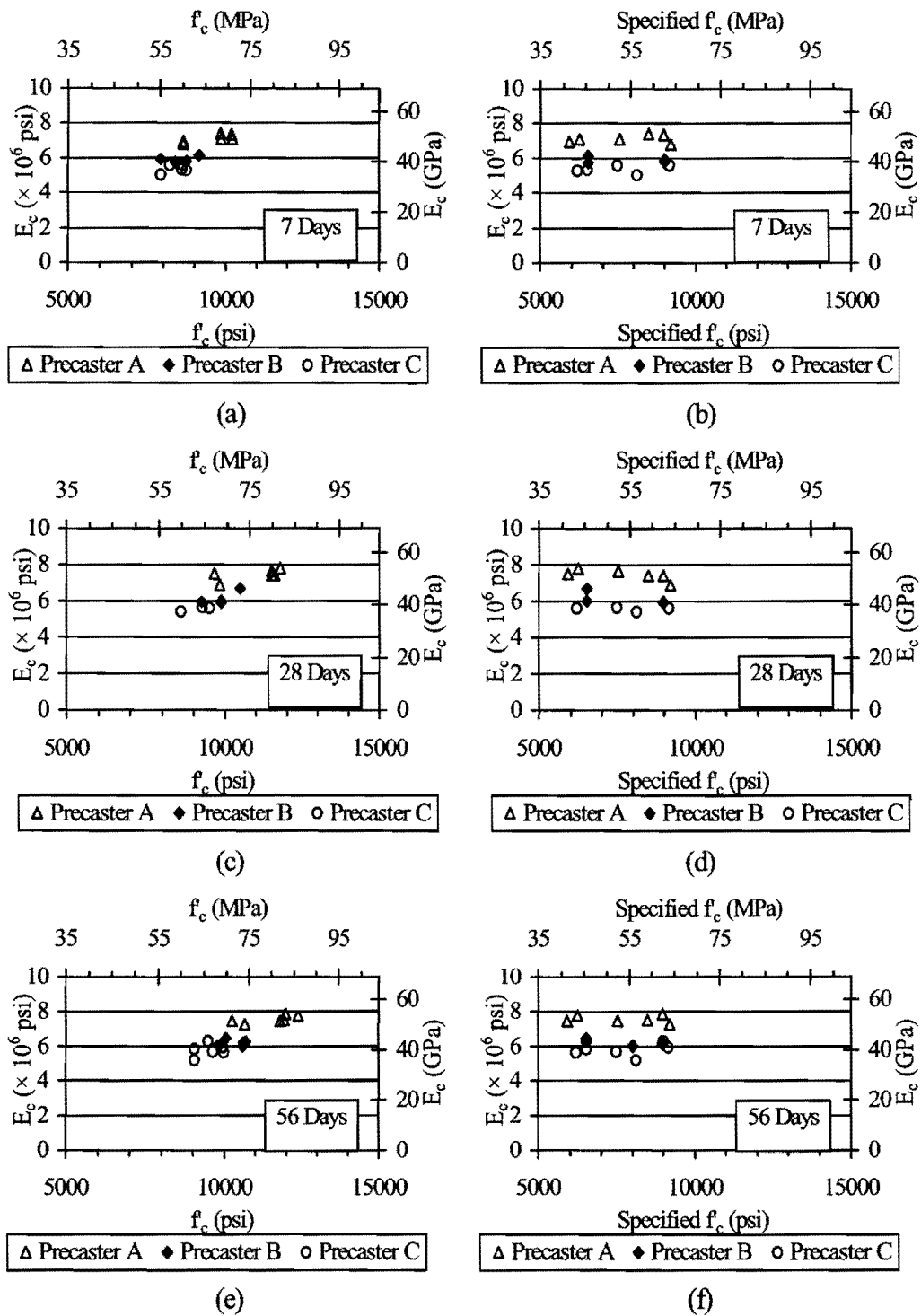
Figure 4.14. Modulus of Elasticity versus Compressive Strengths by Age.

From Figure 4.14 (a), (c), and (e), the age does not seem to have a substantial effect on the relationship between the modulus of elasticity and the compressive strength since the relationships appear to be similar for all ages at each precaster. On the other hand, the precaster that the samples were collected from appears to have a more significant effect on the modulus of elasticity. The moduli of elasticity of the samples from Precaster A are substantially higher than those from Precasters B and C, whereas the moduli of elasticity of the samples from Precasters B and C are similar to each other. This can be clearly seen in Figure 4.15.
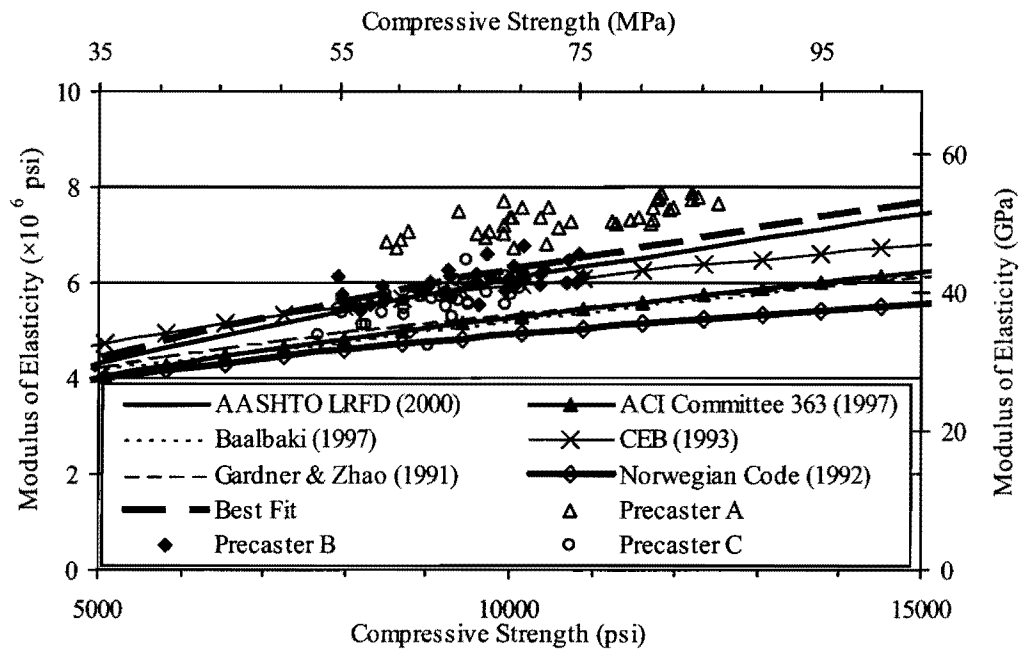
Figure 4.15. Differences in Modulus of Elasticity among Precasters.

The most likely explanation of the difference is the influence of the coarse aggregate. Precaster A used river gravels for making concrete, while Precasters B and C used crushed limestone aggregate. It has been reported that the properties of coarse aggregate, especially its modulus of elasticity, have an influence on the modulus of elasticity of the concrete (Zia et al. 1991, Cetin and Carrasquillo 1998). In addition, the effect of aggregate is more significant in

HSC than in NSC because the stronger transition zone allows transfer of stress from cement paste to the coarse aggregate more effectively.

It can be seen in Figure 4.15 that the relationship between the modulus of elasticity and compressive strength for Precaster A appears to be different from that for Precasters B and C. The accuracy of the prediction can be improved if an aggregate property such as the modulus of elasticity is incorporated in the prediction. Unit weight is often used in the prediction of modulus of elasticity because it gives an indication of the porosity and stiffness of the aggregate and is easier to determine than the modulus of elasticity of aggregate. ACI Committee 318 (1999), ACI Committee 363 (1997), and the Norwegian Code (1992) use a 1.5 power of the unit weight of concrete as a modification factor. Average unit weights of concrete samples from this study are provided in Table 4.20. Also in Table 4.20 are the 1.5 power of the ratio of the unit weight to the unit weight of Precaster A (taken as the baseline), the best fit equation for each precaster, and the ratio of the best fit equation to the best fit equation of Precaster A.

Table 4.20. Effect of Unit Weight on Modulus of Elasticity.

Precaster	Average Unit Weight (w_c)	$\left(\dfrac{w_c}{w_{c,a}}\right)^{1.5}$	Best Fit Equation	Ratio to Best Fit Equation of Precaster A
Precaster A	150.6 pcf (2413 kg/m^3)	1.00	$71000\sqrt{f'_c}$ psi	1.00
Precaster B	149.1 pcf (2388 kg/m^3)	0.99	$62000\sqrt{f'_c}$ psi	0.87
Precaster C	147.2 pcf (2358 kg/m^3)	0.97	$58000\sqrt{f'_c}$ psi	0.82

It can be seen from observing the unit weights and the best fit equations that the modulus of elasticity tends to be higher with higher unit weight concrete. However, by comparing the ratios of the 1.5 power of the unit weights and the ratios of the prediction equations, it can be seen that the difference in the modulus of elasticity is substantially greater than that predicted by

using 1.5 power of the unit weight. It is possible that other properties of aggregate not reflected by the unit weight can also influence the modulus of elasticity of concrete. These properties include size, shape, and surface texture of coarse aggregate.

Figure 4.16 shows the bias factor plot using the best fit equation to determine the nominal value from the specified design compressive strength. This plot is very similar to Figure 4.11 because the best fit equation and AASHTO LRFD Specifications (2000) equation yield similar predicted values. Again, it can be seen that the bias factor tends to be greater than 1.0. This is considered conservative for long-term conditions. Table 4.21 provides a summary of the bias factor for modulus of elasticity calculated using the best fit equation.
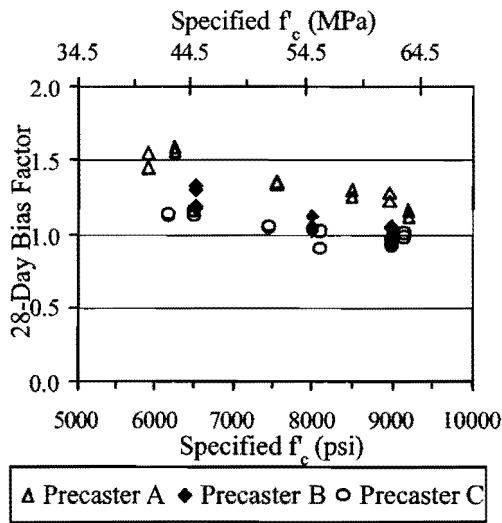
Figure 4.16. Bias Factor for Modulus of Elasticity (Using Best Fit Equation).

Table 4.21. Bias Factor for Modulus of Elasticity (Using Best Fit Equation).

Specified Compressive Strength Level	Bias Factor
6000 ± 1000 psi (41.4 ± 6.9 MPa)	1.26
8000 ± 1000 psi (55.2 ± 6.9 MPa)	1.09
10000 ± 1000 psi (68.9 ± 6.9 MPa)	1.05

141

4.2.2.6 Discussion of Implications for Design Provisions

Modulus of elasticity of concrete is used in the design of prestressed concrete members in the calculation of prestress loss due to elastic shortening and for the calculation of camber and deflections.

Although a new relationship between modulus of elasticity and specified compressive strength could be developed because the modulus of elasticity is considerably underestimated when the design strength is used, it must be realized that the difference between the design and the actual compressive strengths depends on the current practice at a particular time and location. It is possible that the difference can become smaller or larger depending on proportioning, mixing, materials, and/or location. For design purposes, it is often more conservative to evaluate the prediction formula based on the actual compressive strength because the actual compressive strength is always greater than the design compressive strength. This will tend to result in an underestimation of the actual value when the design compressive strength is used. However, underestimation of the modulus of elasticity does not always result in a conservative design. Underestimation of the modulus of elasticity for long-term conditions is conservative because the actual deflection of the member will be less than the predicted value. On the other hand, underestimation of the modulus of elasticity at release will result in a smaller prestress loss than predicted, which can cause excessive stresses and camber immediately after transfer.

To account for the differences between the design and actual compressive strengths, it seems most appropriate to choose a prediction equation that gives the best fit when using the actual compressive strength. When the difference of the design and actual compressive strengths is taken into account, it will result in an underestimation of the modulus of elasticity for long-term conditions, which is conservative. For release of the prestressing strands, the actual compressive strength at release is often close to the specified release strength (the 1-day bias factor for compressive strength is close to 1.0). Therefore, there is only a small effect due to the difference between the specified release strength and the actual release strength. As a result,

using the equation that gives the best estimation based on the actual compressive strength will result in a relatively accurate prediction for the modulus of elasticity at release when the specified release strength is used. It should be noted that the relationship between the modulus of elasticity and compressive strength at 1 day (release) is not determined in this project, but the study of the relationships at the age of 7, 28, and 56 days suggests that the age does not considerably affect the relationship. Therefore, it may be reasonable to assume that this finding is also true at 1 day.

There is no conservative way to overcome the uncertainties in the estimation due to the influence of aggregate. Although incorporation of aggregate properties can substantially improve the prediction, it is not practical to do so because the mixture proportion and type of aggregate are usually not known during the design process. Therefore, the best predicted equation based on several types of aggregate may be used with appropriate reduction factors or resistance factors in the design to account for the variability in the estimation. Nevertheless, if a higher degree of accuracy is necessary, it is recommended that the design should be refined based on an established relationship between the modulus of elasticity and actual compressive strength using the actual mixture proportion and aggregate once the precaster has been selected.

4.2.3 Splitting Tensile Strength

This section presents experimental data and analyses for splitting tensile strength. The samples included in the analysis are summarized in Table 4.22. For each test age, three 4×8 inch (100×200 mm) cylindrical specimens per batch were used to determine the splitting tensile strength. Results from 322 specimens are included in this analysis.

143

Table 4.22. Summary of Data Used in the Analysis for Splitting Tensile Strength.

Precaster	Design f'_c Classification* (psi)	Batch No.	Test Ages		
			7 Days	28 Days	56 Days
Precaster A Set 1	6000	A15-A16	X	X	X
	8000	A5-A6	X	X	X
		A13-A14	NT	NT	NT
	10000	A17-A18	X	X	X
Precaster A Set 2	6000	A7-A8	X	X	X
	8000	A9-A10	X	X	X
	10000	A11-A12	X	X	X
Precaster B Set 1	6000	B3-B4	X	X	X
		B11-B12	NT	NT	NT
	8000	B15-B16	X	X	X
	10000	B7-B8	X	X	X
Precaster B Set 2	6000	B9-B10	X	X	X
	8000	B13-B14	X	X	X
	10000	B5-B6	X	X	X
Precaster C Set 1	6000	C15-C16	X	X	X
	8000	C3-C4	X	X	X
		C13-C14	NT	NT	NT
	10000	C17-C18	X	X	X
Precaster C Set 2	6000	C7-C8	X	X	X
	8000	C11-C12	X	X	X
	10000	C9-C10	X	X	X

Notes:
* = Nominal range
X = Tested
NT = Not tested

The tension failures of the splitting tensile strength specimens were brittle. Each cylinder split at the loading plane into two pieces. The failure surface of concrete made using limestone aggregates was usually flat; the failure plane cut through coarse aggregate particles and hydrated cement paste indicating the paste was stronger than the aggregate. On the other hand, the failure surface of concrete made using river gravel contained both failures through coarse aggregate particles and bond failure at the interface of the cement and coarse aggregate. The failures of both types of concrete under splitting tension are shown in Figure 4.17.
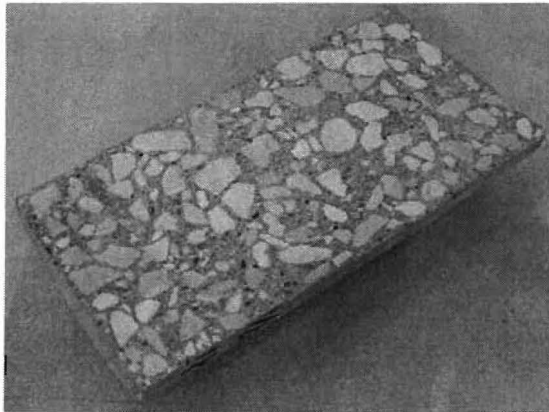
(a) Concrete with Limestone Aggregate   (b) Concrete with River Gravel Aggregate

Figure 4.17. Failure of Splitting Tensile Strength Specimens.

4.2.3.1 Development of Splitting Tensile Strength with Time

Table 4.23 provides a summary of the mean ratio of batch average to the 28-day batch average for each precaster. Individual values for each batch are provided in Appendix B. It can be seen from Table 4.23 that the compressive strength at 7 days was approximately 96 percent of the compressive strength at 28 days for all precasters. The increase in the compressive strength from 28 days to 56 days was found to be small with the overall average increase of 4 percent. The decrease in the 56-day ratio in Precaster B appears to be due to randomness rather than the actual decrease of splitting tensile strength with time because the decreasing trends are neither consistently observed in both batches that were collected at the same time, nor can they be correlated with the decrease in other material properties tested at the same day.

Table 4.23. Ratio of Batch Average to 28-Day Batch Average for Splitting Tensile Strength.

Precaster	Ratio to 28-Day Average		
	7 Days	28 Days	56 Days
Precaster A	0.96	1.00	1.07
Precaster B	0.96	1.00	0.98
Precaster C	0.96	1.00	1.02
Overall	0.96	1.00	1.02

4.2.3.2 Probability Distribution

Quantile plots for splitting tensile strength are shown in Figure 4.18.

(a) Normal Distribution   (b) Lognormal Distribution
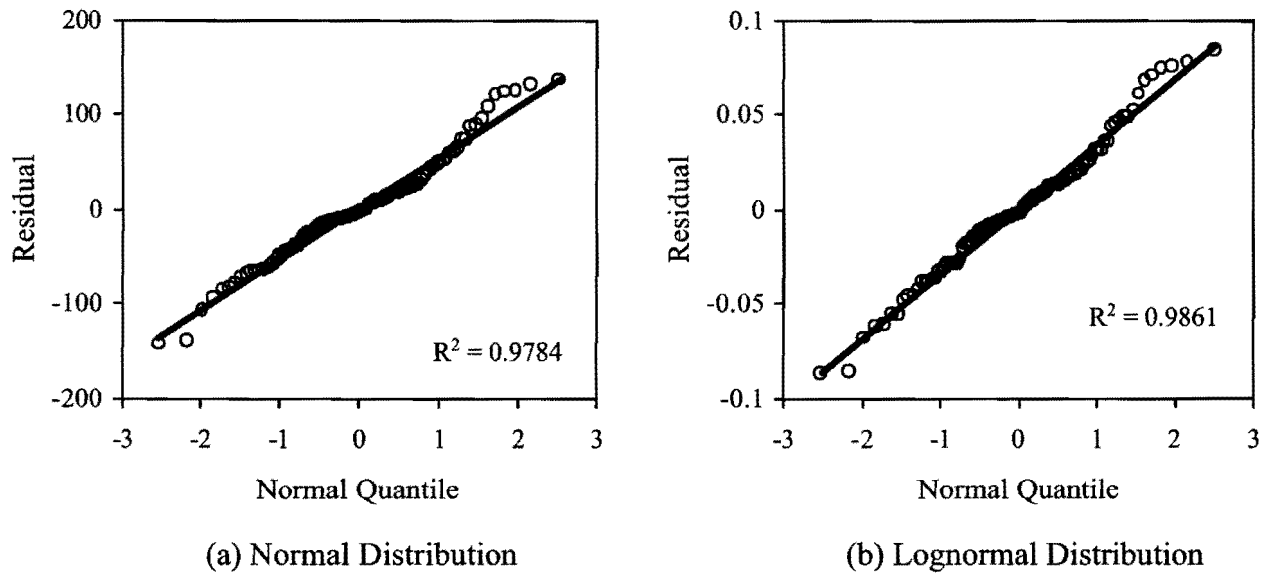
Figure 4.18. Quantile Plots for Splitting Tensile Strength.

Based on observations from Figure 4.18, either normal or lognormal distributions could have been reasonably assumed. The splitting tensile strength is assumed to follow a lognormal distribution because using CV in the analysis, as appropriate for the assumption of lognormal distribution, provides more information about the relative variation of the data.

4.2.3.3 Mean and Coefficient of Variation

Figure 4.19 shows scatter plots of the batch average and CV_{Batch} of the splitting tensile strength. The ANOVA is shown in Table 4.24.
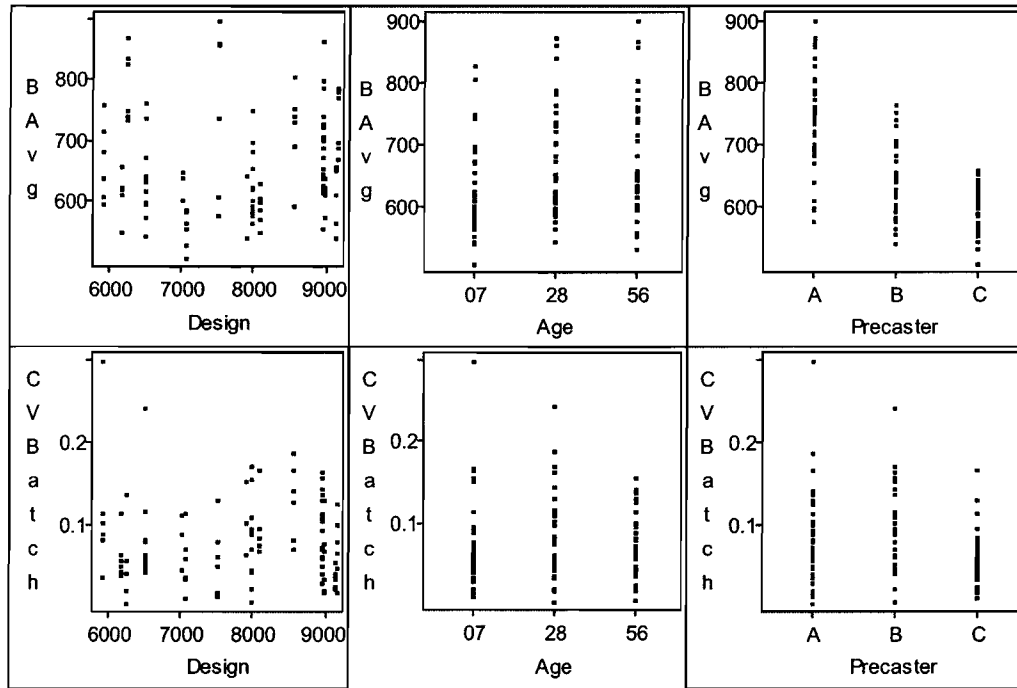
Figure 4.19. Scatter Plots of Batch Average and Coefficient of Variation within a Batch for Splitting Tensile Strength.

Table 4.24. ANOVA Table of Coefficient of Variation within a Batch for Splitting Tensile Strength.

```
Dependent Variable: CVBatch

                                    Sum of
       Source             DF       Squares     Mean Square   F Value   Pr > F

       Model              26     0.07564770    0.00290953      1.18    0.2774

       Error              81     0.19897210    0.00245645

       Corrected Total   107     0.27461980


              R-Square    Coeff Var    Root MSE    CVBatch Mean

              0.275463    59.65250     0.049563      0.083085


       Source             DF      Type I SS    Mean Square   F Value   Pr > F

       Precaster           2     0.02218501    0.01109251      4.52    0.0138
       Age                 2     0.00418249    0.00209125      0.85    0.4306
       Precaster*Age       4     0.01627917    0.00406979      1.66    0.1681
       Class               2     0.00298496    0.00149248      0.61    0.5471
       Precaster*Class     4     0.00372574    0.00093144      0.38    0.8229
       Age*Class           4     0.00826357    0.00206589      0.84    0.5032
       Precaster*Age*Class 8     0.01802675    0.00225334      0.92    0.5067
```

From Figure 4.19, the batch average increases slightly with age but does not appear to increase with the design compressive strength. The batch average of samples from Precaster A tends to be greater than those from Precasters B and C. The concrete from Precaster C tends to have the lowest splitting tensile strength. From Table 4.24, the means of CV_{Batch} are significantly different at the 0.05 level among precasters. The difference is due to the low CV_{Batch} for Precaster C, as can be seen in Figure 4.19. The overall mean of the CV_{Batch} is 8.3 percent.

The mixture average and the CV_{Mix} of the splitting tensile strength are plotted with the design compressive strength, age, precaster, and strength classification in Figure 4.20. The ANOVA of the CV_{Mix} is given in Table 4.25.

148
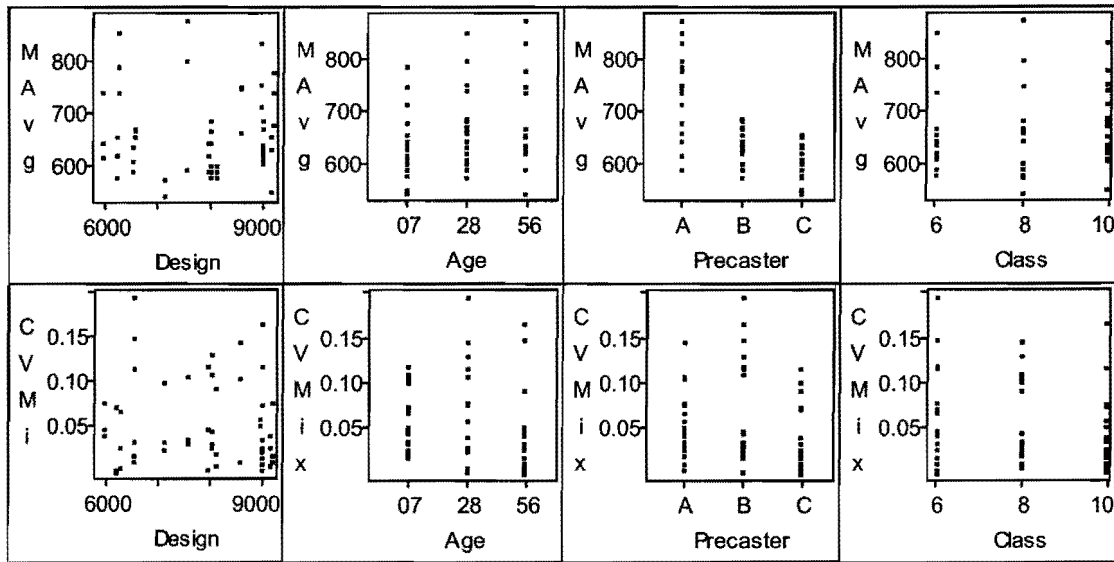
Figure 4.20. Scatter Plots of Mixture Average and Coefficient of Variation within a Mixture for Splitting Tensile Strength.

Table 4.25. ANOVA Table of Coefficient of Variation within a Mixture for Splitting Tensile Strength.

```
Dependent Variable: CVMix

                                   Sum of
Source                 DF         Squares      Mean Square    F Value    Pr > F

Model                  26      0.05052585      0.00194330       0.71     0.8058

Error                  27      0.07375514      0.00273167

Corrected Total        53      0.12428100


            R-Square      Coeff Var      Root MSE      CVMix Mean

            0.406545      92.31077       0.052265      0.056619


Source                 DF      Type I SS     Mean Square    F Value    Pr > F

Precaster               2     0.01207322     0.00603661       2.21     0.1292
Age                     2     0.00588347     0.00294173       1.08     0.3548
Precaster*Age           4     0.00804164     0.00201041       0.74     0.5756
Class                   2     0.00237660     0.00118830       0.44     0.6517
Precaster*Class         4     0.00532987     0.00133247       0.49     0.7446
Age*Class               4     0.00225185     0.00056296       0.21     0.9328
Precaster*Age*Class     8     0.01456921     0.00182115       0.67     0.7158
```

It can be seen from Table 4.25 that the mean of the CV_{Mix} is not significantly different among various groups. Thus, the assumption of lognormal distribution of the splitting tensile

149

strength appears to be valid. The mean value of the CV_{Mix} is determined by averaging all the CV_{Mix} values; it is 5.7 percent.

Because the batch average was assumed to have a lognormal distribution, the mean of the log of the batch average was tested. It was found that the mean of the log of the batch average is also not significantly different among various categories, as can be seen in Table 4.26. Although the analysis shows that the mean of the log of the batch average is not different among ages, separate analyses will be performed for each age because, in fact, the concrete is anticipated to gain strength with time.

Table 4.26. ANOVA Table of the Mean of the Logarithm of Batch Averages for Splitting Tensile Strength.

Dependent Variable: MLogBAvg

Source	DF	Sum of Squares	Mean Square	F Value	Pr > F
Model	17	0.09015627	0.00530331	4.58	<.0001
Error	36	0.04168424	0.00115790		
Corrected Total	53	0.13184052			

R-Square	Coeff Var	Root MSE	MLogBAvg Mean
0.683828	1.206877	0.034028	2.819498

Source	DF	Type III SS	Mean Square	F Value	Pr > F
Design	1	0.00006874	0.00006874	0.06	0.8089
Precaster	2	0.00107100	0.00053550	0.46	0.6334
Age	2	0.00010928	0.00005464	0.05	0.9540
Precaster*Age	4	0.00101201	0.00025300	0.22	0.9264
Design*Precaster	2	0.00033849	0.00016925	0.15	0.8645
Design*Age	2	0.00009780	0.00004890	0.04	0.9587
Design*Precaster*Age	4	0.00120676	0.00030169	0.26	0.9013

The mean and the CV_{MixAvg} for each precaster and each age are summarized in Table 4.27. Because the selection of precasters was not a completely random process, it is more conservative that the estimated mixture average is taken as the lowest value at 28 days of the three precasters and the CV_{MixAvg} is taken as the highest value. The mean mixture average of the splitting tensile

150

strength is 610 psi (4.21 MPa), and the estimated CV_{MixAvg} is 10.8 percent. Using Equation 4.5, the $CV_{BatchAvg}$ of the splitting tensile strength can be estimated to be 12.2 percent.

Table 4.27. Summary of the Mean and Coefficient of Variation of Mixture Averages for Splitting Tensile Strength.

Precaster	Age	N Obs	N	Mean	Coeff of Variation
A	07	7	6	695.8028613	10.9785778
	28	7	6	748.8387878	10.7535843
	56	7	6	792.6471193	7.4155880
B	07	7	6	632.0399166	4.1151552
	28	7	6	661.3268582	6.3167133
	56	7	6	640.7595552	4.6178278
C	07	7	6	583.2723840	4.6172668
	28	7	6	610.3349360	3.4239921
	56	7	6	622.2079565	7.1373289

If the mean values of the CV_{MixAvg} and mixture averages for all precasters are of interest, the mean mixture averages of the splitting tensile strength at 28 days can be determined by averaging all the mixture averages and is found to be 674 psi (4.65 MPa). The mean CV_{MixAvg} for the 28-day compressive strengths is found to be 7.5 percent. The corresponding $CV_{BatchAvg}$ determined by Equation 4.5 is 9.4 percent.

Table 4.27 provides a summary of the coefficients of variation for splitting tensile strength from this project and from Ellingwood et al. (1980). Again, the coefficient of variation for this project is less than those reported by Ellingwood et al. (1980), which were used in the calibration of the AASHTO LRFD Specifications (2000). Note that the CV was assumed by Ellingwood et al. (1980) to be equal to those for compressive strengths having the specified strength of 3000 and 4000 psi (20.7 MPa and 27.6 MPa).

Table 4.28. Comparison of Coefficient of Variation for Splitting Tensile Strength.

Source	Specified Compressive Strength Level	CV (%)
This Study	5900 - 9200 psi (40.7 - 63.4 MPa)	12.2 (9.4[+])
Ellingwood et al. (1980)	3000 psi (20.7 MPa)	18*
	4000 psi (27.6 MPa)	18*
	5000 psi (34.5 MPa)	18*

Note:

[+] = Value based on average values for all precasters

* = Values assumed for in-situ condition

4.2.3.4   Bias Factors

The bias factors for the splitting tensile strength are shown in Figure 4.21. The plot is based on the nominal value calculated by AASHTO LRFD Specifications (2000) using the corresponding specified compressive strength. It can be seen that the bias factor decreases slightly with an increase in compressive strength. This is because the actual splitting tensile strength does not increase with the specified compressive strength because there was not a great deal of variation in the mixture proportions used over the specified strength range. However, the predicted value increases with the design strength. As a result, the bias decreases with the design compressive strength. When the AASHTO LRFD Specifications (2000) equation is used, the bias factors within a batch range from 0.86 to 1.50 and the bias factors within a mixture range from 0.88 to 1.47. Table 4.29 provides a summary of the mean bias factor for splitting tensile strength when calculated using the AASHTO LRFD Specifications (2000) equation.
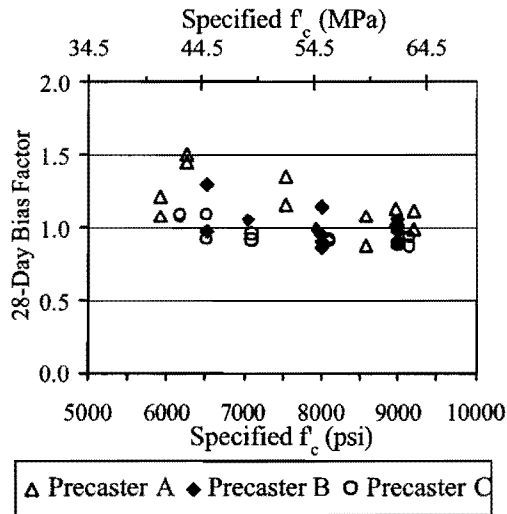
Figure 4.21. Bias Factor for Splitting Tensile Strength (Using AASHTO Equation).

Table 4.29. Bias Factor for Splitting Tensile Strength (Using AASHTO Equation).

Specified Compressive Strength Level	Bias Factor
6000 ± 1000 psi (41.4 ± 6.9 MPa)	1.14
8000 ± 1000 psi (55.2 ± 6.9 MPa)	1.00
10000 ± 1000 psi (68.9 ± 6.9 MPa)	0.98

4.2.3.5 Prediction Formulas

In this section, prediction formulas relating the splitting tensile strength with the compressive strength are investigated. The prediction formulas are summarized in Table 4.30.

Table 4.30. Equations for Determining the Splitting Tensile Strength from the Compressive Strength of Concrete.

Author(s)	Equation	Units of Tensile Strength
ACI Committee 318 (1999)	$6.7 \cdot \sqrt{f_c'}$	psi
Carrasquillo et al. (1981a, 1982) ACI Committee 363 (1997) AASHTO LRFD Specifications (2000)	$7.4 \cdot \sqrt{f_c'}$, 3000 psi $< f'_c <$ 12,000 psi	psi
Ahmad and Shah (1985)	$4.34 \cdot \left(f_c'\right)^{0.55}$, $f'_c <$ 12,000 psi	psi
Burg and Ost (1992)	$7.3 \cdot \sqrt{f_c'}$ for moist-cured specimens	psi
Oluokun (1991)	$1.38 \cdot \left(f_c'\right)^{0.69}$	psi
CEB-FIP Model Code 1990 (CEB 1993)	$1.56 \cdot \left(\dfrac{f_c' - 8}{10}\right)^{\frac{2}{3}}$	MPa

Based on the plot of the splitting tensile strengths with the corresponding compressive strengths from the testing (Figure 4.22), the AASHTO LRFD Specifications (2000), CEB-FIP Model Code 1990 (CEB 1993), and Oluokun (1991) equations overestimate the splitting tensile strength values. The recommended equations by ACI Committee 318 (1999) and Ahmad and Shah (1985) seem to give similar estimations of the splitting tensile strength and appear to fit the test data well.

154
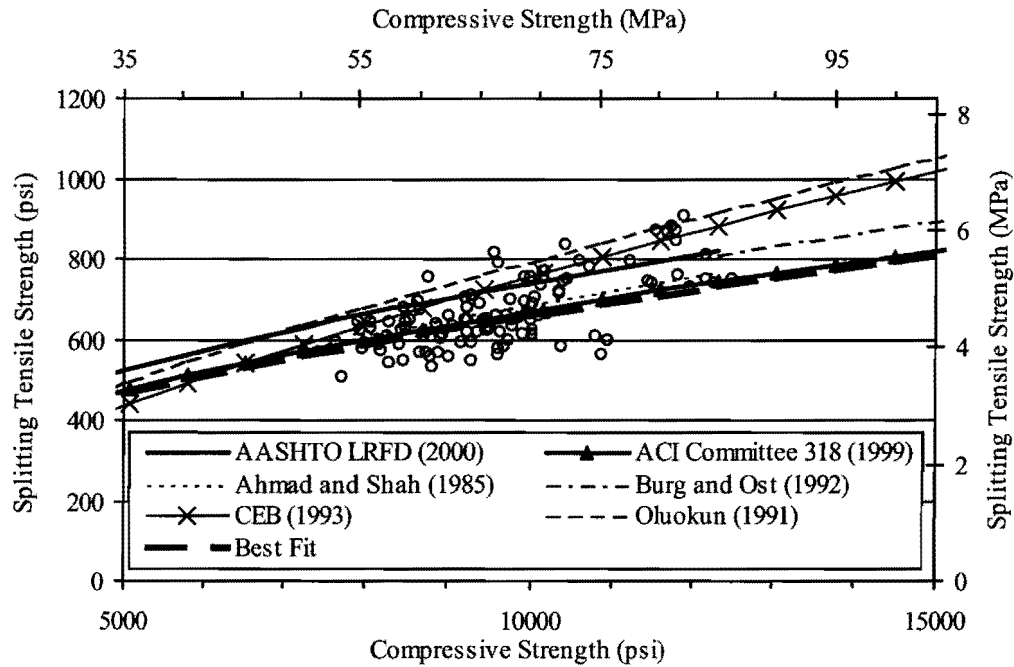
Figure 4.22. Splitting Tensile Strength versus Compressive Strength.

The goodness of fit of the prediction formulas expressed in terms of relative prediction errors are summarized in Table 4.31. It can be seen that the ACI Committee 318 (1999) equation is the best fit at all ages for the data in this project. The equation by Ahmad and Shah (1985) also fits the data almost equally well.

In order to determine a best-fit equation, the prediction model must be determined first. However, the data in this project cover only a relatively small range of compressive strength, and there are significant variations in the data. The square root model used by ACI Committee 318 (1999) and AASHTO LRFD Specifications (2000) was chosen for consistency. Then, the coefficient for the best-fit equation was determined such that the relative prediction errors are minimized for all ages. The best-fit equation for the data from this project is:

$$f_t = 6.6\sqrt{f'_c} \tag{4.14}$$

155

where f_t is the splitting tensile strength in psi and f'_c is the compressive strength in psi. The best-fit equation is also plotted in Figure 4.22, and its relative prediction errors values are summarized in Table 4.31. It can be seen in Figure 4.22 that the best-fit equation provides an estimation similar to the ACI Committee 318 (1999) equation (ACI uses 6.7 as a coefficient) and yields only slightly lower relative prediction errors. Therefore, the existing ACI Committee 318 (1999) equation can be used to predict the splitting tensile strength for HSC similar to those used in this project; no modification appears to be necessary.

Table 4.31. Relative Prediction Errors of Prediction Formulas for Splitting Tensile Strength When Using Compressive Strength from Tests.

Equation	Age of Concrete			
	7 Days	28 Days	56 Days	Overall
AASHTO LFRD Specifications (2000)	0.0227	0.0229	0.0303	0.0253
ACI Committee 318 (1997)	0.0100	0.0084	0.0128	0.0104
Ahmad and Shah (1985)	0.0105	0.0096	0.0149	0.0117
Burg and Ost (1992)	0.0195	0.0195	0.0264	0.0218
CEB-FIP Model Code 1990 (CEB 1993)	0.0194	0.0271	0.0392	0.0286
Oluokun (1991)	0.0372	0.0478	0.0623	0.0491
Best Fit	0.0099	0.0081	0.0121	0.0100

The splitting tensile strength data are plotted with the design compressive strength in Figure 4.23. The relative prediction errors for each equation when using the design compressive strength are summarized in Table 4.32. Initial observations indicate the data points in Figure 4.23 are scattered and there are many data points that are overestimated in the lower compressive strength range. Table 4.32 suggests that the best estimator is the ACI 363 Committee (1997) equation, mainly because it gives the highest predicted values in this range. Upon closer examination, however, it can be observed that the splitting tensile strength does not appear to increase with the specified compressive strength at all. This agrees with the analysis of the mean in the previous section. Therefore, the concept of fitting the splitting tensile strength with the design compressive strength in Figure 4.23 and Table 4.32 may not be appropriate for the data in

this project. Nevertheless, Figure 4.23 does show that the resulting predicted values for the tensile resistance will be on the lower side when the specified compressive strength is used in the prediction. This is considered conservative for design.
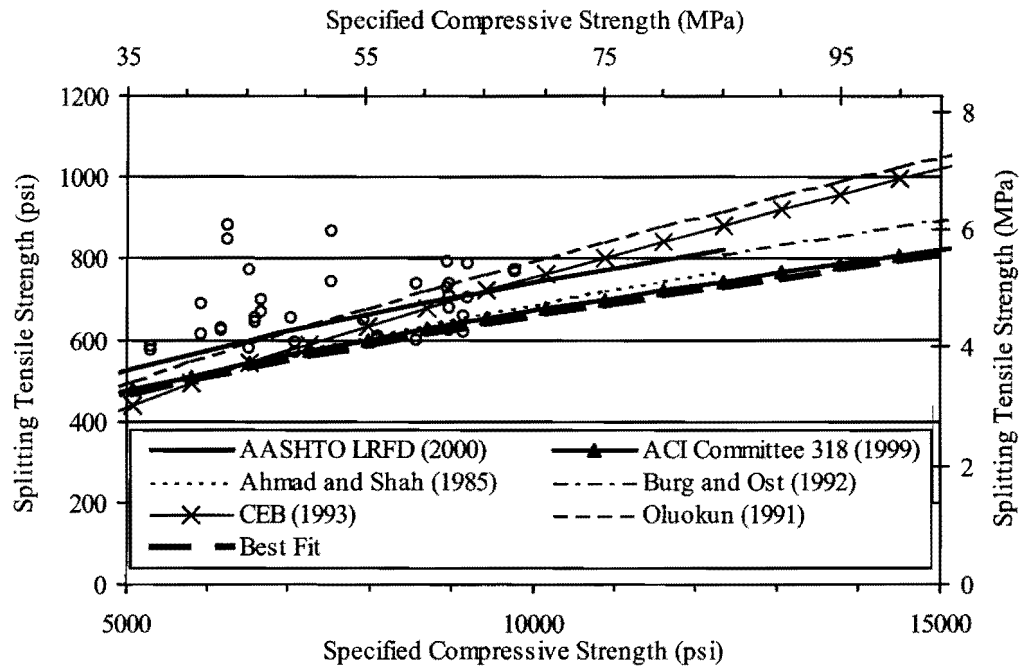
Figure 4.23. Splitting Tensile Strength versus Specified Compressive Strength.

Table 4.32. Relative Prediction Errors of Prediction Formulas for Splitting Tensile Strength When Using Specified Compressive Strength.

Equation	28 Days
AASHTO LFRD Specifications (2000)	0.0156
ACI Committee 318 (1997)	0.0266
Ahmad and Shah (1985)	0.0251
Burg and Ost (1992)	0.0161
CEB-FIP Model Code 1990 (CEB 1993)	0.0215
Oluokun (1991)	0.0198
Best Fit	0.0295

157

Figure 4.24 shows plots of the splitting tensile strength with both compressive strength from tests and specified compressive strength. Plots are made separately for each age, and different markers are used for each precaster. The age of testing does not seem to have a significant effect on the relationships because all trends are the same for all ages. Figure 4.24 (a), (c), and (e) show that the splitting tensile strength increases slightly with compressive strength from tests, but Figure 4.24 (b), (d), and (f) show no increase in splitting tensile strength with the increase in the specified compressive strength. Precasters do not appear to have a significant effect on the relationship between splitting tensile strength and compressive strength, partly because the data are somewhat scattered and clustered in small compressive strength ranges.

Figure 4.25 shows the plot of bias factors for splitting tensile strength when the best-fit equation is used. Compared with Figure 4.25, it can be seen that the bias factor for the best-fit equation has a fewer number of data points that are lower than 1.0. This can be considered conservative for the splitting tensile strength. The bias factors calculated using the best-fit equation range from 0.96 to 1.69 for bias factors within a batch and from 0.98 to 1.65 for bias factors within a mixture. Table 4.33 provides a summary of the mean bias factor for splitting tensile strength when calculated using the best-fit equation.
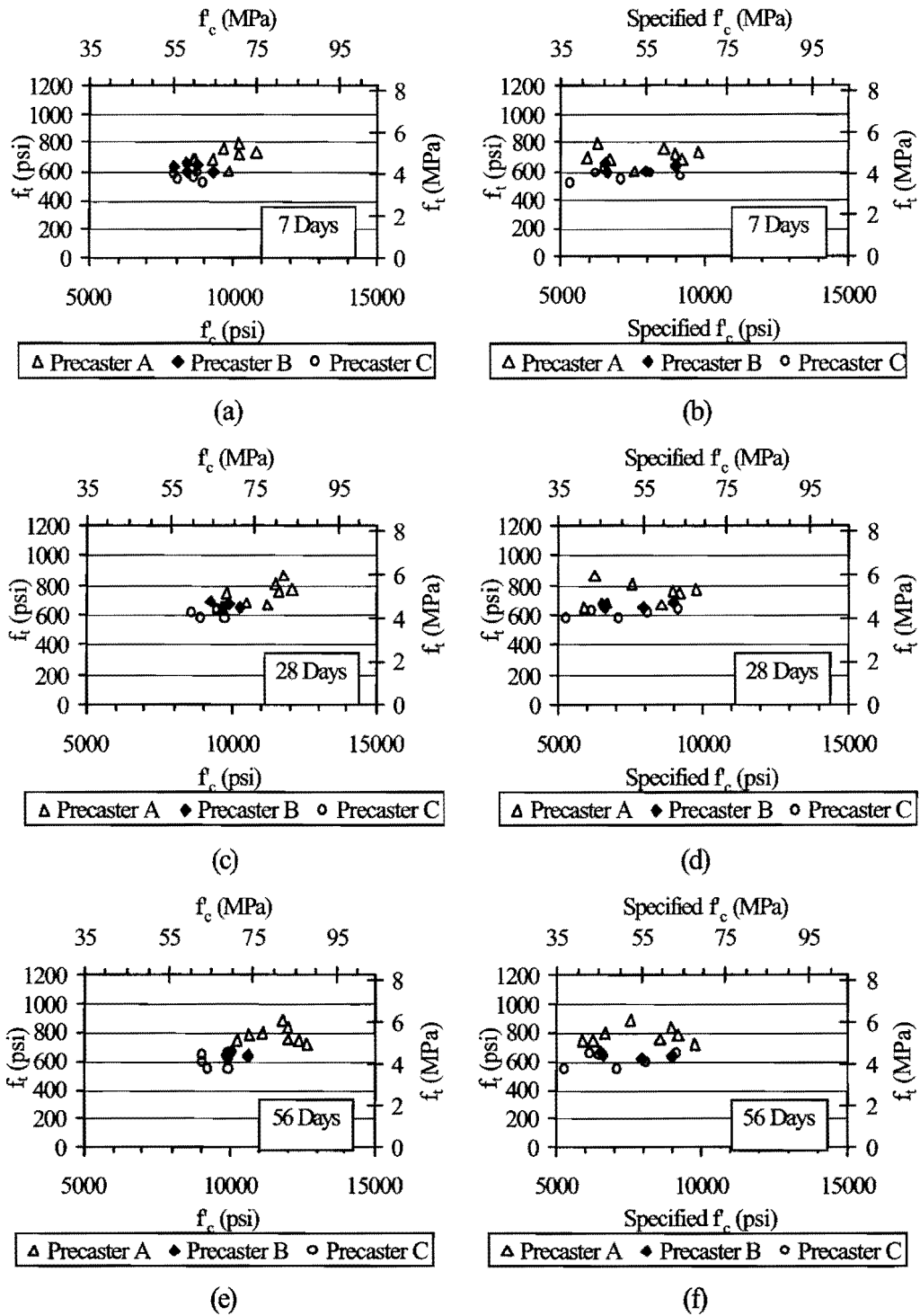
Figure 4.24. Splitting Tensile Strength versus Compressive Strengths by Age.
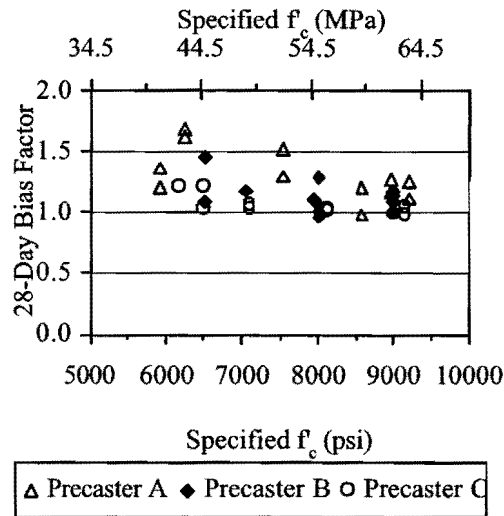
Figure 4.25. Bias Factor for Splitting Tensile Strength (Using Best Fit Equation).

Table 4.33. Bias Factor for Splitting Tensile Strength (Using Best Fit Equation).

Specified Compressive Strength Level	Bias Factor
6000 ± 1000 psi (41.4 ± 6.9 MPa)	1.28
8000 ± 1000 psi (55.2 ± 6.9 MPa)	1.12
10000 ± 1000 psi (68.9 ± 6.9 MPa)	1.10

4.2.3.6   Discussion of Implications for Design Provisions

The shear capacity of prestressed concrete beams depends on the shear resistance provided by concrete, steel stirrups, and the vertical component of the prestressing force. Variability in any of these parameters could affect the variability of the shear resistance of the beam. The shear strength provided by concrete can be related to its splitting tensile strength because shear failures occur due to excessive diagonal tensile stresses. It was found in this project that the coefficient of variation of concrete in splitting tension is larger than the coefficient of variation of concrete under compression. Therefore, it is not reasonable to assume

160

the same coefficient of variation values for both splitting tensile strength and compressive strength. In addition, it was found that the coefficient of variation of the splitting tensile strength for HSC in this project is less than those previously reported for NSC by Ellingwood et al. (1980). Therefore, there may be a possibility that the resistance factor for shear can be increased based on the smaller coefficient of variation. However, the CV reported in this project is not adjusted for in-situ conditions. Limited data are available regarding the relationship between the in-situ CV and CV from the test specimen for splitting tensile strength. Moreover, additional analysis is necessary to assess the effect of concrete splitting tensile strength on the overall resistance parameters for shear.

For design purposes, the prediction formula that should be used in predicting the tensile strength should be the formula that provides the best prediction when the actual compressive strength is used. This tends to result in an underestimation of the actual splitting tensile strength when the design compressive strength is used, which is considered to be conservative. It should be noted that fitting a prediction formula using the specified design strength is not very meaningful in this project. This is because the splitting tensile strength did not change significantly with the specified compressive strength for the concrete sampled from each precaster. The mixture proportions for concrete produced at a particular precast plant were almost always the same for the specified strength range sampled. The ACI Committee 318 (1999) prediction equation was found to be satisfactory for HSC in this project. However, the equation in the AASHTO LRFD Specifications (2000) was found to overestimate the splitting tensile strength.

4.2.4 Modulus of Rupture

In this section, the experimental data and analyses for modulus of rupture are presented. Table 4.34 provides a summary of the data included in the analysis. Three 6×6×20 inch (150×150×500 mm) beam specimens from each batch were used at each test age to determine the modulus of rupture for a total of 323 specimens.

Table 4.34. Summary of Data Used in the Analysis for Modulus of Rupture.

Precaster	Design f'_c Classification* (psi)	Batch No.	Test Ages		
			7 Days	28 Days	56 Days
Precaster A Set 1	6000	A15-A16	X	X	X
	8000	A5-A6	X	X	X
		A13-A14	NT	NT	NT
	10000	A17-A18	X	X	X
Precaster A Set 2	6000	A7-A8	X	X	X
	8000	A9-A10	X	X	X
	10000	A11-A12	X	X	X
Precaster B Set 1	6000	B3-B4	X	X	X
		B11-B12	NT	NT	NT
	8000	B15-B16	X	X	X
	10000	B7-B8	X	X	X
Precaster B Set 2	6000	B9-B10	X	X	X
	8000	B13-B14	X	X	X
	10000	B5-B6	X	X	X
Precaster C Set 1	6000	C15-C16	X	X	X
	8000	C3-C4	X	X	X
		C13-C14	NT	NT	NT
	10000	C17-C18	X	X	X
Precaster C Set 2	6000	C7-C8	X	X	X
	8000	C11-C12	X	X	X
	10000	C9-C10	X	X	X

Notes:

    *   = Nominal range

    X   = Tested

    NT   = Not tested

Failure of specimens under flexural tension in this test was brittle. The failure occurred instantly without noticeable cracks or deflection. The locations of the failure plane of all specimens were within the middle third of the span. In the case of concrete made using limestone aggregate, the failure plane cut through the coarse aggregate particle and hydrated cement paste. The failure plane of concrete made using river gravel went through and around coarse aggregate particles. The failure planes for both types of concrete are shown in Figure 4.26.
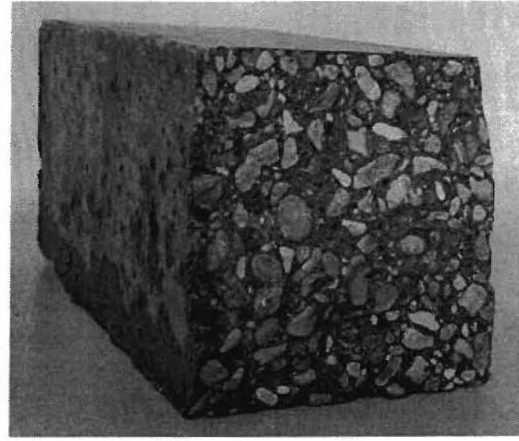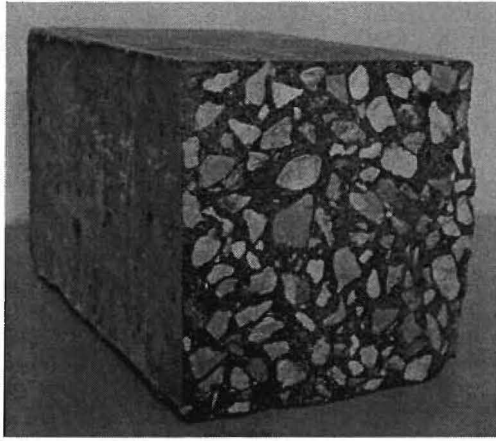
(a) Concrete with Limestone Aggregate   (b) Concrete with River Gravel Aggregate

Figure 4.26. Failures of Modulus of Rupture Specimens.

4.2.4.1   Development of Modulus of Rupture with Time

The ratio of batch average to the 28-day batch average for the modulus of rupture data is provided in Table 4.35. Individual values for each batch are provided in Appendix B. From Table 4.35, the modulus of rupture at 7 days was about 91 percent of the modulus of rupture at 28 days. All precasters appear to have similar trends in this case. The modulus of rupture at 56 days was 4 percent higher than the modulus of rupture at 28 days on average. However, it can be seen from Table 4.35 that the ratio is noticeably higher for Precaster A than those for Precasters B and C, indicating that the difference in materials and mixture proportions can have a significant effect on the long-term development of the modulus of rupture. The increases in the modulus of rupture from 28 days to 56 days for Precasters B and C appear to be small. The small decrease in the 56-day ratio in Precaster B appears to be due to the variations in the modulus of rupture between specimens and the variations from the test.

Table 4.35. Ratio of Batch Average to 28-Day Batch Average for Modulus of Rupture.

Precaster	Ratio to 28-Day Average		
	7 Days	28 Days	56 Days
Precaster A	0.91	1.00	1.12
Precaster B	0.94	1.00	1.02
Precaster C	0.90	1.00	0.98
Overall	0.91	1.00	1.04

4.2.4.2 Probability Distribution

Quantile plots for modulus of rupture are shown in Figure 4.27.

(a) Normal Distribution   (b) Lognormal Distribution
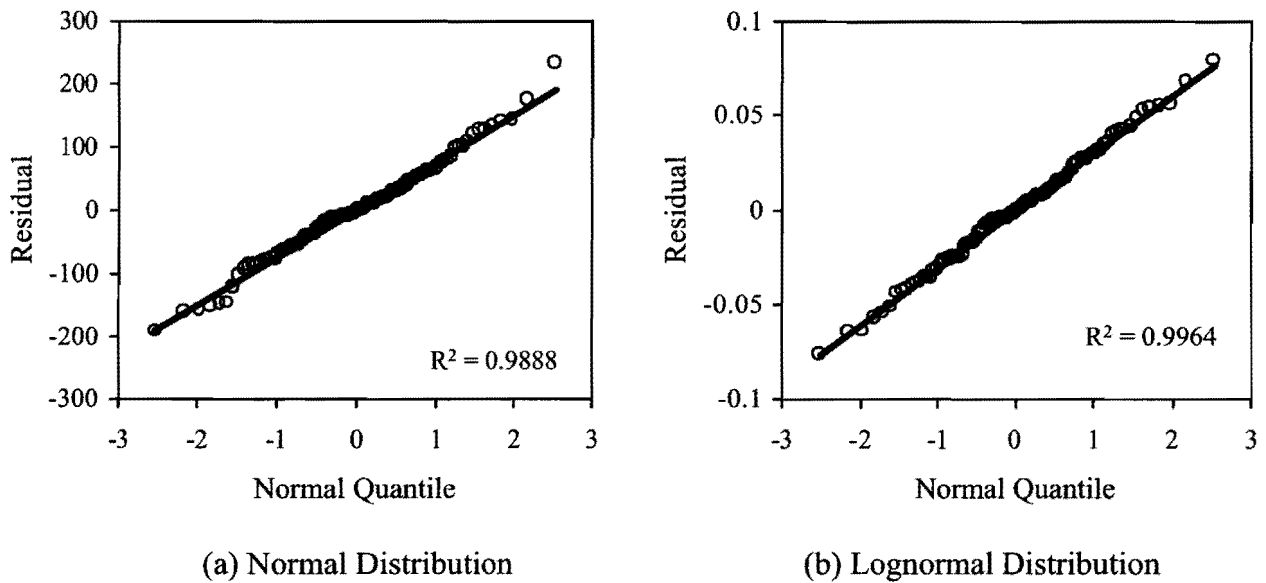
Figure 4.27. Quantile Plots for Modulus of Rupture.

From Figure 4.27, there does not appear to be enough evidence to prefer one distribution over the other since both of them provide a similar fit. Nevertheless, further analyses will be based on the assumption of lognormal distribution because of the convenience of using CV in the analysis and so that the analysis will be consistent with other properties.

164

4.2.4.3 Mean and Coefficient of Variation

The batch average and CV_{Batch} of the modulus of rupture are plotted in Figure 4.28.
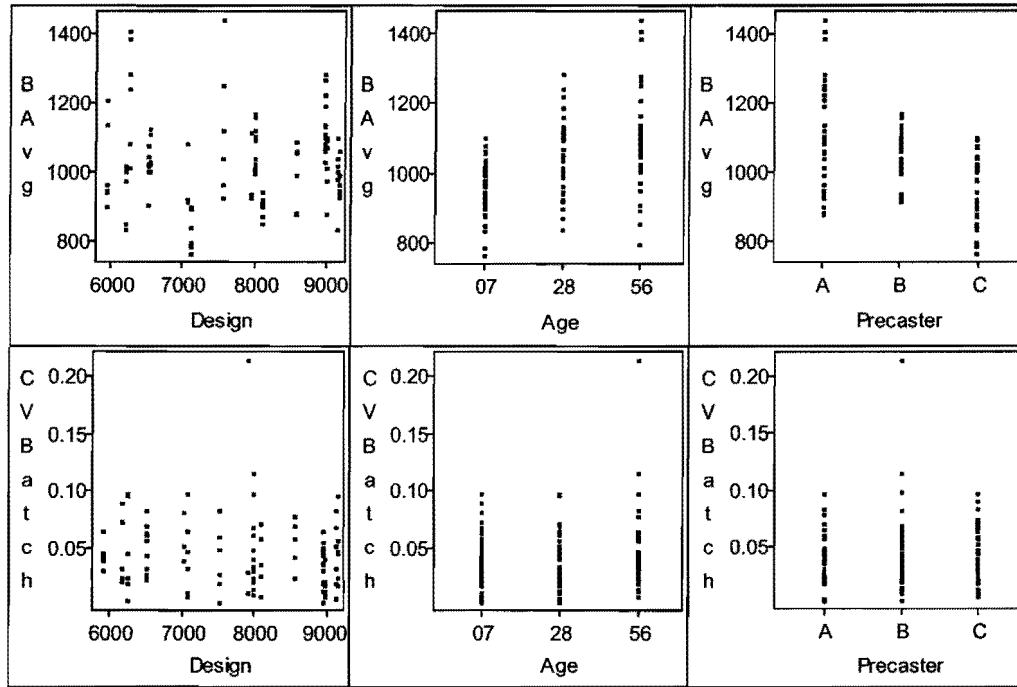
Figure 4.28. Scatter Plots of Batch Average and Coefficient of Variation within a Batch for Modulus of Rupture.

From Figure 4.28, the batch average does not appear to change with an increase in the design strength. The increase in the batch average from 7 days to 28 days can be observed, but the change from 28 days to 56 days is small. The difference between the batch averages among precasters can be seen. The batch average from Precaster A varies over a wider range than Precasters B and C because there were several mixture proportions used by Precaster A, as opposed to one mixture proportion per precaster used for the samples collected from Precasters B and C. Based on the CV_{Batch} plot, the CV_{Batch} appears to have a constant mean for all design strength classifications, ages, and precasters. The ANOVA in Table 4.36 also shows that there is

no difference at 0.05 level in any group. Therefore, the CV_{Batch} can be assumed to be constant with the estimated value of 4.6 percent.

Table 4.36. ANOVA Table of Coefficient of Variation within a Batch for Modulus of Rupture.

```
Dependent Variable: CVBatch

                                   Sum of
       Source            DF        Squares      Mean Square    F Value    Pr > F

       Model             26      0.02663993     0.00102461       1.14     0.3192

       Error             81      0.07275799     0.00089825

       Corrected Total  107      0.09939792


                R-Square     Coeff Var      Root MSE     CVBatch Mean

                0.268013     65.33363       0.029971       0.045873


       Source            DF      Type I SS    Mean Square    F Value    Pr > F

       Precaster          2     0.00105722    0.00052861       0.59     0.5575
       Age                2     0.00217529    0.00108765       1.21     0.3033
       Precaster*Age      4     0.00522520    0.00130630       1.45     0.2238
       Class              2     0.00387242    0.00193621       2.16     0.1224
       Precaster*Class    4     0.00154952    0.00038738       0.43     0.7857
       Age*Class          4     0.00038711    0.00009678       0.11     0.9795
       Precaster*Age*Class 8    0.01237318    0.00154665       1.72     0.1057
```

Scatter plots for the CV_{Mix} of the modulus of rupture are provided in Figure 4.29. Table 4.37 is the ANOVA for the CV_{Mix} of the modulus of rupture.

166
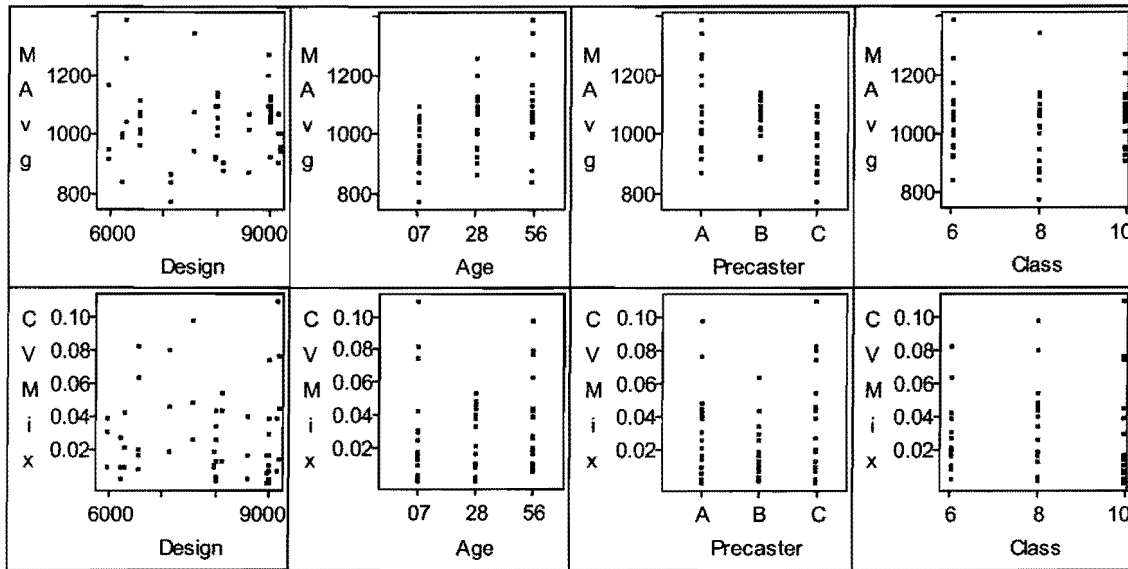
Figure 4.29. Scatter Plots of Mixture Average and Coefficient of Variation within a Mixture for Modulus of Rupture.

Table 4.37. ANOVA Table of Coefficient of Variation within a Mixture for Modulus of Rupture.

```
Dependent Variable: CVMix
```

Source	DF	Sum of Squares	Mean Square	F Value	Pr > F
Model	26	0.02266340	0.00087167	1.57	0.1246
Error	27	0.01497102	0.00055448		
Corrected Total	53	0.03763443			

R-Square	Coeff Var	Root MSE	CVMix Mean
0.602199	76.54996	0.023547	0.030761

Source	DF	Type I SS	Mean Square	F Value	Pr > F
Precaster	2	0.00366589	0.00183295	3.31	0.0520
Age	2	0.00148685	0.00074343	1.34	0.2785
Precaster*Age	4	0.00312043	0.00078011	1.41	0.2584
Class	2	0.00089089	0.00044544	0.80	0.4582
Precaster*Class	4	0.00154032	0.00038508	0.69	0.6023
Age*Class	4	0.00604453	0.00151113	2.73	0.0502
Precaster*Age*Class	8	0.00591449	0.00073931	1.33	0.2698

Based on Table 4.37, the mean of the CV_{Mix} of the modulus of rupture is not significantly different at 0.05 significant level for all groups. The mean CV_{Mix} is 3.1 percent.

The hypothesis tests of the means of the logarithm of the batch average are summarized in Table 4.38. No significant difference is found in all groups. Again, separate analyses will be carried out for each age even though there is no statistical difference among age groups.

Table 4.38. ANOVA Table of the Mean of the Logarithm of Batch Averages for Modulus of Rupture.

Dependent Variable: MLogBAvg

Source	DF	Sum of Squares	Mean Square	F Value	Pr > F
Model	17	0.07921336	0.00465961	2.85	0.0040
Error	36	0.05877101	0.00163253		
Corrected Total	53	0.13798437			

R-Square	Coeff Var	Root MSE	MLogBAvg Mean
0.574075	1.339925	0.040405	3.015433

Source	DF	Type III SS	Mean Square	F Value	Pr > F
Design	1	0.00013642	0.00013642	0.08	0.7742
Precaster	2	0.00726125	0.00363063	2.22	0.1228
Age	2	0.00308811	0.00154406	0.95	0.3978
Precaster*Age	4	0.00176313	0.00044078	0.27	0.8953
Design*Precaster	2	0.00375564	0.00187782	1.15	0.3279
Design*Age	2	0.00130496	0.00065248	0.40	0.6735
Design*Precaster*Age	4	0.00106014	0.00026504	0.16	0.9560

Table 4.39 provides the summary of the mean and CV_{MixAvg} of the modulus of rupture for each precaster and for each test age. The minimum 28-day modulus of rupture was determined to be 1000 psi (6.91 MPa). The maximum CV_{MixAvg} was 11.8 percent at Precaster A. The $CV_{BatchAvg}$ was found according to Equation 4.5 to be 12.2 percent.

168

Table 4.39. Summary of the Mean and Coefficient of Variation of Mixture Averages for Modulus of Rupture.

```
                      Analysis Variable : MAvg

                          N                            Coeff of
    Precaster    Age     Obs     N        Mean         Variation
    ------------------------------------------------------------
    A            07       7      6        983.45       8.5481126

                 28       7      6       1089.44      11.8483566

                 56       7      6       1221.82      12.6968076

    B            07       7      6       1022.94       5.0457836

                 28       7      6       1091.71       7.0785815

                 56       7      6       1105.68       2.8540461

    C            07       7      6        895.24       7.6597763

                 28       7      6       1001.51       8.9291118

                 56       7      6        981.46       9.1530006
    ------------------------------------------------------------
```

For the case when the mean values of the CV_{MixAvg} and mixture averages for all precasters are of interest, the mean mixture average of the modulus of rupture was determined to be 1060 psi (7.31 MPa), and the mean CV_{MixAvg} for the 28-day compressive strength was 9.5 percent. The $CV_{BatchAvg}$, determined by Equation 4.5 and using the average CV_{Mix} of 3.1 percent, was found to be 10.0 percent.

4.2.4.4 Bias Factors

The bias factors for the modulus of rupture are shown in Figure 4.30. The plot is based on the nominal value calculated by the AASHTO LRFD Specifications (2000) using the specified compressive strengths. The bias factor appears to decrease slightly with the specified compressive strength between the specified compressive strengths of 6000 and 7000 psi (41.4 and 48.3 MPa) and remain relatively constant at about 1.5 at higher strengths. The decrease in the bias factor is due to the fact that the actual modulus of rupture does not increase with the specified design strength. Again, this is due to consistency in concrete mixture proportions used by a precaster for the specified compressive strength range in this project. In addition, the prediction formula used to determine the nominal value can affect the trend of the bias factor.

When the AASHTO LRFD Specifications (2000) equation is used, the bias factor ranges from 1.30 to 2.18 for a bias factor within a batch and from 1.34 to 2.14 for a bias factor within a mixture. High values of bias factors indicate that the modulus of rupture is considerably underestimated when using the specified compressive strength in the prediction. Table 4.40 provides a summary of the mean bias factor for modulus of rupture when calculated using the AASHTO LRFD Specifications (2000) equation.
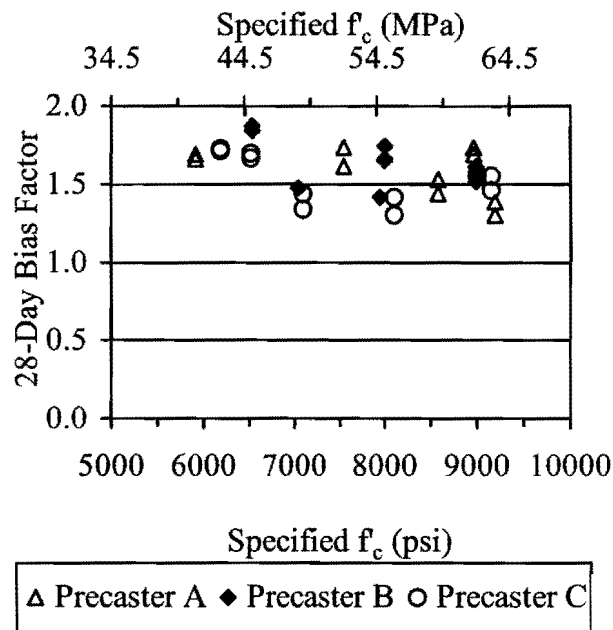
Figure 4.30. Bias Factors for Modulus of Rupture (Using AASHTO Equation).

Table 4.40. Bias Factor for Modulus of Rupture (Using AASHTO Equation).

Specified Compressive Strength Level	Bias Factor
6000 ± 1000 psi (41.4 ± 6.9 MPa)	1.77
8000 ± 1000 psi (55.2 ± 6.9 MPa)	1.54
10000 ± 1000 psi (68.9 ± 6.9 MPa)	1.54

In this section, the goodness of fit of the prediction formulas relating the compressive strength to the modulus of rupture is investigated. The formulas under study include those shown in Table 4.41. The equations are also listed in Section 2.4.4, with a description of the variables. The equation proposed by Ahmad and Shah (1985) is the same equation as that recommended by Raphael (1984), which was originally developed for lower strength concrete (up to approximately 7000 psi (48.3 MPa)).

Table 4.41. Equations for Determining Modulus of Rupture (MOR) from the Compressive Strength of Concrete.

Author(s)	Equation	Units of MOR
ACI Committee 318 (1999) AASHTO LRFD Specifications (2000)	$7.5 \cdot \sqrt{f_c'}$	psi
ACI Committee 363 (1997) Carrasquillo et al. (1981a)	$11.7 \cdot \sqrt{f_c'}$, 3000 psi $< f_c' < 12,000$ psi	psi
Burg and Ost (1992)	$12.4 \cdot \sqrt{f_c'}$, for Moist-Cured Specimens	psi
CEB-FIP Model Code 1990 (CEB 1993)	$1.40 \cdot \dfrac{1+1.5 \cdot \left(\frac{h_b}{h_o}\right)^{0.7}}{1.5 \cdot \left(\frac{h_b}{h_o}\right)^{0.7}} \cdot \left(\dfrac{f_c'-8}{10}\right)^{2/3}$	MPa
Khayat et al. (1995)	$0.23 + 0.12 \cdot \left(f_c'\right) - 0.000218 \cdot \left(f_c'\right)^2$	MPa
Raphael (1984) Ahmad and Shah (1985)	$2.3 \cdot \left(f_c'\right)^{2/3}, f_c' < 12,000$ psi	psi

The relationship between the measured compressive strength and modulus of rupture is plotted in Figure 4.31. Each point in the plot consists of the average results from three modulus of rupture specimens (beam specimens) and three compressive strength specimens. From the plot, it can be seen that the predicted values from all the formulas are similar except those from the AASHTO LRFD Specifications (2000) equation. This estimate is significantly lower than the others. Additionally, the equation for HSC recommended by the ACI Committee 363 (1997) does not result in a good prediction because it overestimates most of the test data. The majority of the test data fall between the equation from the AASHTO LRFD Specifications (2000) and the equation from ACI Committee 363 (1997).
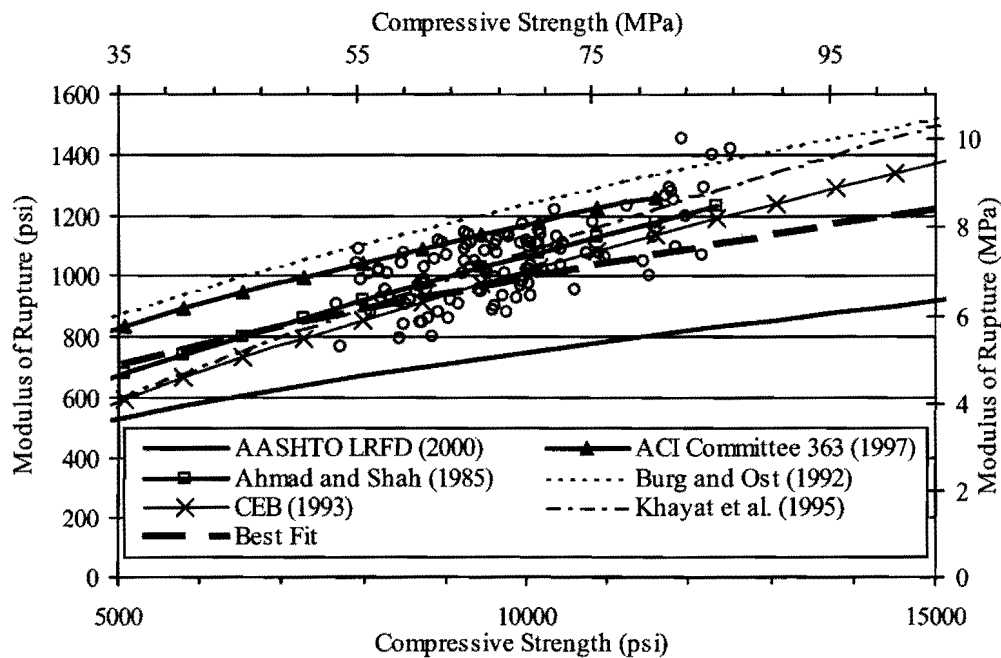
Figure 4.31. Modulus of Rupture versus Compressive Strength.

Table 4.42 is the summary of the relative prediction errors for each equation. The best existing prediction formula for this data is the CEB-FIP Model Code 1990 (CEB 1993) formula followed by the Ahmad and Shah (1985) equation.

The best fit equation for the modulus of rupture in this project is:

$$f_r = 10\sqrt{f'_c} \qquad\qquad (4.15)$$

where f_r is the modulus of rupture in psi and f'_c is the compressive strength in psi. This equation was determined by finding a coefficient in front of the square root such that the relative prediction errors are minimized. The equation is based on the square root model used by the AASHTO LRFD Specifications (2000) and ACI Committee 363 (1997). It can be seen from Figure 4.31 that the trend of the best fit curve is somewhat different from the CEB-FIP Model Code 1990 (CEB 1993) equation. This is because the CEB-FIP Model Code 1990 (CEB 1993) equation uses the 2/3 power rather than square root. The data in this project covers a relatively small range of compressive strengths, and there are variations in the data; therefore, the best fit model was selected based on currently accepted prediction relationships.

Table 4.42. Relative Prediction Errors for Modulus of Rupture When Using Compressive Strength from Tests.

Equation	Age of Concrete			
	7 Days	28 Days	56 Days	Overall
AASHTO LFRD Specifications (2000)	0.0632	0.0781	0.0861	0.0807
ACI Committee 363 (1997)	0.0244	0.0402	0.0268	0.0324
Ahmad and Shah (1985)/Raphael (1984)	0.0075	0.0181	0.0111	0.013
Burg and Ost (1992)	0.0447	0.0673	0.0485	0.0569
CEB-FIP Model Code 1990 (CEB 1993)	0.0084	0.0149	0.0097	0.0117
Khayat et al. (1995)	0.008	0.021	0.0129	0.0149
Best Fit	0.0069	0.0142	0.0117	0.0116

The modulus of rupture is plotted with the design compressive strength in Figure 4.32, and the relative prediction errors are summarized in Table 4.43. When the design compressive strength is used, the equation from the ACI Committee 363 (1997) is the best prediction equation.
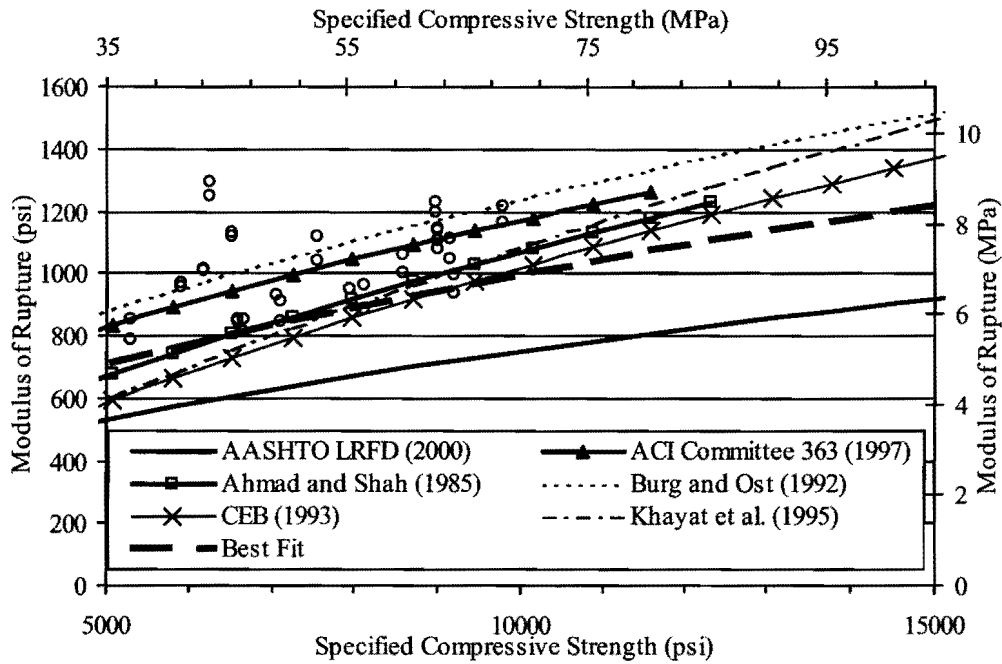
Figure 4.32. Modulus of Rupture versus Specified Compressive Strength.

Table 4.43. Relative Prediction Errors for Modulus of Rupture When Using Specified Compressive Strength.

Equation	28 Days
AASHTO LFRD Specifications (2000)	0.1356
ACI Committee 363 (1997)	<u>0.0122</u>
Ahmad and Shah (1985)/Raphael (1984)	0.0279
Burg and Ost (1992)	0.0168
CEB-FIP Model Code 1990 (CEB 1993)	0.0216
Khayat et al. (1995)	0.0387
Best Fit	0.0309

The modulus of rupture is plotted separately for each age with both actual compressive strength and specified compressive strength and using different markers for each precaster in Figure 4.33.
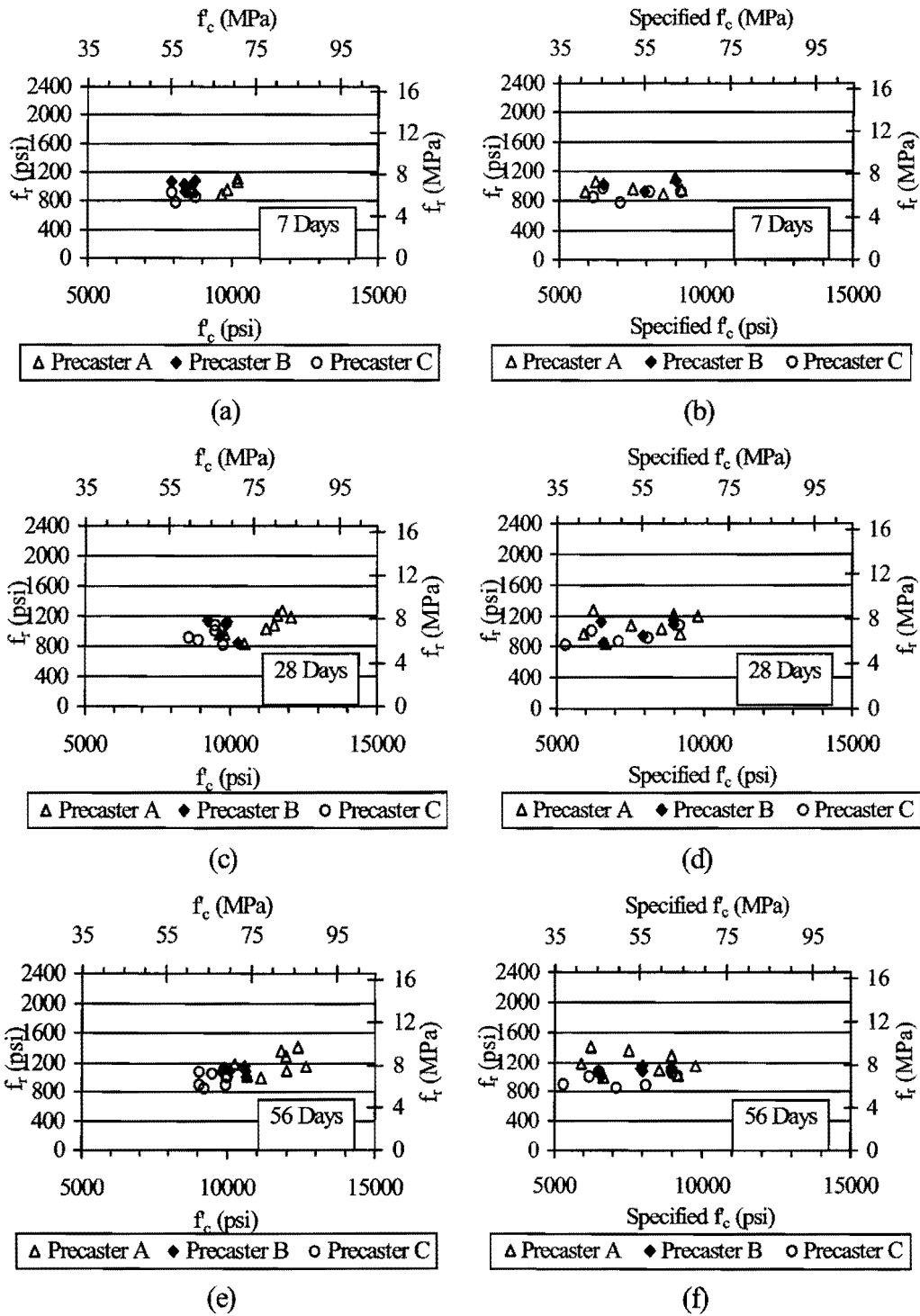
Figure 4.33. Modulus of Rupture versus Compressive Strengths by Age.

It can be observed from Figure 4.33 (a), (c), and (e) that the data for each age are somewhat scattered for each precaster, making it difficult to observe a trend. The relationships between the modulus of rupture and the compressive strength are clearer at the ages of 28 and 56 days than the relationship at 7 days.

From Figure 4.33 (b), (d), and (f), it can be seen that the modulus of rupture does not seem to increase with the specified compressive strength. The reason is the same as in the case of the other properties previously mentioned. That is, the same mixture proportion was used for all the specimens collected from Precasters B and C, and other factors can be as important as the design strength in the selection of the mixture proportion for Precaster A.

Figure 4.34 shows the plot of bias factors for the modulus of rupture when the best fit equation is used. In this case, the bias factors within a batch range from 0.97 to 1.64 and those within a mixture range from 1.01 to 1.61. Table 4.44 provides a summary of the mean bias factor for the modulus of rupture when calculated using the best fit equation.
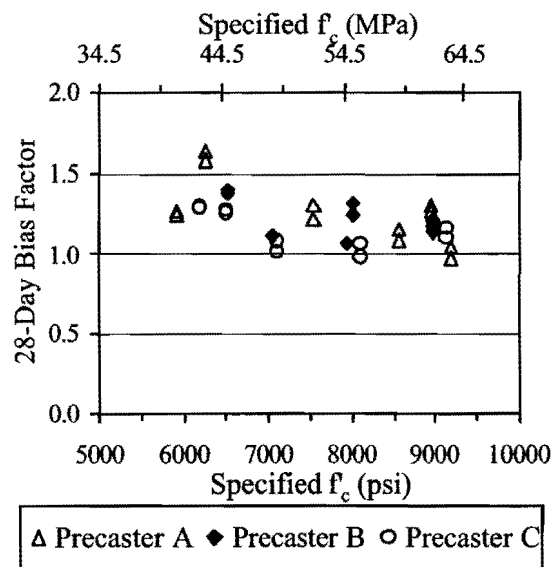

Figure 4.34. Bias Factor for Modulus of Rupture (Using Best Fit Equation).

Table 4.44. Bias Factor for Modulus of Rupture (Using Best Fit Equation).

Specified Compressive Strength Level	Bias Factor
6000 ± 1000 psi (41.4 ± 6.9 MPa)	1.28
8000 ± 1000 psi (55.2 ± 6.9 MPa)	1.12
10000 ± 1000 psi (68.9 ± 6.9 MPa)	1.10

4.2.4.6   Discussions of Implications for Design Provisions

Because the modulus of rupture is used in design to estimate the stress at which a prestressed concrete member begins to crack in bending and expose the prestressing strands to a corrosive environment, it is conservative to underestimate the value of modulus of rupture. However, it must be noted that underestimation of modulus of rupture is not always conservative in design. If the actual modulus of rupture is greater than the estimated value used in the design, the actual cracking moment will also be greater than the calculated value. If the cracking moment is close to the nominal moment capacity of the beam, a sudden failure of the beam can occur immediately after the beam cracks without significant deflection to serve as a warning of the impending failure. Nevertheless, this appears to be rare because one of the problems facing bridge designers is not that the beam has too few prestressing strands but rather the standard section is not big enough to fit all the desired prestressing strands. This leads to the use of 0.6 inch (15 mm) prestressing strands instead of standard 0.5 inch (13 mm) prestressing strands to increase the area of the prestressing steel. Therefore, underestimation of the modulus of rupture should not be a major concern as long as it is not considerably underestimated and there is a sufficient amount of longitudinal reinforcement.

Again, because the design strength depends on current practices, it is not desirable to recommend a prediction formula based on how accurate it is using specified design strengths. Rather, the prediction formula that gives the most accurate prediction using the actual compressive strengths should be selected. Design criteria can then be developed based on this best fit expression such that the probability of exceeding a limit state in design is acceptably low.

Based on the test data of the modulus of rupture, the allowable tensile stress of $6\sqrt{f'_c}$ (in psi) seems to be conservative. Figure 4.35 shows a plot of the modulus of rupture and the actual compressive strength similar to Figure 4.31. In this plot, the allowable stress calculated from compressive strength values is plotted along with the AASHTO LRFD Specifications (2000) relationship for the allowable tensile stress in bending. The allowable stress happens to be 80 percent of the modulus of rupture used for design ($0.8 \times 7.5\sqrt{f'_c}$). Also on this plot are the best fit equation and the 80 percent of the best fit values. Different markers are used to distinguish the data for different test ages.

It can be seen that the allowable stress of $6\sqrt{f'_c}$ is substantially lower than all the data from this project. The allowable stress is only 60 percent of the modulus of rupture values predicted by the best fit equation. At 80 percent of the best fit values, nearly all of the test data are still above this line. Therefore, based on the modulus of rupture from the test, there is a potential that the allowable tensile stress can be increased. However, Nilson (1985) pointed out that the cracking stress of an actual structural member could be less than the modulus of rupture of laboratory samples due to the difference in curing conditions in the laboratory and in the field. However, no such comparison was made for this project.
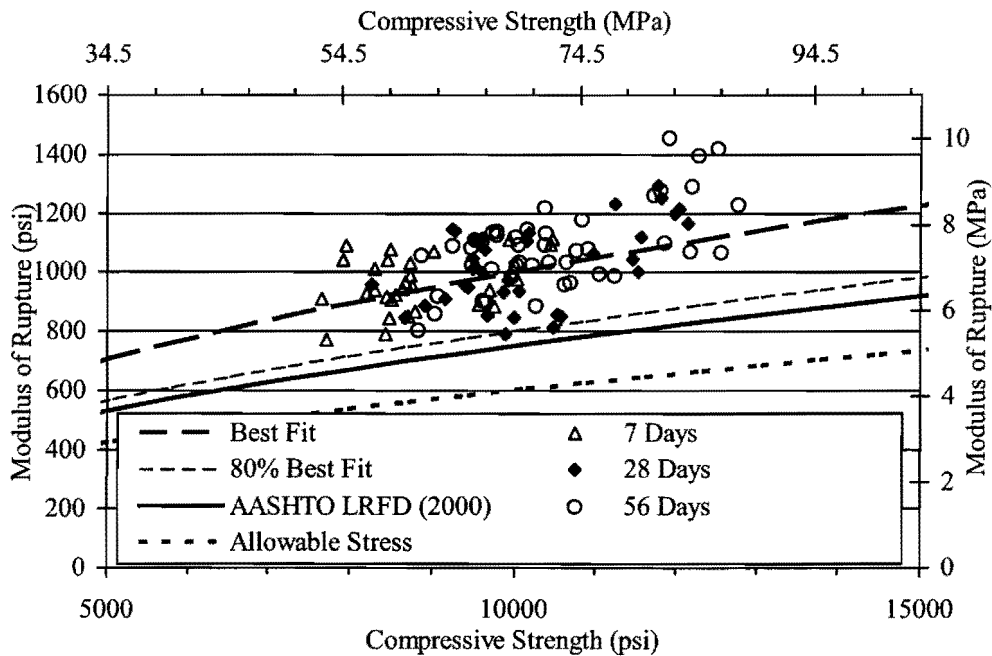
Figure 4.35. Allowable Stresses and Modulus of Rupture.

Nevertheless, HSC has a very dense structure that can prevent the escape of moisture, as can be seen later from the low drying shrinkage of HSC. Therefore, the curing condition of the bulk concrete may be considered as the same as the curing condition of the moist-cured laboratory specimens. In addition, when Type III portland cement is used in HSC, the majority of the long-term strength is gained while the concrete is still in the mold. Therefore, it will not be affected by the curing condition as much as NSC. To determine what the allowable tensile stress value should be, the study of the effect of the curing conditions on the modulus of rupture may be required.

4.2.5 Creep and Shrinkage

In this section, the measurements of creep and shrinkage are presented. A summary of the data included in this analysis is provided in Table 4.45.

Table 4.45. Summary of Data Used in the Analysis for Creep and Shrinkage.

Precaster	Design f'_c Classification* (psi)	Batch No.	Last Reading Creep & Shrinkage (Cylinders)	Last Reading Shrinkage (Prisms)
Precaster A Set 1	6000	A15-A16	NT	NT
	8000	A5-A6	NT	NT
		A13-A14	NT	NT
	10000	A17-A18	NT	64 weeks
Precaster A Set 2	6000	A7-A8	670 days	64 weeks
	8000	A9-A10	650 days	64 weeks
	10000	A11-A12	600 days	64 weeks
Precaster B Set 1	6000	B3-B4	NT	NT
		B11-B12	NT	64 weeks
	8000	B15-B16	NT	64 weeks
	10000	B7-B8	NT	64 weeks
Precaster B Set 2	6000	B9-B10	580 days	64 weeks
	8000	B13-B14	510 days	64 weeks
	10000	B5-B6	590 days	64 weeks
Precaster C Set 1	6000	C15-C16	NT	64 weeks
	8000	C3-C4	NT	NT
		C13-C14	NT	NT
	10000	C17-C18	NT	64 weeks
Precaster C Set 2	6000	C7-C8	650 days	64 weeks
	8000	C11-C12	630 days	64 weeks
	10000	C9-C10	630 days	64 weeks

Notes:
* = Nominal range
NT = Not Tested

Creep of concrete for each sample collection was tested beginning at the age of 7 days using four 4×8 inch (100×200 mm) cylindrical specimens (two specimens per batch) loaded in a creep frame. Two unloaded 4×8 inch (100×200 mm) specimens (one specimen per batch) were used to monitor shrinkage strains in the same environment (control specimens). The specimens

180

in the creep frames were loaded to approximately 30 percent of the average compressive strength for the two batches at an age of 7 days, corresponding to the age at loading. Table 4.46 provides a summary of the load regime for the creep samples. The load losses were computed by multiplying the average change in the height of the spring with the corresponding spring stiffness (27 kips/inch [4.7 kN/mm]). Strains were measured using electronic strain gages, with the data recorded at one-hour increments. A 64-channel data acquisition system with signal conditioners was used, limiting the creep testing to one sample collection for each strength range and precaster. A total of nine creep frames with six channels each were used.

Table 4.46. Load Summary for Creep Specimens.

Batch No.	A7 A8	A9 A10	A11 A12	B5 B6	B9 B10	B13 B14	C7 C8	C9 C10	C11 C12
Mixture Average f'_c at 7 Days (psi)	8626	9862	8646	7929	8376	8705	8749	8604	7928
Load Corresponding to 30% of f'_c (kips)	32.5	37.2	32.6	29.9	31.6	32.8	33.0	32.4	29.9
Initial Load (kips)	29.6	34.2	31.8	29.5	35.1	33.4	30.3	31.4	29.6
Load Loss (kips)	0.0	1.7	0.0	1.7	1.7	2.4	1.8	2.2	2.2
Creep Load (kips) (% of f'_c)	29.6 27.3	32.5 26.2	31.8 29.3	27.9 28.0	33.4 31.8	31.0 28.4	28.5 25.9	29.2 27.0	27.3 27.4

Shrinkage was also tested using 4×4×11.25 inch (100×100×285 mm) prism specimens. A length comparator was used to measure the change in length of the shrinkage specimens at 1 day after casting (initial reading); 28 days after casting (second reading); 4, 7, 14, and 28 days after the second reading; and 8, 16, 32, and 64 weeks after the second reading. Details on the test methods and equipment setup for both the creep and shrinkage testing are discussed in Sections 3.2.5, 3.2.6, 3.3.6, and 3.3.7 and in Appendix D. Strain measurements for each individual sample can be found in Appendix B.

4.2.5.1 Prediction of Creep and Shrinkage with Time

The creep and shrinkage strain measurements from creep testing (ASTM C 512 1992) are plotted along with prediction formulas in Figures 4.36 through 4.44. Creep strain is defined as the difference between the average of two total strains from two specimens in the creep frame

and the shrinkage strain from the control specimen, all within the same batch. This is based on the widely accepted assumption that the creep and shrinkage are additive. The creep strains from the two batches of a mixture were then averaged to obtain the creep curve shown in the plots. The shrinkage curve was obtained from the average of two control specimens, one from each batch of a mixture. The equations for prediction of creep and shrinkage are provided in Tables 4.47 and 4.48. The description of terms is provided in Section 2.4.4.6.4.

Table 4.47. Equations for Predicting Creep as a Function of Time.

Author(s)	Equation
AASHTO LRFD (2000)	$3.5 k_c k_f \left(1.58 - \dfrac{H}{120}\right) t_j^{-0.118} \dfrac{(t - t_j)^{0.6}}{10.0 + (t - t_j)^{0.6}}$
ACI Committee 209 (1992)	$\dfrac{t^{0.6}}{10.0 + t^{0.6}} \nu_u$
CEB (1993)	$\dfrac{\sigma_c(t_0)}{E_{ci}} \phi(t, t_0)$
Bazant and Panula (BP) (1984)	$\dfrac{1}{E_0} + C_0(t, t') + C_d(t, t', t_0) - C_p(t, t', t_0)$
Bazant and Panula (BP Simplified) (1980)	$\dfrac{1}{E_0} + A(t')F(\bar{t}) + k'_h P(\Delta_d) B(t') f\left(\dfrac{\hat{t}}{\tau_{sh}}\right)$

Table 4.48. Equations for Predicting Shrinkage as a Function of Time.

Author(s)	Equation
AASHTO LRFD (2000)	$-k_s k_h \left(\dfrac{t}{35.0 + t}\right) 0.51 \times 10^{-3}$
ACI Committee 209 (1992)	$\dfrac{t}{35 + t} (\varepsilon_{sh})_u$
CEB (1993)	$\varepsilon_{cso} \beta_s (t - t_s)$
Bazant and Panula (BP) (1984)	$\varepsilon_{sh\infty} k_h S(\hat{t})$
Bazant and Panula (BP Simplified) (1980)	$\varepsilon_{sh\infty} k_h S\left(\dfrac{\hat{t}}{\tau_{sh}}\right)$
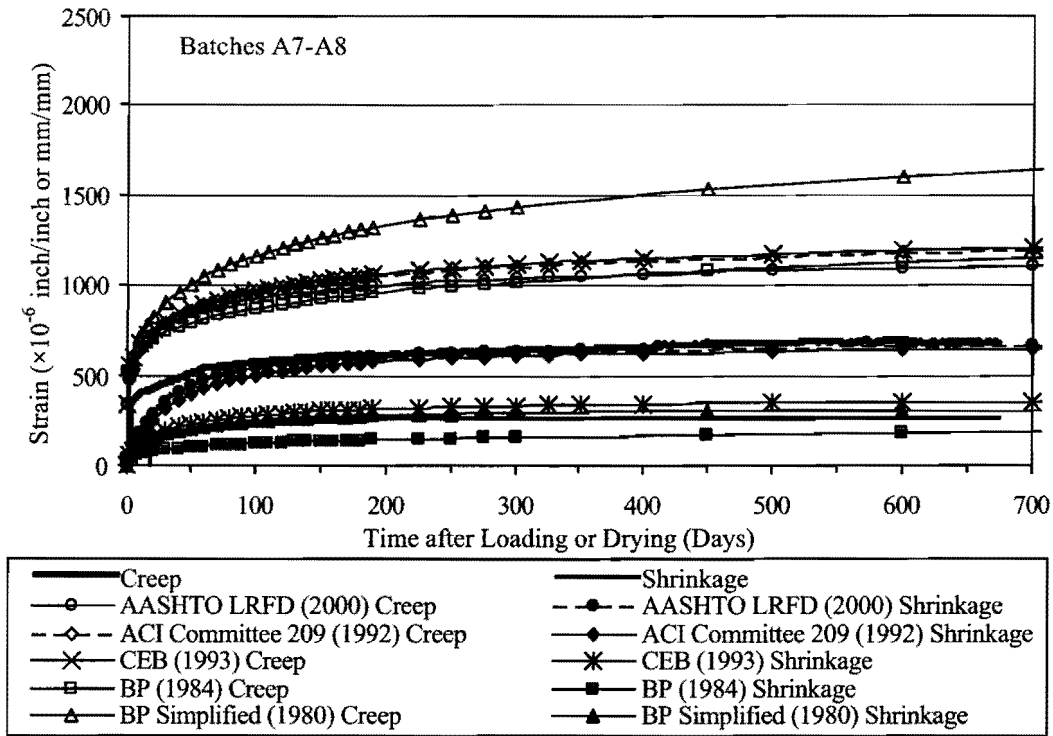
Figure 4.36. Creep and Shrinkage Strains for Batches A7-A8.
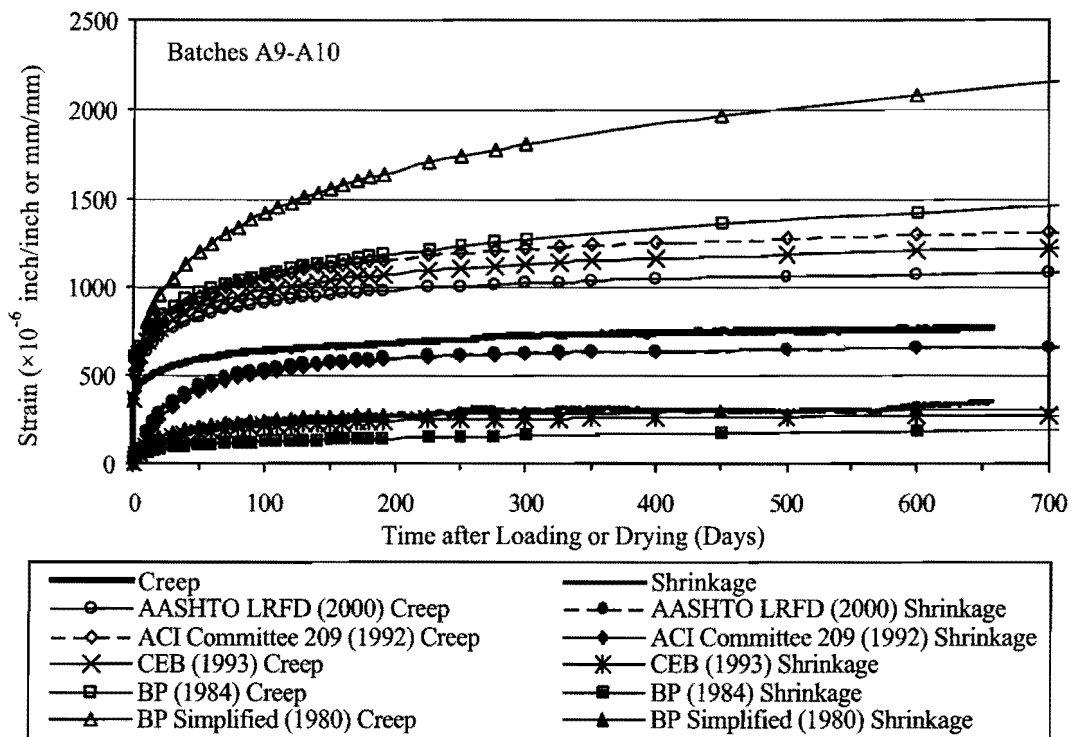
Figure 4.37. Creep and Shrinkage Strains for Batches A9-A10.

183
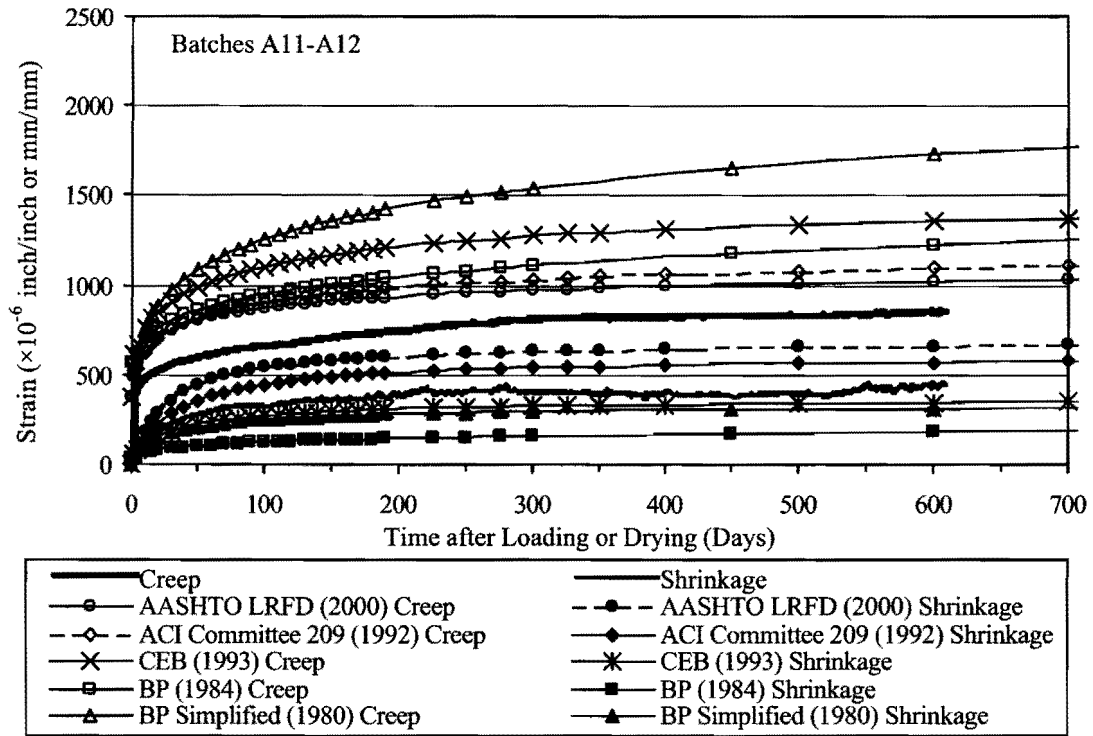
Figure 4.38. Creep and Shrinkage Strains for Batches A11-A12.
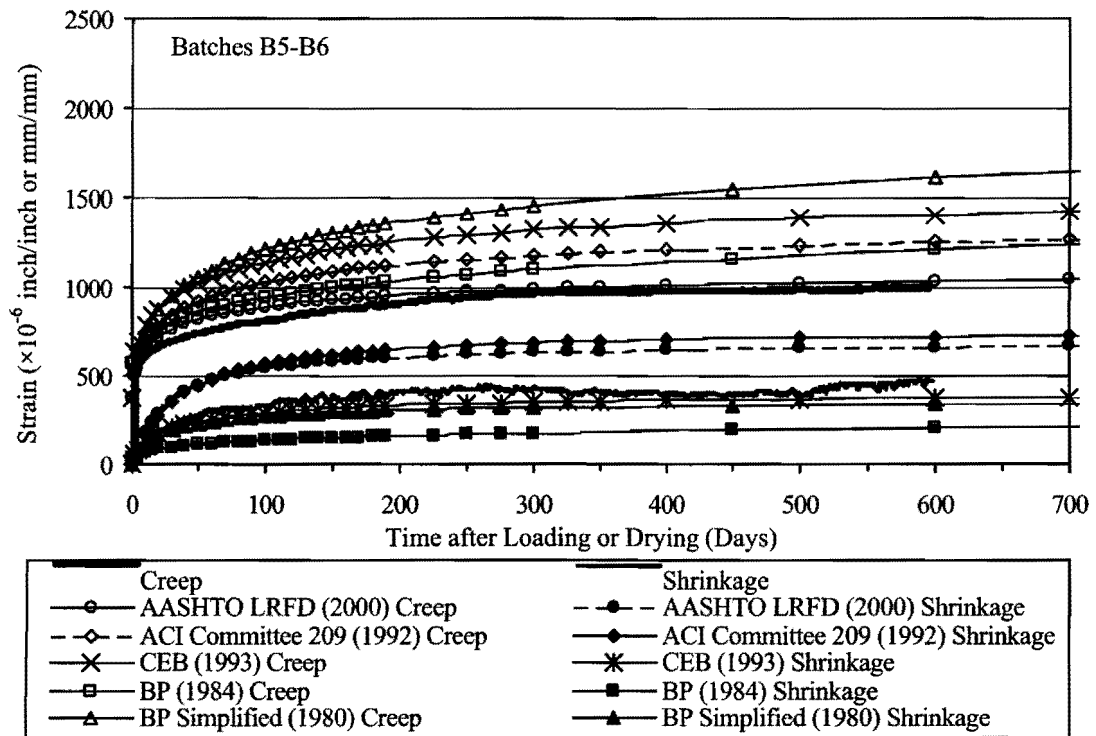
Figure 4.39. Creep and Shrinkage Strains for Batches B5-B6.

184
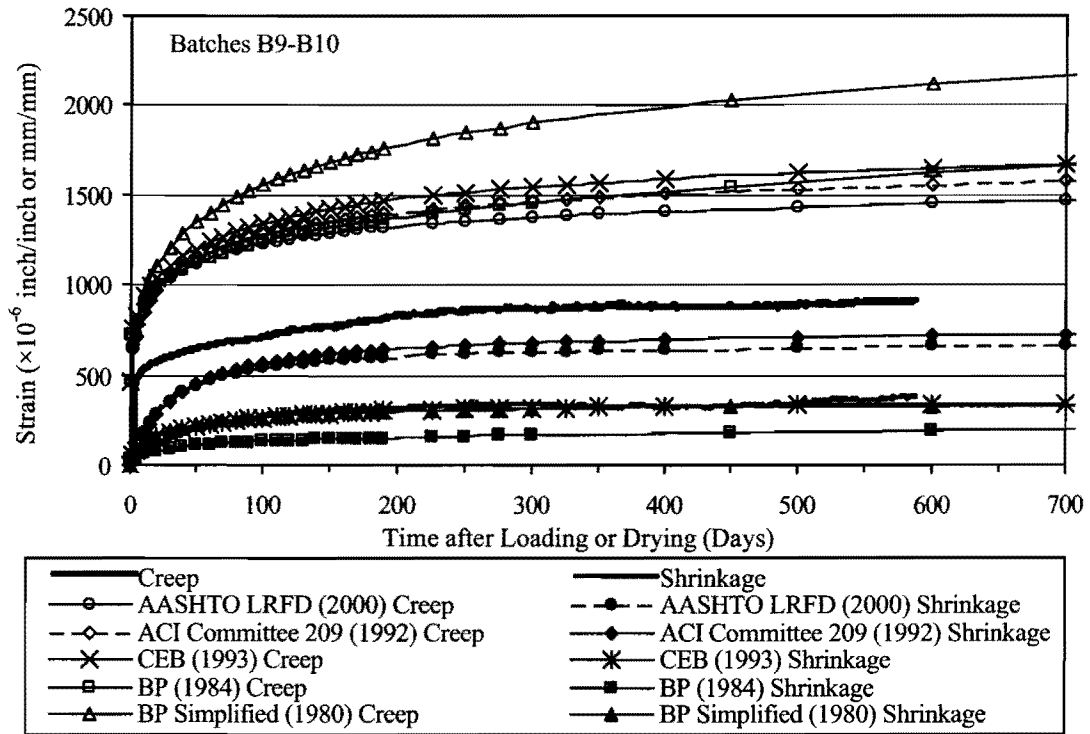
Figure 4.40. Creep and Shrinkage Strains for Batches B9-B10.
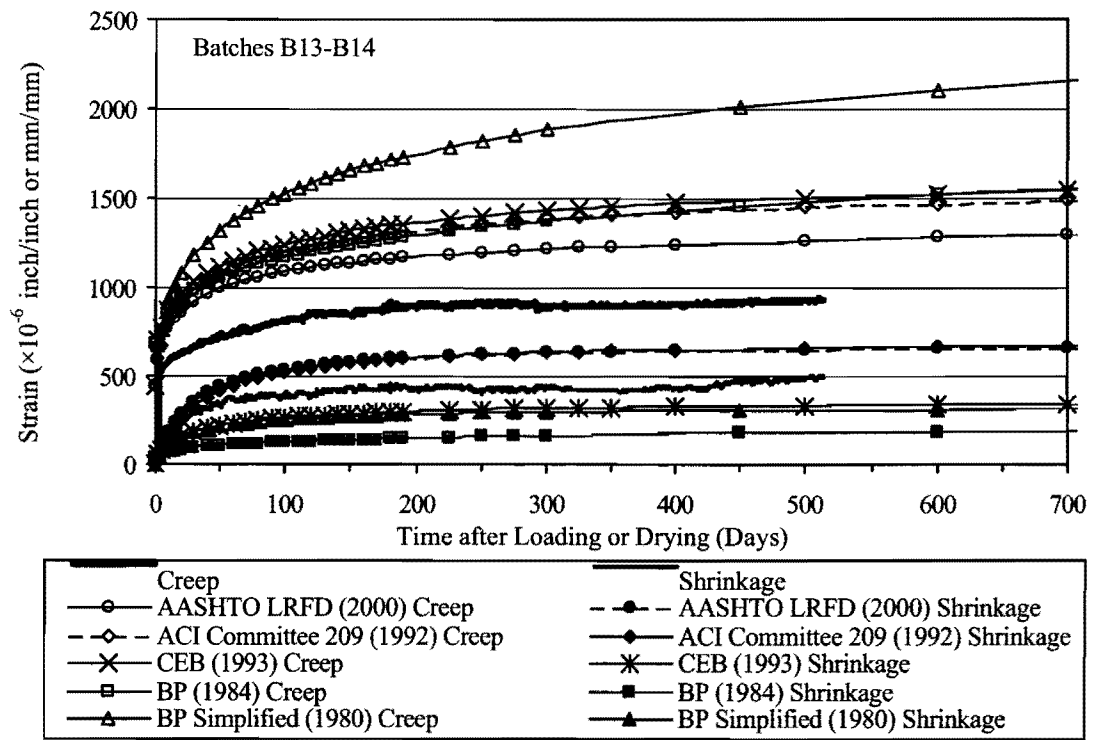
Figure 4.41. Creep and Shrinkage Strains for Batches B13-B14.

185
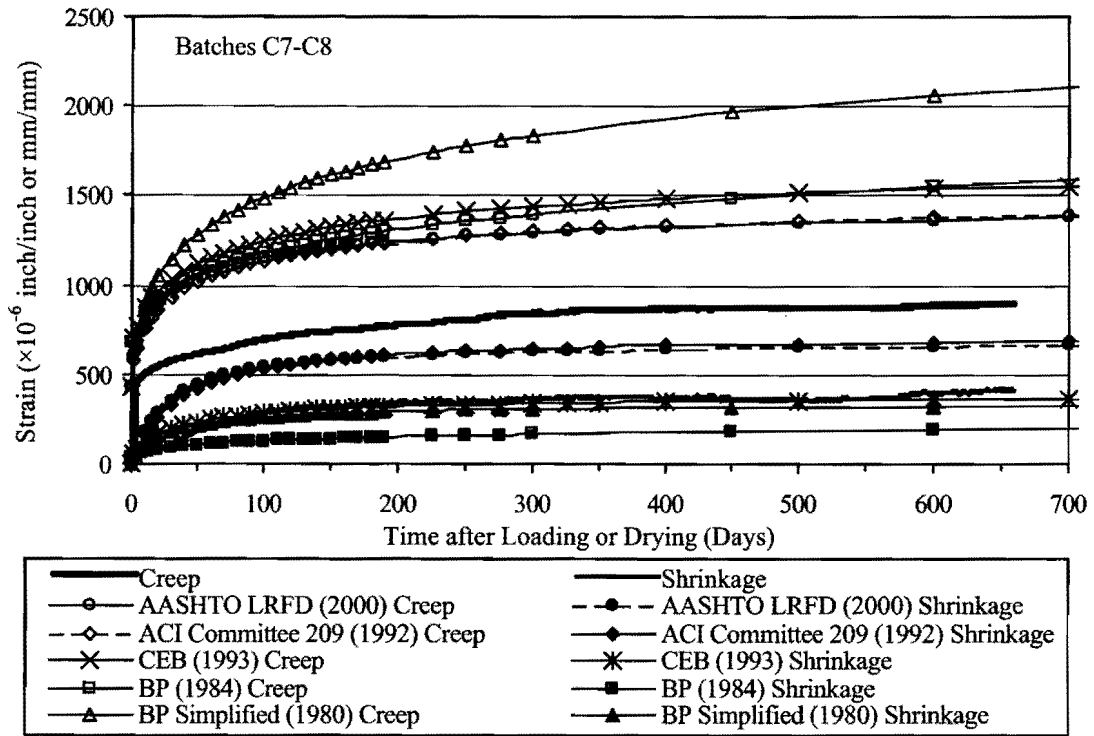
Figure 4.42. Creep and Shrinkage Strains for Batches C7-C8.
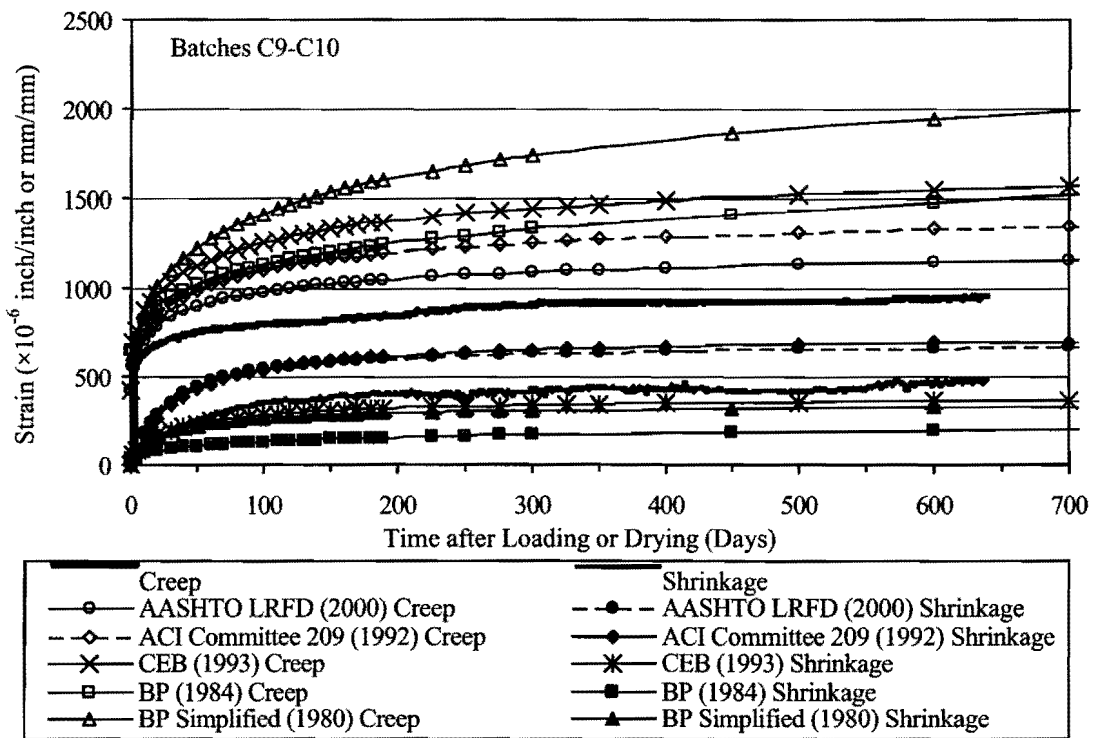
Figure 4.43. Creep and Shrinkage Strains for Batches C9-C10.

186
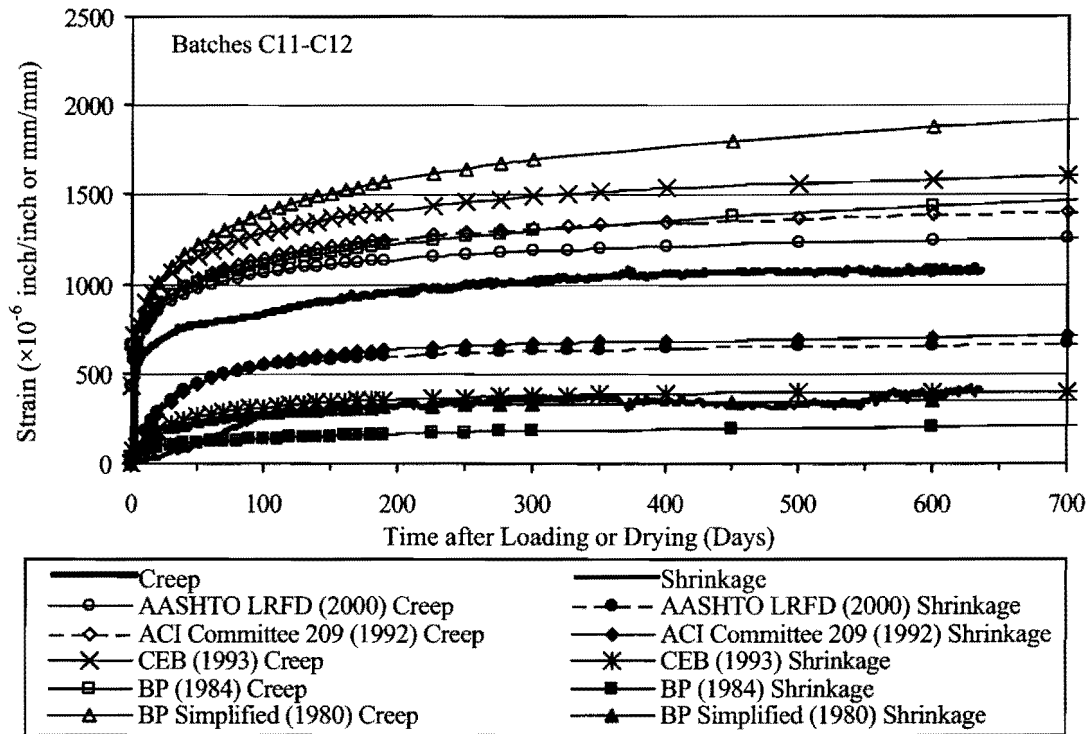
Figure 4.44. Creep and Shrinkage Strains for Batches C11-C12.

It can be observed from the plots that all the prediction formulas overestimate creep strains for all concrete mixtures tested. Equations from the AASHTO LRFD Specifications (2000), ACI Committee 209 (1992), and Bažant and Panula (1978b, 1978c, 1978d, 1979a, 1979b, 1984) usually yield lower predicted values of creep compared with equations from CEB-FIP Model Code 1990 (CEB 1993) and the simplified equation from Bažant and Panula (1980). Even the lowest predicted values overestimated the creep of all the HSC samples tested, and this overestimation was significant in most cases.

For many of the specimens, the creep strains became nearly constant after they were loaded for about 150 to 200 days. On the other hand, some prediction equations, especially the simplified equation from Bažant and Panula (1980) and CEB-FIP Model Code 1990 (CEB 1993), still show an increasing trend at 200 days.

The corresponding shrinkage of the control specimens was predicted with much better accuracy by current equations. The CEB-FIP Model Code 1990 (CEB 1993) equation and the simplified equation from Bažant and Panula (1980) predict the shrinkage of all the samples

relatively well. The ACI Committee 209 (1992) equation and AASHTO LRFD Specifications (2000) equation overestimate shrinkage strains by as much as 100 percent. Like the creep strains, most of the shrinkage strains also begin to stabilize after the specimens have been exposed to drying for about 150 to 200 days.

In all of the prediction formulas, the relative humidity and temperature (where required for the model) are assumed to be constant at 50 percent and 70 °F (21.1 °C), respectively. These are close to the average relative humidity and temperature in the laboratory where the specimens were stored. The relative humidity and temperature histories for the laboratory are shown in Figure 4.45. The samples were collected at different times, and so the creep specimens were loaded between about 10 and 160 days according to the timescale provided in the graphs.
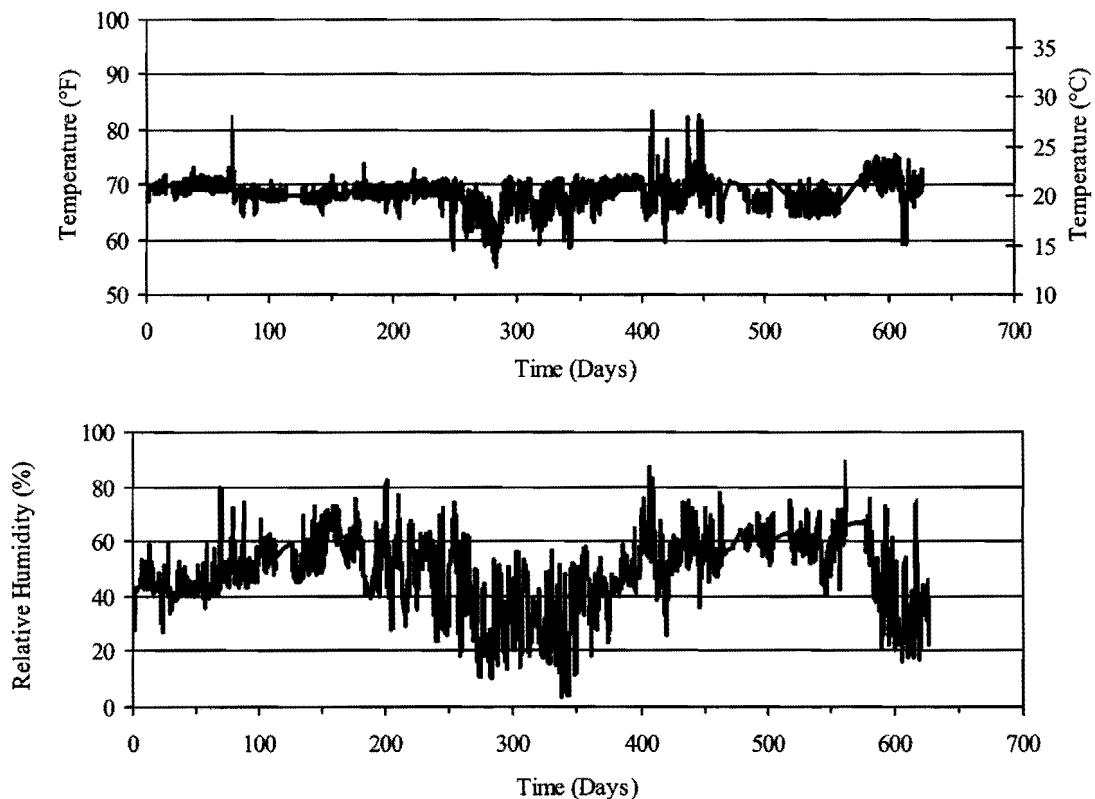
Figure 4.45. History of Temperature and Relative Humidity for Creep Test.

Figure 4.46 shows a variation of temperature and relative humidity over a 5-day period. Vertical lines indicate midnight (12:00 a.m.). There are some fluctuations of the temperature and relative humidity within a 24-hour period, and there is a tendency for the highest temperature and relative humidity to occur in the afternoon. The effect of temperature on the measured strains was minimized by determining the magnitude of the thermal strain with the use of strain gages mounted on a steel block. The longitudinal strain of each concrete sample, which is a combination of creep, shrinkage strain, and thermal strain, was adjusted by subtracting the thermal strain from the measured longitudinal strain. The adjusted longitudinal strain is provided in this report.
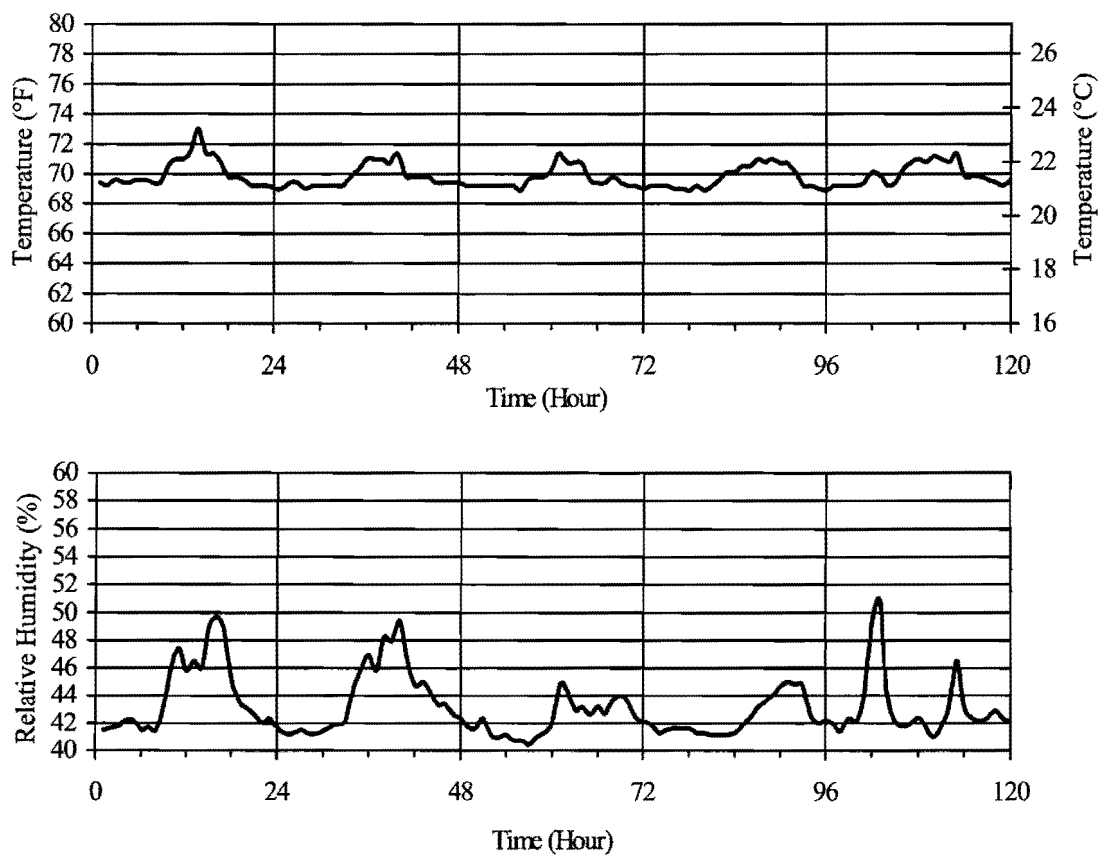
Figure 4.46. Sample Daily Variations of Temperature and Humidity.

The measured shrinkage strains from the prism specimens (ASTM C 157 [1999c]) are plotted versus predicted values as a function of time in Figures 4.47 through 4.61. The shrinkage at each age is typically the average shrinkage for six specimens from two batches (three specimens per batch).

189
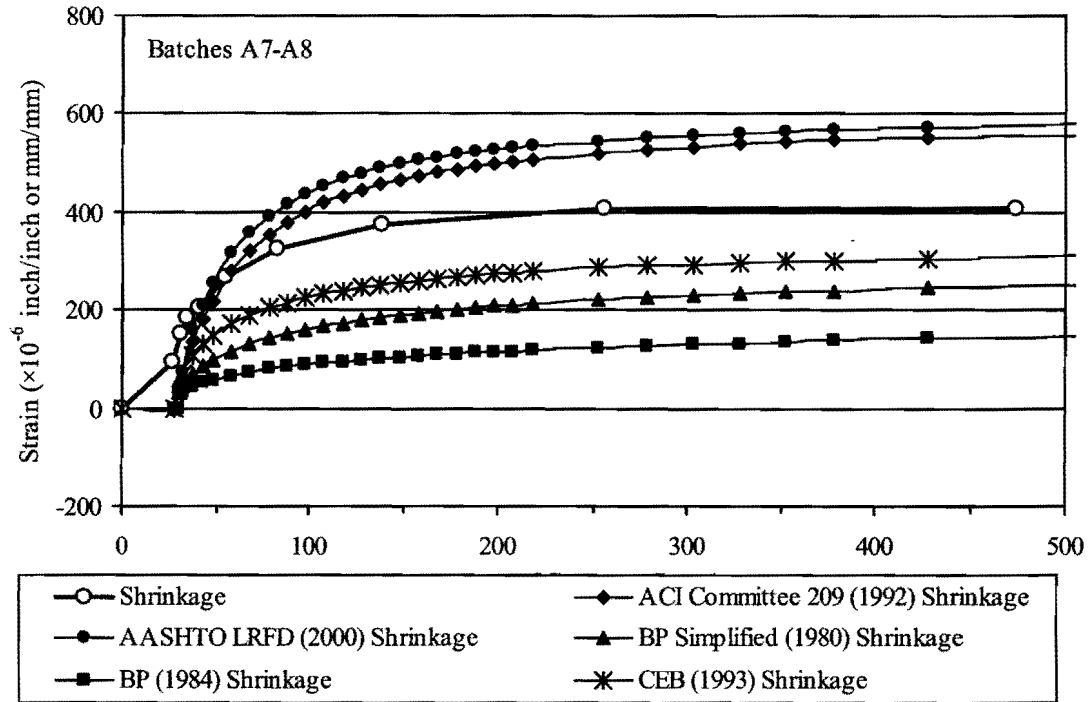
Figure 4.47. Shrinkage Strains of Prism Specimens for Batches A7-A8.
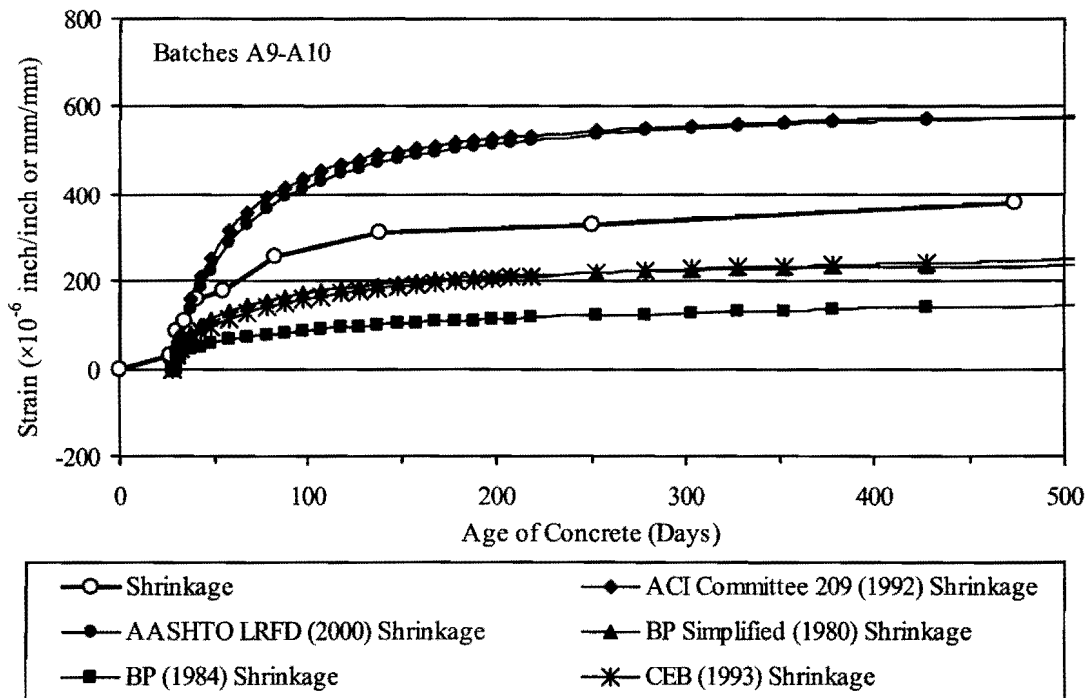
Figure 4.48. Shrinkage Strains of Prism Specimens for Batches A9-A10.

190
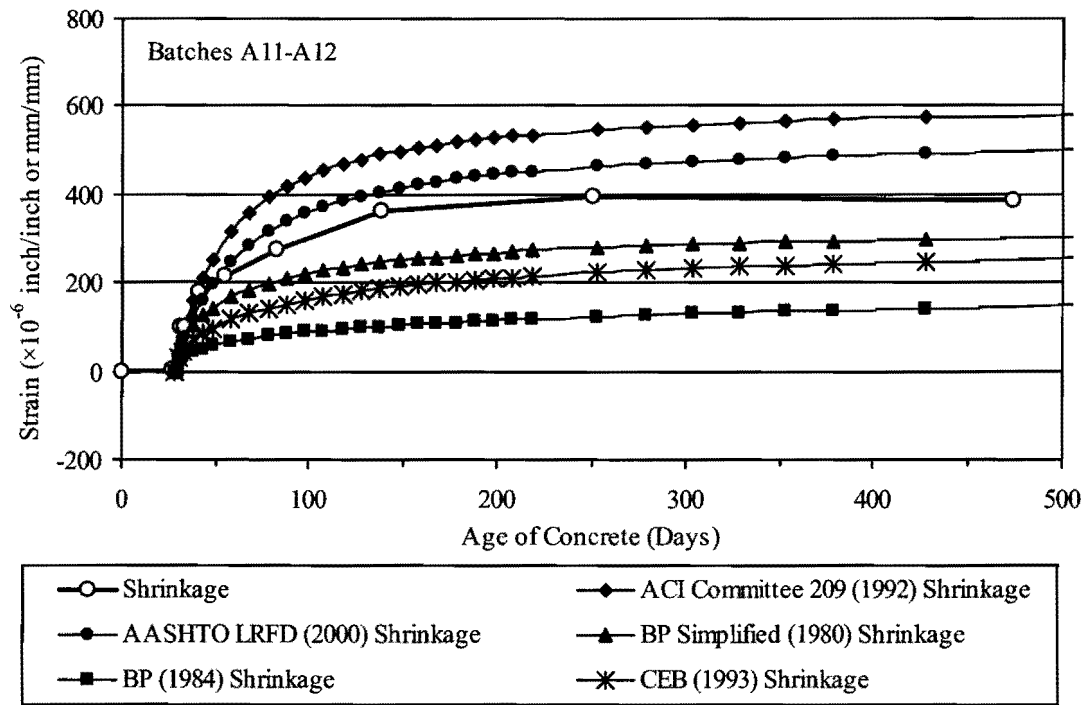
Figure 4.49. Shrinkage Strains of Prism Specimens for Batches A11-A12.
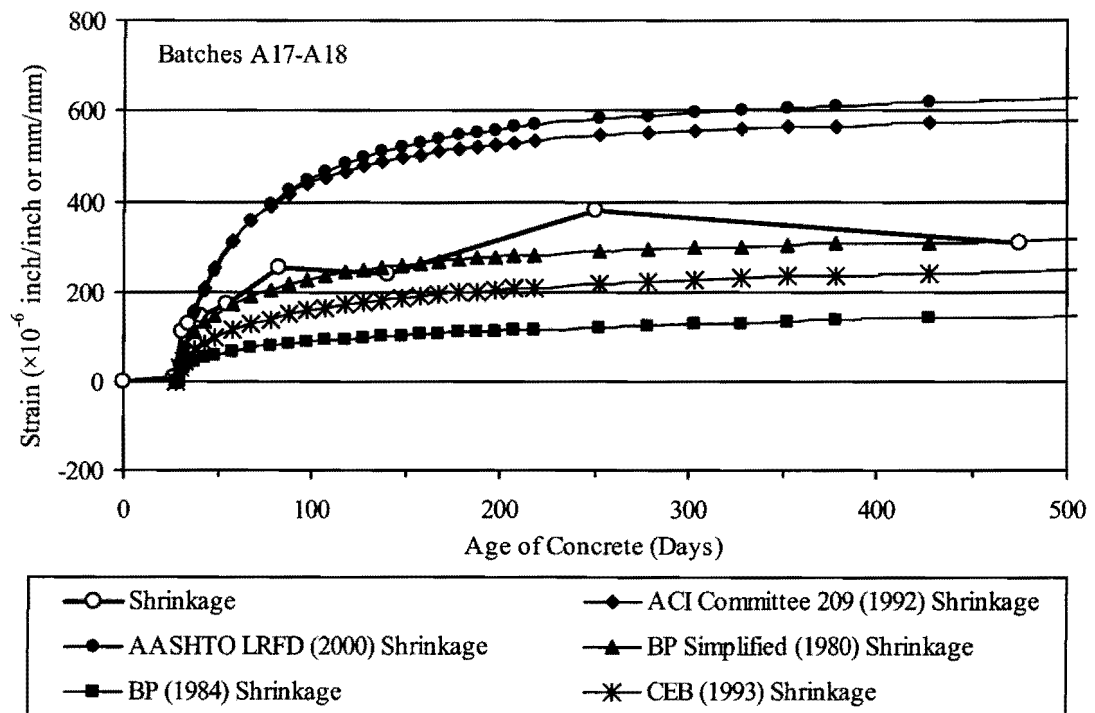
Figure 4.50. Shrinkage Strains of Prism Specimens for Batches A17-A18.

191
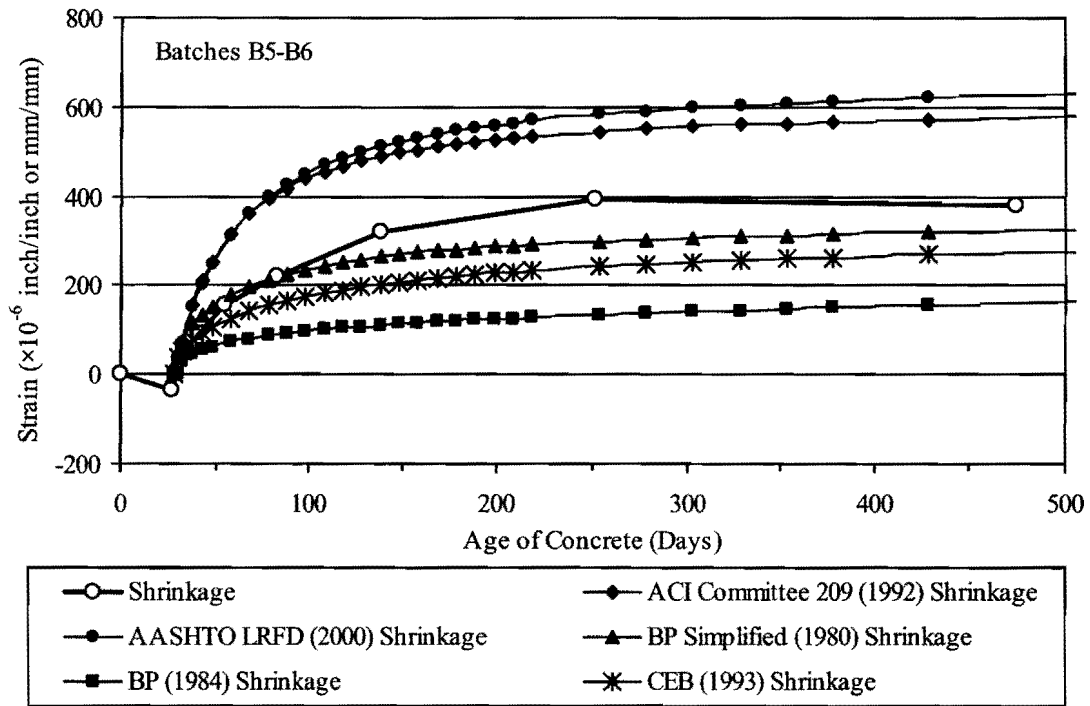
Figure 4.51. Shrinkage Strains of Prism Specimens for Batches B5-B6.
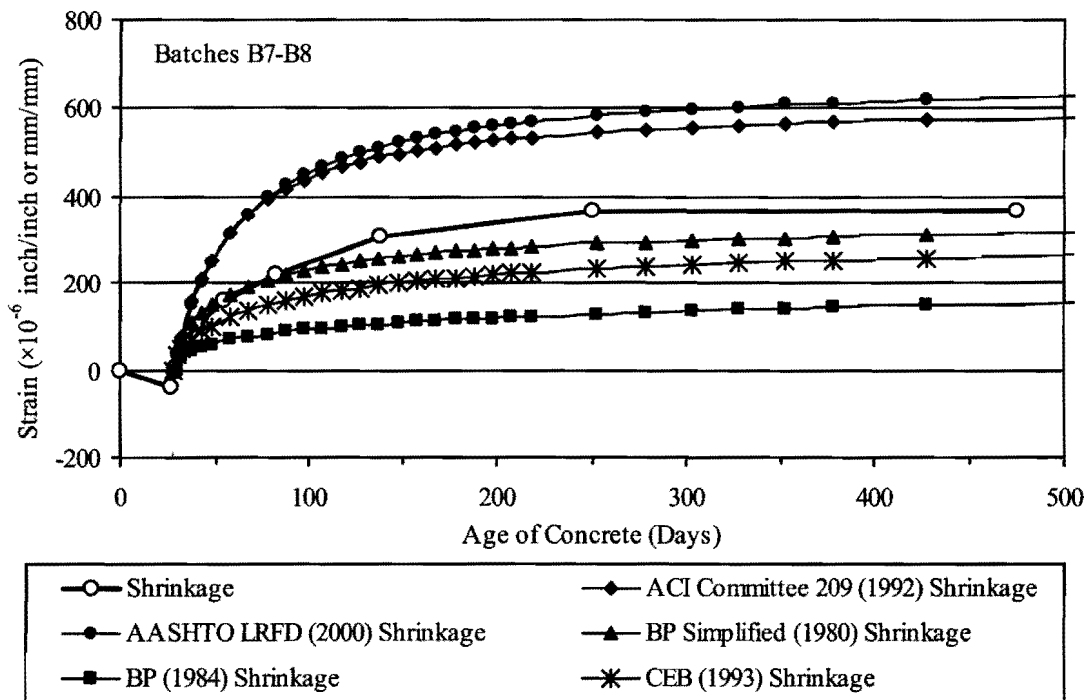
Figure 4.52. Shrinkage Strains of Prism Specimens for Batches B7-B8.

192
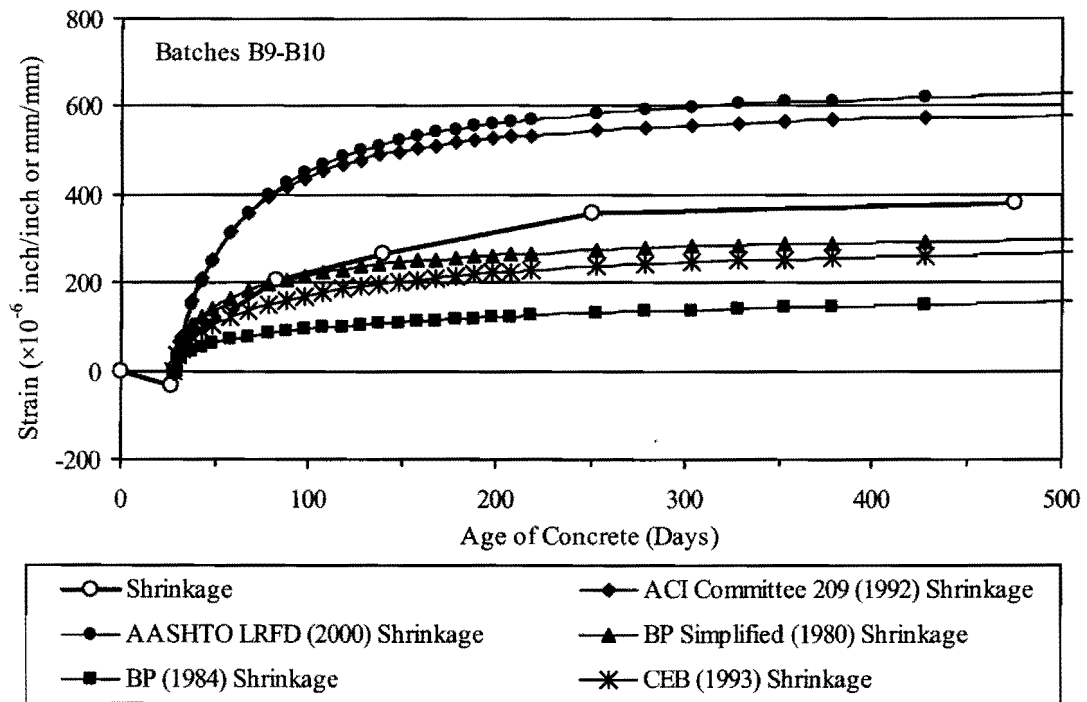
Figure 4.53. Shrinkage Strains of Prism Specimens for Batches B9-B10.
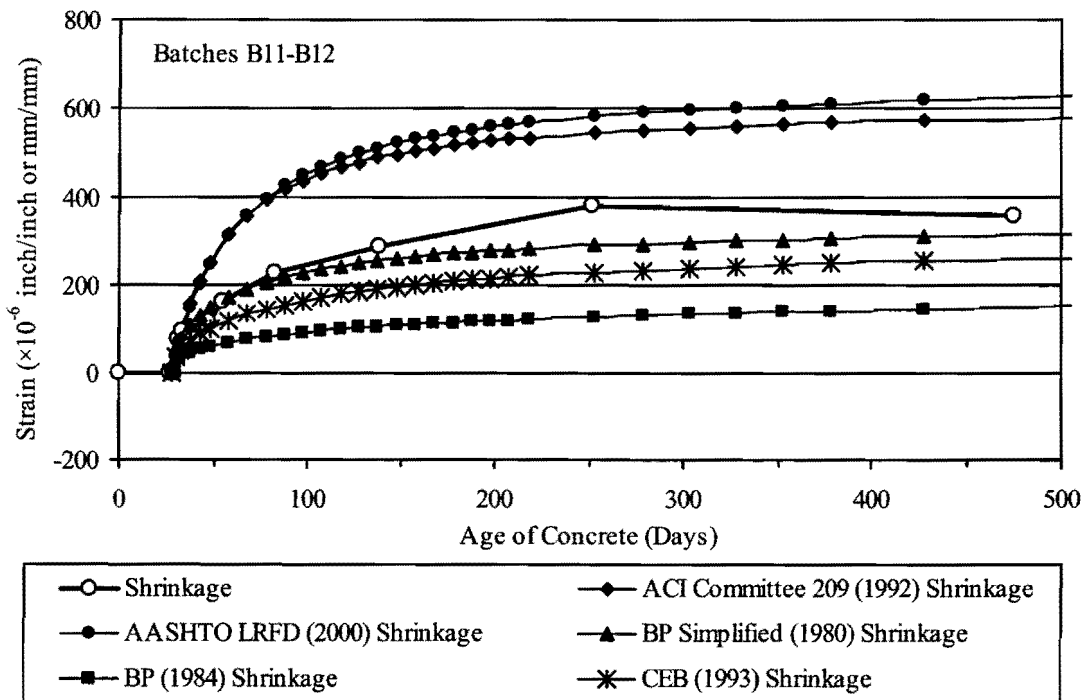
Figure 4.54. Shrinkage Strains of Prism Specimens for Batches B11-B12.
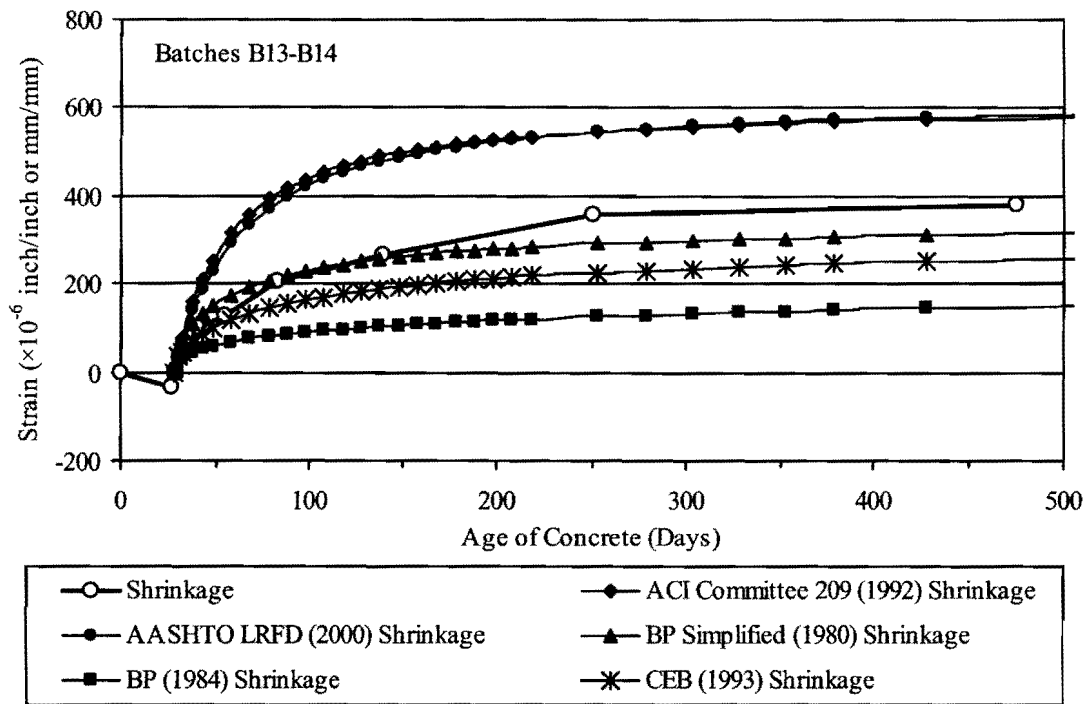
Figure 4.55. Shrinkage Strains of Prism Specimens for Batches B13-B14.
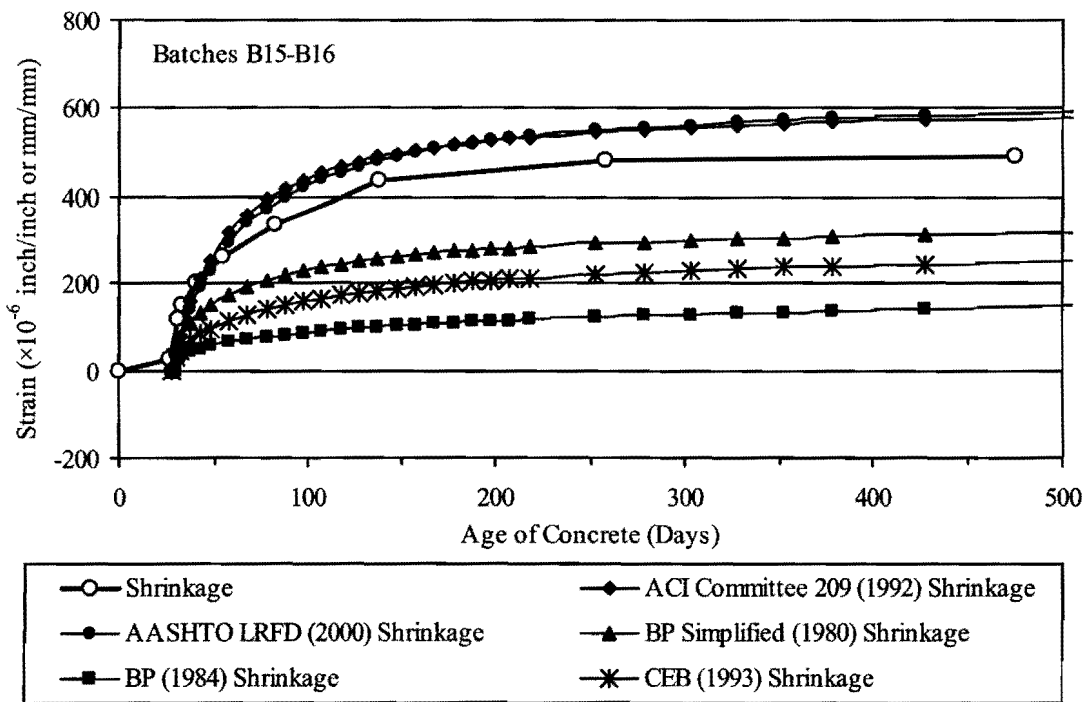
Figure 4.56. Shrinkage Strains of Prism Specimens for Batches B15-B16.

194
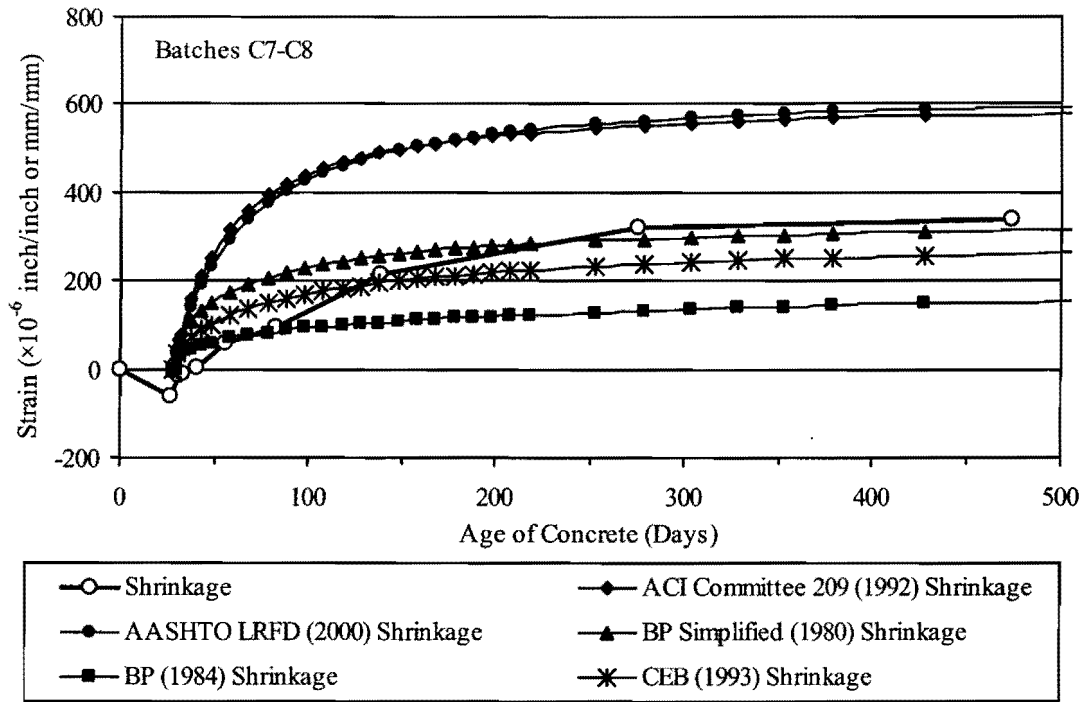
Figure 4.57. Shrinkage Strains of Prism Specimens for Batches C7-C8.
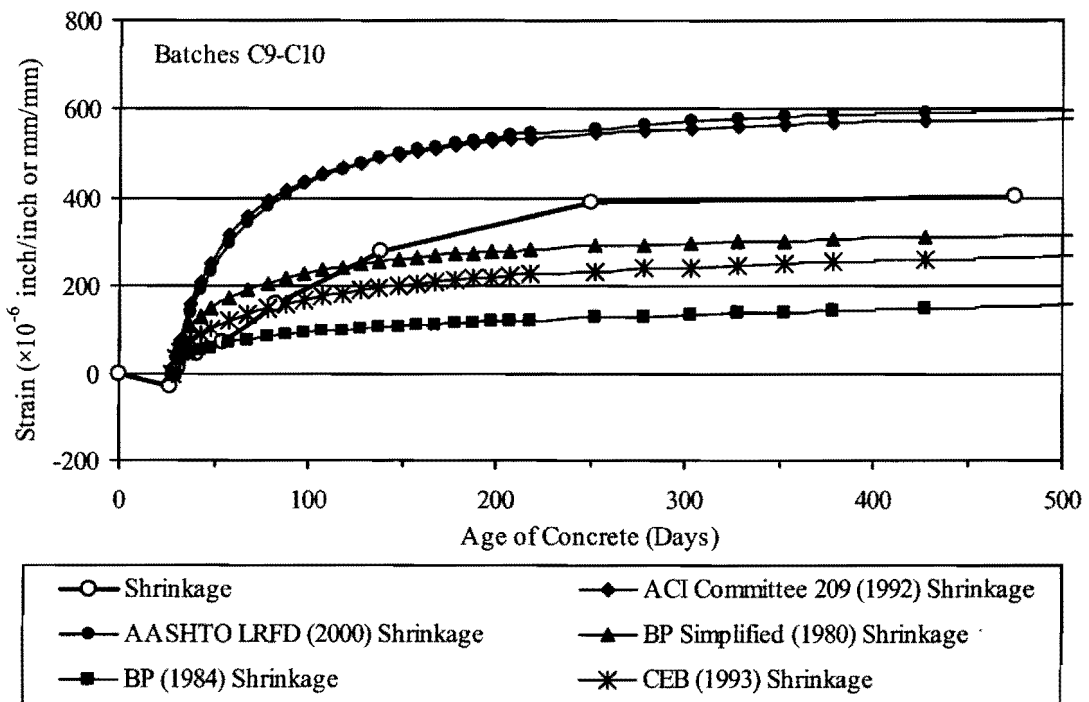
Figure 4.58. Shrinkage Strains of Prism Specimens for Batches C9-C10.

195
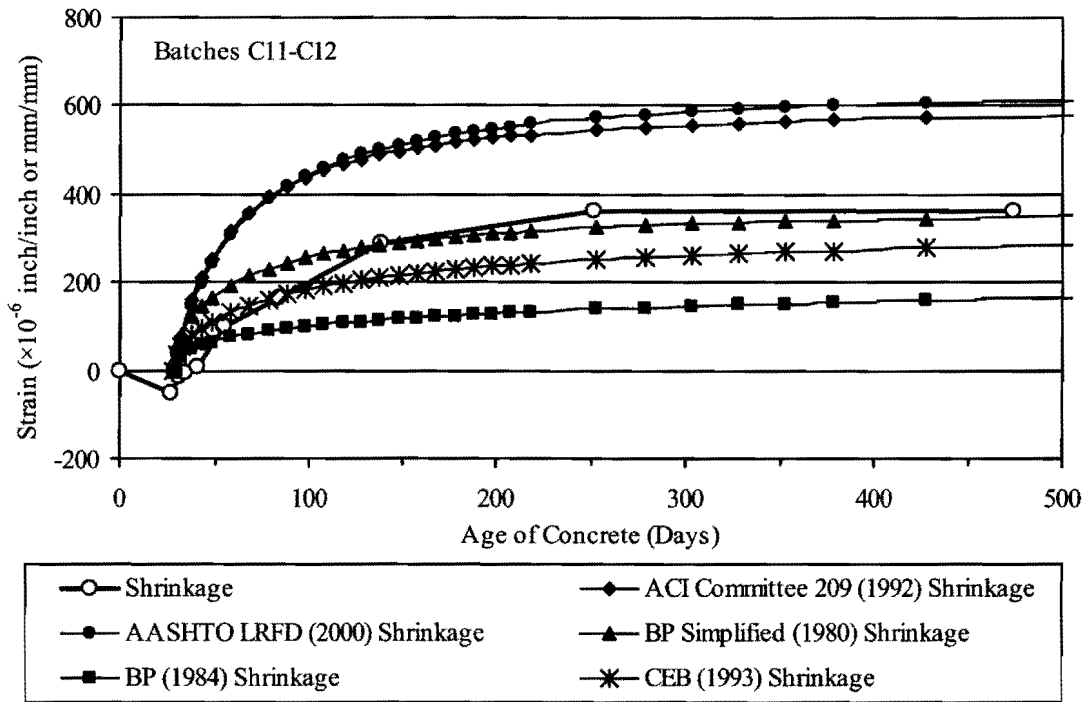
Figure 4.59. Shrinkage Strains of Prism Specimens for Batches C11-C12.
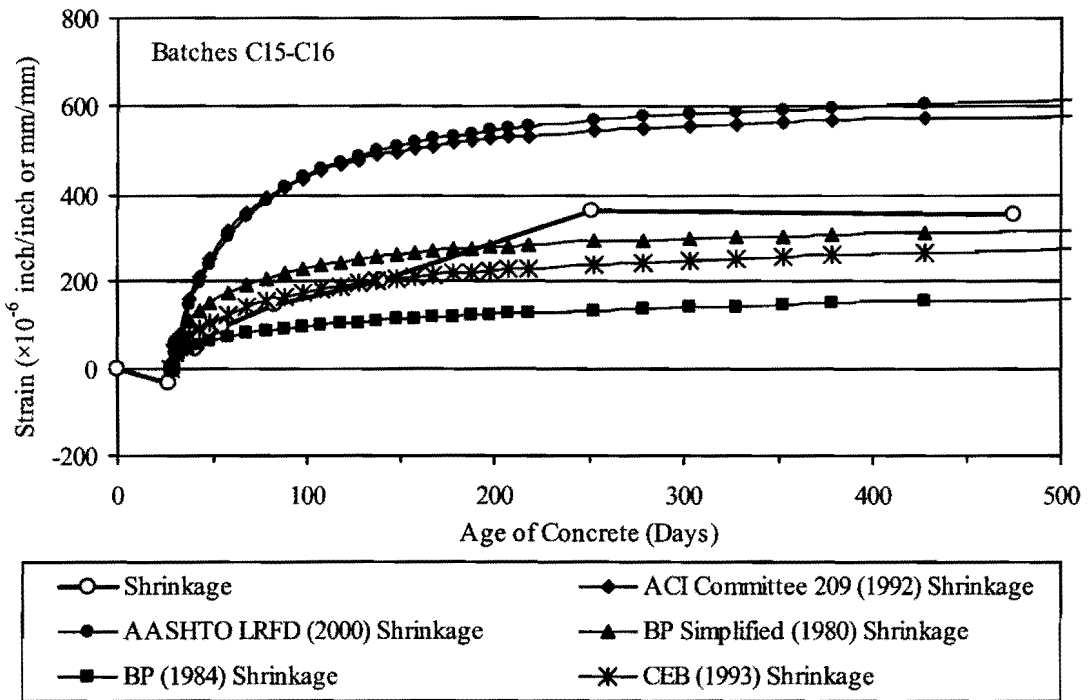
Figure 4.60. Shrinkage Strains of Prism Specimens for Batches C15-C16.

196
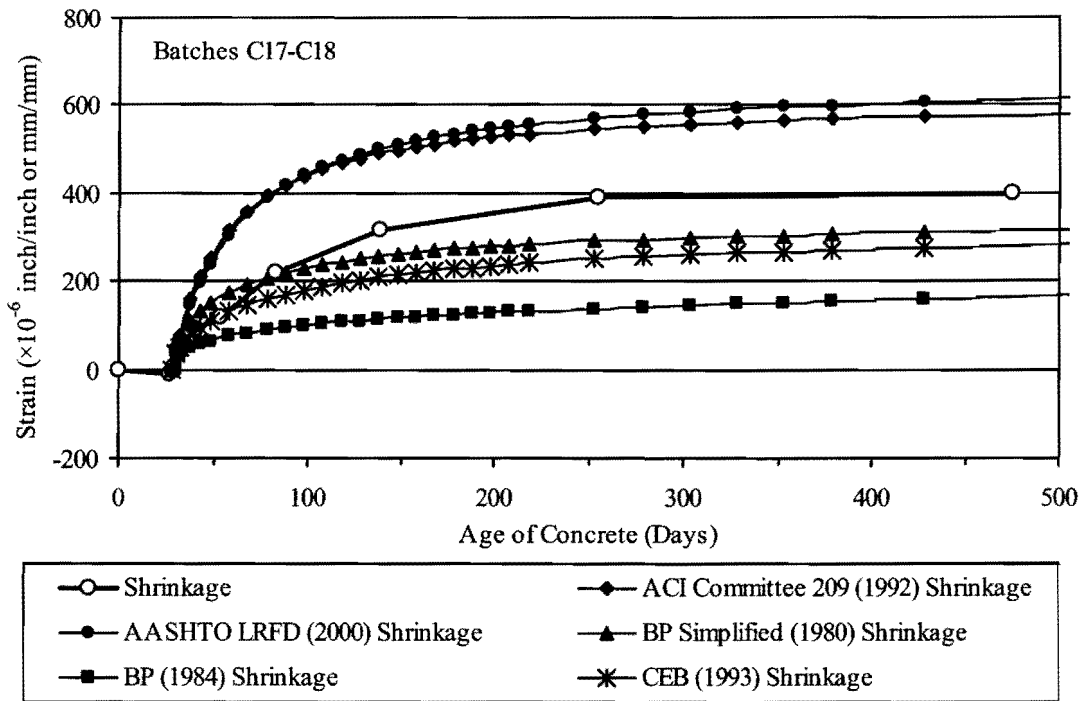
Figure 4.61. Shrinkage Strains of Prism Specimens for Batches C17-C18.

The comparisons between the measured shrinkage strain for prism specimens and predicted strains based on mixture information yield the same conclusion as for the unloaded control cylindrical specimens from the creep test (also called shrinkage specimens). The ACI Committee 209 (1992) and AASHTO LRFD Specifications (2000) equations overestimate the shrinkage stains measured for the HSC samples in this project. By the time the initial readings have occurred (first 28 days of drying), these two equations typically provide an upper bound to the measured shrinkage values. Therefore, the current AASHTO expression can be said to be conservative in estimating shrinkage for the duration considered in this project. The remaining three expressions underpredicted the measured shrinkage values. In most cases, the simplified model from Bažant and Panula (1980) tended to provide the closest prediction of the shrinkage strains, although this is an under-prediction. The CEB-FIP Model Code 1990 (CEB 1993) expression gave a slightly lower curve, and the equation from Bažant and Panula (1984) gave an even smaller predicted shrinkage.

197

For the prediction of shrinkage for the prism specimens, the ambient relative humidity and temperature were also assumed to be constant at 50 percent and 70 °F (21.1 °C), respectively. The relative humidity and temperature in the laboratory where the shrinkage specimens were stored were recorded only at the times that the shrinkage readings were taken. This location is different than where the creep specimens and their control specimens were stored. The temperature and relative humidity measurements for the prism specimens are shown in Figure 4.62.
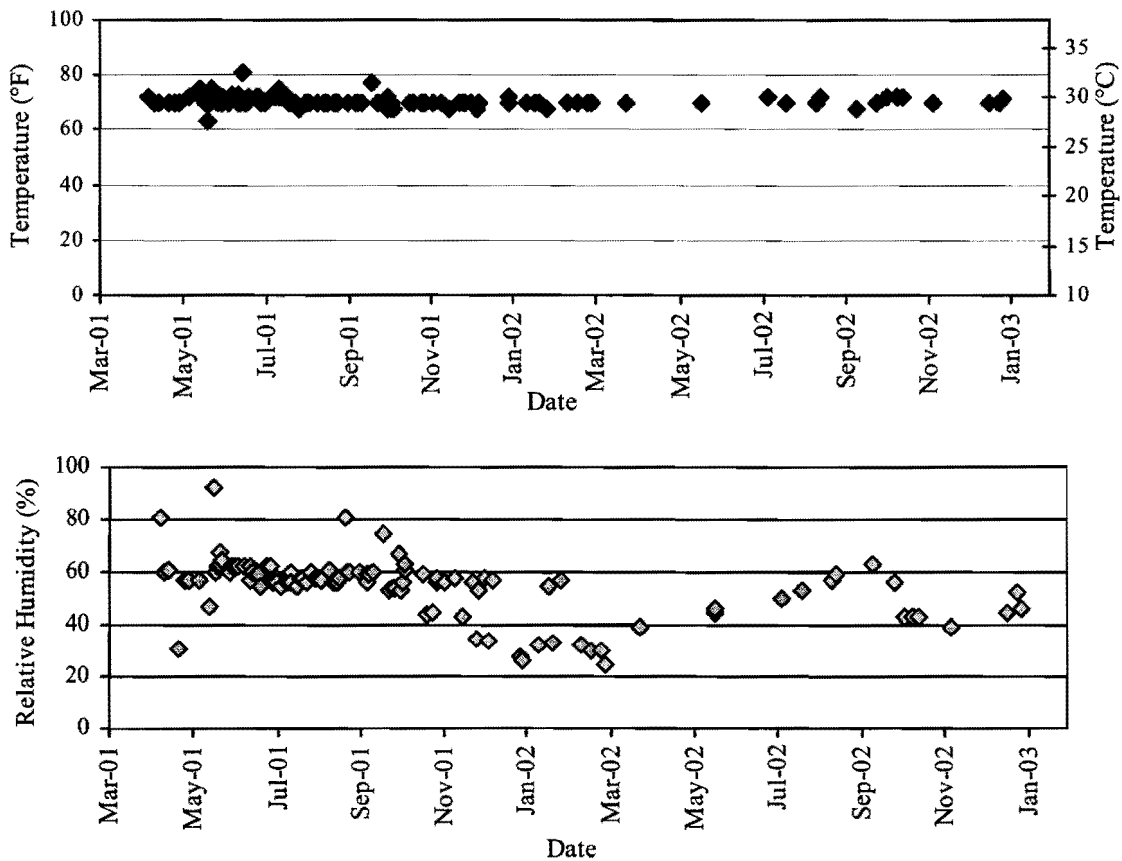
Figure 4.62. History of Temperature and Relative Humidity for Shrinkage Test.

A comparison of the creep coefficients (defined as the ratio between the additional strain due to creep and the initial elastic strain) is presented in Figure 4.63. The line types are consistent for samples corresponding to each precaster. The samples show relatively stable creep coefficients for the later readings, although a small positive slope can be observed.
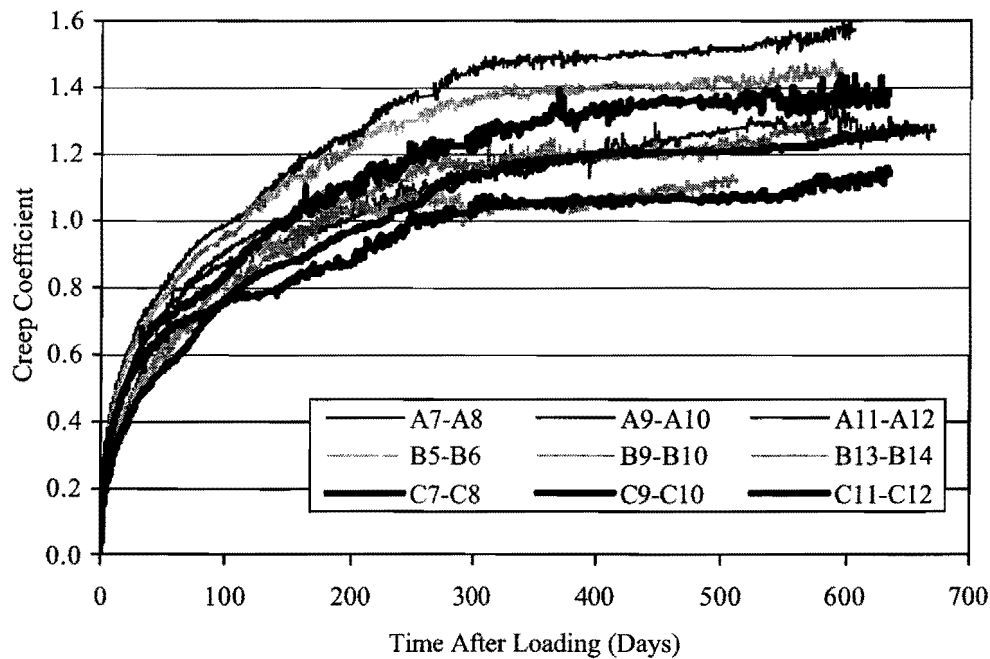
Figure 4.63. Comparison of Creep Coefficients.

It can be seen that the creep coefficient can be quite different among the samples from a particular precaster even though the concrete has the same mixture proportions, as in the case of concrete mixtures from Precasters B and C. Part of this may be due to the variations in concrete batching, mixing, and curing; as well as testing conditions of each sample set. Table 4.49 provides a summary of creep coefficients at 500 days and the creep coefficients for the last available reading. Compared within the same precaster, the set that has a higher compressive strength at 28 days tends to have a smaller creep coefficient at 500 days. However, as noted above, there are many more factors that affect the creep of concrete other than the associated compressive strength. Additional factors include differences in the temperature and humidity history during curing for each set. It should be noted that the environment in the laboratory where all the samples were stored could not be strictly controlled (see Figure 4.45).

199

Table 4.49. Comparison of Creep Coefficients.

Batch No.	Design f'_c Classification (psi)	28-Day Compressive Strength (psi)	Creep Coefficient at 500 Days	Creep Coefficient at Last Reading	Last Reading (Days)
A7-A8	6000	9657	1.26	1.26	670
A9-A10	8000	11508	1.22	1.26	650
A11-A12	10000	9853	1.52	1.57	600
B9-B10	6000	9896	1.23	1.27	580
B13-B14	8000	9993	1.12	1.12	510
B5-B6	10000	9258	1.43	1.45	590
C7-C8	6000	9506	1.20	1.27	650
C11-C12	8000	8586	1.35	1.37	630
C9-C10	10000	9734	1.07	1.14	630
		Minimum	1.07	1.12	
		Average	1.27	1.30	
		Maximum	1.52	1.57	

A comparison of the shrinkage strains from the control specimens in the creep test is presented in Figure 4.64. Similar plots with the data from prism specimens are shown in Figure 4.65. In each graph, a consistent line type is used to identify samples from a particular precaster. From Figure 4.64, all the specimens appear to show similar shrinkage values at later ages. In contrast, Figure 4.65 shows that the shrinkage can be quite different from precaster to precaster. There appears to be no correlation between the shrinkage and the actual 28-day compressive strength for either set of tests.

Comparisons of shrinkage from both tests are provided for each precaster in Figures 4.66 through 4.68. In each graph, a consistent line type is used to identify control cylinders and shrinkage prisms from the same sample set. Additional shrinkage prisms that came from different batches than the control cylinders are also included for each precaster.
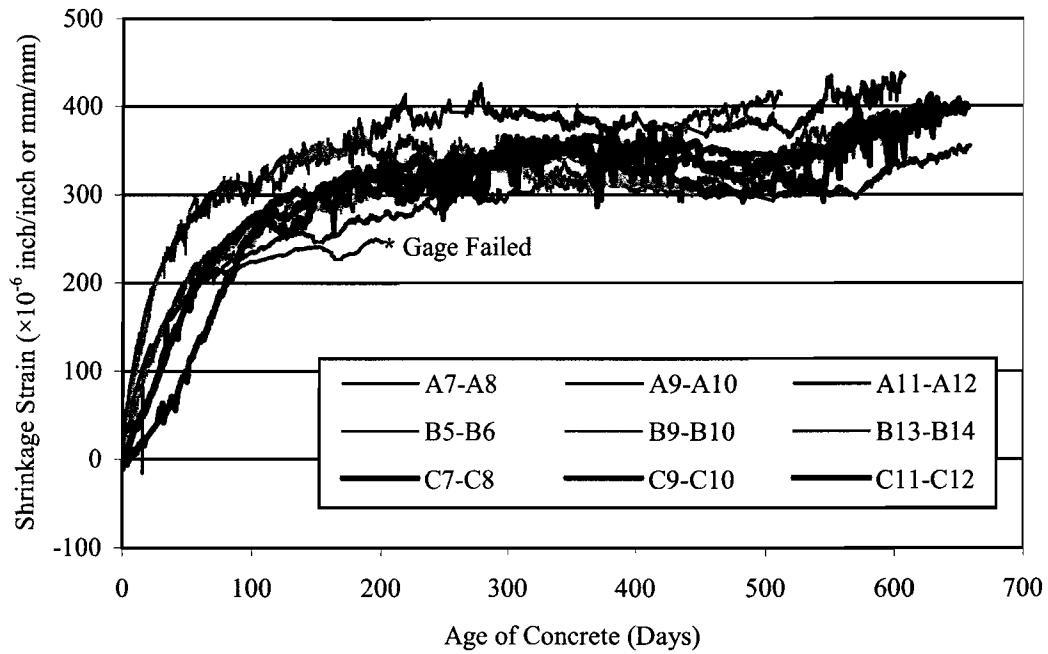
Figure 4.64. Comparison of Shrinkage Strains of Control Specimens from Creep Test.
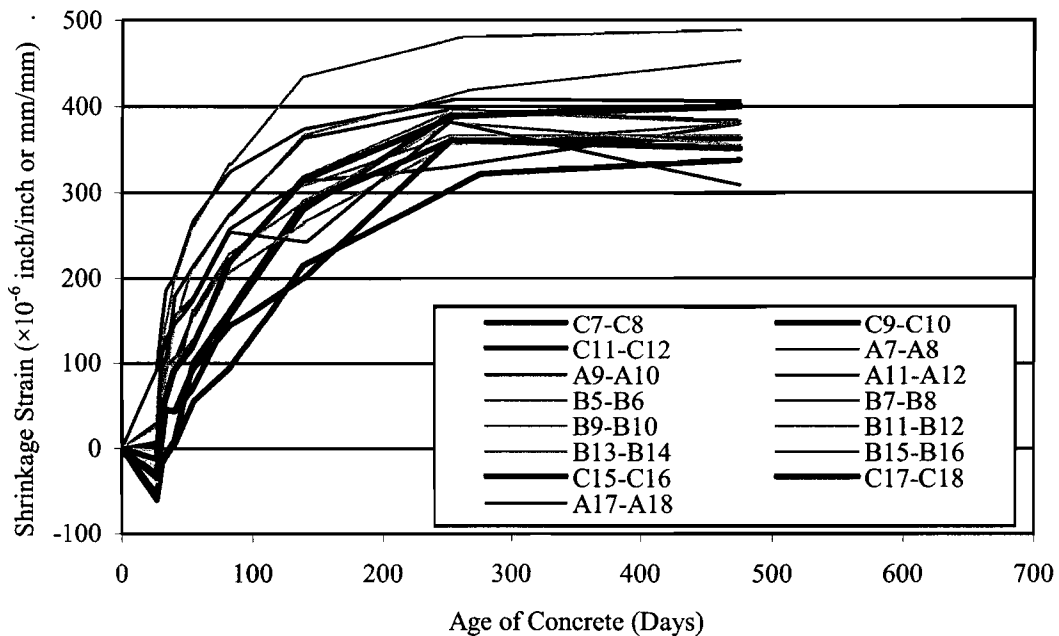
Figure 4.65. Comparison of Shrinkage Strains of Prism Specimens.

201
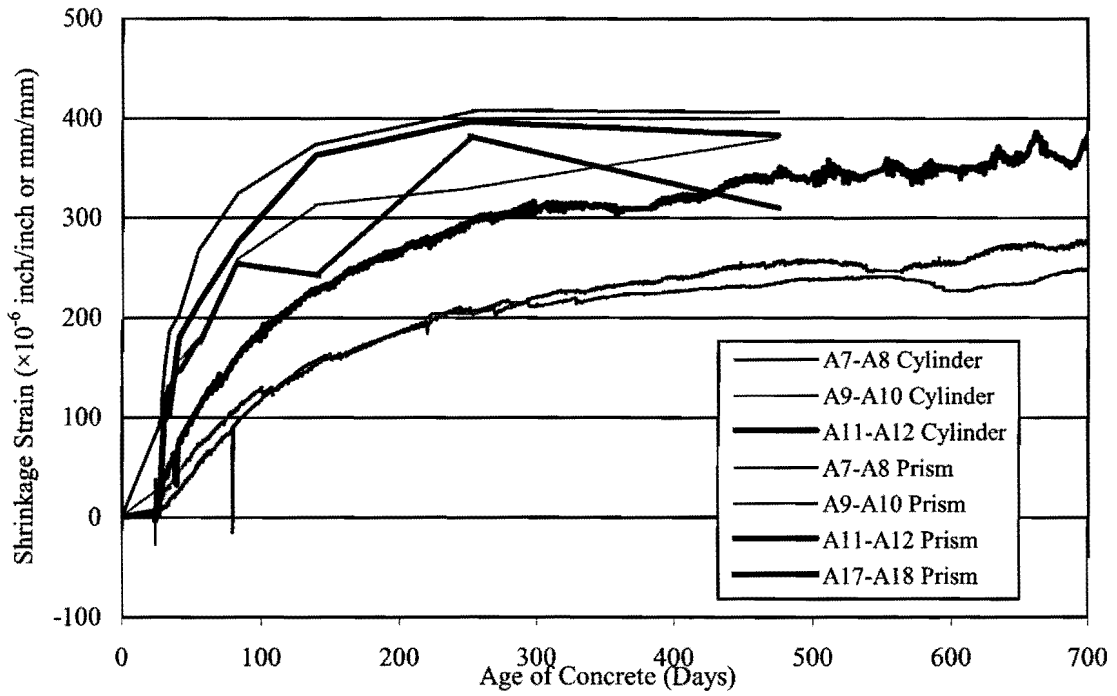
Figure 4.66. Comparison of Shrinkage Strains for Precaster A.
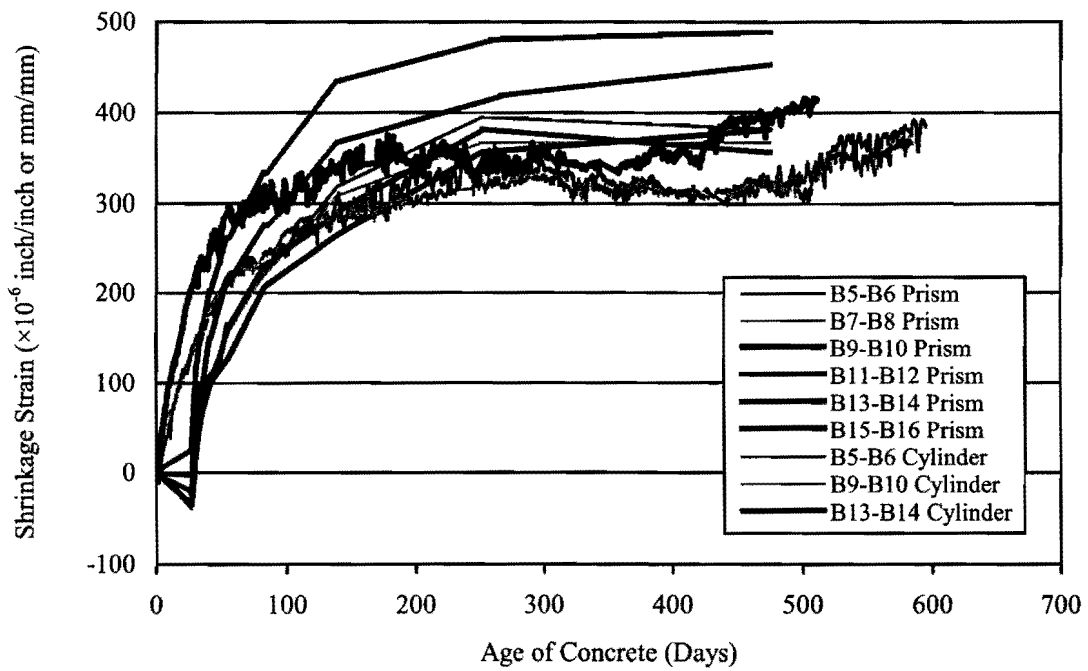
Figure 4.67. Comparison of Shrinkage Strains for Precaster B.

202
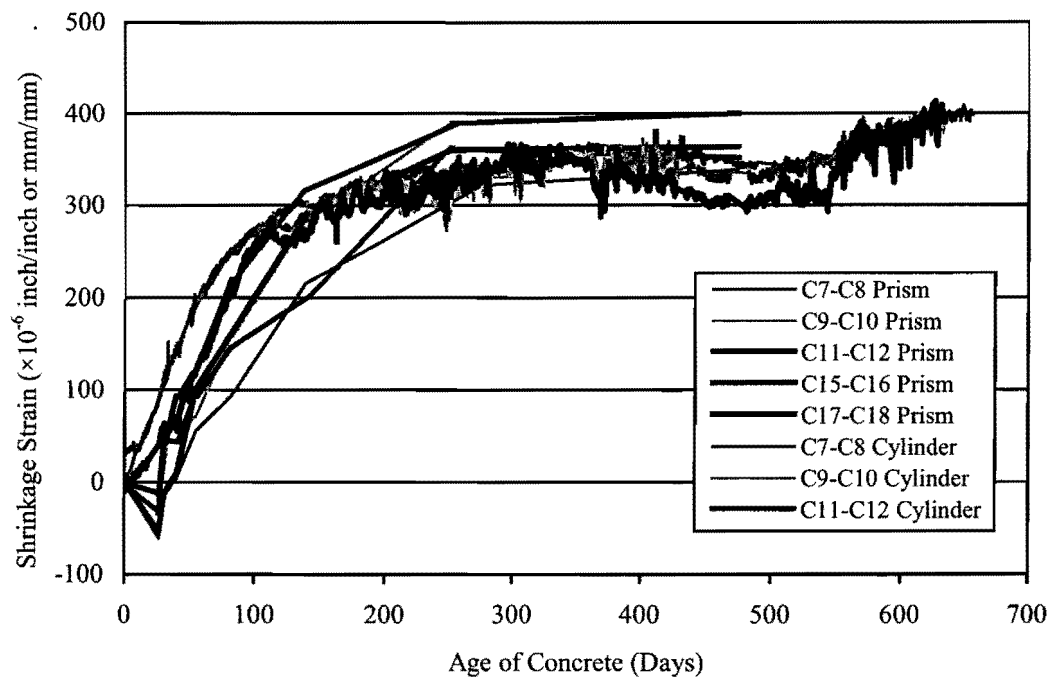
Figure 4.68. Comparison of Shrinkage Strains for Precaster C.

Comparing the shrinkage strains from two tests (Figures 4.66 through 4.68), it can be seen that there are some inconsistencies between the shrinkage at the same age for each batch. This is mainly due to the different ages at first drying and the curing condition during the test. For the control specimens of the creep test, each specimen was moist-cured for 7 days before the shrinkage measurements began, at which time it was put into the laboratory and allowed to dry. On the other hand, the length of a prism specimen was first measured at one day after casting, and then the specimen was cured in a lime solution for 28 days before it was allowed to dry. For the prism specimens, some sets of samples exhibited swelling between the initial and second readings when they were cured in the lime solution. The trend that the drying shrinkage of concrete is lower when the drying begins at later ages is not seen here, as the shrinkage of prism specimens appears to be in the same range as the shrinkage for the control specimens of the creep test. This may be because the modulus of elasticity of concrete, which is often used as an indication of the ability to resist the shrinkage of concrete, is not substantially different between the age of 7 days to 56 days (Section 4.2.2.1). In addition, it may be because the differences in the drying environment and variability inherited in both tests have a greater effect than the effect

203

of the age at first drying. Moreover, the difference in the shrinkage can be attributed to the different types of specimens used for the two tests. The shape of the specimen may affect the development of shrinkage even though they all have the same volume-surface ratio.

It can be seen that the variation of shrinkage measured for the control cylinders is somewhat lower in Figure 4.64 compared with that for the prisms shown in Figure 4.65. This may be due to the effect of autogenous shrinkage. At one day after casting, the hydration of concrete is not yet completed. As a result, autogenous shrinkage can continue developing after the initial reading in the prism specimen. This can be seen from some specimens that show shrinkages between the initial and second reading. Therefore, the shrinkage shown in Figure 4.65 is the combination of the autogenous shrinkage and the drying shrinkage, and a more significant difference in the shrinkage is observed for the different precasters. On the other hand, at 7 days, a larger portion of the hydration has been completed, and the autogenous shrinkage after this time may be negligible. As a result, the shrinkage strains in Figure 4.64 can be attributed to the drying shrinkage only (the carbonation shrinkage is usually negligible under these conditions). The drying shrinkage depends mainly on the ambient relative humidity. The mixture proportion and materials used are considered to be of lesser importance. Therefore, the difference between the shrinkage among precasters is less pronounced in this case.

Concrete samples from Precasters A and B appear to have larger shrinkage strains than samples from Precaster C, despite the use of a lower water-cement ratio and a higher measured modulus of elasticity of concrete for Precaster A. This indicates that other factors have a greater impact on the shrinkage than the water-cement ratio and modulus of elasticity. The difference may be related to the type of the coarse aggregate. The two sample sets that give the highest final shrinkage values for Precaster B are those using river gravel for the coarse aggregate (B13-B14 and B15-B16), while the other samples from the same precaster use crushed limestone. The smooth surface of the river gravel used for all Precaster A and some Precaster B mixtures may not help restrain the shrinkage as well as the rough surface of the crushed limestone aggregate used for all Precaster C and some Precaster B mixtures. In addition, the differences in cement and chemical admixtures used can affect the shrinkage of the concrete.

204

In basic design procedures, a long-term value of the creep coefficient and shrinkage strain is of interest for estimating prestress losses; the prediction of the creep and shrinkage with time, as described in Section 4.2.5.1, is often not necessary. The following section discusses the assumptions behind the formulas for estimating creep and shrinkage losses specified in the standards. These estimates are then compared with the measured data.

4.2.5.2.1   Ultimate Creep and Shrinkage from Design Equations for Prestress Losses

Zia et al. (1979) proposed the following equation to estimate the prestress loss due to creep (Δf_{pCR}):

$$\Delta f_{pCR} = K_{CR} \left(\frac{E_p}{E_c} \right) (f_{cgp} - \Delta f_{cdp}) \qquad (4.16)$$

where K_{CR} is 2.0 for normal weight concrete, E_c is the modulus of elasticity of concrete at 28 days, E_p is the modulus of elasticity of the prestressing strand, f_{cgp} is the stress in concrete at the level of the prestressing strand due to prestressing force at transfer and the self-weight of the member, and Δf_{cdp} is the change in concrete stress at the center of gravity of prestressing steel due to additional permanent loads after prestress transfer. Rearranging the terms and substituting the value of K_{CR}:

$$\left(\frac{\Delta f_{pCR}}{E_p} \right) = 2.0 \left(\frac{f_{cgp} - \Delta f_{cdp}}{E_c} \right) \qquad (4.17)$$

$$\Delta \varepsilon_{pCR} = 2.0 \varepsilon_{ci} \qquad (4.18)$$

where $\Delta \varepsilon_{pCR}$ is the change in strain at the center of gravity (c.g.) level of the prestressing strand due to the creep of concrete and ε_{ci} is the initial sustained stress of the concrete at the c.g. level

of the prestressing strands. For pretensioned members, the change in strain of the prestressing strain is equal to the change in strain of concrete at the same level, $\Delta\varepsilon_{cCR}$. Therefore:

$$\frac{\Delta\varepsilon_{pCR}}{\varepsilon_{ci}} = \frac{\Delta\varepsilon_{cCR}}{\varepsilon_{ci}} = 2.0 \tag{4.19}$$

The creep coefficient is defined as the ratio of the creep strain to the initial strain due to sustained load. Therefore, from Equation 4.19, the creep coefficient is assumed to be 2.0. In fact, the assumed creep coefficient should be slightly less than 2.0 because the modulus of elasticity of concrete, E_c, used in the equation is the 28-day E_c, not at the age when the prestressing strands are released. Because prestressing strands are usually released prior to 28 days (releases at 1 day were commonly observed in this project), the modulus of elasticity at release would be less than that at 28 days. Therefore, the actual initial strain of concrete should be higher.

For estimating the shrinkage loss (Δf_{pSR}), Zia et al. (1979) recommended the following equation:

$$\Delta f_{pSR} = 8.2 \times 10^{-6} K_{SH} E_p \left(1 - 0.06\frac{V}{S}\right)(100 - H) \tag{4.20}$$

where K_{SH} is equal to 1.0 for pretensioned members and H is the relative humidity in percent. Rearranging terms and substituting the value of K_{SH}:

$$\left(\frac{\Delta f_{pSR}}{E_p}\right) = 8.2 \times 10^{-6} \times 1.0 \times \left(1 - 0.06\frac{V}{S}\right)(100 - H) \tag{4.21}$$

Note that the left term is the change in strain in prestressing strands due to shrinkage, $\Delta\varepsilon_{pSR}$. Substituting the volume-surface ratio of 1.0 for a 4×8 inch (100×200 mm) specimen and using 50 percent relative humidity standard conditions:

206

$$\Delta\varepsilon_{pSR} = 8.2\times10^{-6}\times1.0\times(1-0.06\times1.0)(100-50) = 385\times10^{-6} \text{ inch/inch} \qquad (4.22)$$

Again, the change in strain of prestressing strands is equal to the change in strain of concrete at the same level for a pretensioned member:

$$\Delta\varepsilon_{cSR} = 385\times10^{-6} \text{ inch/inch} \qquad (4.23)$$

where $\Delta\varepsilon_{cSR}$ is the change in strain of concrete due to shrinkage at the level of the c.g. of the prestressing strands. This is, in fact, the ultimate shrinkage strain.

The loss due to creep in Section 5.9.5.4.3 of the AASHTO LRFD Specifications (2000) is calculated by the equation proposed by Hernandez and Gamble (1975) as:

$$\Delta f_{pCR} = 12 f_{cgp} - 7.0\Delta f_{cdp} \qquad (4.24)$$

The term Δf_{cdp} is equal to zero because there is no additional load after the first loading. Dividing both sides by the modulus of elasticity of the prestressing strand will result in a change in strain:

$$\Delta\varepsilon_{pCR} = \frac{\Delta f_{pCR}}{E_p} = \frac{12 f_{cgp}}{E_p} \qquad (4.25)$$

To obtain the creep coefficient, divide both sides with the elastic strain, $\varepsilon_{ci} = \dfrac{f_{cgp}}{E_c}$. Note here that the change in strain of the prestressing strand is equal to the change in strain of concrete at the same level in a pretensioned member:

$$\frac{\Delta\varepsilon_{cCR}}{\varepsilon_{ci}} = \frac{\Delta\varepsilon_{pCR}}{\varepsilon_{ci}} = \frac{12 E_c}{E_p} \qquad (4.26)$$

The left term in Equation 4.26 is equal to the creep coefficient. The modulus of elasticity of the prestressing strand can be taken as 29×10^6 psi (200 GPa). For example, if the modulus of elasticity of concrete is 6,000,000 psi, then the creep coefficient will be 2.48.

For estimating shrinkage loss, the following equation is recommended in Section 5.9.5.4.2 of the AASHTO LRFD Specifications (2000):

$$\Delta f_{pSR} = 17 - 0.150H \qquad (4.27)$$

Dividing both sides by the modulus of elasticity of the prestressing strands to obtain the change in strain due to shrinkage and substituting the relative humidity of 50 percent:

$$\varepsilon_{pSR} = \frac{\Delta f_{pSR}}{E_p} = \frac{17 - 0.150H}{29000} = 328 \times 10^{-6} \text{ inch/inch} \qquad (4.28)$$

Again, the change in strain of the prestressing strands is equal to the change in strain of concrete at the same level. Therefore, the ultimate shrinkage strain of concrete assumed in this equation is 328 $\mu\varepsilon$.

4.2.5.2.2   Comparison with Experimental Data

The creep coefficients and shrinkage strains from the tests are summarized in Table 4.50 and Table 4.51, respectively, along with the ultimate creep coefficients and ultimate shrinkage strains calculated from prediction and design equations. The ultimate creep coefficients and shrinkage strains from the prediction formulas (in Section 4.2.5.1) are the creep coefficient and shrinkage strains at 75 years, the design lifetime of a structure. The ultimate creep coefficients and shrinkage strains from design equations are discussed in Section 4.2.5.1.

Table 4.50. Summary of Ultimate Creep Coefficients.

	Batch Number								
	A7 **A8**	**A9** **A10**	**A11** **A12**	**B5** **B6**	**B9** **B10**	**B13** **B14**	**C7** **C8**	**C9** **C10**	**C11** **C12**
ASTM C 512									
Creep Coefficient	1.26	1.26	1.57	1.45	1.27	1.12	1.27	1.14	1.37
Duration (days)	670	650	600	590	580	510	650	630	630
Predicted Ultimate Creep Coefficient ($\mu\epsilon$)									
AASHTO	2.6	2.3	2.0	2.1	2.5	2.2	2.6	2.1	2.2
AASHTO Design	2.9	2.9	2.8	2.5	2.4	2.3	2.2	2.3	2.1
ACI 209	2.9	3.0	2.3	2.8	2.8	2.8	2.6	2.6	2.6
CEB-FIP	3.1	2.8	3.0	3.1	3.0	3.0	3.1	3.1	3.3
BP	4.8	6.2	4.8	4.7	5.3	5.2	5.7	5.6	4.9
BP (Simplified)	7.3	11.9	7.3	6.0	6.8	7.5	7.6	7.3	6.0
Zia et al.*	2.0	2.0	2.0	2.0	2.0	2.0	2.0	2.0	2.0

Notes:
* = Value does not depend on mixture properties
AASHTO = Section 5.4.2.3.2 of AASHTO LRFD Specifications (2000)
AASHTO Design = Equation 4.26
ACI 209 = Section 2.4 to 2.6 of ACI Committee 209 (1992)
CEB-FIP = Section 2.16.4.3 of CEB-FIP Model Code 1990 (CEB 1993)
BP = Bažant and Panula (1978b, 1978c, 1978d, 1979a, 1979b, 1984)
BP Simplified = Bažant and Panula (1980)
Zia et al. (1979) = Equation 4.19

Table 4.51. Summary of Ultimate Shrinkage Strains.

	Batch Number														
	A7	A9	A11	A17	B5	B7	B9	B11	B13	B15	C7	C9	C11	C15	C17
	A8	A10	A12	A18	B6	B8	B10	B12	B14	B16	C8	C10	C12	C16	C18
ASTM C 157 (Prism Specimens)															
Shrinkage (με)	407	381	383	310	382	367	381	355	453	489	402	363	407	352	400
Last Rdg. (weeks[+])	64	64	64	64	64	64	64	64	64	64	64	64	64	64	64
ASTM C 512 (Control Specimens of Creep Test)															
Shrinkage (με)	246	355	433	-	387	-	366	-	414	-	399	393	395	-	-
Duration (days)	670	650	600	-	590	-	580	-	510	-	650	630	630	-	-
Predicted Ultimate Shrinkage (με)															
AASHTO*	688	688	688	612	688	612	688	612	688	612	688	688	688	612	612
AASHTO Design*	328	328	328	328	328	328	328	328	328	328	328	328	328	328	328
ACI 209	675	698	601	672	758	674	758	673	708	633	719	724	743	657	659
CEB-FIP	375	289	367	255	394	326	361	301	360	324	382	382	425	353	360
BP	284	282	286	251	311	266	304	263	290	252	299	302	322	273	285
BP (Simplified)	323	320	326	287	354	305	346	301	330	287	340	343	366	313	326
Zia et al.*	385	385	385	385	385	385	385	385	385	385	385	385	385	385	385

Notes:

+ = Weeks after the second reading
* = Value does not depend on mixture properties
AASHTO = Section 5.4.2.3.3 of AASHTO LRFD Specifications (2000)
AASHTO Design = Equation 4.28
ACI 209 = Section 2.4 to 2.6 of ACI Committee 209 (1992)
CEB-FIP = Section 2.16.4.4 of CEB-FIP Model Code 1990 (CEB 1993)
BP = Bažant and Panula (1978a, 1979b, 1984)
BP Simplified= Bažant and Panula (1980)
Zia et al. (1979) = Equation 4.23

It should be noted that not all of the creep and shrinkage values from the tests shown in Tables 4.50 and 4.51 have stabilized enough to be considered as ultimate values. However, based on the plot in Figure 4.63, the creep coefficient curves begin to flatten at the creep coefficient values of about 1.0 to 1.5, which are considerably less than the majority of the creep coefficients from the equations listed in Table 4.50. Note that the creep coefficient from the simplified equation recommended by Bažant and Panula (1980) does not appear to converge to a limiting value. The ultimate creep coefficient values from the design equation and the equation for estimating the creep in the AASHTO LRFD Specifications (2000) are similar.

Comparing the shrinkage strains in Figures 4.64 and 4.65, with the ultimate shrinkage values in Table 4.51, indicates that the ultimate shrinkage values assumed for computing prestress losses recommended by Zia et al. (1979) (385 με) and the AASHTO LRFD Specifications (2000) (328 με) are reasonable considering the variations of the shrinkage tests. However, it should also be noted that these values are less than the maximum measured shrinkage strain among all the test samples.

The ultimate shrinkage from the equation proposed by Zia et al. (1979) and design equation from the AASHTO LRFD Specifications (2000) are in relatively close agreement with the Bažant and Panula (1978a, 1979b, 1984), Bažant and Panula (1980), and CEB-FIP Model Code 1990 (CEB 1993) equations. The ultimate shrinkage values from ACI Committee 209 (1992) and the AASHTO LRFD Specifications (2000) (equation for estimating shrinkage) appear to overestimate the ultimate shrinkage of the data by almost a factor of two in some cases, according to the latest measurements.

4.2.5.3 Discussion of Implications for Design Provisions

Based on the experimental data, the creep of the HSC in this project is overestimated by all of the design equations and the equations that estimate the development of creep with time, including the ACI 209 and AASHTO equations. On the other hand, the development of the shrinkage of HSC with time was most closely predicted using the Bažant and Panula (1980) expression, although this did result in an under-prediction of the shrinkage.

The ultimate shrinkage strain assumed in the equations to compute prestress losses due to shrinkage from ACI Committee 423 (Zia et al. 1979) and the AASHTO LRFD Specifications (2000) appears to be close to the expected values for the measured data, based on measurements for shrinkage at 450 to 600 days.

The creep and shrinkage from the test specimens could overestimate the actual creep and shrinkage because the humidity near the prestressing strands can be substantially higher than the humidity in the laboratory where specimens were stored. On the other hand, prestressed

members are released at 1 day rather than 7 days as the test specimens. This tends to increase the creep and can offset the effect of humidity.

When considering both the effect of creep and shrinkage, the loss due to time-dependent deformation of concrete appears to be overestimated in a standard design procedure based on measurements for the HSC samples in this project. In general, it is conservative when the actual long-term loss is less than the predicted value because the actual tensile stress at the bottom fiber of the beam and the compressive stress at the top fiber are less than the value calculated in the design and should be less than the allowable stresses. However, it is not clear just by considering the creep and shrinkage of concrete whether this will result in a conservative situation because the relaxation of the prestressing strands also depends on the creep and shrinkage of concrete. The interaction of the relaxation loss and the losses due to creep and shrinkage should be considered. If the combined effect of creep and shrinkage of concrete is significantly lower than the predicted value, then the sustained strain in the prestressing strands at any time will be larger than that used in the formulation of the relaxation loss. As a result, the rate of relaxation loss can be higher than predicted. If the resulting decrease in the actual versus specified creep loss is greater than the increase in the actual versus specified relaxation loss, the design will still be conservative.

5 SUMMARY AND CONCLUSIONS

5.1 SUMMARY

This research is Phase 1 of the TxDOT Project 0-2101, *Allowable Stresses and Resistance Factors for High Strength Concrete*. The objective of the overall project was to evaluate the allowable stresses and resistance factors in the AASHTO LRFD Specifications for design of HSC girders used in Texas bridges. Hueste et al. (2003a) summarized the complete project. Phase 1 of the project focused on evaluating the applicability of current prediction equations for estimation of mechanical properties of HSC and determining statistical parameters for mechanical properties of HSC. Phase 2 included defining the current state of practice and identifying critical areas for refining design provisions for HSC prestressed bridge girders (Hueste and Cuadros 2003). Phase 3 focused on assessing the impact of different curing conditions on the compressive and flexural strength of HSC and developing appropriate recommendations for HSC prestressed bridge girders (Hueste et al. 2003b).

As a first step toward evaluating the applicability of current AASHTO design provisions for HSC prestressed bridge members, Phase 1 of this project focused on evaluating the mechanical properties of HSC produced by Texas precasters. HSC samples were collected from three selected precasters in Texas. These precasters are considered to be representative of the eight precasters in Texas that produce prestressed bridge members at the time of this project. As much as possible, precasters were selected to cover different geographical locations in Texas, coarse aggregate type (coarse river gravel and crushed limestone), and precaster production capacities. For each precaster, concrete samples were categorized by specified design compressive strength into three classes, 41 ±7 MPa (6000 ±1000 psi), 55 ±7 MPa (8000 ± 1000 psi), and 69 ±7 MPa (10000 ±1000 psi), so that effects of the specified design compressive strength on other concrete properties could be observed. For each strength class, two collections were made from each precaster on different days to capture variability within mixtures used by a precaster for the same specified design compressive strength. Two sets of

concrete samples were made during each collection, sampling from two different batches of the same mixture on the same collection date, to account for variability in the mixing and batching procedures.

In the majority of cases, the concrete evaluated in the research project was obtained directly from the precast plants during casting of prestressed bridge members. However, for three collections, the concrete was specifically produced at the plant for the research project because these particular specified design strengths were not available from the precasters during the time frame of this program. In these cases, the precaster produced their standard concrete mixtures for the given specified design compressive strength. Type III high early strength portland cement was used for all concrete mixtures sampled in this project.

The samples were tested in the laboratory at 7, 28, and 56 days of age for compressive strength, modulus of rupture, splitting tensile strength, and modulus of elasticity. The experimental data were analyzed to determine mean values, bias factors, and coefficients of variation for each of these four mechanical properties. In addition, creep and shrinkage were monitored for a period of approximately 450 to 700 days, depending on the sample set. One-day compressive strength data were obtained from the precasters. In addition, analyses were performed to evaluate the applicability of prediction formulas in current design codes and the literature to HSC. Based on the mechanical properties determined for plant-produced HSC, a preliminary assessment of the current design provisions as they apply to HSC prestressed members was made, and areas for potential modification are identified.

5.2 CONCLUSIONS

The following conclusions were made based on the data obtained in the experimental program for HSC produced by Texas precasters. A summary of the statistical data is followed by general conclusions, and conclusions for each mechanical property are provided.

5.2.1 Summary of Statistical Data

Tables 5.1 and 5.2 provide a summary of the mean and coefficients of variation for compressive strength, modulus of elasticity, splitting tensile strength, and modulus of rupture obtained from the statistical analysis in this project.

Although the precasters for this project were selected to be representative of precasters in Texas, it was not possible to choose precasters in a completely random way. Therefore, for the determination of resistance parameters by simulations using statistical parameters of mechanical properties from this project, the maximum coefficient of variation and lowest mean among precasters are considered conservative for representing the overall practice in Texas. Alternatively, simulations can be performed using the mean and coefficient of variation for each precaster (because the lowest mean and highest coefficient of variation do not necessarily occur for the same precaster), and then the resistance parameters can be chosen conservatively among precasters.

Table 5.1. Summary of Mean and Coefficient of Variation (Conservative Estimates).

Property	Mean at 28 Days psi (MPa) (1)	CV (%)			
		Within a Batch (2)	Within a Mixture (2)	Mix Average (3)	Batch Average (4)
Compressive Strength	9240 (63.7)	2.4	2.4	8.8	9.1
Modulus of Elasticity	5,660,000 (39,000)	3.6	3.3	5.2	6.1
Splitting Tensile Strength	610 (4.21)	8.3	5.7	10.8	12.2
Modulus of Rupture	1000 (6.91)	4.6	3.1	11.8	12.2

Notes:
(1) Minimum value among precasters at 28 days
(2) Average value for all precasters and all ages
(3) Maximum value among precasters
(4) Calculated using Equation 4.5

215

Table 5.2. Summary of Mean and Coefficient of Variation (Average Estimates).

Property	Mean at 28 Days psi (MPa) (1)	CV (%)			
		Within a Batch (2)	Within a Mixture (2)	Mix Average (1)	Batch Average (3)
Compressive Strength	10000 (68.9)	2.4	2.4	6.4	6.9
Modulus of Elasticity	6,360,000 (43,900)	3.6	3.3	4.3	5.4
Splitting Tensile Strength	674 (4.65)	8.3	5.7	7.5	9.4
Modulus of Rupture	1060 (7.31)	4.6	3.1	9.5	10.0

Notes:
(1) Average value for all precasters at 28 days
(2) Average value for all precasters and all ages
(3) Calculated using Equation 4.5

5.2.2 General Conclusions

1. Because of typical practices for the Texas precasters who participated in this project, very little or no increase in the average compressive strength, modulus of elasticity, splitting tensile strength, and modulus of rupture was found with an increase in the specified compressive strength. In general, the precasters did not use many different mixture proportions for prestressed concrete work and may use only one mixture proportion for a wide range of specified compressive strengths. Where various mixture proportions were available, the specified compressive strength was not the only factor in the selection of the mixture proportions. Factors such as time of day of casting and ambient temperature played a significant role in the selection of the mixture proportions. In addition, for compressive strength, splitting tensile strength, and modulus of rupture, the mean of the logarithm of the batch average (equivalent to mixture average if the data are normally distributed) was found not to be significantly different at the 0.05 level among precasters, ages, design compressive strengths, and their interaction groups.

2. Compressive strength, modulus of elasticity, splitting tensile strength, and modulus of rupture can be assumed to follow a lognormal distribution. However, a normal distribution may also be reasonably assumed.

216

3. Overall, the 28-day bias factors (mean-to-nominal ratios) decrease with an increase in design compressive strength due to the relative uniformity of mixture proportions provided for the specified strength range. Nevertheless, the 28-day bias factors are greater than or equal to 1.00, except for the bias factor for splitting tensile strength for the 10000 psi (69 MPa) strength class.

4. The coefficient of variation within a batch and the coefficient of variation (CV) within a mixture for the compressive strength, modulus of elasticity, splitting tensile strength, and modulus of rupture were not significantly different at the 0.05 level among specified design compressive strength classes and any design compressive strength interactions. However, these CVs may be significantly different among precasters and ages. Details are provided for each property below and in Chapter 4.

5. The CVs for the compressive and spitting tensile strength for the HSC samples in this project are lower than those previously used in the development of the AASHTO LRFD Specifications (2000).

6. The code equations that gave the closest prediction of the mechanical properties of the HSC tested in this project are as follows:

   - Modulus of Elasticity: AASHTO LRFD Specifications (2000)/ACI 318 (1999)

   - Splitting Tensile Strength: ACI 318 (1999)

   - Modulus of Rupture: CEB-FIP Model Code 1990 (CEB 1993)

   Best-fit equations were also developed to give the lowest relative prediction error, while maintaining a relatively simple expression.

5.2.3 Compressive Strength

1. The increase in compressive strength was substantial from release (typically 1 day) to 7 days and from 7 days to 28 days. The compressive strengths at release and at 7 days

were found to be an average of 69 percent and 88 percent of the 28-day compressive strength, respectively. The increase of compressive strength from 28 days to 56 days was small with an average of a 4 percent increase. All precasters appear to have a similar trend.

2. The 28-day bias factor (mean-to-nominal ratio) was found to decrease with an increase in design compressive strength due to the fact that the actual compressive strength did not significantly increase with the specified design compressive strength. Nevertheless, the bias factor is greater than 1.0.

3. The concept of a bias factor may not provide the best description for the HSC produced by the precasters in this project because the mean compressive strength was found to be constant regardless of the specified compressive strengths. However, it is useful to compare the bias factors to the values used in the development of the AASHTO LRFD Specifications (2000).

4. The coefficient of variation within a batch and coefficient of variation within a mixture of the compressive strength were not significantly different among precasters, ages, design compressive strengths, and their interaction groups.

5. The coefficient of variation of the batch average for design compressive strengths between 5900 to 9200 psi (40.7 MPa to 63.4 MPa) could be taken conservatively (because precasters were not selected in a purely random manner) as 9.1 percent or 6.9 percent on average. The mean 28-day compressive strength could be taken conservatively as 9204 psi (63.4 MPa) or 9986 psi (68.9 MPa) as an average.

6. The estimated coefficient of variation for HSC in this project (even for the conservative case) is significantly smaller than those previously used in the development of the AASHTO LRFD Specifications (2000).

7. There is a possibility that the resistance factor for flexural design of prestressed concrete members can be increased for HSC based on the smaller coefficient of variation and

larger bias factor for the compressive strength. However, the mean compressive strength (which was found to be constant regardless of the specified compressive strengths) may be more relevant than a bias factor in the simulation of resistance parameters for this group of precasters. For composite beams, information on the statistical parameters of the deck concrete is also important for establishing the resistance factor for flexure.

8. Because TxDOT allows the use of either 4×8 inch (100×200 mm) or 6×12 inch (150×300 mm) specimens and either neoprene or sulfur capping for compressive strength testing, no adjustment to the bias factor is necessary to account for the differences in the compressive strength due to the differences in the size and capping of the test specimens. Based on current literature, the coefficient of variation of 6×12 inch (150×300 mm) cylinders can be expected to be the same or smaller than that for 4×8 inch (100×200 mm) cylinders. Therefore, the reported coefficient of variation value here can be considered as a conservative estimate of the coefficient of variation of concrete tested using 6×12 inch (150×300 mm) cylinders.

5.2.4 Modulus of Elasticity

1. The increase of modulus of elasticity with time was not substantial from 7 days to 28 days and from 28 days to 56 days. The 7-day and 56-day modulus of elasticity values were about 96 percent and 102 percent of the 28-day modulus of elasticity. All precasters appear to have a similar trend.

2. The bias factor for modulus of elasticity (where the nominal value is calculated using AASHTO LRFD Specifications [2000]equation) was found to decrease with an increase in specified compressive strength. This is because the modulus of elasticity was found not to increase with the specified compressive strength while the predicted value does increase.

3. The coefficient of variation of the modulus of elasticity within a batch was significantly different among ages. The coefficient of variation within a mixture of the modulus of

elasticity can be assumed to be the same among precasters, ages of test, design compressive strengths, and their interaction groups.

4. The mean of the modulus of elasticity was not significantly different among design strengths but was different among precasters. The differences among precasters could be attributed to the type of coarse aggregate used.

5. For concrete having design compressive strength between 5900 to 9200 psi (41.4 MPa to 62.0 MPa), the coefficient of variation can be taken as 6.1 percent as a conservative value (because precasters were not selected in a purely random manner) or 5.4 percent as an average value. A minimum 28-day mean of the modulus of elasticity among precasters was found to be 5,660,000 psi (39.0 GPa). The mean 28-day of the modulus of elasticity for all precasters was found to be 6,360,000 psi (43.9 GPa).

6. When the actual compressive strength was used for prediction of modulus of elasticity, all prediction equations under investigation underestimated the modulus of elasticity. AASHTO LRFD Specifications (2000) equation, which is the same as the equation recommended by ACI Committee 318 (1999), provided the best estimation for the data in this project. It only slightly underestimated the experimental data when compared with the best-fit equation.

7. The ACI Committee 363 (1997) equation for HSC was found to underestimate the modulus of elasticity of HSC in this project.

8. When the specified compressive strength was used in the prediction, all prediction equations under investigation underestimated the modulus of elasticity.

9. The modulus of elasticity cannot be accurately predicted by the design equations because it is strongly influenced by the type of coarse aggregate. If a high degree of accuracy is required, the modulus of elasticity should be obtained from tests.

5.2.5 Splitting Tensile Strength

1. The splitting tensile strength did not increase substantially after the age of 7 days. The 7-day and 56-day splitting tensile strengths were about 96 percent and 102 percent of the 28-day splitting tensile strength, respectively. All precasters appear to have a similar trend.

2. The coefficient of variation within a batch for splitting tensile strength was significantly different among precasters. The coefficient of variation within a mixture for splitting tensile strength was not significantly different among precasters, ages, design compressive strengths, and their interaction groups.

3. For a specified design compressive strength between 5900 and 9200 psi (41.4 MPa to 62.0 MPa), the mean and coefficient of variation for splitting tensile strength could be taken conservatively (because precasters were not selected in a purely random manner) as 610 psi (4.21 MPa) and 12.2 percent, respectively. The mean splitting tensile strength and the mean coefficient of variation for all precasters could be taken as 674 psi (4.65 MPa) and 9.4 percent, respectively.

4. The coefficient of variation of the batch average of the splitting tensile strength for HSC in this project appears to be lower than that previously reported for NSC by Ellingwood et al. (1980). Therefore, there is a potential that the resistance factor for shear design can be increased for HSC members. Additional data should be collected to evaluate the difference between the splitting tensile strength of laboratory and field concrete.

5. The bias factor for splitting tensile strength (where the nominal value is found using the AASHTO LFRD Specification [2000] equation) decreased with an increase in the specified design compressive strength because the splitting tensile strength remains relatively constant while the predicted value increases with the specified compressive strength.

6. The relationship between the actual splitting tensile strength and the actual compressive strength in this project is predicted well using the ACI 318 (1999) equation. It was also found to be in close agreement with the best fit equation.

7. The AASHTO LRFD Specifications (2000) equation, which was proposed by Carrasquillo et al. (1981a, 1982) and also used by ACI Committee 363 (1997), overestimated the splitting tensile strength when actual compressive strength values were used.

8. When using the specified design compressive strength, the splitting tensile strength was best estimated with the equation proposed by the AASHTO LRFD Specifications (2000) equation. The ACI Committee 318 (1999) equation underestimated the splitting tensile strength.

9. Based on the data in this project, the ACI Committee 318 (1999) equation is the most appropriate equation among all the equations under investigation because it gave the best prediction for the splitting tensile strength based on the actual value of compressive strength and gives a conservative estimate when design compressive strength is used.

5.2.6 Modulus of Rupture

1. The modulus of rupture values at 7 days and 56 days were 91 percent and 104 percent of the modulus of rupture value at 28 days, respectively. Differences in the trend among precasters were found at 56 days.

2. The coefficient of variation within a batch and the coefficient of variation within a mixture of the modulus of rupture were not significantly different among ages, precasters, and design compressive strengths.

3. For specified design compressive strength between 5900 and 9200 psi (41.4 MPa to 62.0 MPa), the mean and coefficient of variation for modulus of rupture can be taken conservatively (because precasters were not selected in a purely random manner) as

1000 psi (6.89 MPa) and 12.2 percent, respectively; or they can be taken as average to be 1060 psi (7.31 MPa) and 10.0 percent, respectively.

4. The bias factor for the modulus of rupture when using the AASHTO LRFD Specifications (2000) equation decreases with the specified compressive strength because the modulus of rupture remained relatively constant while the predicted value increased with the specified compressive strength.

5. When using the actual compressive strength in the prediction, the equation recommended by the AASHTO LRFD Specifications (2000), which is the same as that recommended by ACI Committee 318 (1999), underestimated the modulus of rupture. Prediction equations recommended for HSC by ACI Committee 363 (1997) overestimated the modulus of rupture in this project.

6. The CEB-FIP Model Code 1990 (CEB 1993) equation provided the best estimate of the modulus of rupture when actual compressive strength was used for the prediction. The modulus of rupture can also be predicted using the best-fit equation $f_r = 10\sqrt{f'_c}$.

7. The equation proposed by ACI Committee 363 (1997) gives the closest prediction of the modulus rupture for the materials used in this project when the design compressive strength was used. The ACI Committee 318 (1999) equation was found to underestimate the modulus of rupture considerably.

8. The underestimation of the modulus of rupture is conservative in terms of crack prevention. However, this underestimation can result in a higher actual cracking moment than predicted, which could result in abrupt failure of the girder after the cracking of concrete. This may occur without significant deformation warning if the cracking moment is too close to the ultimate moment.

9. Based on the modulus of rupture value, the allowable tensile stress in the AASHTO LRFD Specifications (2000) appears to be conservative. However, curing conditions can affect the modulus of rupture. Therefore, when accounting for the curing condition in the

field, concrete could crack at a lower stress than the modulus of rupture found in the laboratory. Phase 3 evaluated the effect of field curing on the modulus of rupture. The findings were documented by Hueste et al. (2003b).

5.2.7 Creep and Shrinkage

The following conclusions for creep and shrinkage are based on creep and shrinkage samples that were monitored between about 450 to 700 days.

1. All of the time-dependent creep prediction formulas that were evaluated, including the ACI Committee 209 (1992) and AASHTO LRFD Specifications (2000) expressions, overestimated the creep strains for all HSC mixtures tested.

2. The corresponding shrinkage of the control specimens was predicted with much better accuracy than the creep. The CEB-FIP Model Code 1990 (CEB 1993) equation and the simplified equation from Bažnt and Panula (1980) predict the shrinkage of all the samples relatively well. The ACI Committee 209 (1992) equation and AASHTO LRFD Specifications (2000) equation overestimate shrinkage strains by as much as 100 percent.

3. The development of shrinkage with time for the laboratory-cured HSC prism specimens was most closely predicted using the Bazant and Panula (1980) expression. However, this expression results in an under-prediction of shrinkage, which is not conservative for design. The ACI Committee 209 (1992) and AASHTO LRFD Specifications (2000) equations overestimated the development of shrinkage with time for these specimens. Both expressions provide an upper bound to the measured shrinkage values, which is generally conservative for design.

4. The creep and shrinkage values begin to stabilize after the specimens have been exposed to drying for about 150 to 200 days. However, a small positive slope can be observed for the later readings, indicating that some increase can be expected over time and the final values reported cannot be considered ultimate values. It was observed that the measured

creep coefficients begin to stabilize at values of about 1.0 to 1.5, which are considerably less than the referenced ultimate values from design codes and the literature.

5. The ultimate shrinkage strain in the design equation for computing prestress losses provided by the AASHTO LRFD Specifications (2000) and ACI Committee 423 (☒ et al. 1979) appears to be reasonable. However, in some cases the estimated values are less than the maximum measured values, which is not conservative for design.

6. The ultimate shrinkage values from ACI Committee 209 (1992) and the AASHTO LRFD Specifications (2000) equation for estimating shrinkage as a function of time appear to overestimate the ultimate shrinkage of the data by almost a factor of two in some cases, according to the latest measurements available.

7. The creep coefficient and shrinkage strain during the time of testing were not always smaller for concrete with a higher compressive strength or higher modulus of elasticity. Other characteristics of concrete, curing conditions, or testing variables appear to have a significant impact on the creep and shrinkage.

5.3 DISCUSSION

The conclusions from testing of plant-produced HSC from precasters in Texas point to possible advantages for HSC prestressed member design. A smaller CV, when combined with a larger bias factor (as observed for the compressive strength), can lead to a smaller probability of failure. Therefore, there is a potential for an increase in the resistance factors developed specifically for HSC members in flexure and shear versus those developed for NSC. However, several issues must be considered. First, the lower CVs are likely a result of the relatively consistent mixture proportions used by each of the three precasters selected for this project. The CVs may be larger if one were to randomly select from a very large group of precasters across the country. Second, the differences in the behavior of HSC members versus NSC members must be considered in any future code changes. Third, the greatest potential for increasing the economy of prestressed girders lies in increasing the allowable stresses for release and service conditions, and the ultimate flexural limit state does not typically control the maximum spans

that can be achieved with standard prestressed girder cross-sections. Therefore, further attention should be given to the allowable stress values. Based on the modulus of rupture data, the allowable tensile stress in the AASHTO LRFD Specifications may be too conservative. However, curing conditions can affect the MOR. For this reason, additional work was performed to compare the MOR for lab-cured and field-cured HSC specimens (Hueste et al. 2003a, Hueste et al. 2003b).

5.4 RECOMMENDATIONS FOR FUTURE RESEARCH

The following areas for additional work are recommended based on the findings from this project:

1. Additional experimental study to obtain mechanical property data for HSC having a specified compressive strength greater than 10000 psi (68.9 MPa) is recommended. Mixture proportions for a specified compressive strength greater than 10000 psi (68.9 MPa) can be substantially different from those used for the samples in this project.

2. Additional experimental and analytical study of the variation of concrete used for making the concrete deck of prestressed concrete bridges is encouraged. This will provide data for determining the resistance parameters for composite bridge girders.

3. Further study investigating the difference of mechanical property values and the corresponding coefficient of variations between the concrete in a structure (in-situ) and from laboratory test specimens is recommended. Nilson (1985) pointed out that the cracking stress of an actual structural member could be less than the modulus of rupture of laboratory samples due to the difference in curing conditions in the laboratory and in the field. In addition, Bazant and Li (1995) reported that as the sample size increases, the apparent cracking stress is decreased. Therefore, further research to quantify the impact of field curing conditions and size effects for HSC prestressed bridge girders would be beneficial in establishing appropriate allowable stress limits for design. Phase 3 of this project (Hueste et al. 2003b) investigated the impact of field curing conditions on the

compressive strength and MOR. However, the scope of this project did not include a study on the impact of size effects.

4. Long-term monitoring of creep and shrinkage would be useful for determining the ultimate creep coefficients and shrinkage strains. Further study seeking to modify current design equations for estimation of creep and shrinkage for HSC would also be useful based on long-term data.

REFERENCES

AASHTO (1989). *Standard specifications for highway bridges.* Fourteenth edition, Washington, D.C.

AASHTO (1994). *AASHTO LRFD bridge design specifications.* First edition, Washington, D.C.

AASHTO (1999). *1999 interim revisions to the standard specifications for highway bridges.* Sixteenth edition, Washington, D.C.

AASHTO (2000). *2000 interim AASHTO LRFD bridge design specifications.* Customary U.S. units, Second edition, Washington, D.C.

ACI Committee 209 (1992). "Prediction of creep, shrinkage, and temperature effects in concrete structures." *ACI 209R-92*, Farmington Hills, Michigan.

ACI Committee 211 (1993). "Guide for selecting proportions for high-strength concrete with portland cement and fly ash." *ACI 211.4R-93*, Farmington Hills, Michigan.

ACI Committee 318 (1977). "Building code requirements for reinforced concrete." *ACI 318-77*, Farmington Hills, Michigan.

ACI Committee 318 (1999). "Building code requirements for structural concrete (318-99) and commentary (318r-99)." *ACI 318-99/318R-99*, Farmington Hills, Michigan.

ACI Committee 423 (1999). "State-of-the-art report on partially prestressed concrete." *ACI 423.5R-99*, Farmington Hills, Michigan.

ACI Committee 363 (1997). "State-of-the-art report on high-strength concrete." *ACI 363R-92 (reapproved 1997)*, Farmington Hills, Michigan.

Ahmad, S. H. and Shah, S. P. (1985). "Structural properties of high-strength concrete and its implication for precast prestressed concrete." *PCI J.*, 30(6), 92-119.

Aïtcin, P. C. (1998). *High-performance concrete.* Routledge, New York.

ASTM (1992). "Standard test method for creep of concrete in compression." *C 512–87 (reapproved 1992)*, West Conshohocken, Pennsylvania.

ASTM (1994a). "Standard test method for flexural strength of concrete (using simple beam with third-point loading)." *C 78–94*, West Conshohocken, Pennsylvania.

ASTM (1994b). "Standard test method for static modulus of elasticity and Poisson's ratio of concrete in compression." *C 469–94*, West Conshohocken, Pennsylvania.

ASTM (1994c). "Standard practice for capping cylindrical concrete specimens." *C 617–94*, West Conshohocken, Pennsylvania.

ASTM (1996). "Standard test method for splitting tensile strength of cylindrical concrete specimens." *C 496–96*, West Conshohocken, Pennsylvania.

ASTM (1998a). "Standard practice for making and curing concrete test specimens in the field." *C 31/C 31M–98*, West Conshohocken, Pennsylvania.

ASTM (1998b). "Standard test method for compressive strength of hydraulic cement mortars (using 2-in. [or 50 mm] cube specimens)." *C 109/C 109M–98*, West Conshohocken, Pennsylvania.

ASTM (1998c). "Standard practice for making and curing concrete specimens in the laboratory." *C 192/ C 192M–98*, West Conshohocken, Pennsylvania.

ASTM (1998d). "Standard specification for molds for forming concrete test cylinders vertically." *C 470–98*, West Conshohocken, Pennsylvania.

ASTM (1999a). "Standard specification for concrete aggregates." *C 33–99a*, West Conshohocken, Pennsylvania.

ASTM (1999b). "Standard test method for compressive strength of cylindrical concrete specimens." *C 39/C 39M–99*, West Conshohocken, Pennsylvania.

ASTM (1999c). "Standard test method for length change of hardened hydraulic-cement mortar and concrete." *C 157/ C 157M–99*, West Conshohocken, Pennsylvania.

ASTM (1999d). "Standard specification for chemical admixtures for concrete." *C 494/C 494M–99a*, West Conshohocken, Pennsylvania.

ASTM (2000a). "Standard specification for portland cement." *C 150–00*, West Conshohocken, Pennsylvania.

ASTM (2000b). "Standard practice for use of unbonded caps in determination of compressive strength of hardened concrete cylinders." *C 1231/C 1231M–00*, West Conshohocken, Pennsylvania.

ASTM (2000c). "Standard test method for rubber property–durometer hardness." *D 2240-00*, West Conshohocken, Pennsylvania.

Baalbaki, W. (1997). "Analyse expérimentale et prévisionnelle de module d'élasticité des bétons." Ph.D. dissertation, Université de Sherbrooke, Québec, Canada.

Baalbaki, W., Aïtcin, P. C., and Ballivy, G. (1992a). "On predicting modulus of elasticity in high-strength concrete." *ACI Materials J.*, 89(5), 517-520.

Baalbaki, W., Baalbaki, M., Benmokrane, B., and Aïtcin, P. C. (1992b). "Influence of specimen size on compressive strength and elastic modulus of high-performance concrete." *Cement, Concrete, and Aggregates*, ASTM, 14(2), 113-117.

Bažant, Z. P., and Panula, L. (1978a). "Practical prediction of time-dependent deformations of concrete. I: Shrinkage." *Materials and Structures*, 11(65), 307-316.

Bažant, Z. P., and Panula, L. (1978b). "Practical prediction of time-dependent deformations of concrete. II: Basic creep." *Materials and Structures*, 11(65), 317-328.

Bažant, Z. P., and Panula, L. (1978c). "Practical prediction of time-dependent deformations of concrete. III: Drying creep." *Materials and Structures*, 11(66), 415-423.

Bažant, Z. P., and Panula, L. (1978d). "Practical prediction of time-dependent deformations of concrete. IV: Temperature effect on basic creep." *Materials and Structures*, 11(66), 423-434.

Bažant, Z. P., and Panula, L. (1979a). "Practical prediction of time-dependent deformations of concrete. V: Temperature effect on drying creep." *Materials and Structures*, 12(69), 169-174.

Bažant, Z. P., and Panula, L. (1979b). "Practical prediction of time-dependent deformations of concrete. VI: Cyclic creep, nonlinearity and statistical scatter." *Materials and Structures*, 12(69), 174-183.

Bažant, Z. P., and Panula, L. (1980). "Creep and shrinkage characterization for analyzing prestressed concrete structures." *PCI J.*, 25(3), 86-122.

Bažant, Z. P., and Panula, L. (1984). "Practical prediction of creep and shrinkage of high-strength concrete." *Materials and Structures*, 17(101), 375-378.

Buil, M., and Acker, P. (1985). "Creep of a silica fume concrete." *Cement and Concrete Research*, 15(3), 463-466.

Burg, R. G., and Ost, B. W. (1992). "Engineering properties of commercially available high-strength concretes." *Research and Development Bulletin RD104T*, PCA, Skokie, Illinois.

Canadian Standards Association (CSA) (1994). "Design of concrete structures." *A23.3-94*, Toronto, Canada.

Carino, N. J., Guthrie, W. F., and Lagergren, E. S. (1994). "Effects of testing variables on the measured compressive strength of high-strength (90 MPa) concrete." *Report No. PB95-179040*, NIST, Gaithersburg, Maryland.

Carrasquillo, P. M., and Carrasquillo, R. L. (1987). "Improved concrete quality control procedures using third point loading." *Report 1119-1F*, Center for Transportation Research, The University of Texas at Austin, Austin, Texas.

Carrasquillo, P. M., and Carrasquillo, R. L. (1988a). "Evaluation of the use of current concrete practice in the production of high-strength concrete." *ACI Materials J.*, 85(1), 49-54.

Carrasquillo, P. M., and Carrasquillo, R. L. (1988b). "Effect of using unbonded capping system on the compressive strength of concrete cylinders." *ACI Materials J.*, 85(3), 141-147.

Carrasquillo, R. L., Slate, F. O., and Nilson, A. H. (1981a). "Properties of high-strength concrete subjected to short-term loads." *ACI Journal, Proceedings*, 78(3), 171-178.

Carrasquillo, R. L., Slate, F. O., and Nilson A.H. (1981b). "Microcracking and behavior of high-strength concrete subject to short-term loading." *ACI Journal, Proceedings*, 78(3), 179-186.

Carrasquillo, R. L., Slate, F. O., and Nilson, A. H. (1982). "Discussion: Properties of high-strength concrete subjected to short-term loads." *ACI Journal, Proceedings*, 79(2), 162-163.

Castrodale, R. W., Kreger, M. E., and Burns, N. H. (1988). "A study of pretensioned high-strength concrete girders in composite highway bridges–Design considerations." *Report*

381-4F, Center for Transportation Research, The University of Texas at Austin, Austin, Texas.

Cetin, A., and Carrasquillo, R. L. (1998). "High-performance concrete: Influence of coarse aggregates on mechanical properties." *ACI Materials J.*, 95(3), 252-261.

Comite Euro-International du Beton (CEB) (1993). *CEB-FIP Model Code 1990*, Thomas Telford, London.

Date, C. G., and Schnormeier, R. H. (1984). "Day-to-day comparison of 4- and 6-inch diameter concrete cylinder strengths." *Concrete International: Design and Construction*, ACI, 6(8), 24-26.

De Larrard, F. (1990). "Creep and shrinkage of high-strength field concrete." *High-Strength Concrete: Second International Symposium, Publication SP 121*, W. T. Hester, ed., ACI, Farmington Hills, Michigan, 576-587.

Dewar, J. D. (1964). "The indirect tensile strength of concretes of high compressive strength." *Technical Report No. 42.377*, Cement and Concrete Association, Wexham Springs, UK.

Durning, T. A., and Rear, K. B. (1993). "Braker Lane bridge–High strength concrete in prestressed bridge girders." *PCI J.*, 38(3), 46-51.

Ellingwood, B., Galabos, T. V., MacGregor, J. G., and Cornell, C.A. (1980). "Development of a probability-based load criterion for American National Standard A58, building code requirements for minimum design loads in buildings and other structures." *NBS Special Publication 577*, National Bureau of Standards, Washington, D.C.

Féret, R. (1892). "Sur la compacité des mortiers hydrauliques." *Mémoires et Documents Relatifs à l'Art des Constructions et au Service de l'Ingénieur, Annales des Ponts et Chaussées*, 4(2), 5-61.

Forstie, D. A., and Schnormeier, R. (1981). "Development and use of 4 by 8 inch concrete cylinders in Arizona." *Concrete International: Design and Construction*, ACI, 3(7), 42-45.

French, C. W., and Mokhtarzadeh, A. (1993). "High-strength concrete: Effects of materials, curing, and test procedures on short-term compressive strength." *PCI J.*, 38(3), 76-87.

Gardner, N. J., and Zhao, J. W. (1991). "Mechanical properties of concrete for calculating long-term deformations." *Proceedings, Second Canadian Symposium on Cement and*

Concrete, S. Hindess, ed., University of British Columbia Press, Vancouver, Canada, 150-159.

Gonnerman, H. F. (1925). "Effect of size and shape of test specimen on compressive strength of concrete." *ASTM Proceedings*, ASTM, 25(2), 237-250.

Gross, S. P., and Burns, N. H. (2000). "Field performance of prestressed high performance concrete highway bridges in Texas." *Report 580/589-2 Revised Preliminary Review Copy*, Center for Transportation Research, The University of Texas at Austin, Austin, Texas.

Haldar, A., and Mahadevan, S. (2000). *Probability, reliability, and statistical methods in engineering design*. John Wiley and Sons, New York.

Hasofer, A. M., and Lind, N. (1974). "An exact and invariant first-order reliability format." *J. of Engineering Mechanics*, 100(1), 111-121.

Hernandez, H. D., and Gamble, W. L. (1975). "Time-dependent prestress losses in pretensioned concrete construction." *Structural Research Series 0069-4274 No. 417*, Department of Civil Engineering, University of Illinois, Urbana, Illinois.

Hester, W. T. (1980). "Field testing high-strength concretes: A critical review of the state-of-the-art." *Concrete International: Design and Construction*, ACI, 2(2), 27-38.

Hindy, E. E., Buquan, M., Chaallal, O., and Aïtcin, P. C. (1994). "Drying shrinkage of ready-mixed high-performance concrete." *ACI Structural J.*, 91(3), 300-305.

Hueste, M. D., and Cuadros, G. (2003). "Flexural design of high strength concrete prestressed bridge girders – Review of current practice and parametric study." *Report 2101-3*, Texas Transportation Institute, Texas A&M University, College Station, Texas.

Hueste, M. D., Trejo, D., Cline, D. and Keating, P. (2003a). "Investigation of flexural design parameters for high strength concrete prestressed bridge girders – project overview." *Research Report 2101-1*, Texas Transportation Institute, Texas A&M University, College Station, Texas.

Hueste, M. D., Moutassem, F., Trejo, D. and Cline, D. (2003b). "Impact of field exposure conditions on high strength concrete produced for prestressed bridge girders." *Research Report 2101-4*, Texas Transportation Institute, Texas A&M University, College Station, Texas.

Khan, A. A., Cook, W. D., and Mitchell, D. (1997). "Creep, shrinkage, and thermal strains in normal, medium, and high-strength concrete during hydration." *ACI Materials J.*, 94(2), 156-163.

Khayat, K. H., Bickley, J. A., and Hooton, R. D. (1995). "High-strength concrete properties derived from compressive strength values." *Cement, Concrete, and Aggregates*, 17(2), 126-133.

Kim, J. K., Yi, S. T., Park, C. K., and Seok, H. O. (1999). "Size effect on compressive strength of plain and spirally reinforced concrete cylinders." *ACI Structural J.*, 96(1), 88-94.

Lessard, M., Chaallal, O., and Aïtcin, P. C. (1993). "Testing high-strength concrete compressive strength." *ACI Materials J.*, 90(4), 303-308.

Lin, T. Y., and Burns, N. H. (1982). *Design of prestressed concrete structures, SI version*, John Wiley and Sons, New York.

Malhotra, V. M. (1970). "Effect of specimen size on tensile strength of concrete." *ACI Journal, Proceedings*, 67(6), 467-469.

Malhotra, V. M. (1976). "Are 4 × 8 inch concrete cylinders as good as 6 × 12 inch cylinders for quality control of concrete?" *ACI Journal, Proceedings*, 73(1), 33-36.

Maso, F. (1980). *Proceedings of the seventh international congress on the chemistry of cements*. Vol. 1, Editions Septima, Paris.

Mehta, P. K., and Aïtcin, P. C. (1990). "Microstructural basis of selection of materials and mix proportions for high-strength concrete." *High-Strength Concrete, Second International Symposium*, W. T. Hester, ed., ACI, Farmington Hills, Michigan, 265-286.

Mehta, P. K., and Monteiro, P. J. M. (1993). *Concrete: Structure, properties, and materials*. Prentice Hall, Englewood Cliffs, New Jersey.

Milton, J. S., and Arnold, J. C. (1995). *Introduction to probability and statistics: Principles and applications for engineering and the computing sciences*. McGraw-Hill, New York.

Mirza, S. A., Hatzinikolas, M., and MacGregor, J. G. (1979). "Statistical description of strength of concrete." *J. of the Structural Division*, 105(6), 1021-1037.

Mokhtarzadeh, A., and French, C. (2000a). "Mechanical properties of high-strength concrete with consideration for precast applications." *ACI Materials J.*, 97(2), 136-147.

Mokhtarzadeh, A., and French, C. (2000b). "Time-dependent properties of high-strength concrete with consideration for precast applications." *ACI Materials J.*, 97(3), 263-271.

Myers, J. J., and Carrasquillo, R. L. (1998). "Production and quality control of high performance concrete in Texas bridge structures." *Report 580/589-1 Preliminary Review Copy*, Center for Transportation Research, The University of Texas at Austin, Austin, Texas.

Naaman, A. E., and Siriaksorn, A. (1982). "Reliability of partially prestressed beams at serviceability limit states." *PCI J.*, 27(6), 66-85.

Neville, A. M. (1996). *Properties of concrete*. John Wiley and Sons, New York.

Ngab, A. S., Nilson, A. H., and Slate, F. O. (1981). "Shrinkage and creep of high-strength concrete." *ACI Journal, Proceedings*, 78(4), 255-261.

Nilson, A. H. (1985). "Design implications of current research on high-strength concrete." *High-Strength Concrete, SP-87*, H. G. Russell, ed., ACI, Farmington Hills, Michigan, 85-118.

Norwegian Council for Standardization (1992). "Design of concrete structures." *NS 3473*, Oslo, Norway.

Nowak, A. S. (1999). "Calibration of LRFD bridge design code." *NCHRP Report 368*, National Research Council, Washington, D.C.

Nowak, A. S., and Collins, K. R. (2000). *Reliability of structures*. International edition, McGraw Hill, Singapore.

Nowak, A. S., Yamani, A. S., and Tabsh, S. W. (1994). "Probabilistic models for resistance of concrete bridge girders." *ACI Structural J.*, 91(3), 269-276.

Oluokun, F. A. (1991). "Prediction of concrete tensile strength from its compressive strength: Evaluation of existing relations for normal weight concrete." *ACI Materials J.*, 88(3), 302-309.

Ozyildirim, C. (1985). "Neoprene pads for capping concrete cylinders." *Cement, Concrete, and Aggregates*, ASTM, 7(1), 25-28.

PCI Industry Handbook Committee (1992). *PCI design handbook*. Fourth edition, PCI, Chicago.

236

Penttala, V., and Rautanen, T. (1990). "Microporosity, creep and shrinkage of high-strength concretes." *High-Strength Concrete: Second International Symposium, Publication SP 121*, W. T. Hester, ed., ACI, Detroit, Michigan, 409-432.

Pistilli, M. F., and Willems, T. (1993). "Evaluation of cylinder size and capping method in compression strength testing of concrete." *Cement, Concrete, and Aggregates*, 15(1), 59-69.

Rackwitz, R., and Fiessler, B. (1978). "Structural reliability under combined random load sequences." *Computer and Structures*, 9(5), 484-494.

Raphael, J. M. (1984). "Tensile strength of concrete." *J. American Concrete Institute*, 81(2), 158-165.

Richardson, D. N. (1990). "Effects of testing variables on the comparison of neoprene pad and sulfur mortar-capped concrete test cylinders." *ACI Materials J.*, 87(5), 489-495.

Russell, B. W. (1994). "Impact of high-strength concrete on the design and construction of pretensioned girder bridges." *PCI J.*, 39(4), 76-89.

Russell, H. G. (1999). "ACI defines high-performance concrete." *Concrete International: Design and Construction*, 21(2), 56-57.

SAS user's manual-version 8.01 (1999). SAS Institute Inc., Cary, North Carolina.

Senor, S. (1997). "Size effect tests of high-strength concrete." *J. of Materials in Civil Engrg.*, ASCE, 9(1), 46-48.

Smadi, M. M., Slate, F. O., and Nilson, A. H. (1987). "Shrinkage and creep of high-, medium-, and low-strength concretes, including overloads." *ACI Materials J.*, 84(3), 224-234.

Tabsh, S. W. (1992). "Reliability based parametric study of pretensioned AASHTO bridge girders." *PCI J.*, 3(5), 56-67.

Tabsh, S. W., and Aswad, A. (1995). "Statistical properties of plant-produced high-strength concrete in compression." *PCI J.*, 40(4), 72-76.

Tabsh, S. W., and Aswad, A. (1997). "Statistics of high-strength concrete cylinders." *ACI Materials J.*, 94(5), 361-364.

Tabsh, S. W., and Nowak, A. S. (1991). "Reliability of highway girder bridges." *J. Struct. Engrg.*, 117(8), 2372-2388.

Taylor, H. F. W. (1997). *Cement chemistry.* Thomas Telford, London.

Vecchio, F. J., and Collins, M. P. (1986). "The modified compression field theory for reinforced concrete elements subjected to shear." *J. American Concrete Institute*, 83(2), 219-231.

Zia, P., Leming, M. L., and Ahmad, S. H. (1991). "High performance concretes: A state-of-the-art report." *Report No. SHRP-C/FR-91-103*, National Research Council, Washington, D.C.

Zia, P., Preston, H. K., Scott, N. L., and Workman, E. B. (1979). "Estimating prestress losses." *Concrete International: Design and Construction*, 1(6), 32-38.

Zia, P., Schemmel, J. J., and Tallman, T. E. (1989). "Structural application of high-strength concrete." *Research Project 23241-87-3, Final Report*, Center for Transportation Engineering Studies, North Carolina State University, Raleigh, North Carolina.

Zsutty, T. C. (1971). "Shear strength prediction for separate categories of simple beam tests." *J. American Concrete Institute*, 68(2), 138-143.

APPENDIX A

MIXTURE INFORMATION

Summary of mixture proportion, design requirements, and other information are provided in Table A.1, Table A.2, and Table A.3 for HSC samples collected from Precasters A, B, and C, respectively. The summary contains the batch number, which is used throughout the report; design requirements, including specified compressive strength and required release strength; mixture proportion, mainly used for the prediction of creep and shrinkage; fresh concrete properties; and ambient conditions during casting of samples in the field. Precaster name and specific information about mixture proportions such as brand of cement, brand of admixtures, and source of aggregates are omitted.

Table A.1. Mixture Information for Precaster A.

	Set 1				Set 2		
Compressive Strength Category	6000 psi	8000 psi	8000 psi (2)	10000 psi	6000 psi	8000 psi	10000 psi
Designation	A15-A16	A5-A6	A13-A14	A17-A18	A7-A8	A9-A10	A11-A12
Date Collected	6/20/01	9/15/00	6/18/01	6/25/01	3/19/01	4/2/01	5/23/01
Design Requirements							
Specified f'_c (psi)	6250	8573	8484	8963	5909	7540	9196
Design f'_{ci} (psi)	6250	5416	6324	6252	5284	5890	6919
Mixture Proportions							
Coarse Aggregate Type Quantity (pcy)	CRG 1989	¾" CRG 2016	CRG 1989	CRG 1989	CRG 2035	CRG 2034	CRG 1989
Fine Aggregate Type Quantity (pcy)	NRS 1214	NRS 1243	NRS 1214	NRS 1214	NRS 1232	NRS 1151	NRS 1214
Cement ASTM C 150 Type Quantity (pcy)	III 705	III 611	III 705	III 705	III 611	III 705	III 705
W/C	0.28	0.34	0.28	0.28	0.34	0.29	0.28
Retarder ASTM C 494 Type Quantity (oz/100 lb cement)	D 3.5	D 3.5	D 3.5	D 3.5	D 3.5	D 3.5	D 3.5
HRWR ASTM C 494 Type Quantity (oz/100 lb cement)	F 29	F 26	F 29	F 29	F 26	F 29	F 29
Fly Ash Type Quantity (pcy)	N/A	N/A	N/A	N/A	N/A	N/A	N/A
Silica Fume	N/A	N/A	N/A	N/A	N/A	N/A	N/A
Fresh Concrete							
Slump (inch)	8	7.75	8	8	6.5-7	7.5	8
Ambient Temperature (°F)	90	75	88	91	61	77	92
Ambient Relative Humidity (%)	47	98	50	51	37	97	24

Conversion Factors:
> 1000 psi = 6.895 MPa
> 1 lb/yd^3 = 0.5933 kg/m^3
> 1 oz = 2.957 × 10^{-5} m^3
> 1 inch = 25.4 mm
> °F = (9/5) °C + 32

Abbreviations:
> CRG = Coarse river gravel
> NRS = Natural river sand

240

Table A.2. Mixture Information for Precaster B.

	Set 1				Set 2		
Compressive Strength Category	6000 psi	6000 psi (2)	8000 psi	10000 psi	6000 psi	8000 psi	10000 psi
Designation	B3-B4	B11-B12	B15-B16	B7-B8	B9-B10	B13-B14	B5-B6
Date Collected	9/20/00	6/21/01	9/4/01	6/7/01	6/14/01	8/27/01	6/4/01
Design Requirements							
Specified f'_c (psi)	6525	6598	8000*	8983	6525	8000*	8983
Design f'_{ci} (psi)	6525	6517	Not Specified	6555	6525	Not Specified	6555
Mixture Proportions							
Coarse Aggregate Type / Quantity (pcy)	CL / 1872	CL / 1853	CRG / 1998	CL / 1850	CL / 1850	CRG / 2010	CL / 1859
Fine Aggregate Type / Quantity (pcy)	NRS / 1421	NRS / 1490	NRS / 1369	NRS / 1490	NRS / 1490	NRS / 1356	NRS / 1493
Cement ASTM C 150 Type / Quantity (pcy)	III / 658	III / 658	III / 658	III / 658	III / 658	III / 658	III / 658
W/C	0.34		0.34	0.34	0.34	0.34	0.34
Retarder ASTM C 494 Type / Quantity (oz/100 lb cement)	B, D / 3.0	B, D / 3.0	B, D / 3.0	B, D / 3.0	B, D / 3.0	B, D / 3.0	B, D / 3.0
HRWR ASTM C 494 Type / Quantity (oz/100 lb cement)	A, F / 15	A, F / 15	A, F / 15	A, F / 15	A, F / 15	A, F / 15	A, F / 15
Fly Ash Type / Quantity (pcy)	N/A	N/A	N/A	N/A	N/A	N/A	N/A
Silica Fume	N/A	N/A	N/A	N/A	N/A	N/A	N/A
Fresh Concrete							
Slump (inch)	5.5	5.5	5.5	5.5	5.5	5.5	5.5
Ambient Temperature (°F)	102	90	79	93	91	91	95
Ambient Relative Humidity (%)	No Data	53	78	53	57	57	56

Notes: * Specified compressive strength provided by author. Concrete was made for this project with the batch size of 1 yd³.

Conversion Factors:
    1000 psi = 6.895 MPa
    1 lb/yd³ = 0.5933 kg/m³
    1 oz = 2.957 × 10⁻⁵ m³
    1 inch = 25.4 mm
    °F = (9/5) °C + 32

Abbreviations:
    CL = Crushed limestone
    CRG = Coarse river gravel
    NRS = Natural river sand

241

Table A.3. Mixture Information for Precaster C.

	Set 1				Set 2		
Compressive Strength Category	6000 psi	8000 psi	8000 psi (2)	10000 psi	6000 psi	8000 psi	10000 psi
Designation	C15-C16	C3-C4	C13-C14	C17-C18	C7-C8	C11-C12	C9-C10
Date Collected	7/18/01	9/25/00	6/13/01	9/07/01	4/4/01	4/26/01	4/24/01
Design Requirements							
Specified f'_c (psi)	6512	7099	7469	9000*	6178	8102	9152
Design f'_{ci} (psi)	5816	5716	6048	Not Specified	5204	6590	7034
Mixture Proportions							
Coarse Aggregate Type Quantity (pcy)	CL 1775	CL 1910	CL 1781	CL 1759	CL 1847	CL 1760	CL 1837
Fine Aggregate Type Quantity (pcy)	NRS 1475	NRS 1384	NRS 1477	NRS 1474	NRS 1427	NRS 1483	NRS 1448
Cement ASTM C 150 Type Quantity (pcy)	III 658	III 658	III 658	III 658	III 658	III 658	III 658
W/C	0.34	0.34	0.34	0.34	0.34	0.34	0.34
Retarder ASTM C 494 Type Quantity (oz/100 lb cement)	B, D 3.0	B, D 3.0	B, D 3.0	B, D 3.0	B, D 3.0	B, D 3.0	B, D 3.0
HRWR ASTM C 494 Type Quantity (oz/100 lb cement)	A, F 20	A, F 20	A, F 20	A, F 20	A, F 20	A, F 20	A, F 20
Fly Ash Type Quantity (pcy)	N/A	N/A	N/A	N/A	N/A	N/A	N/A
Silica Fume	N/A	N/A	N/A	N/A	N/A	N/A	N/A
Fresh Concrete							
Slump (inch)	4.5	4.5	4.5	4.5	4.5	4.5	4.5
Ambient Temperature (°F)	No Data	61	88	77	72	68	63
Ambient Relative Humidity (%)	No Data	60	45	84	98	45	No Data

Notes: * Specified compressive strength provided by author. Concrete samples were collected from concrete used in the casting of girders with different strength requirements.

Conversion Factors:
   1000 psi = 6.895 MPa
   1 lb/yd^3 = 0.5933 kg/m^3
   1 oz = 2.957 × 10^{-5} m^3
   1 inch = 25.4 mm
   °F = (9/5) °C + 32

Abbreviations:
   CL = Crushed limestone
   NRS = Natural river sand

APPENDIX B

EXPERIMENTAL DATA

The experimental data from all the tests are provided in this section. The results are organized by the precaster who produced the concrete for the samples. The summary of compressive strength tests is shown in Table B.1 to Table B.3. Samples are arranged by set (1 or 2) and then the design compressive strength ranges. The averages of compressive strength and coefficients of variation are also provided for each batch and each mixture. Similar tables are also provided for modulus of elasticity in Table B.4 to Table B.6, splitting tensile strength in Table B.7 to Table B.9, and modulus of rupture in Table B.10 to Table B.12. Stress-strain plots for the determination of the modulus of elasticity are provided in Figure B.1 to Figure B.18. Each plot consists of the stress-strain plot from two cycles of loading for each of the two specimens in a batch. The ratio of batch average to the 28-day batch average for compressive strength, modulus of elasticity, splitting tensile strength, and modulus of rupture are provided in Table B.13 to Table B.16. Bias factors for compressive strength, modulus of elasticity, splitting tensile strength, and modulus of rupture are provided in Table B.17 to Table B.20. Unit weight measurements for each set of samples are summarized in Table B.21.

The following notations are used in Table B.1 to Table B.21:

N/A = Not applicable

NI = Not included in the analysis

NR = Test results are not reported due to insufficient data

NT = Not tested

The symbol NT used for specimen D in all the tables indicates that the specimen is not needed for the test. Some tests have four specimens because there were some specimens that yielded questionable results, and the additional specimen was tested to confirm the result.

Table B.1. Summary of Compressive Strength for Precaster A.

Batch No.	Set	Age Tested	f'c Category	Specimen A (psi)	B (psi)	C (psi)	D (psi)	Batch Avg. (psi)	Batch CV (%)	Mix Avg. (psi)	Mix CV (%)
A15	1	7 days	6000 psi	9565	10088	10348	NT	10000	4.0		
A16	1	7 days	6000 psi	10018	10775	10508	NT	10433	3.7	10217	3.0
A15	1	28 days	6000 psi	11970	11803	11667	NT	11813	1.3		
A16	1	28 days	6000 psi	11742	11657	11911	NT	11770	1.1	11791	0.3
A15	1	56 days	6000 psi	12473	11863	12493	NT	12277	2.9		
A16	1	56 days	6000 psi	12545	12503	12496	NT	12515	0.2	12396	1.4
A5	1	7 days	8000 psi	9832	9895	9540	NT	9755	1.9		
A6	1	7 days	8000 psi	9215	9864	9626	NT	9568	3.4	9662	1.4
A5	1	28 days	8000 psi	11490	11601	11466	NT	11519	0.6		
A6	1	28 days	8000 psi	10779	10944	11173	NT	10965	1.8	11242	3.5
A5	1	56 days	8000 psi	12145	12220	12151	NT	12172	0.3		
A6	1	56 days	8000 psi	11769	12196	11560	NT	11841	2.7	12007	1.9
A13	1	7 days	8000 psi	9738	9816	9687	NT	9747	0.7		
A14	1	7 days	8000 psi	10162	9762	9821	NT	9915	2.2	9831	1.2
A13	1	28 days	8000 psi	11573	11162	11118	NT	11285	2.2		
A14	1	28 days	8000 psi	11650	11993	11517	NT	11720	2.1	11502	2.7
A13	1	56 days	8000 psi	11398	12054	11651	NT	11701	2.8		
A14	1	56 days	8000 psi	11993	12401	12164	NT	12186	1.7	11944	2.9
A17	1	7 days	10000 psi	10061	10213	9539	NT	9938	3.6		
A18	1	7 days	10000 psi	10234	10364	10779	NT	10459	2.7	10198	3.6
A17	1	28 days	10000 psi	11406	10898	11416	NT	11240	2.6		
A18	1	28 days	10000 psi	12023	11881	12025	NT	11976	0.7	11608	4.5
A17	1	56 days	10000 psi	11471	12005	11928	NT	11801	2.4		
A18	1	56 days	10000 psi	12005	12235	12327	NT	12189	1.4	11995	2.3
A7	2	7 days	6000 psi	8871	8756	8644	NT	8757	1.3		
A8	2	7 days	6000 psi	8541	8585	8360	NT	8495	1.4	8626	2.1
A7	2	28 days	6000 psi	10167	9785	9808	NT	9920	2.2		
A8	2	28 days	6000 psi	9631	9406	9142	NT	9393	2.6	9657	3.9
A7	2	56 days	6000 psi	10539	9964	10579	NT	10360	3.3		
A8	2	56 days	6000 psi	10468	9623	10373	NT	10155	4.6	10258	1.4
A9	2	7 days	8000 psi	9524	9685	9879	NT	9696	1.8		
A10	2	7 days	8000 psi	10010	10164	9909	NT	10027	1.3	9862	2.4
A9	2	28 days	8000 psi	11121	11701	11541	NT	11454	2.6		
A10	2	28 days	8000 psi	11614	11405	11664	NT	11561	1.2	11508	0.7
A9	2	56 days	8000 psi	11489	12236	11427	NT	11717	3.8		
A10	2	56 days	8000 psi	11443	11619	12667	NT	11910	5.6	11814	1.2
A11	2	7 days	10000 psi	8484	8851	8551	NT	8629	2.3		
A12	2	7 days	10000 psi	8512	8624	8856	NT	8664	2.0	8646	0.3
A11	2	28 days	10000 psi	10098	9870	10203	NT	10057	1.7		
A12	2	28 days	10000 psi	9082	9988	9771	NT	9614	4.9	9835	3.2
A11	2	56 days	10000 psi	10626	11241	10365	NT	10744	4.2		
A12	2	56 days	10000 psi	10361	10584	10859	NT	10601	2.4	10673	0.9

244

Table B.2. Summary of Compressive Strength for Precaster B.

Batch No.	Set	Age Tested	f'c Category	Specimen A (psi)	B (psi)	C (psi)	D (psi)	Batch Avg. (psi)	Batch CV (%)	Mix Avg. (psi)	Mix CV (%)
B3	1	7 days	6000 psi	8437	8303	8897	NT	8546	3.6		
B4	1	7 days	6000 psi	8629	8130	8437	7992	8297	3.5	8404	2.1
B3	1	28 days	6000 psi	9738	10243	9613	NT	9865	3.4		
B4	1	28 days	6000 psi	9393	9483	NT	NT	9438	0.7	9694	3.1
B3	1	56 days	6000 psi	9978	9379	10754	NT	10037	6.9		
B4	1	56 days	6000 psi	9617	9950	NT	NT	9783	2.4	9936	1.8
B11	1	7 days	6000 psi	9012	9415	9332	NT	9253	2.3		
B12	1	7 days	6000 psi	9069	8968	9065	NT	9034	0.6	9144	1.7
B11	1	28 days	6000 psi	10931	10701	10895	NT	10842	1.1		
B12	1	28 days	6000 psi	10335	9876	10291	NT	10167	2.5	10505	4.5
B11	1	56 days	6000 psi	10996	10513	10618	NT	10709	2.4		
B12	1	56 days	6000 psi	10766	10615	10670	NT	10684	0.7	10696	0.2
B13	1	7 days	8000 psi	9264	9094	9309	NT	9222	1.2		
B14	1	7 days	8000 psi	7659	8678	8224	NT	8187	6.2	8705	8.4
B13	1	28 days	8000 psi	9889	9867	10356	NT	10037	2.8		
B14	1	28 days	8000 psi	10196	10013	9637	NT	9949	2.9	9993	0.6
B13	1	56 days	8000 psi	10121	11183	11164	NT	10822	5.6		
B14	1	56 days	8000 psi	10044	10578	10510	NT	10378	2.8	10600	3.0
B7	1	7 days	10000 psi	8583	8178	8713	NT	8491	3.3		
B8	1	7 days	10000 psi	8935	9015	9081	NT	9010	0.8	8751	4.2
B7	1	28 days	10000 psi	9682	9321	9902	NT	9635	3.0		
B8	1	28 days	10000 psi	10406	9696	10332	NT	10145	3.8	9890	3.6
B7	1	56 days	10000 psi	10015	10500	10584	NT	10366	3.0		
B8	1	56 days	10000 psi	10736	10815	11113	NT	10888	1.8	10627	3.5
B9	2	7 days	6000 psi	8349	8795	8231	NT	8458	3.5		
B10	2	7 days	6000 psi	8383	8487	8012	NT	8294	3.0	8376	1.4
B9	2	28 days	6000 psi	10058	10199	10275	NT	10177	1.1		
B10	2	28 days	6000 psi	9591	9902	9353	NT	9615	2.9	9896	4.0
B9	2	56 days	6000 psi	10257	10523	10461	NT	10414	1.3		
B10	2	56 days	6000 psi	9862	9880	9464	NT	9735	2.4	10075	4.8
B15	2	7 days	8000 psi	7985	7847	8346	NT	8059	3.2		
B16	2	7 days	8000 psi	8008	8012	8506	NT	8175	3.5	8117	1.0
B15	2	28 days	8000 psi	8897	8699	9093	NT	8896	2.2		
B16	2	28 days	8000 psi	8836	9439	9607	NT	9294	4.4	9095	3.1
B15	2	56 days	8000 psi	9855	9167	9761	NT	9594	3.9		
B16	2	56 days	8000 psi	9670	10201	10278	NT	10050	3.3	9822	3.3
B5	2	7 days	10000 psi	7946	7989	7902	NT	7946	0.5		
B6	2	7 days	10000 psi	7824	7714	8201	NT	7913	3.2	7929	0.3
B5	2	28 days	10000 psi	9116	9412	9189	NT	9239	1.7		
B6	2	28 days	10000 psi	9403	9109	9321	NT	9278	1.6	9258	0.3
B5	2	56 days	10000 psi	9404	10235	9708	NT	9782	4.3		
B6	2	56 days	10000 psi	10110	9609	10316	NT	10012	3.6	9897	1.6

Table B.3. Summary of Compressive Strength for Precaster C.

Batch No.	Set	Age Tested	f'$_c$ Category	Specimen A (psi)	B (psi)	C (psi)	D (psi)	Batch Avg. (psi)	Batch CV (%)	Mix Avg. (psi)	Mix CV (%)
C15	1	7 days	6000 psi	8134	8597	8594	NT	8442	3.2		
C16	1	7 days	6000 psi	8739	9058	8373	NT	8723	3.9	8583	2.3
C15	1	28 days	6000 psi	9258	9144	9211	NT	9204	0.6		
C16	1	28 days	6000 psi	9272	9129	9499	NT	9300	2.0	9252	0.7
C15	1	56 days	6000 psi	9197	9328	9191	NT	9239	0.8		
C16	1	56 days	6000 psi	8173	9406	9006	NT	8861	7.1	9050	2.9
C3	1	7 days	8000 psi	7634	7934	7575	NT	7714	2.5		
C4	1	7 days	8000 psi	8420	8720	8130	NT	8423	3.5	8069	6.2
C3	1	28 days	8000 psi	8695	8932	8392	NT	8673	3.1		
C4	1	28 days	8000 psi	9238	9023	9208	NT	9156	1.3	8915	3.8
C3	1	56 days	8000 psi	9040	8832	8604	NT	8826	2.5		
C4	1	56 days	8000 psi	9417	9577	9845	NT	9613	2.3	9219	6.0
C13	1	7 days	8000 psi	7686	7934	8126	NT	7916	2.8		
C14	1	7 days	8000 psi	8597	8444	8479	NT	8506	0.9	8211	5.1
C13	1	28 days	8000 psi	9293	9069	9113	NT	9158	1.3		
C14	1	28 days	8000 psi	9442	8974	9771	NT	9396	4.3	9277	1.8
C13	1	56 days	8000 psi	9398	9300	9219	NT	9306	1.0		
C14	1	56 days	8000 psi	9654	10034	10128	NT	9939	2.5	9622	4.7
C17	1	7 days	10000 psi	7788	7957	8139	NT	7961	2.2		
C18	1	7 days	10000 psi	8060	8032	8126	NT	8073	0.6	8017	1.0
C17	1	28 days	10000 psi	8995	8901	8956	NT	8951	0.5		
C18	1	28 days	10000 psi	9237	9310	9184	NT	9244	0.7	9097	2.3
C17	1	56 days	10000 psi	9382	9541	9475	NT	9466	0.8		
C18	1	56 days	10000 psi	9477	9341	9617	NT	9478	1.5	9472	0.1
C7	2	7 days	6000 psi	9008	8542	8816	NT	8789	2.7		
C8	2	7 days	6000 psi	8895	8581	8651	NT	8709	1.9	8749	0.6
C7	2	28 days	6000 psi	9513	9634	9347	NT	9498	1.5		
C8	2	28 days	6000 psi	9603	9379	9559	NT	9513	1.2	9506	0.1
C7	2	56 days	6000 psi	10235	9680	9969	NT	9961	2.8		
C8	2	56 days	6000 psi	9944	9930	10172	NT	10015	1.4	9988	0.4
C11	2	7 days	8000 psi	7426	7871	7670	NT	7656	2.9		
C12	2	7 days	8000 psi	8147	8001	8455	NT	8201	2.8	7928	4.9
C11	2	28 days	8000 psi	8281	8206	8296	NT	8261	0.6		
C12	2	28 days	8000 psi	9483	8695	8554	NT	8911	5.6	8586	5.3
C11	2	56 days	8000 psi	9087	8952	9036	NT	9025	0.8		
C12	2	56 days	8000 psi	8617	9426	9153	NT	9065	4.5	9045	0.3
C9	2	7 days	10000 psi	8482	8463	8487	NT	8478	0.1		
C10	2	7 days	10000 psi	9032	8285	8875	NT	8731	4.5	8604	2.1
C9	2	28 days	10000 psi	9304	9366	9391	NT	9354	0.5		
C10	2	28 days	10000 psi	10275	10094	9976	NT	10115	1.5	9734	5.5
C9	2	56 days	10000 psi	9625	9980	9549	NT	9718	2.4		
C10	2	56 days	10000 psi	10379	10397	9842	NT	10206	3.1	9962	3.5

Table B.4. Summary of Modulus of Elasticity for Precaster A.

Batch No.	Set	Age Tested	f'c Category	Specimen A (psi)	Specimen B (psi)	Batch Avg. (psi)	Batch CV (%)	Mix Avg. (psi)	Mix CV (%)
A15	1	7 days	6000 psi	7193022	7492242	7342632	2.9		
A16	1	7 days	6000 psi	7275540	6368959	6822249	9.4	7082441	5.2
A15	1	28 days	6000 psi	7798467	7968707	7883587	1.5		
A16	1	28 days	6000 psi	7931598	7553847	7742723	3.4	7813155	1.3
A15	1	56 days	6000 psi	7765567	7794774	7780171	0.3		
A16	1	56 days	6000 psi	7527507	7786850	7657179	2.4	7718675	1.1
A5	1	7 days	8000 psi	NR	NR	N/A	N/A		
A6	1	7 days	8000 psi	NR	NR	N/A	N/A	N/A	N/A
A5	1	28 days	8000 psi	NR	NR	N/A	N/A		
A6	1	28 days	8000 psi	NR	NR	N/A	N/A	N/A	N/A
A5	1	56 days	8000 psi	NR	NR	N/A	N/A		
A6	1	56 days	8000 psi	NR	NR	N/A	N/A	N/A	N/A
A13	1	7 days	8000 psi	7419377	6721918	7070648	7.0		
A14	1	7 days	8000 psi	7756991	7668044	7712517	0.8	7391583	6.1
A13	1	28 days	8000 psi	7322847	7166730	7244789	1.5		
A14	1	28 days	8000 psi	7306061	7805460	7555760	4.7	7400275	3.0
A13	1	56 days	8000 psi	7357257	7146397	7251827	2.1		
A14	1	56 days	8000 psi	7297194	8218378	7757786	8.4	7504807	4.8
A17	1	7 days	10000 psi	7083307	7299260	7191284	2.1		
A18	1	7 days	10000 psi	7446334	7668845	7557589	2.1	7374436	3.5
A17	1	28 days	10000 psi	7386399	7154229	7270314	2.3		
A18	1	28 days	10000 psi	7387486	7779627	7583556	3.7	7426935	3.0
A17	1	56 days	10000 psi	7650159	7963208	7806684	2.8		
A18	1	56 days	10000 psi	7836103	7891079	7863591	0.5	7835137	0.5
A7	2	7 days	6000 psi	7316343	6790461	7053402	6.1		
A8	2	7 days	6000 psi	7127744	6588802	6858273	3.5	6955837	2.0
A7	2	28 days	6000 psi	7075511	6930413	7002962	4.9		
A8	2	28 days	6000 psi	7472863	7469732	7471298	1.5	7237130	4.6
A7	2	56 days	6000 psi	7339524	7350022	7344773	0.1		
A8	2	56 days	6000 psi	7393920	7764993	7579456	3.5	7462115	2.2
A9	2	7 days	8000 psi	6790834	7104502	6947668			
A10	2	7 days	8000 psi	7131932	7595465	7363699	5.7	7155683	4.1
A9	2	28 days	8000 psi	7473746	7128533	7301139			
A10	2	28 days	8000 psi	7442584	7274443	7358513	2.1	7329826	0.6
A9	2	56 days	8000 psi	7291097	7329953	7310525			
A10	2	56 days	8000 psi	7874952	7212790	7543871	6.2	7427198	2.2
A11	2	7 days	10000 psi	6606848	6851163	6729006	2.6		
A12	2	7 days	10000 psi	7031056	6761138	6896097	2.8	6812551	1.7
A11	2	28 days	10000 psi	6808697	6677200	6742949	1.4		
A12	2	28 days	10000 psi	6764696	7275636	7020166	5.1	6881557	2.8
A11	2	56 days	10000 psi	6957503	7632689	7295096	6.5		
A12	2	56 days	10000 psi	6910363	7361697	7136030	4.5	7215563	1.6

247

Table B.5. Summary of Modulus of Elasticity for Precaster B.

Batch No.	Set	Age Tested	f'_c Category	Specimen A (psi)	Specimen B (psi)	Batch Avg. (psi)	Batch CV (%)	Mix Avg. (psi)	Mix CV (%)
B3	1	7 days	6000 psi	NR	NR	N/A	N/A		
B4	1	7 days	6000 psi	NR	NR	N/A	N/A	N/A	N/A
B3	1	28 days	6000 psi	NR	NR	N/A	N/A		
B4	1	28 days	6000 psi	NR	NR	N/A	N/A	N/A	N/A
B3	1	56 days	6000 psi	NR	NR	N/A	N/A		
B4	1	56 days	6000 psi	NR	NR	N/A	N/A	N/A	N/A
B11	1	7 days	6000 psi	6620863	5916210	6268537	7.9		
B12	1	7 days	6000 psi	6468265	5512182	5990224	11.3	6129380	3.2
B11	1	28 days	6000 psi	7009763	6197383	6603573	8.7		
B12	1	28 days	6000 psi	6839979	6687586	6763782	1.6	6683678	1.7
B11	1	56 days	6000 psi	6745407	6173501	6459454	6.3		
B12	1	56 days	6000 psi	6053262	5974099	6013680	0.9	6236567	5.1
B13	1	7 days	8000 psi	5966816	5553039	5759927	5.1		
B14	1	7 days	8000 psi	4940056	5881423	5410739	12.3	5585333	4.4
B13	1	28 days	8000 psi	6423089	6217442	6320265	2.3		
B14	1	28 days	8000 psi	5919562	5764649	5842106	1.9	6081185	5.6
B13	1	56 days	8000 psi	5840885	6196880	6018883	4.2		
B14	1	56 days	8000 psi	5919474	5995994	5957734	0.9	5988308	0.7
B7	1	7 days	10000 psi	5902066	5403142	5652604	6.2		
B8	1	7 days	10000 psi	5880353	5913065	5896709	0.4	5774656	3.0
B7	1	28 days	10000 psi	5437302	5659760	5548531	2.8		
B8	1	28 days	10000 psi	6498189	5938763	6218476	6.4	5883503	8.1
B7	1	56 days	10000 psi	6349292	6008796	6179044	3.9		
B8	1	56 days	10000 psi	5882640	6411823	6147232	6.1	6163138	0.4
B9	2	7 days	6000 psi	5886675	5954274	5920475	0.8		
B10	2	7 days	6000 psi	5291631	5737822	5514727	5.7	5717601	5.0
B9	2	28 days	6000 psi	6199098	5909912	6054505	3.4		
B10	2	28 days	6000 psi	5808654	6165672	5987163	4.2	6020834	0.8
B9	2	56 days	6000 psi	6057450	6429083	6243267	4.2		
B10	2	56 days	6000 psi	6673801	6508843	6591322	1.8	6417295	3.8
B15	2	7 days	8000 psi	5231018	5874600	5552809	8.2		
B16	2	7 days	8000 psi	5175138	5691796	5433467	6.7	5493138	1.5
B15	2	28 days	8000 psi	6178768	5552964	5865866	7.5		
B16	2	28 days	8000 psi	5798090	5701750	5749920	1.2	5807893	1.4
B15	2	56 days	8000 psi	6379198	5978162	6178680	4.6		
B16	2	56 days	8000 psi	5984886	5844718	5914802	1.7	6046741	3.1
B5	2	7 days	10000 psi	5891028	5593492	5742260	3.7		
B6	2	7 days	10000 psi	6312851	5958225	6135538	4.1	5938899	4.7
B5	2	28 days	10000 psi	5891028	5593492	5742260	3.7		
B6	2	28 days	10000 psi	6312851	5958225	6135538	4.1	5938899	4.7
B5	2	56 days	10000 psi	6121466	6081983	6101724	0.5		
B6	2	56 days	10000 psi	6025755	6149994	6087874	1.4	6094799	0.2

248

Table B.6. Summary of Modulus of Elasticity for Precaster C.

Batch No.	Set	Age Tested	f'_c Category	Specimen A (psi)	Specimen B (psi)	Batch Avg. (psi)	Batch CV (%)	Mix Avg. (psi)	Mix CV (%)
C15	1	7 days	6000 psi	5225878	5497897	5361887	3.6		
C16	1	7 days	6000 psi	5205697	5427403	5316550	2.9	5339219	0.6
C15	1	28 days	6000 psi	5880257	5823905	5852081	0.7		
C16	1	28 days	6000 psi	5655565	5683016	5669291	0.3	5760686	2.2
C15	1	56 days	6000 psi	5406820	6130859	5768839	8.9		
C16	1	56 days	6000 psi	6109553	5637770	5873662	5.7	5821250	1.3
C3	1	7 days	8000 psi	NR	NR	N/A	N/A		
C4	1	7 days	8000 psi	NR	NR	N/A	N/A	N/A	N/A
C3	1	28 days	8000 psi	NR	NR	N/A	N/A		
C4	1	28 days	8000 psi	NR	NR	N/A	N/A	N/A	N/A
C3	1	56 days	8000 psi	NR	NR	N/A	N/A		
C4	1	56 days	8000 psi	NR	NR	N/A	N/A	N/A	N/A
C13	1	7 days	8000 psi	5654434	5279890	5467162	4.8		
C14	1	7 days	8000 psi	5674553	5775289	5724921	1.2	5596041	3.3
C13	1	28 days	8000 psi	5894216	5513644	5703930	4.7		
C14	1	28 days	8000 psi	5632035	5640187	5636111	0.1	5670020	0.8
C13	1	56 days	8000 psi	5174246	5338758	5256502	2.2		
C14	1	56 days	8000 psi	6310280	5973175	6141728	3.9	5699115	11.0
C17	1	7 days	10000 psi	5273199	5486595	5379897	2.8		
C18	1	7 days	10000 psi	5701415	5342122	5521769	4.6	5450833	1.8
C17	1	28 days	10000 psi	5539207	5898680	5718944	4.4		
C18	1	28 days	10000 psi	5596304	5410099	5503201	2.4	5611072	2.7
C17	1	56 days	10000 psi	5968366	6155361	6061863	2.2		
C18	1	56 days	10000 psi	6447829	6482039	6464934	0.4	6263398	4.6
C7	2	7 days	6000 psi	4978966	4857199	4918083	7.4		
C8	2	7 days	6000 psi	5638183	5288313	5463248	3.4	5190666	7.4
C7	2	28 days	6000 psi	5532824	5623984	5578404	1.2		
C8	2	28 days	6000 psi	5703411	5398721	5551066	3.9	5564735	0.3
C7	2	56 days	6000 psi	5477480	5604929	5541205	1.6		
C8	2	56 days	6000 psi	5843174	5674283	5758729	2.1	5649967	2.7
C11	2	7 days	8000 psi	4955229	4833481	4894355	1.8		
C12	2	7 days	8000 psi	5301557	4942604	5122080	5.0	5008218	3.2
C11	2	28 days	8000 psi	5170674	5045677	5108175	1.7		
C12	2	28 days	8000 psi	5793128	5647807	5720468	1.8	5414322	8.0
C11	2	56 days	8000 psi	5148191	4220579	4684385	14.0		
C12	2	56 days	8000 psi	5752283	5583411	5667847	2.1	5176116	13.4
C9	2	7 days	10000 psi	5388938	5750377	5569658	4.6		
C10	2	7 days	10000 psi	5726614	5529750	5628182	2.5	5598920	0.7
C9	2	28 days	10000 psi	5857096	6201799	6029447	4.0		
C10	2	28 days	10000 psi	5663939	6113035	5888487	5.4	5958967	1.7
C9	2	56 days	10000 psi	5639911	5948935	5794423	3.8		
C10	2	56 days	10000 psi	6109884	5964077	6036981	1.7	5915702	2.9

Table B.7. Summary of Splitting Tensile Strength for Precaster A.

Batch No.	Set	Age Tested	f'c Category	Specimen A (psi)	B (psi)	C (psi)	D (psi)	Batch Avg. (psi)	Batch CV (%)	Mix Avg. (psi)	Mix CV (%)
A15	1	7 days	6000 psi	776	748	743	NT	755	2.4		
A16	1	7 days	6000 psi	817	809	876	NT	834	4.4	795	7.0
A15	1	28 days	6000 psi	848	839	846	NT	844	0.6		
A16	1	28 days	6000 psi	850	940	850	NT	880	5.9	862	2.9
A15	1	56 days	6000 psi	621	795	808	NT	741	14.1		
A16	1	56 days	6000 psi	762	697	784	NT	748	6.1	744	0.6
A5	1	7 days	8000 psi	564	738	791	NT	698	17.0		
A6	1	7 days	8000 psi	868	822	749	NT	813	7.4	755	10.8
A5	1	28 days	8000 psi	667	787	759	NT	738	8.5		
A6	1	28 days	8000 psi	533	529	729	NT	597	19.2	667	14.9
A5	1	56 days	8000 psi	642	834	767	NT	748	13.0		
A6	1	56 days	8000 psi	769	646	868	NT	761	14.6	754	1.3
A13	1	7 days	8000 psi	NT	NT	NT	NT	N/A	N/A		
A14	1	7 days	8000 psi	NT	NT	NT	NT	N/A	N/A	N/A	N/A
A13	1	28 days	8000 psi	NT	NT	NT	NT	N/A	N/A		
A14	1	28 days	8000 psi	NT	NT	NT	NT	N/A	N/A	N/A	N/A
A13	1	56 days	8000 psi	NT	NT	NT	NT	N/A	N/A		
A14	1	56 days	8000 psi	NT	NT	NT	NT	N/A	N/A	N/A	N/A
A17	1	7 days	10000 psi	617	724	737	NT	693	9.5		
A18	1	7 days	10000 psi	728	742	776	NT	748	3.3	721	5.5
A17	1	28 days	10000 psi	901	790	690	NT	794	13.3		
A18	1	28 days	10000 psi	777	638	769	NT	728	10.7	761	6.1
A17	1	56 days	10000 psi	930	799	889	NT	873	7.7		
A18	1	56 days	10000 psi	826	847	751	NT	808	6.2	840	5.5
A7	2	7 days	6000 psi	784	504	394	722	753	5.9		
A8	2	7 days	6000 psi	688	577	666	NT	644	9.2	687	11.2
A7	2	28 days	6000 psi	664	637	541	NT	614	10.6		
A8	2	28 days	6000 psi	603	761	699	NT	688	11.6	651	8.0
A7	2	56 days	6000 psi	747	727	690	NT	721	4.0		
A8	2	56 days	6000 psi	842	732	727	NT	767	8.4	744	4.4
A9	2	7 days	8000 psi	549	584	610	NT	581	5.3		
A10	2	7 days	8000 psi	604	622	615	NT	613	1.5	597	3.8
A9	2	28 days	8000 psi	689	764	776	NT	743	6.4		
A10	2	28 days	8000 psi	912	785	908	NT	868	8.3	806	11.0
A9	2	56 days	8000 psi	756	985	854	NT	865	13.3		
A10	2	56 days	8000 psi	887	919	918	NT	908	2.0	887	3.4
A11	2	7 days	10000 psi	750	672	662	NT	694	6.9		
A12	2	7 days	10000 psi	662	689	672	NT	674	2.1	684	2.1
A11	2	28 days	10000 psi	621	746	746	NT	704	10.2		
A12	2	28 days	10000 psi	745	756	863	NT	788	8.3	746	7.9
A11	2	56 days	10000 psi	825	753	758	NT	778	5.2		
A12	2	56 days	10000 psi	840	676	865	NT	794	12.9	786	1.4

Table B.8. Summary of Splitting Tensile Strength for Precaster B.

Batch No.	Set	Age Tested	f'_c Category	Specimen A (psi)	B (psi)	C (psi)	D (psi)	Batch Avg. (psi)	Batch CV (%)	Mix Avg. (psi)	Mix CV (%)
B3	1	7 days	6000 psi	610	671	656	NT	646	4.9		
B4	1	7 days	6000 psi	624	552	455	NT	544	15.6	595	12.2
B3	1	28 days	6000 psi	581	647	730	NT	653	11.4		
B4	1	28 days	6000 psi	631	697	618	NT	648	6.6	650	0.5
B3	1	56 days	6000 psi	574	670	572	NT	605	9.3		
B4	1	56 days	6000 psi	727	605	615	NT	649	10.5	627	4.9
B11	1	7 days	6000 psi	NT	NT	NT	NT	N/A	N/A		
B12	1	7 days	6000 psi	NT	NT	NT	NT	N/A	N/A	N/A	N/A
B11	1	28 days	6000 psi	NT	NT	NT	NT	N/A	N/A		
B12	1	28 days	6000 psi	NT	NT	NT	NT	N/A	N/A	N/A	N/A
B11	1	56 days	6000 psi	NT	NT	NT	NT	N/A	N/A		
B12	1	56 days	6000 psi	NT	NT	NT	NT	N/A	N/A	N/A	N/A
B13	1	7 days	8000 psi	628	753	726	NT	702	9.3		
B14	1	7 days	8000 psi	530	560	707	NT	599	15.9	651	11.2
B13	1	28 days	8000 psi	580	589	706	NT	625	11.2		
B14	1	28 days	8000 psi	830	835	604	NT	756	17.5	691	13.4
B13	1	56 days	8000 psi	573	592	659	NT	608	7.4	0	0.0
B14	1	56 days	8000 psi	621	599	521	NT	580	9.1	594	3.3
B7	1	7 days	10000 psi	599	619	663	NT	627	5.2		
B8	1	7 days	10000 psi	708	664	610	NT	661	7.4	644	3.7
B7	1	28 days	10000 psi	645	709	506	NT	620	16.7		
B8	1	28 days	10000 psi	781	714	712	NT	735	5.3	678	12.1
B7	1	56 days	10000 psi	786	582	770	NT	713	16.0		
B8	1	56 days	10000 psi	594	602	485	NT	560	11.7	637	16.9
B9	2	7 days	6000 psi	672	649	716	NT	679	5.0		
B10	2	7 days	6000 psi	611	643	681	NT	645	5.5	662	3.6
B9	2	28 days	6000 psi	877	726	708	NT	770	12.0		
B10	2	28 days	6000 psi	701	615	422	NT	579	24.7	675	20.0
B9	2	56 days	6000 psi	790	753	691	NT	745	6.7		
B10	2	56 days	6000 psi	574	567	657	NT	600	8.4	672	15.2
B15	2	7 days	8000 psi	584	700	601	NT	628	9.9		
B16	2	7 days	8000 psi	566	575	620	NT	587	4.9	607	4.8
B15	2	28 days	8000 psi	455	628	624	NT	569	17.3		
B16	2	28 days	8000 psi	606	615	563	NT	595	4.7	582	3.1
B15	2	56 days	8000 psi	653	677	646	NT	659	2.5		
B16	2	56 days	8000 psi	687	693	681	NT	687	0.9	673	2.9
B5	2	7 days	10000 psi	662	581	627	NT	623	6.5		
B6	2	7 days	10000 psi	612	656	665	NT	645	4.4	634	2.4
B5	2	28 days	10000 psi	728	744	563	NT	678	14.8		
B6	2	28 days	10000 psi	742	763	616	NT	707	11.2	693	3.0
B5	2	56 days	10000 psi	562	733	605	NT	633	14.1		
B6	2	56 days	10000 psi	651	679	621	NT	650	4.4	642	1.9

251

Table B.9. Summary of Splitting Tensile Strength for Precaster C.

Batch No.	Set	Age Tested	f'_c Category	Specimen A (psi)	B (psi)	C (psi)	D (psi)	Batch Avg. (psi)	Batch CV (%)	Mix Avg. (psi)	Mix CV (%)
C15	1	7 days	6000 psi	668	595	606	NT	623	6.3		
C16	1	7 days	6000 psi	580	647	588	NT	605	6.0	614	2.1
C15	1	28 days	6000 psi	642	682	618	NT	647	5.0		
C16	1	28 days	6000 psi	587	496	556	NT	546	8.4	597	12.0
C15	1	56 days	6000 psi	620	679	646	NT	648	4.6		
C16	1	56 days	6000 psi	614	684	613	NT	637	6.4	643	1.2
C3	1	7 days	8000 psi	543	503	480	NT	509	6.3		
C4	1	7 days	8000 psi	N/A	583	594	NT	589	1.4	541	10.4
C3	1	28 days	8000 psi	547	569	589	NT	568	3.7		
C4	1	28 days	8000 psi	606	N/A	574	NT	590	3.8	577	2.7
C3	1	56 days	8000 psi	570	569	461	NT	533	11.7		
C4	1	56 days	8000 psi	560	603	519	NT	561	7.5	547	3.6
C13	1	7 days	8000 psi	NT	NT	NT	NT	N/A	N/A		
C14	1	7 days	8000 psi	NT	NT	NT	NT	N/A	N/A	N/A	N/A
C13	1	28 days	8000 psi	NT	NT	NT	NT	N/A	N/A		
C14	1	28 days	8000 psi	NT	NT	NT	NT	N/A	N/A	N/A	N/A
C13	1	56 days	8000 psi	NT	NT	NT	NT	N/A	N/A		
C14	1	56 days	8000 psi	NT	NT	NT	NT	N/A	N/A	N/A	N/A
C17	1	7 days	10000 psi	524	598	611	NT	578	8.1		
C18	1	7 days	10000 psi	662	618	655	NT	645	3.7	611	7.8
C17	1	28 days	10000 psi	602	613	630	NT	615	2.3		
C18	1	28 days	10000 psi	617	631	606	NT	618	2.0	617	0.3
C17	1	56 days	10000 psi	563	584	717	NT	621	13.4		
C18	1	56 days	10000 psi	587	627	677	NT	630	7.1	626	1.0
C7	2	7 days	6000 psi	571	512	581	NT	554	6.7		
C8	2	7 days	6000 psi	691	612	546	NT	616	11.8	585	7.5
C7	2	28 days	6000 psi	644	583	648	NT	625	5.9		
C8	2	28 days	6000 psi	600	622	664	NT	628	5.2	627	0.4
C7	2	56 days	6000 psi	643	647	698	NT	663	4.7		
C8	2	56 days	6000 psi	649	693	645	NT	662	4.1	662	0.0
C11	2	7 days	8000 psi	599	689	487	NT	592	17.1		
C12	2	7 days	8000 psi	579	617	527	NT	574	7.9	583	2.1
C11	2	28 days	8000 psi	600	662	568	NT	610	7.8		
C12	2	28 days	8000 psi	544	615	648	NT	602	8.8	606	0.9
C11	2	56 days	8000 psi	613	503	550	NT	555	10.0		
C12	2	56 days	8000 psi	667	N/A	603	NT	635	7.2	595	9.5
C9	2	7 days	10000 psi	551	567	520	NT	546	4.4		
C10	2	7 days	10000 psi	570	547	588	NT	568	3.6	557	2.8
C9	2	28 days	10000 psi	595	643	614	NT	617	3.9		
C10	2	28 days	10000 psi	626	699	644	NT	656	5.8	637	4.3
C9	2	56 days	10000 psi	641	653	675	NT	656	2.6		
C10	2	56 days	10000 psi	685	655	651	NT	664	2.8	660	0.8

Table B.10. Summary of Modulus of Rupture for Precaster A.

Batch No.	Set	Age Tested	f'c Category	Specimen A (psi)	B (psi)	C (psi)	D (psi)	Batch Avg. (psi)	Batch CV (%)	Mix Avg. (psi)	Mix CV (%)
A15	1	7 days	6000 psi	1001	1043	1029	NT	1024	2.1		
A16	1	7 days	6000 psi	1083	1094	1098	NT	1092	0.7	1058	4.5
A15	1	28 days	6000 psi	1108	1333	1308	NT	1250	9.9		
A16	1	28 days	6000 psi	1266	1249	1363	NT	1293	4.7	1271	2.4
A15	1	56 days	6000 psi	1427	1357	1406	NT	1397	2.6		
A16	1	56 days	6000 psi	1484	1519	1259	NT	1420	9.9	1408	1.2
A5	1	7 days	8000 psi	889	828	933	NT	883	6.0		
A6	1	7 days	8000 psi	912	890	865	NT	889	2.7	886	0.5
A5	1	28 days	8000 psi	1002	1044	955	NT	1001	4.4		
A6	1	28 days	8000 psi	1141	1058	989	NT	1063	7.2	1032	4.3
A5	1	56 days	8000 psi	1135	973	1101	NT	1070	8.0		
A6	1	56 days	8000 psi	1056	1151	1088	NT	1099	4.4	1084	1.9
A13	1	7 days	8000 psi	NT	NT	NT	NT	N/A	N/A		
A14	1	7 days	8000 psi	NT	NT	NT	NT	N/A	N/A	N/A	N/A
A13	1	28 days	8000 psi	NT	NT	NT	NT	N/A	N/A		
A14	1	28 days	8000 psi	NT	NT	NT	NT	N/A	N/A	N/A	N/A
A13	1	56 days	8000 psi	NT	NT	NT	NT	N/A	N/A		
A14	1	56 days	8000 psi	NT	NT	NT	NT	N/A	N/A	N/A	N/A
A17	1	7 days	10000 psi	1123	1047	1159	NT	1110	5.2		
A18	1	7 days	10000 psi	1072	1125	1139	NT	1112	3.2	1111	0.2
A17	1	28 days	10000 psi	1288	1241	1166	NT	1232	5.0		
A18	1	28 days	10000 psi	1266	1181	1150	NT	1199	5.0	1215	1.9
A17	1	56 days	10000 psi	1270	1308	1253	NT	1277	2.2		
A18	1	56 days	10000 psi	1248	1345	1281	NT	1291	3.8	1284	0.8
A7	2	7 days	6000 psi	967	984	910	NT	954	4.0		
A8	2	7 days	6000 psi	892	881	955	NT	910	4.4	932	3.4
A7	2	28 days	6000 psi	1013	926	975	NT	971	4.5		
A8	2	28 days	6000 psi	926	932	1009	NT	956	4.8	963	1.1
A7	2	56 days	6000 psi	1230	1247	1173	NT	1217	3.2		
A8	2	56 days	6000 psi	1149	1068	1224	NT	1147	6.8	1182	4.2
A9	2	7 days	8000 psi	967	928	916	NT	937	2.9		
A10	2	7 days	8000 psi	971	1025	927	NT	974	5.0	956	2.8
A9	2	28 days	8000 psi	1047	1050	1054	NT	1050	0.4		
A10	2	28 days	8000 psi	1153	1127	1106	NT	1129	2.1	1089	5.1
A9	2	56 days	8000 psi	1258	1340	1183	NT	1261	6.2		
A10	2	56 days	8000 psi	1455	1578	1329	NT	1454	8.6	1357	10.1
A11	2	7 days	10000 psi	936	937	969	NT	947	1.9		
A12	2	7 days	10000 psi	1032	919	960	NT	970	5.9	959	1.7
A11	2	28 days	10000 psi	848	1032	922	NT	934	9.9		
A12	2	28 days	10000 psi	991	976	1027	NT	998	2.6	966	4.7
A11	2	56 days	10000 psi	1015	1094	1108	NT	1072	4.7		
A12	2	56 days	10000 psi	919	1010	944	NT	958	4.9	1015	8.0

253

Table B.11. Summary of Modulus of Rupture for Precaster B.

Batch No.	Set	Age Tested	f'c Category	Specimen A (psi)	B (psi)	C (psi)	D (psi)	Batch Avg. (psi)	Batch CV (%)	Mix Avg. (psi)	Mix CV (%)
B3	1	7 days	6000 psi	893	1009	863	NT	922	8.4		
B4	1	7 days	6000 psi	927	950	935	NT	937	1.3	929	1.2
B3	1	28 days	6000 psi	926	983	882	NT	930	5.4		
B4	1	28 days	6000 psi	979	945	919	NT	948	3.1	939	1.3
B3	1	56 days	6000 psi	1060	1145	1075	NT	1093	4.1		
B4	1	56 days	6000 psi	1410	987	983	NT	1126	21.8	1110	2.1
B11	1	7 days	6000 psi	NT	NT	NT	NT	N/A	N/A		
B12	1	7 days	6000 psi	NT	NT	NT	NT	N/A	N/A	N/A	N/A
B11	1	28 days	6000 psi	NT	NT	NT	NT	N/A	N/A		
B12	1	28 days	6000 psi	NT	NT	NT	NT	N/A	N/A	N/A	N/A
B11	1	56 days	6000 psi	NT	NT	NT	NT	N/A	N/A		
B12	1	56 days	6000 psi	NT	NT	NT	NT	N/A	N/A	N/A	N/A
B13	1	7 days	8000 psi	988	1068	1087	NT	1047	5.0		
B14	1	7 days	8000 psi	1037	948	1090	NT	1025	7.0	1036	1.5
B13	1	28 days	8000 psi	1155	1079	1101	NT	1112	3.5		
B14	1	28 days	8000 psi	1182	1115	1212	NT	1170	4.3	1141	3.6
B13	1	56 days	8000 psi	1152	1211	1168	NT	1177	2.6		
B14	1	56 days	8000 psi	1150	1128	1116	NT	1131	1.5	1154	2.8
B7	1	7 days	10000 psi	1068	1058	1102	NT	1076	2.2		
B8	1	7 days	10000 psi	1087	1013	1108	NT	1069	4.7	1073	0.5
B7	1	28 days	10000 psi	1100	1038	1095	NT	1077	3.2		
B8	1	28 days	10000 psi	1109	1031	1180	NT	1107	6.7	1092	1.9
B7	1	56 days	10000 psi	1151	1066	1061	NT	1093	4.6		
B8	1	56 days	10000 psi	1116	1088	1033	NT	1079	3.9	1086	0.9
B9	2	7 days	6000 psi	1009	1044	1066	NT	1039	2.8		
B10	2	7 days	6000 psi	978	1047	1009	NT	1011	3.5	1025	1.9
B9	2	28 days	6000 psi	1144	1056	1201	NT	1134	6.5		
B10	2	28 days	6000 psi	1135	1172	1043	NT	1117	6.0	1125	1.0
B9	2	56 days	6000 psi	1115	942	1049	NT	1035	8.4		
B10	2	56 days	6000 psi	1156	1150	1102	NT	1136	2.6	1086	6.6
B15	2	7 days	8000 psi	889	1050	1076	NT	1005	10.1		
B16	2	7 days	8000 psi	1001	1023	1017	NT	1014	1.1	1009	0.6
B15	2	28 days	8000 psi	1096	1142	1101	NT	1113	2.3		
B16	2	28 days	8000 psi	1066	1121	1136	NT	1108	3.3	1110	0.3
B15	2	56 days	8000 psi	1031	1170	1114	NT	1105	6.3		
B16	2	56 days	8000 psi	1039	911	1154	NT	1035	11.8	1070	4.6
B5	2	7 days	10000 psi	1155	1030	1080	NT	1088	5.8		
B6	2	7 days	10000 psi	1042	1035	1044	NT	1041	0.5	1065	3.2
B5	2	28 days	10000 psi	1151	1160	1127	NT	1146	1.5		
B6	2	28 days	10000 psi	1137	1145	1136	NT	1139	0.4	1143	0.4
B5	2	56 days	10000 psi	1120	1115	1182	NT	1139	3.3		
B6	2	56 days	10000 psi	1056	1096	1203	NT	1118	6.8	1129	1.3

Table B.12. Summary of Modulus of Rupture for Precaster C.

Batch No.	Set	Age Tested	f'c Category	Specimen				Batch Avg. (psi)	Batch CV (%)	Mix Avg. (psi)	Mix CV (%)
				A (psi)	B (psi)	C (psi)	D (psi)				
C15	1	7 days	6000 psi	981	867	892	NT	914	6.6		
C16	1	7 days	6000 psi	1086	996	1011	NT	1031	4.6	972	8.5
C15	1	28 days	6000 psi	1077	933	1020	NT	1010	7.2		
C16	1	28 days	6000 psi	1044	1036	997	NT	1025	2.5	1018	1.1
C15	1	56 days	6000 psi	1163	1043	1061	NT	1089	5.9		
C16	1	56 days	6000 psi	1052	1088	1026	NT	1055	3.0	1072	2.2
C3	1	7 days	8000 psi	818	775	714	NT	769	6.8		
C4	1	7 days	8000 psi	783	803	789	NT	792	1.3	780	2.1
C3	1	28 days	8000 psi	865	800	877	NT	847	4.9		
C4	1	28 days	8000 psi	1011	845	866	NT	908	10.0	877	4.9
C3	1	56 days	8000 psi	810	795	802	NT	802	0.9		
C4	1	56 days	8000 psi	919	867	920	NT	902	3.3	852	8.3
C13	1	7 days	8000 psi	NT	NT	NT	NT	N/A	N/A		
C14	1	7 days	8000 psi	NT	NT	NT	NT	N/A	N/A	N/A	N/A
C13	1	28 days	8000 psi	NT	NT	NT	NT	N/A	N/A		
C14	1	28 days	8000 psi	NT	NT	NT	NT	N/A	N/A	N/A	N/A
C13	1	56 days	8000 psi	NT	NT	NT	NT	N/A	N/A		
C14	1	56 days	8000 psi	NT	NT	NT	NT	N/A	N/A	N/A	N/A
C17	1	7 days	10000 psi	1009	963	985	NT	985	2.3		
C18	1	7 days	10000 psi	879	893	878	NT	883	0.9	934	7.7
C17	1	28 days	10000 psi	1084	1126	1112	NT	1107	1.9		
C18	1	28 days	10000 psi	1087	1115	1108	NT	1103	1.3	1105	0.3
C17	1	56 days	10000 psi	1073	1077	1101	NT	1084	1.4		
C18	1	56 days	10000 psi	1002	1071	994	NT	1022	4.2	1053	4.1
C7	2	7 days	6000 psi	814	950	811	NT	858	9.3		
C8	2	7 days	6000 psi	775	855	903	NT	844	7.6	851	1.1
C7	2	28 days	6000 psi	981	1017	1030	NT	1009	2.5		
C8	2	28 days	6000 psi	1053	983	1010	NT	1016	3.5	1013	0.4
C7	2	56 days	6000 psi	997	994	957	NT	983	2.2		
C8	2	56 days	6000 psi	1063	1017	993	NT	1025	3.5	1004	2.9
C11	2	7 days	8000 psi	911	914	899	NT	908	0.9		
C12	2	7 days	8000 psi	899	919	967	NT	928	3.8	918	1.6
C11	2	28 days	8000 psi	923	961	974	NT	953	2.8		
C12	2	28 days	8000 psi	927	805	907	NT	880	7.4	916	5.6
C11	2	56 days	8000 psi	850	918	815	NT	861	6.1		
C12	2	56 days	8000 psi	896	902	957	NT	918	3.7	890	4.6
C9	2	7 days	10000 psi	N/A	800	883	NT	842	7.0		
C10	2	7 days	10000 psi	935	1042	987	NT	988	5.4	929	11.1
C9	2	28 days	10000 psi	1046	1041	1058	NT	1048	0.8		
C10	2	28 days	10000 psi	1069	1121	1143	NT	1111	3.4	1080	4.1
C9	2	56 days	10000 psi	1053	1071	912	NT	1012	8.6		
C10	2	56 days	10000 psi	1050	1015	1009	NT	1025	2.1	1018	0.9
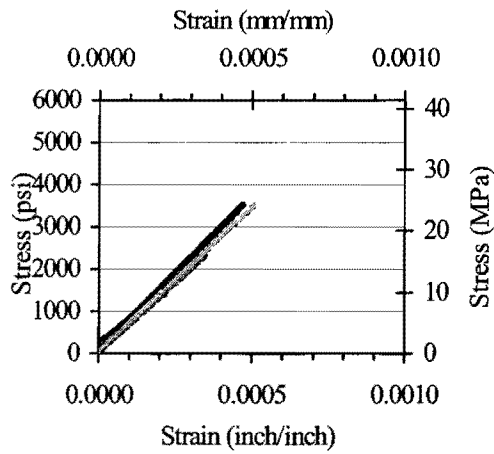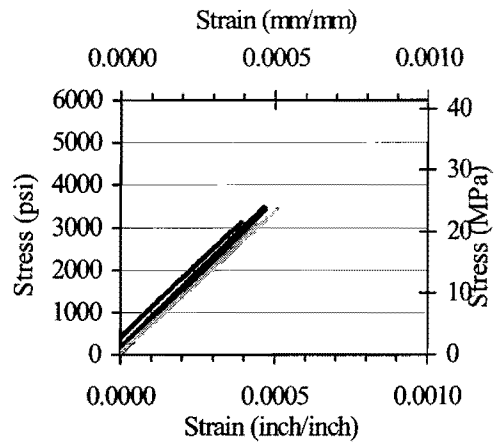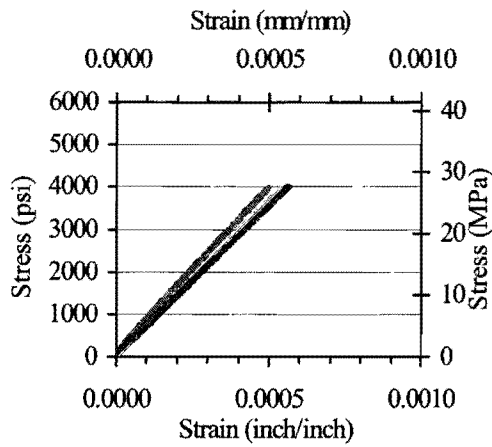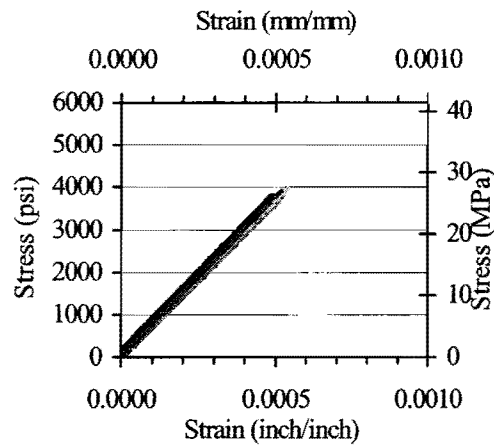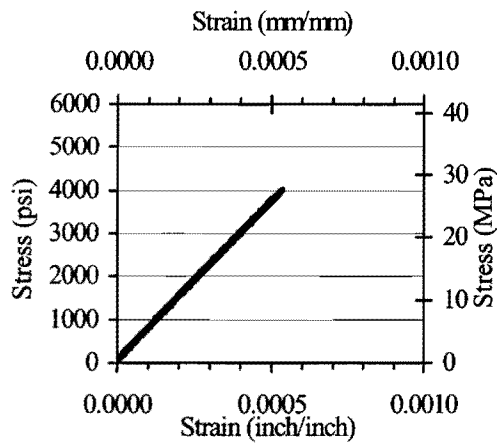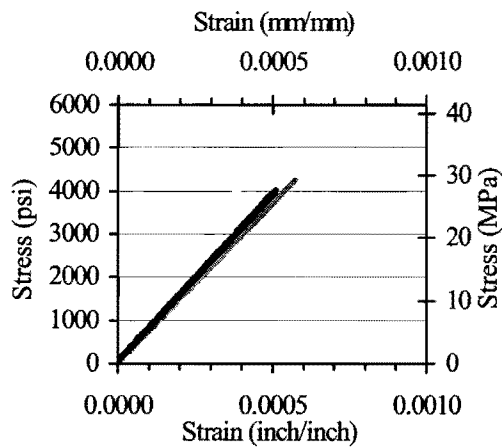
Figure B.1. Stress-Strain Plots for Determination of Modulus of Elasticity for Batches A7-A8.
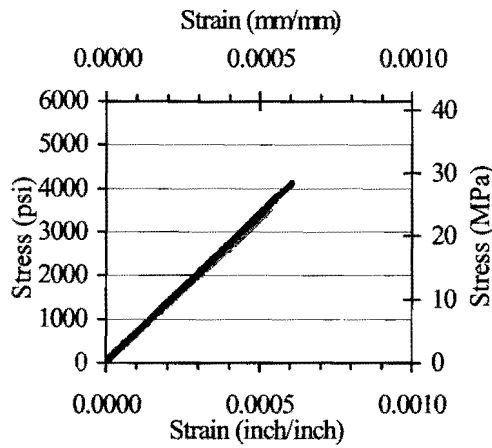
(a) A9 at 7 Days
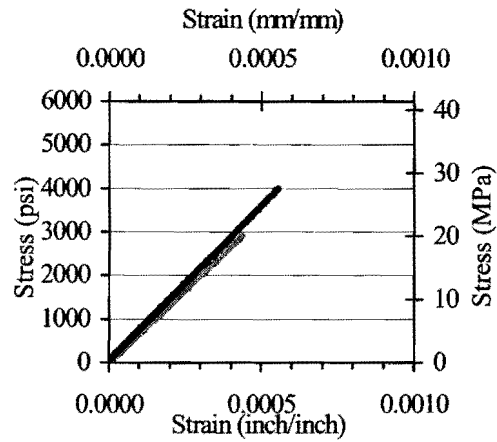
(b) A10 at 7 Days
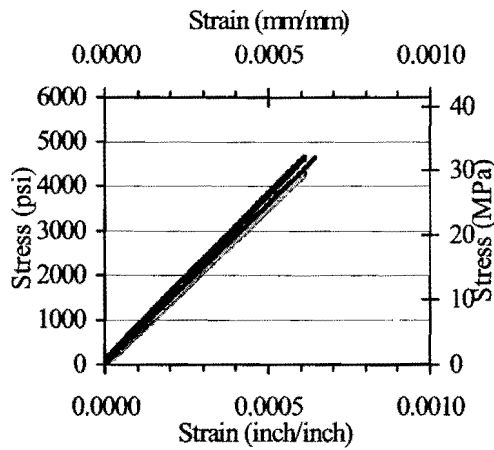
(c) A9 at 28 days
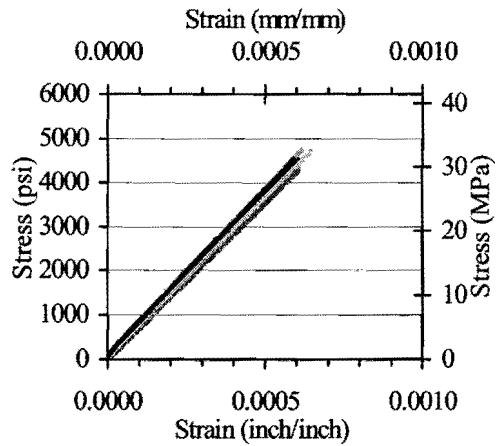
(d) A10 at 28 Days
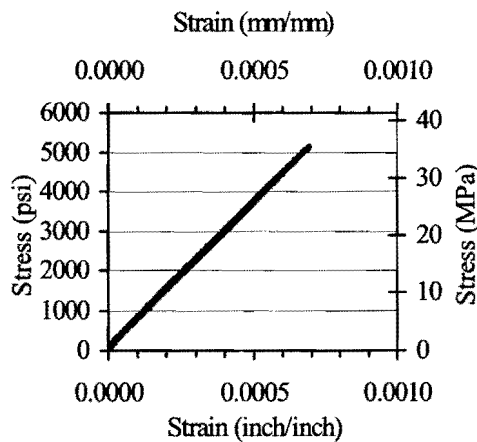
(e) A9 at 56 Days
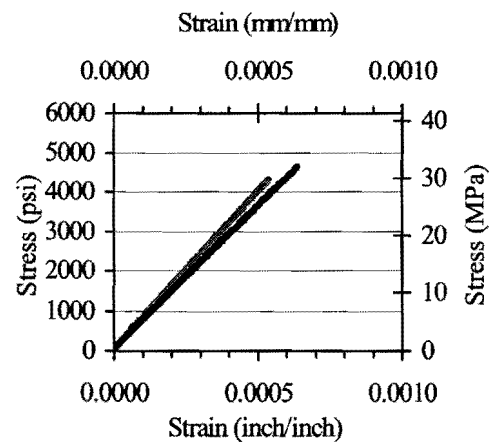
(f) A10 at 56 Days

**Figure B.2. Stress-Strain Plots for Determination of Modulus of Elasticity for Batches A9-A10.**
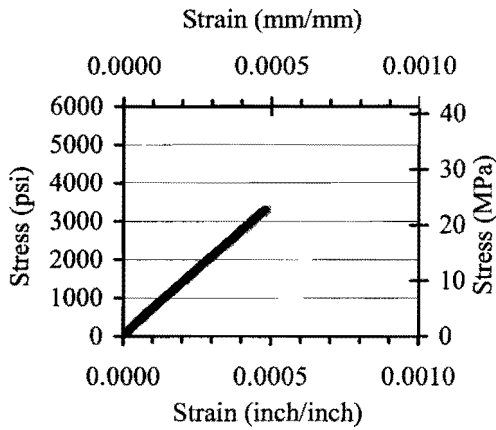
257
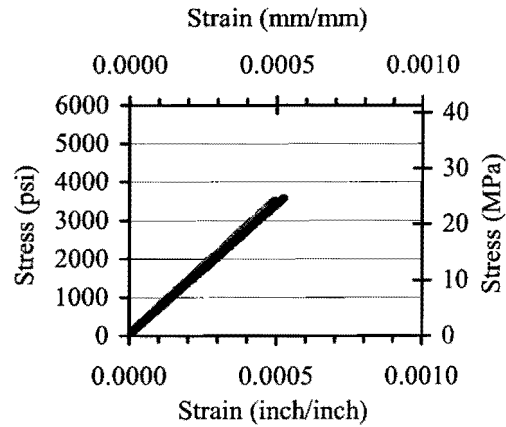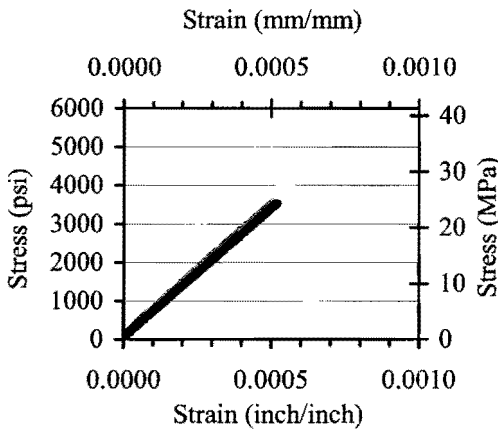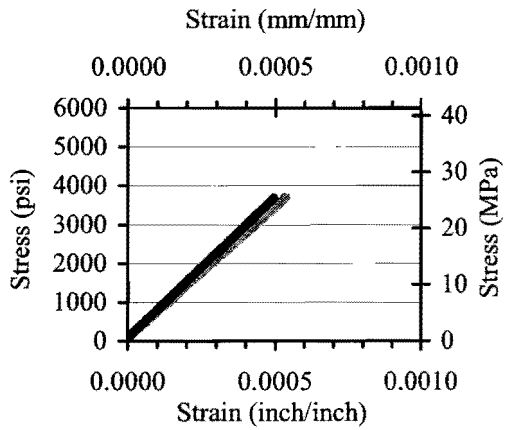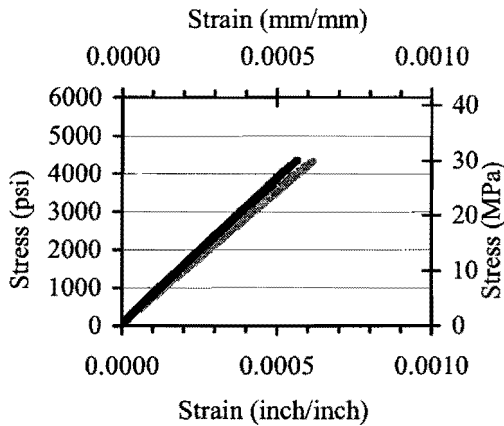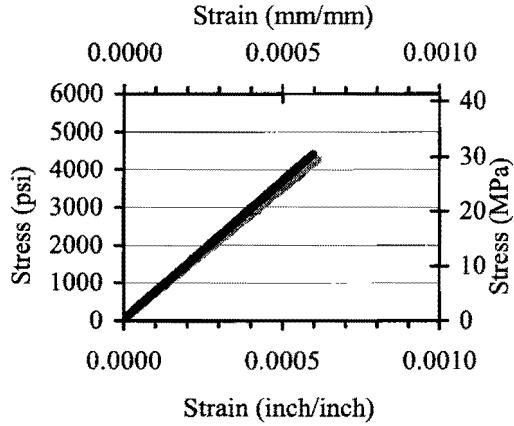
**Figure B.3. Stress-Strain Plots for Determination of Modulus of Elasticity for Batches A11-A12.**

258
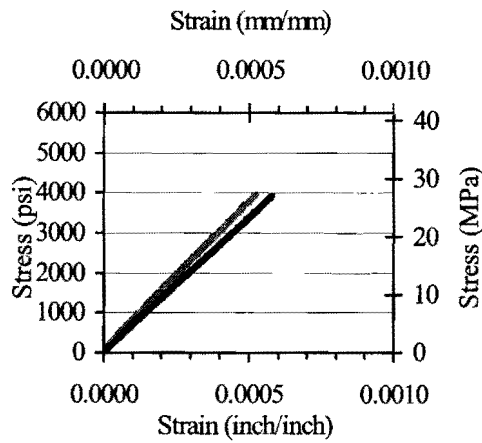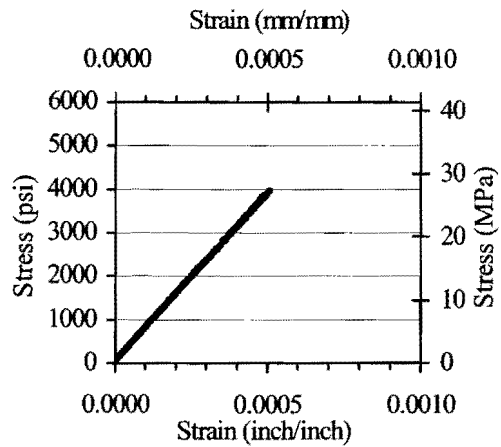
(a) A13 at 7 Days

(b) A14 at 7 Days
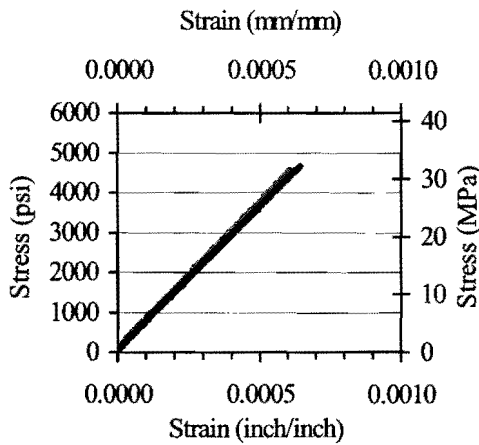
(c) A13 at 28 days
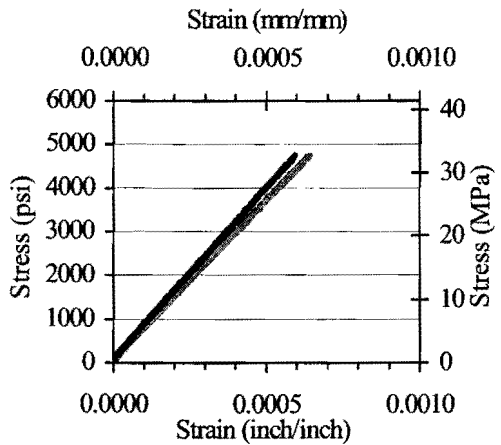
(d) A14 at 28 Days
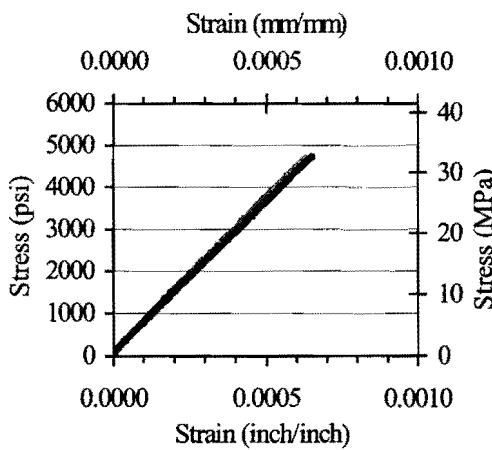
(e) A13 at 56 Days
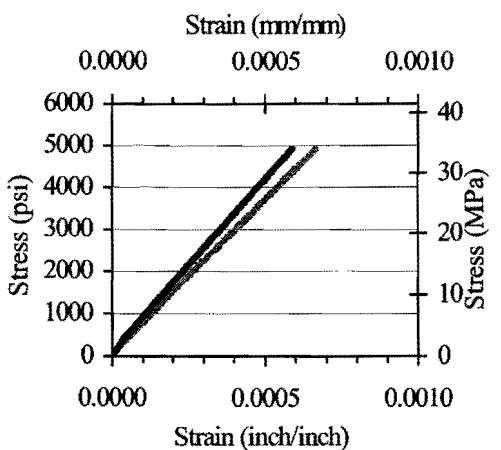
(f) A14 at 56 Days

Figure B.4. Stress-Strain Plots for Determination of Modulus of Elasticity for Batches A13-A14.
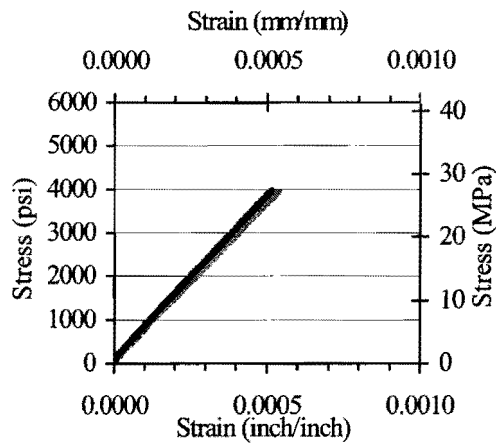
259
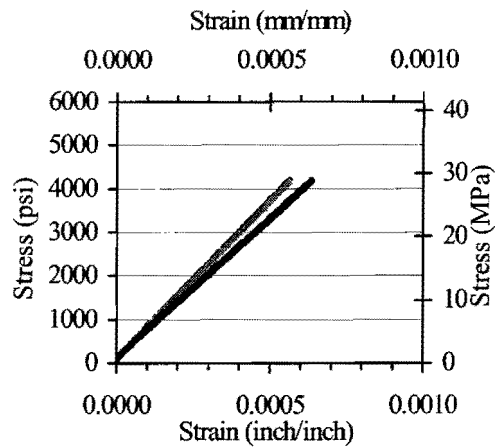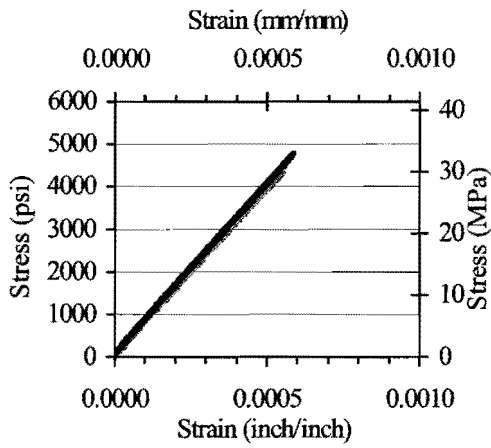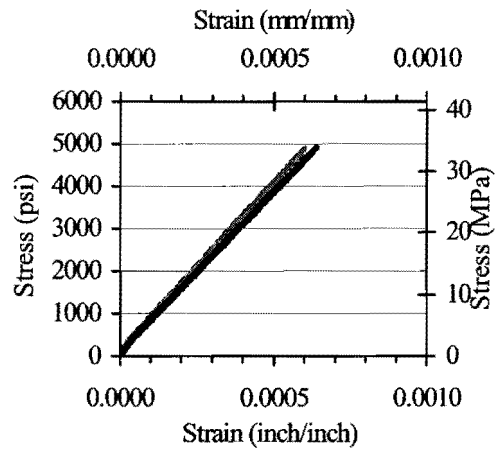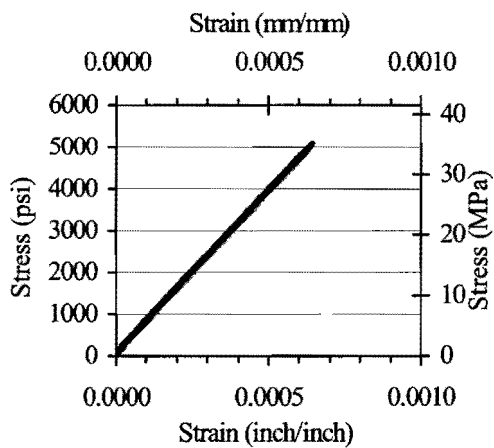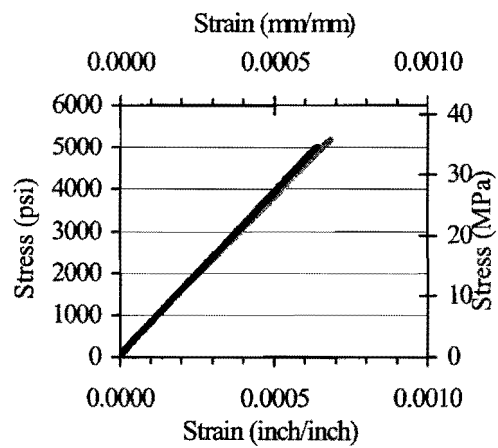
Figure B.5. Stress-Strain Plots for Determination of Modulus of Elasticity for Batches A15-A16.
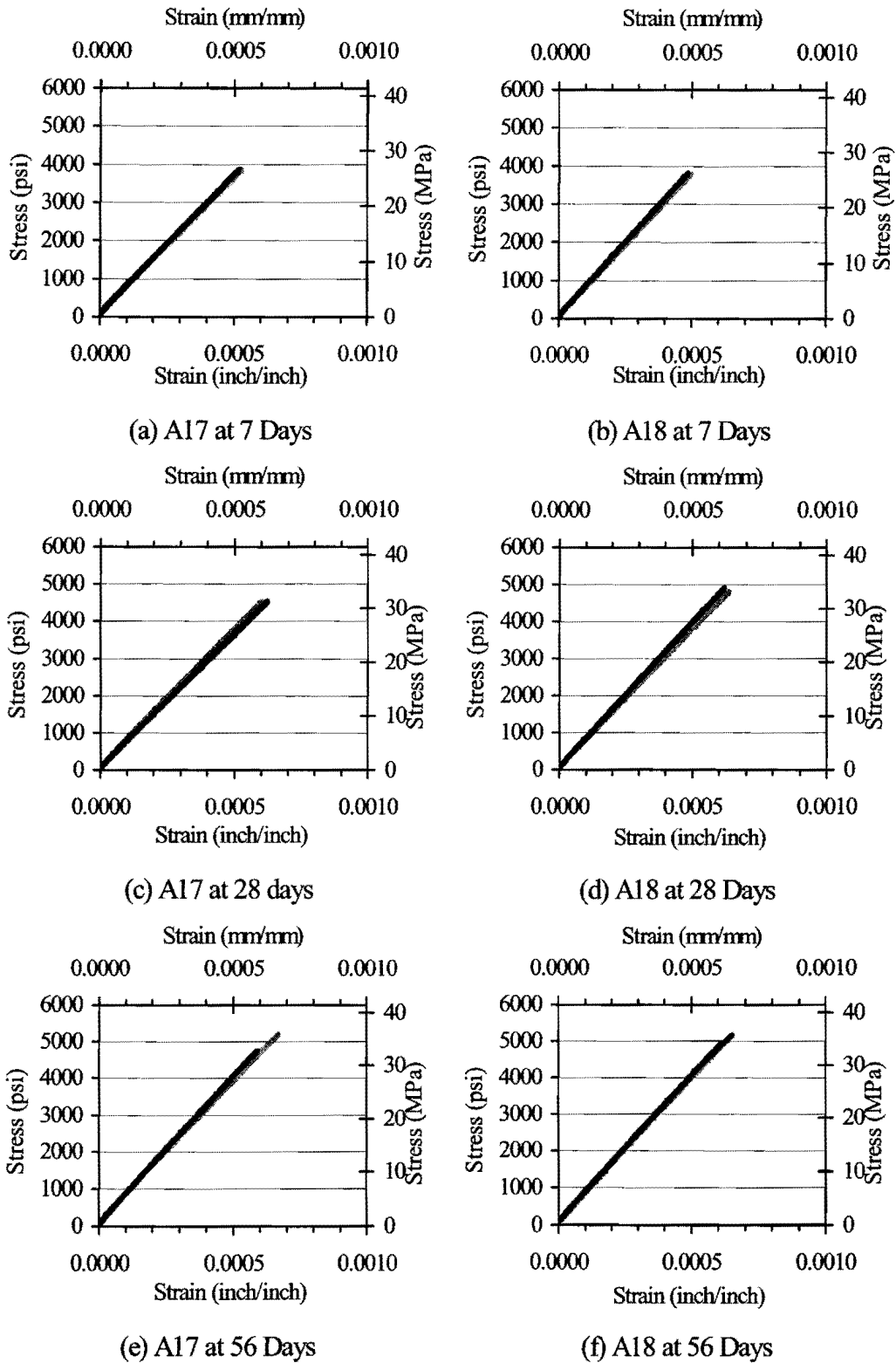
Figure B.6. Stress-Strain Plots for Determination of Modulus of Elasticity for Batches A17-A18.
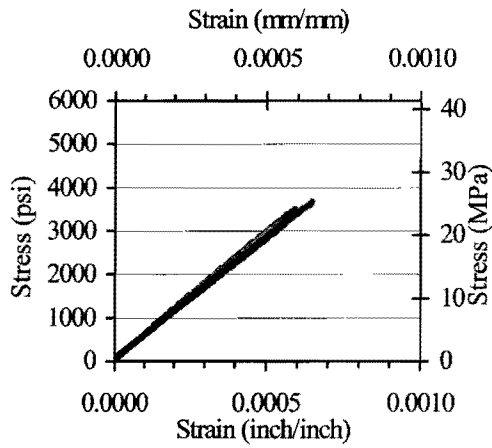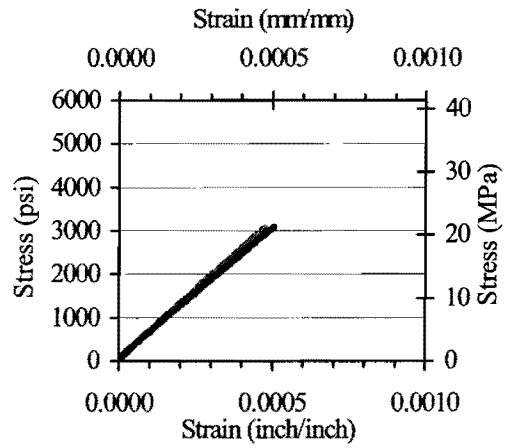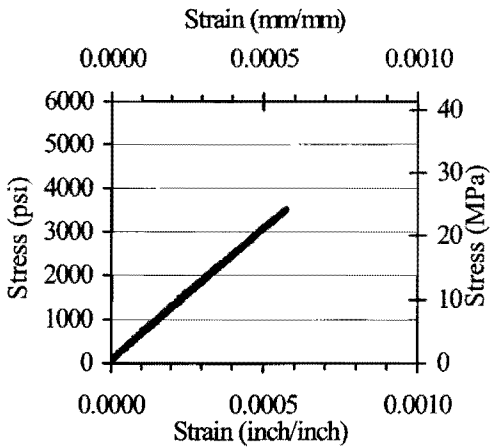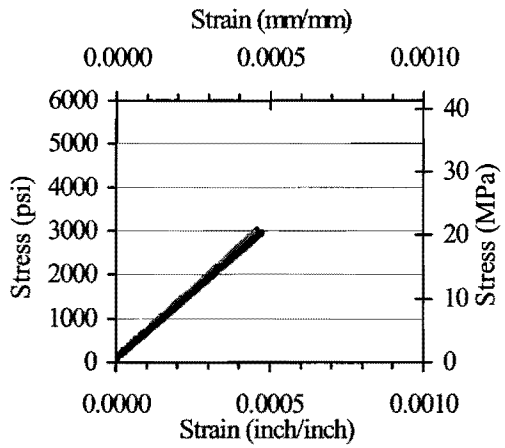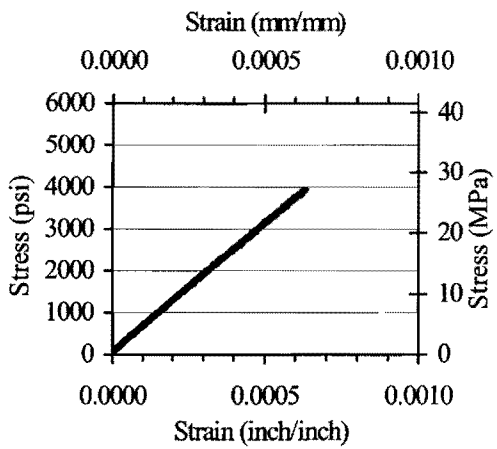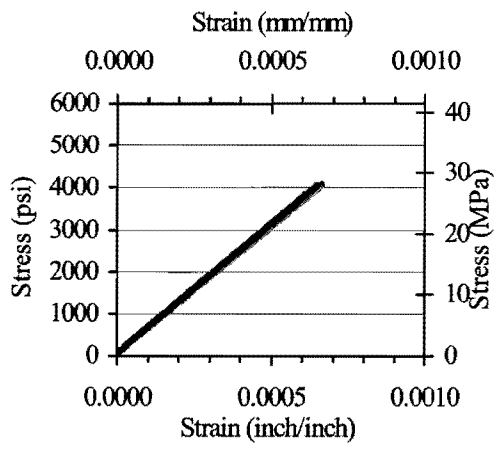
Figure B.7. Stress-Strain Plots for Determination of Modulus of Elasticity for Batches B5-B6.
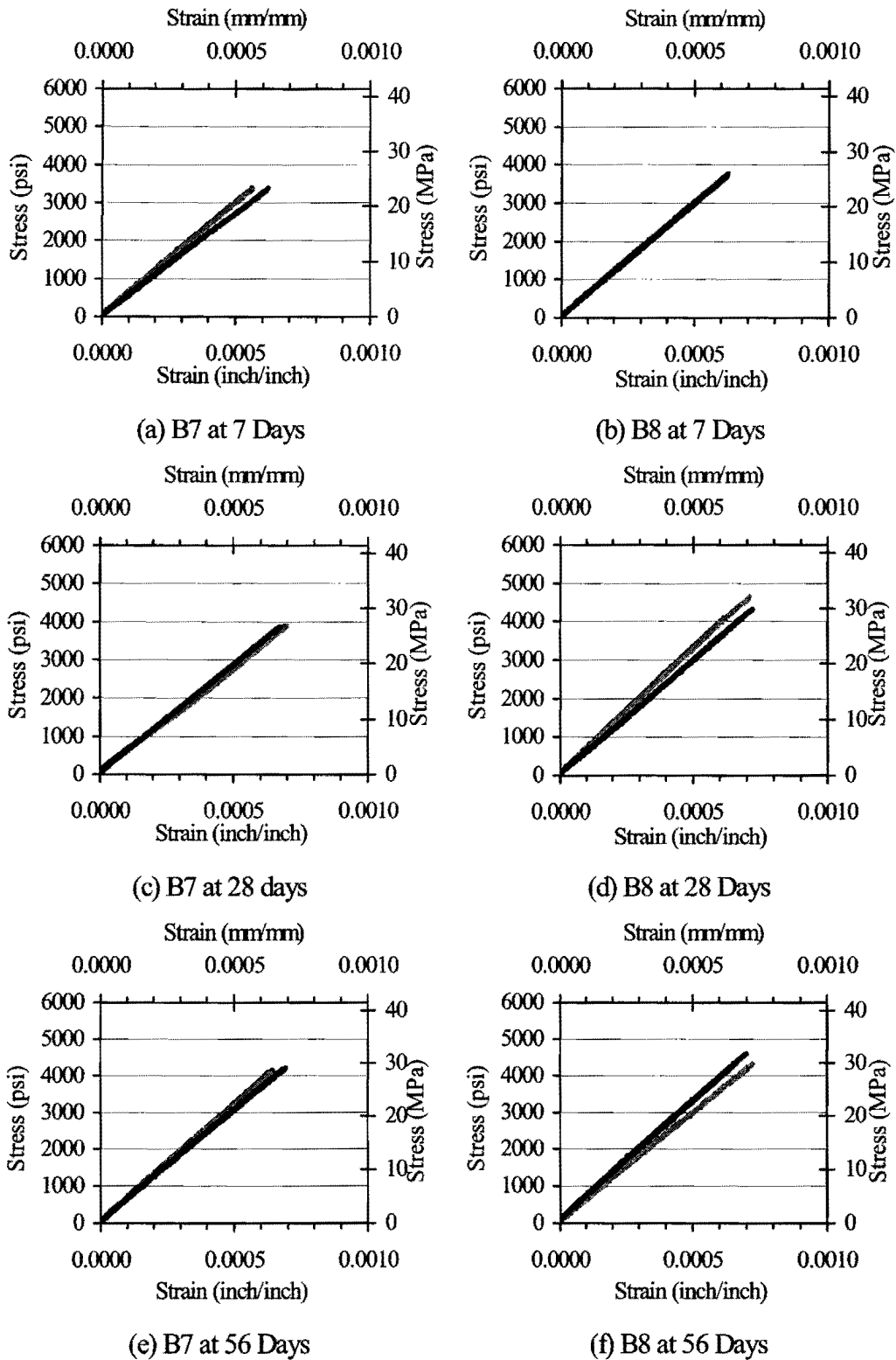
Figure B.8. Stress-Strain Plots for Determination of Modulus of Elasticity for Batches B7-B8.

263
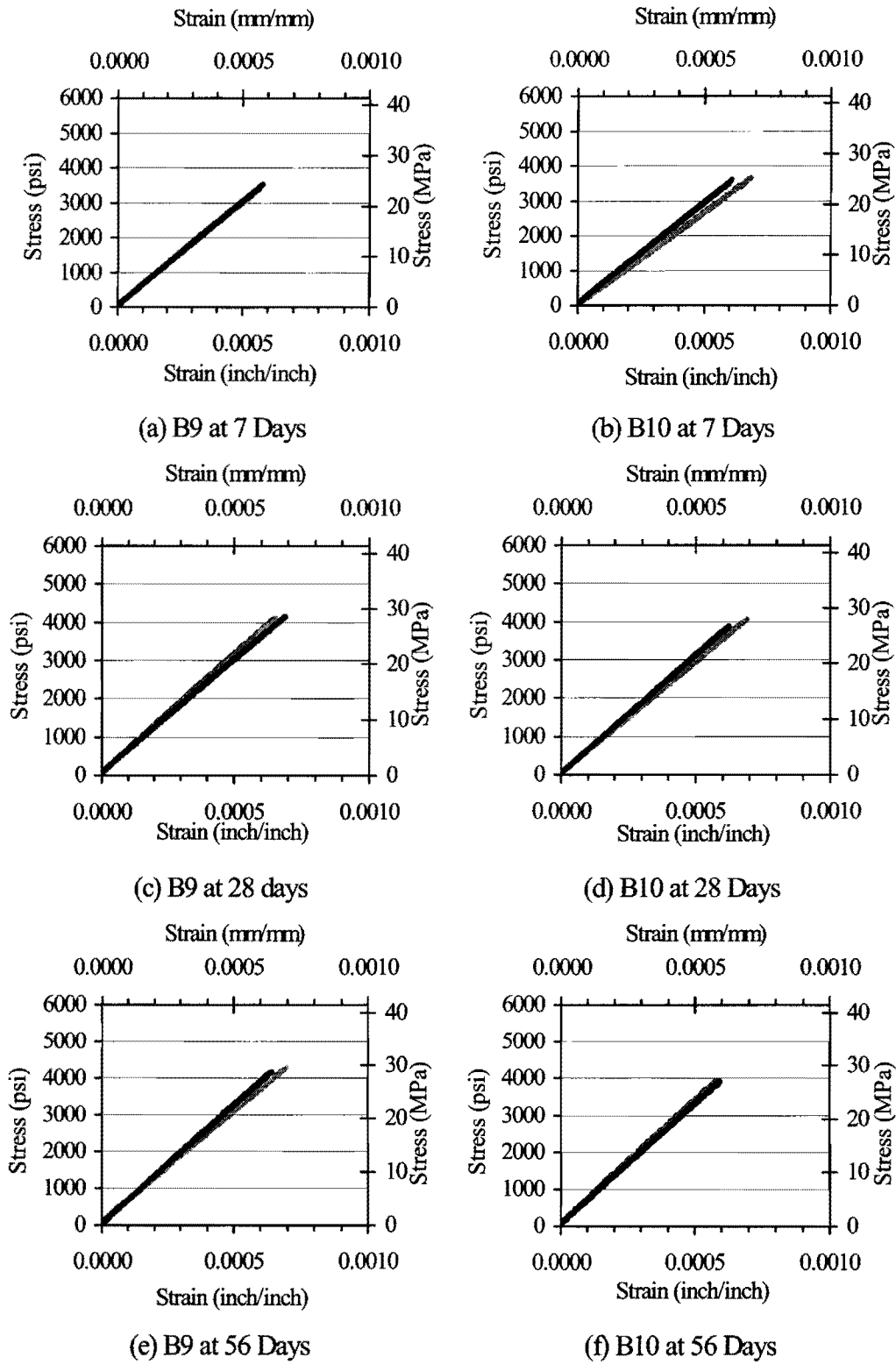
**Figure B.9. Stress-Strain Plots for Determination of Modulus of Elasticity for Batches B9-B10.**
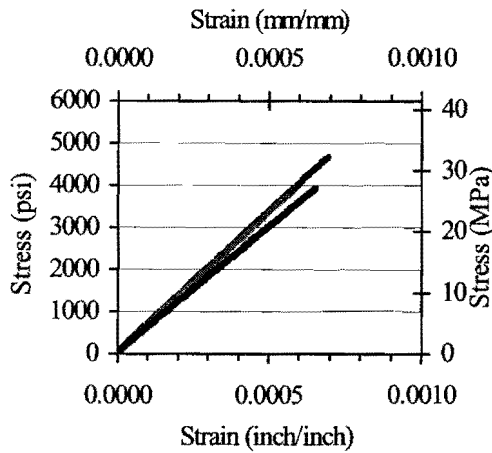
(a) B11 at 7 Days
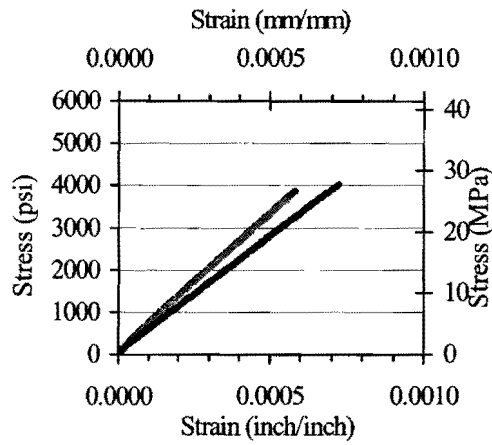
(b) B12 at 7 Days
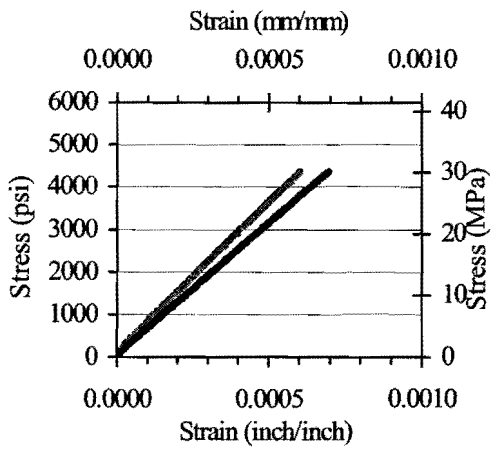
(c) B11 at 28 days
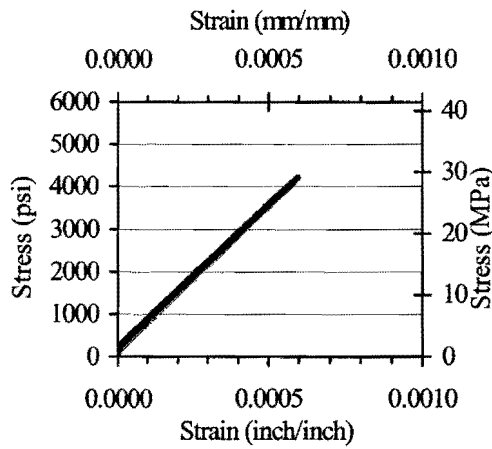
(d) B12 at 28 Days
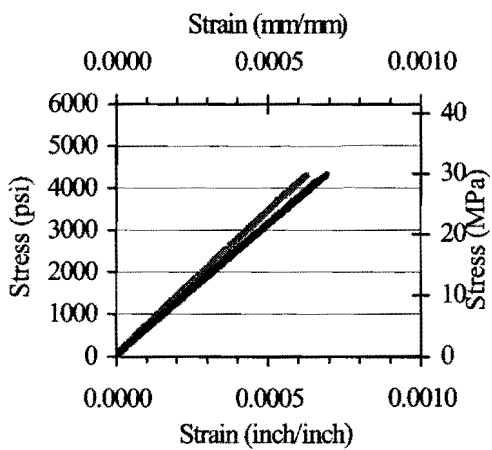
(e) B11 at 56 Days
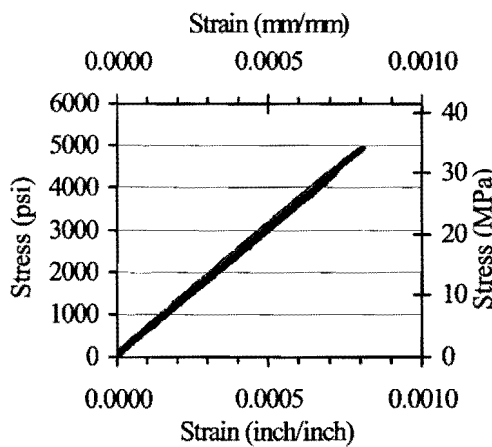
(f) B12 at 56 Days

Figure B.10. Stress-Strain Plots for Determination of Modulus of Elasticity for Batches B11-B12.
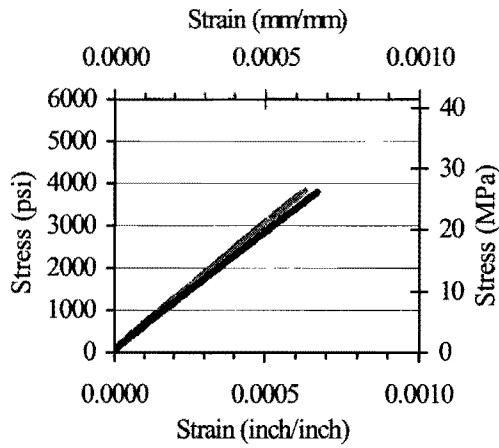
(a) B13 at 7 Days
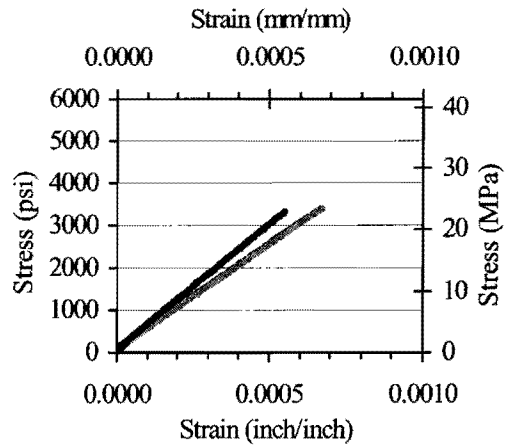
(b) B14 at 7 Days
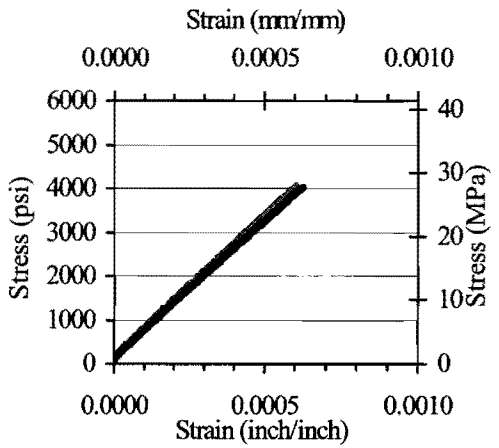
(c) B13 at 28 days
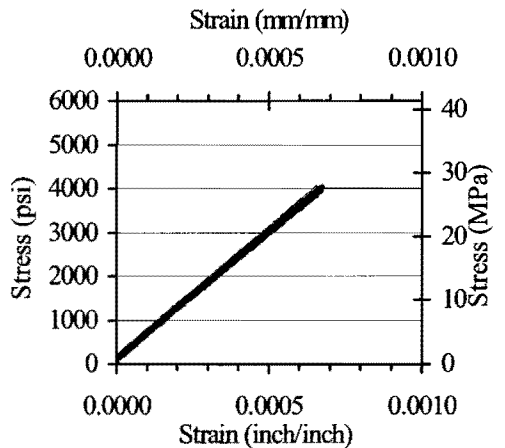
(d) B14 at 28 Days
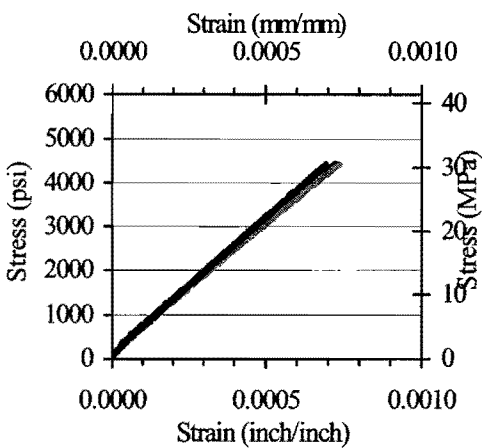
(e) B13 at 56 Days
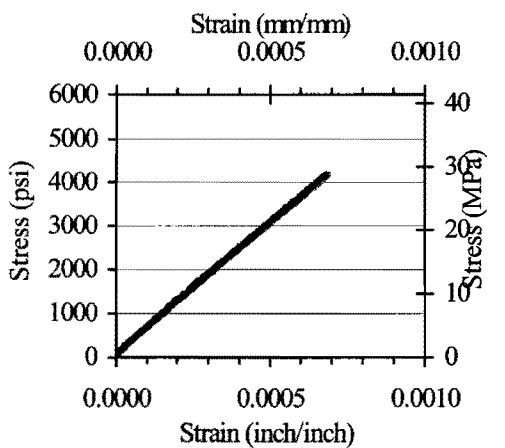
(f) B14 at 56 Days

Figure B.11. Stress-Strain Plots for Determination of Modulus of Elasticity for Batches B13-B14.
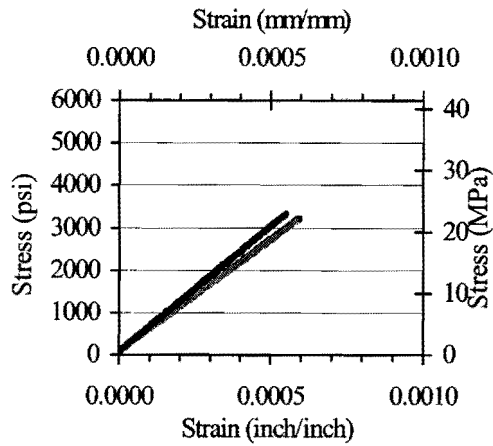
(a) B15 at 7 Days
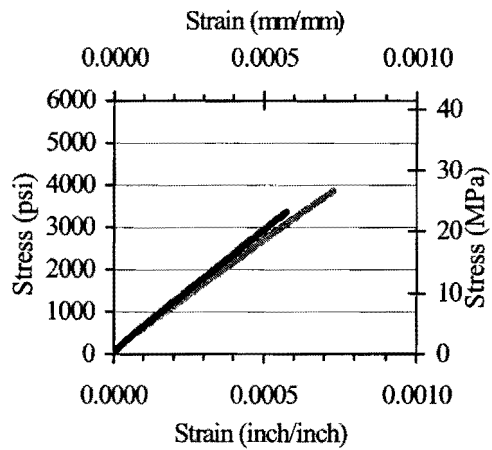
(b) B16 at 7 Days
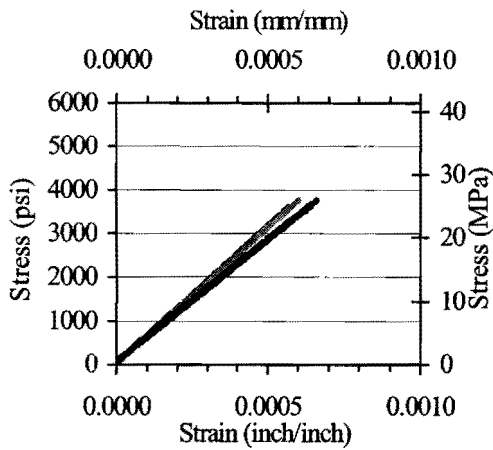
(c) B15 at 28 days
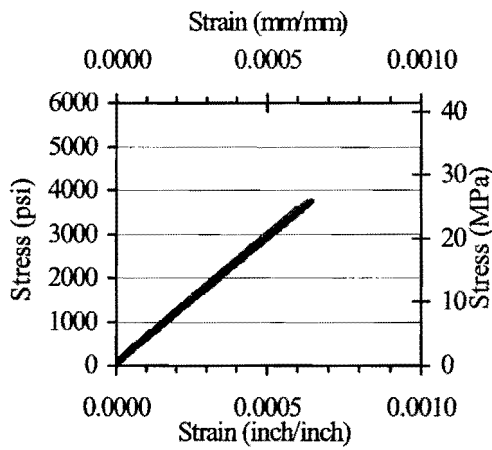
(d) B16 at 28 Days
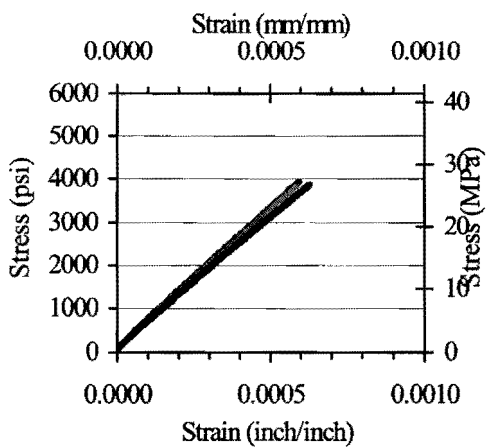
(e) B15 at 56 Days
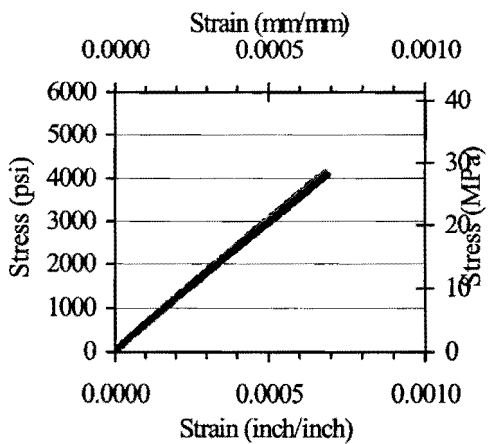
(f) B16 at 56 Days

Figure B.12. Stress-Strain Plots for Determination of Modulus of Elasticity for Batches B15-B16.
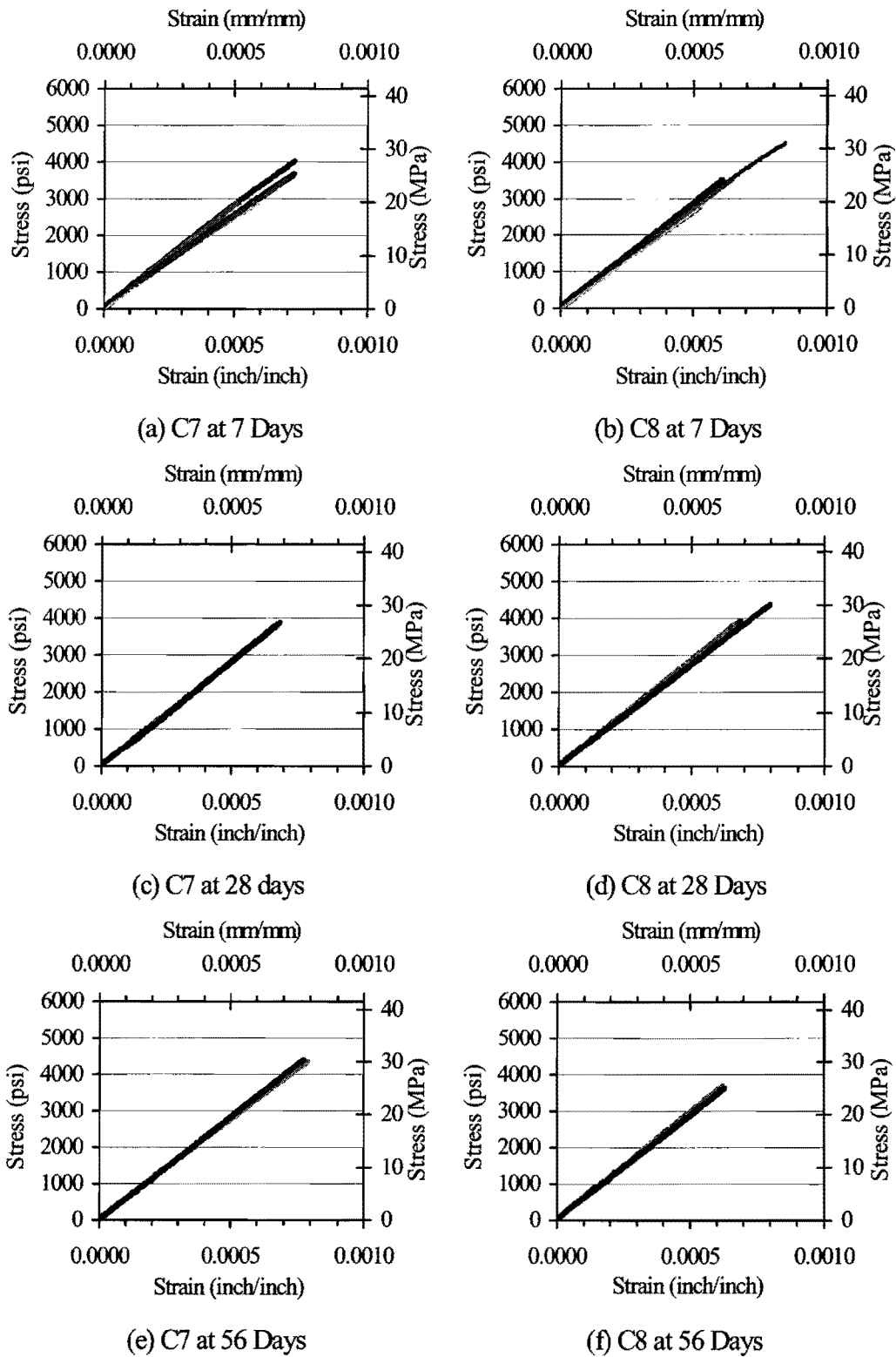
Figure B.13. Stress-Strain Plots for Determination of Modulus of Elasticity for Batches C7-C8.

268
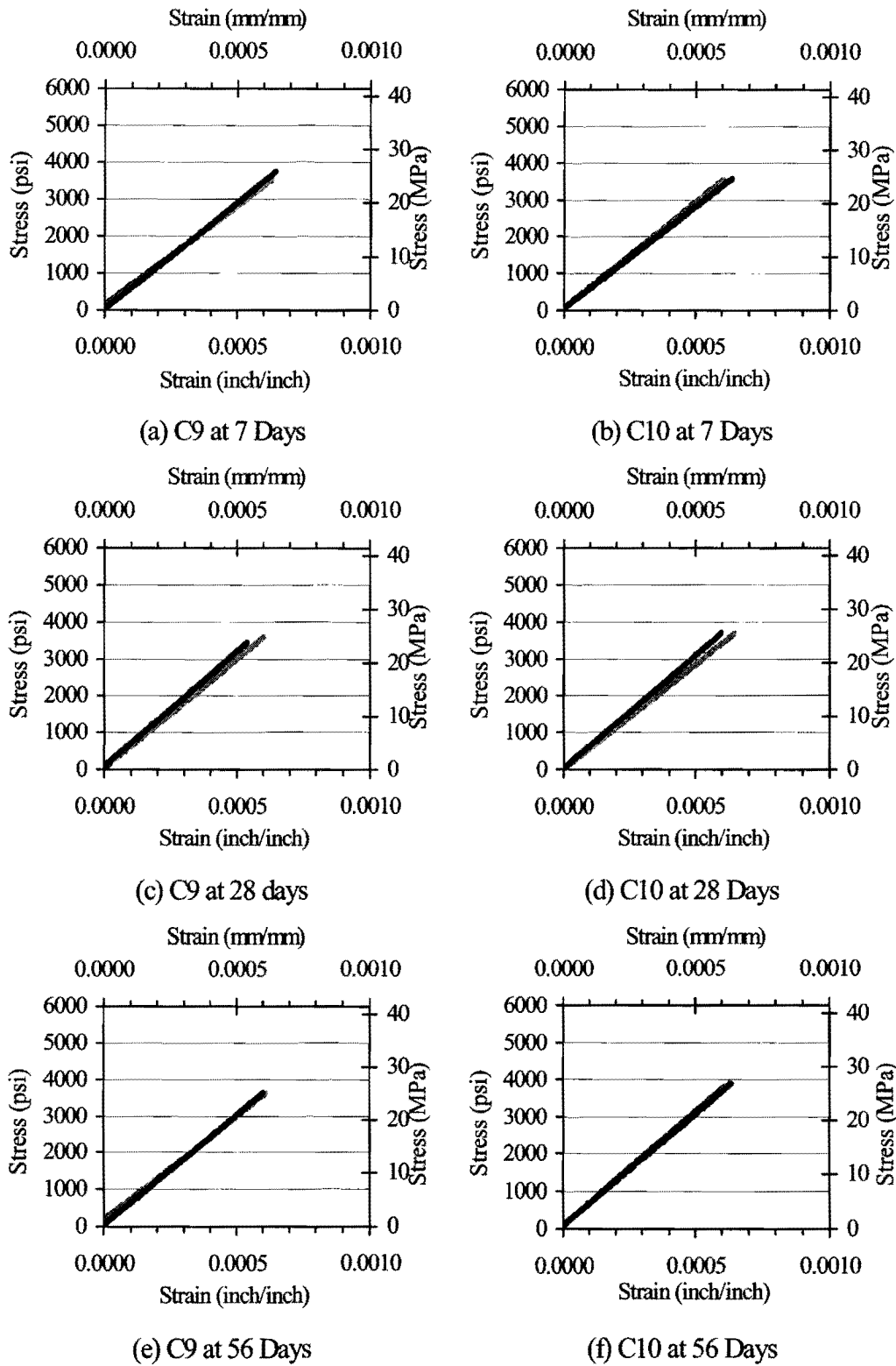
Figure B.14. Stress-Strain Plots for Determination of Modulus of Elasticity for Batches C9-C10.
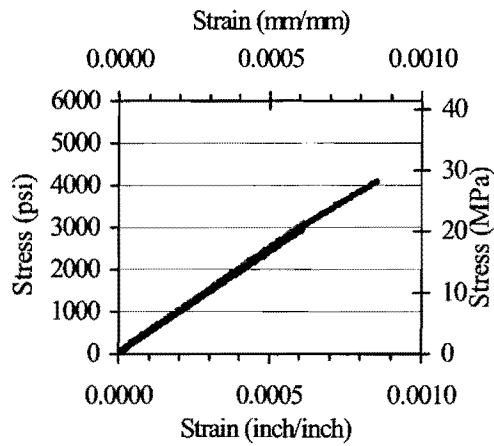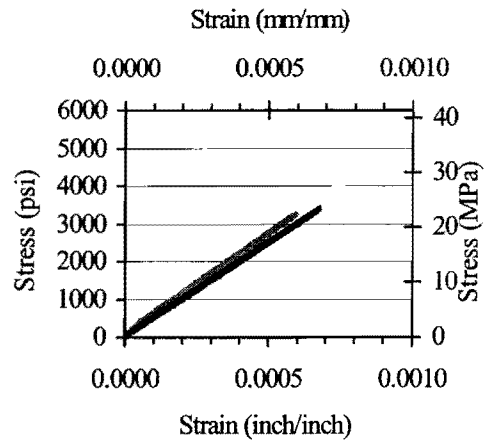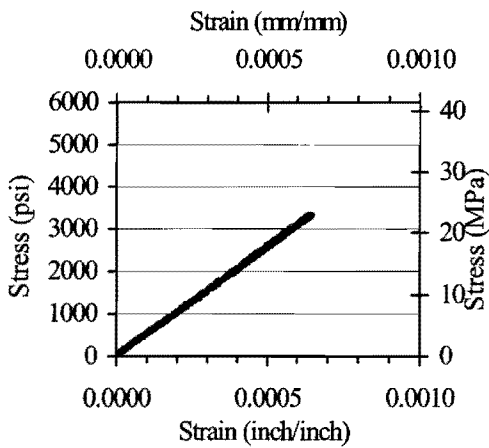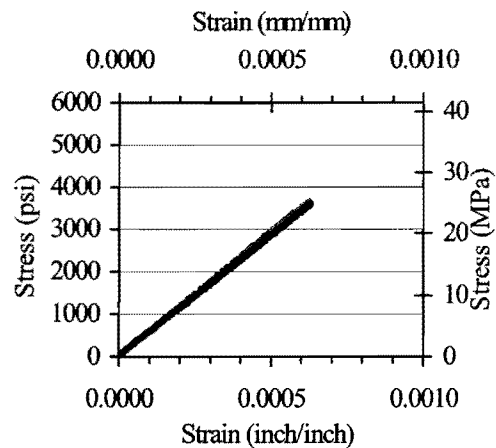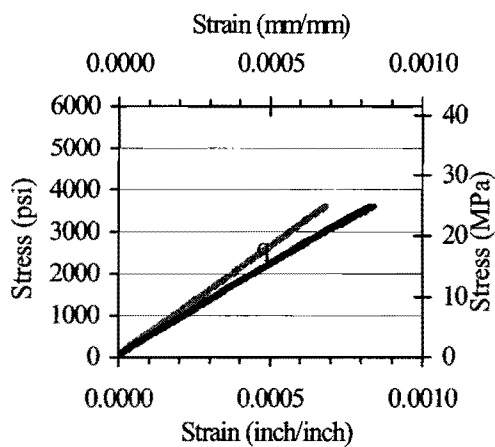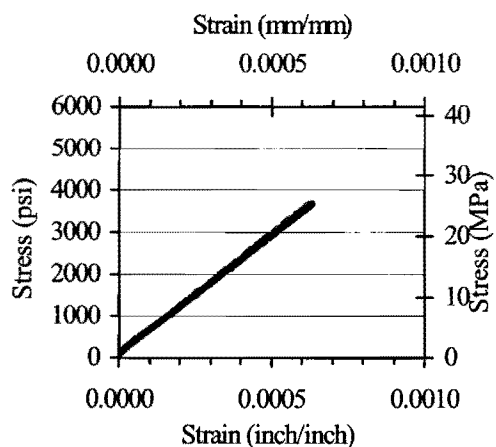
Figure B.15. Stress-Strain Plots for Determination of Modulus of Elasticity for Batches C11-C12.
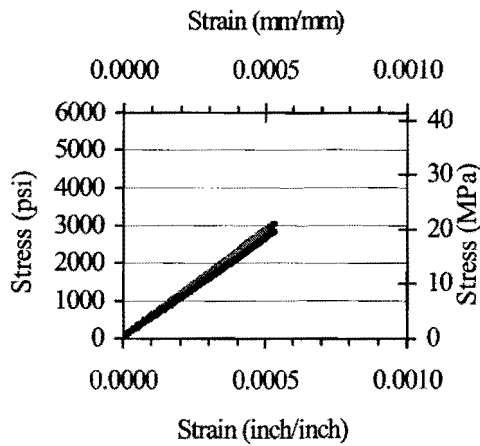
270
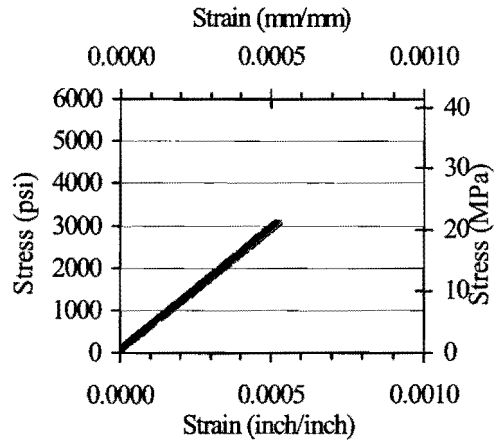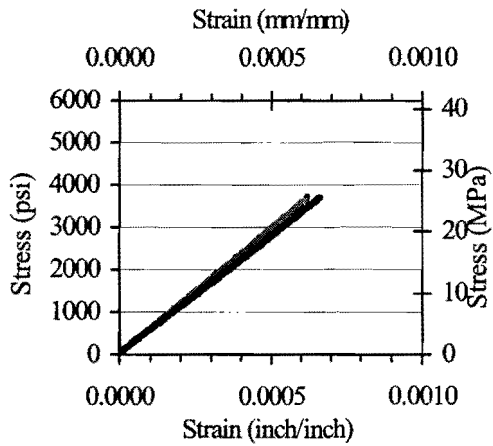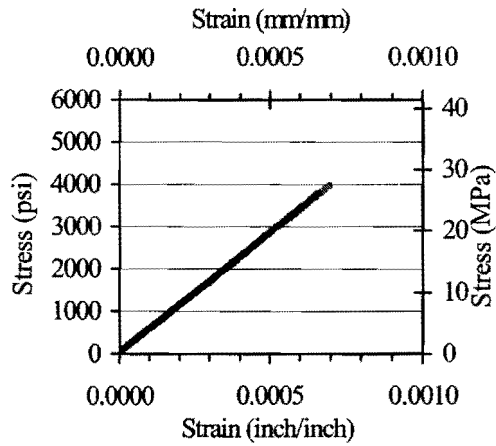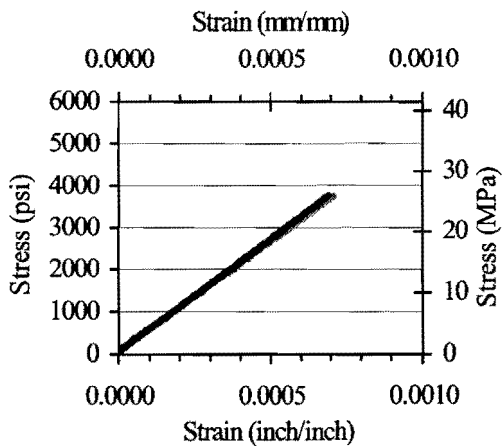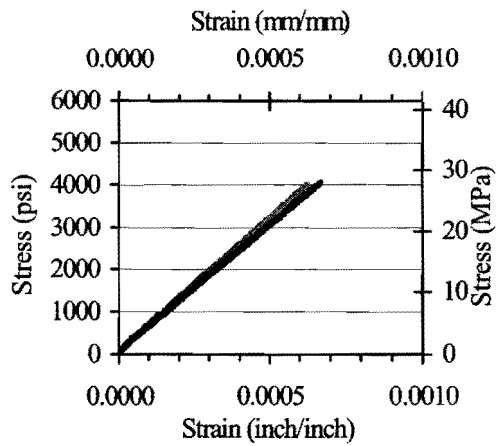
Figure B.16. Stress-Strain Plots for Determination of Modulus of Elasticity for Batches C13-C14.
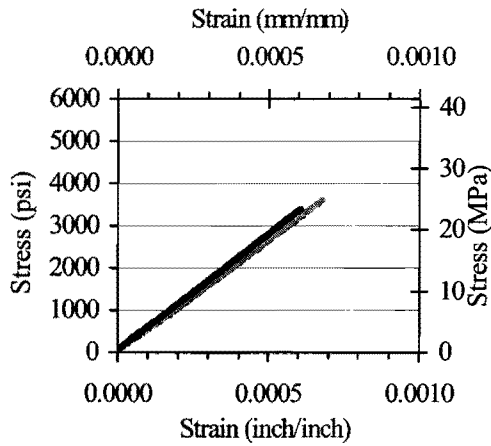
271
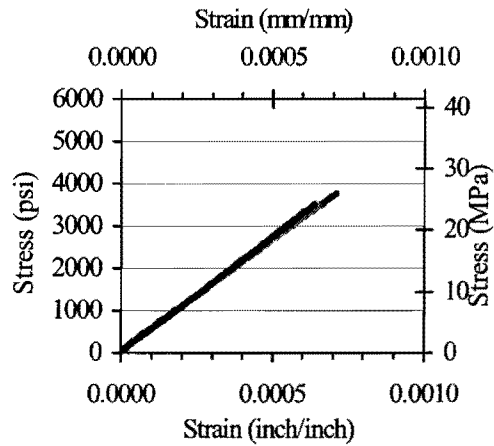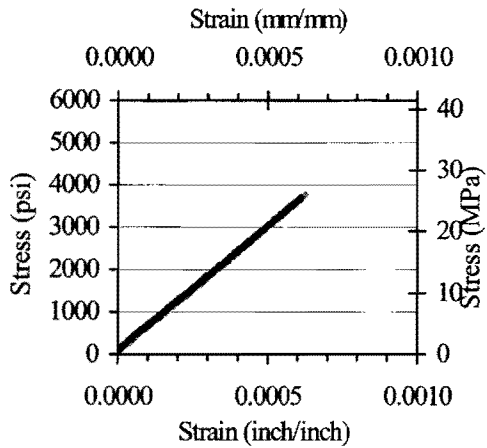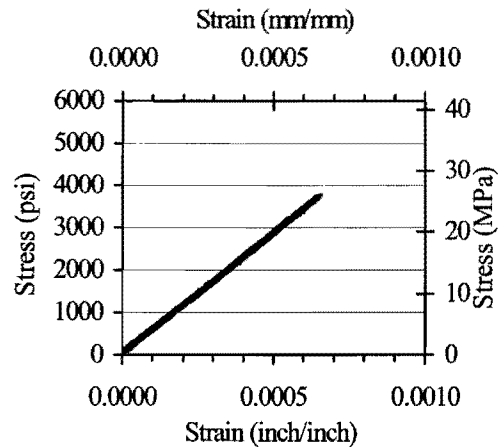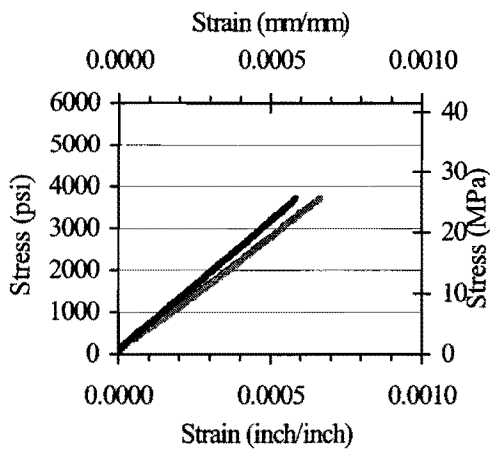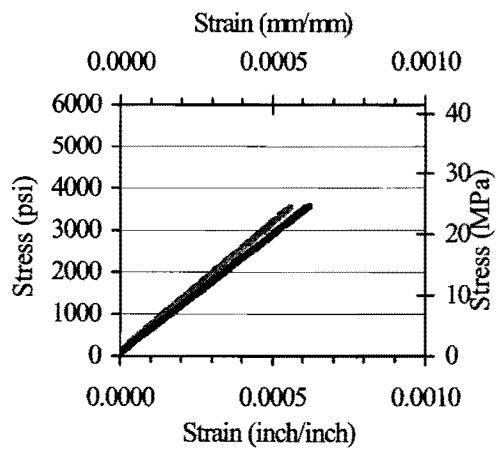
Figure B.17. Stress-Strain Plots for Determination of Modulus of Elasticity for Batches C15-C16.
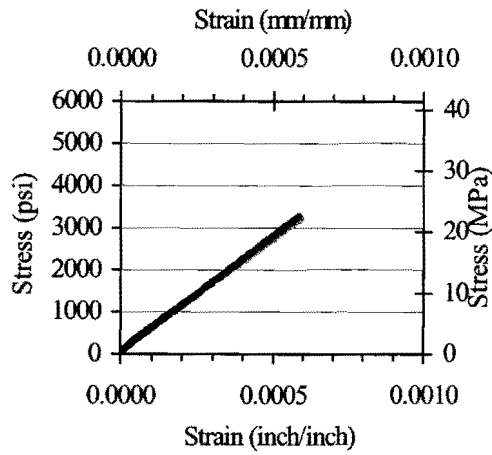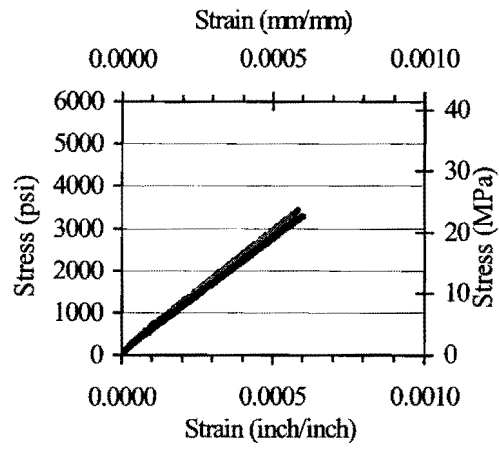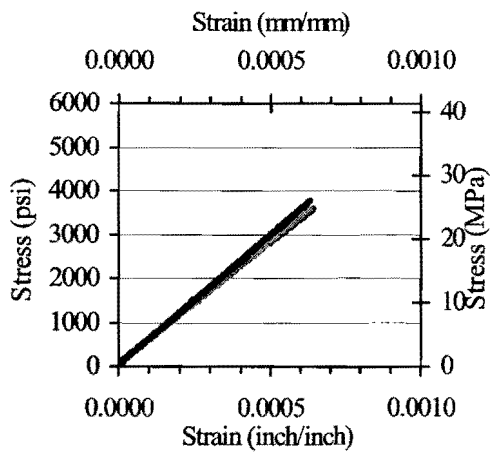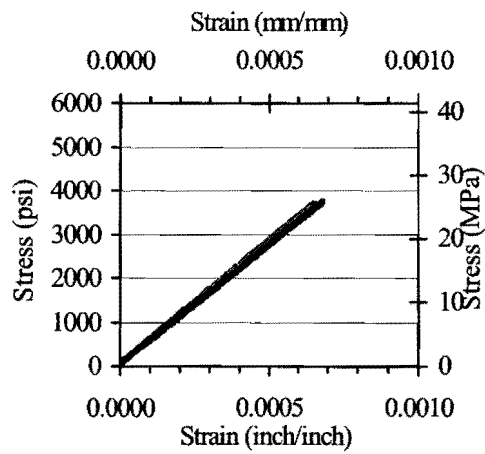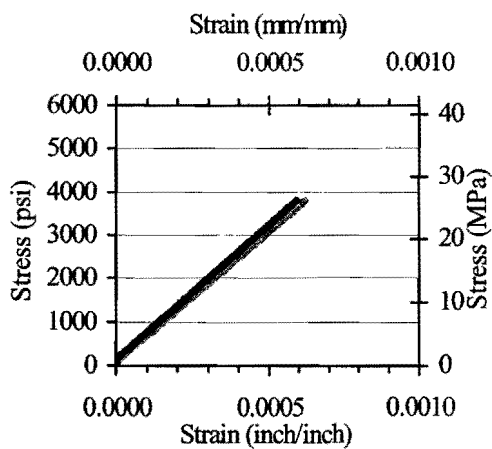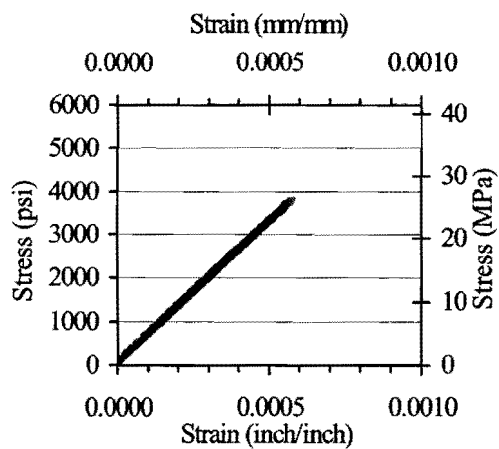
Figure B.18. Stress-Strain Plots for Determination of Modulus of Elasticity for Batches C17-C18.

273

Table B.13. Ratio of Batch Average to 28-Day Batch Average for Compressive Strength.

Batch No.	Set	f'c Class	Batch Average (psi)				Ratio to 28-Day Average			
			Release	7 Days	28 Days	56 Days	Release	7 Days	28 Days	56 Days
A15	1	6000 psi	7800	10000	11813	12277	0.66	0.85	1.00	1.04
A16	1	6000 psi	7800	10433	11770	12515	0.66	0.89	1.00	1.06
A5	1	8000 psi	NI	NI	NI	NI	N/A	N/A	N/A	N/A
A6	1	8000 psi	NI	NI	NI	NI	N/A	N/A	N/A	N/A
A13	1	8000 psi	7800	9747	11285	11701	0.69	0.86	1.00	1.04
A14	1	8000 psi	7800	9915	11720	12186	0.67	0.85	1.00	1.04
A17	1	10000 psi	7020	9938	11240	11801	0.62	0.88	1.00	1.05
A18	1	10000 psi	7020	10459	11976	12189	0.59	0.87	1.00	1.02
A7	2	6000 psi	5695	8757	9920	10360	0.57	0.88	1.00	1.04
A8	2	6000 psi	5695	8495	9393	10155	0.61	0.90	1.00	1.08
A9	2	8000 psi	6370	9696	11454	11717	0.56	0.85	1.00	1.02
A10	2	8000 psi	6370	10027	11561	11910	0.55	0.87	1.00	1.03
A11	2	10000 psi	7100	8629	10057	10744	0.71	0.86	1.00	1.07
A12	2	10000 psi	7100	8664	9614	10601	0.74	0.90	1.00	1.10
						Precaster Average	**0.64**	**0.87**	**1.00**	**1.05**
B3	1	6000 psi	NI	NI	NI	NI	N/A	N/A	N/A	N/A
B4	1	6000 psi	NI	NI	NI	NI	N/A	N/A	N/A	N/A
B11	1	6000 psi	7845	9253	10842	10709	0.72	0.85	1.00	0.99
B12	1	6000 psi	7845	9034	10167	10684	0.77	0.89	1.00	1.05
B13	1	8000 psi	6774	9222	10037	10822	0.67	0.92	1.00	1.08
B14	1	8000 psi	5659	8187	9949	10378	0.57	0.82	1.00	1.04
B7	1	10000 psi	6537	8491	9635	10366	0.68	0.88	1.00	1.08
B8	1	10000 psi	6537	9010	10145	10888	0.64	0.89	1.00	1.07
B9	2	6000 psi	6537	8458	10177	10414	0.64	0.83	1.00	1.02
B10	2	6000 psi	6537	8294	9615	9735	0.68	0.86	1.00	1.01
B15	2	8000 psi	6320	8059	8896	9594	0.71	0.91	1.00	1.08
B16	2	8000 psi	6498	8175	9294	10050	0.70	0.88	1.00	1.08
B5	2	10000 psi	6293	7946	9239	9782	0.68	0.86	1.00	1.06
B6	2	10000 psi	6293	7913	9278	10012	0.68	0.85	1.00	1.08
						Precaster Average	**0.68**	**0.87**	**1.00**	**1.05**
C15	1	6000 psi	7223	8442	9204	9239	0.78	0.92	1.00	1.00
C16	1	6000 psi	7223	8723	9300	8861	0.78	0.94	1.00	0.95
C3	1	8000 psi	NI	NI	NI	NI	N/A	N/A	N/A	N/A
C4	1	8000 psi	NI	NI	NI	NI	N/A	N/A	N/A	N/A
C13	1	8000 psi	6287	7916	9158	9306	0.69	0.86	1.00	1.02
C14	1	8000 psi	6287	8506	9396	9939	0.67	0.91	1.00	1.06
C17	1	10000 psi	7800	7961	8951	9466	0.87	0.89	1.00	1.06
C18	1	10000 psi	7800	8073	9244	9478	0.84	0.87	1.00	1.03
C7	2	6000 psi	6450	8789	9498	9961	0.68	0.93	1.00	1.05
C8	2	6000 psi	6450	8709	9513	10015	0.68	0.92	1.00	1.05
C11	2	8000 psi	6567	7656	8261	9025	0.79	0.93	1.00	1.09
C12	2	8000 psi	6567	8201	8911	9065	0.74	0.92	1.00	1.02
C9	2	10000 psi	7092	8478	9354	9718	0.76	0.91	1.00	1.04
C10	2	10000 psi	7092	8731	10115	10206	0.70	0.86	1.00	1.01
						Precaster Average	**0.75**	**0.90**	**1.00**	**1.03**
						Overall Average	**0.69**	**0.88**	**1.00**	**1.04**

274

Table B.14. Ratio of Batch Average to 28-Day Batch Average for Modulus of Elasticity.

Batch No.	Set	f'c Class	Batch Average (psi) 7 Days	Batch Average (psi) 28 Days	Batch Average (psi) 56 Days	Ratio to 28-Day Average 7 Days	Ratio to 28-Day Average 28 Days	Ratio to 28-Day Average 56 Days
A15	1	6000 psi	7342632	7883587	7780171	0.93	1.00	0.99
A16	1	6000 psi	6822249	7742723	7657179	0.88	1.00	0.99
A5	1	8000 psi	NR	NR	NR	N/A	N/A	N/A
A6	1	8000 psi	NR	NR	NR	N/A	N/A	N/A
A13	1	8000 psi	7070648	7244789	7251827	0.98	1.00	1.00
A14	1	8000 psi	7712517	7555760	7757786	1.02	1.00	1.03
A17	1	10000 psi	7191284	7270314	7806684	0.99	1.00	1.07
A18	1	10000 psi	7557589	7583556	7863591	1.00	1.00	1.04
A7	2	6000 psi	7053402	7002962	7344773	1.01	1.00	1.05
A8	2	6000 psi	6858273	7471298	7579456	0.92	1.00	1.01
A9	2	8000 psi	6947668	7301139	7310525	0.95	1.00	1.00
A10	2	8000 psi	7363699	7358513	7543871	1.00	1.00	1.03
A11	2	10000 psi	6729006	6742949	7295096	1.00	1.00	1.08
A12	2	10000 psi	6896097	7020166	7136030	0.98	1.00	1.02
					Precaster Average	0.97	1.00	1.03
B3	1	6000 psi	NR	NR	NR	N/A	N/A	N/A
B4	1	6000 psi	NR	NR	NR	N/A	N/A	N/A
B11	1	6000 psi	6268537	6603573	6459454	0.95	1.00	0.98
B12	1	6000 psi	5990224	6763782	6013680	0.89	1.00	0.89
B13	1	8000 psi	5759927	6320265	6018883	0.91	1.00	0.95
B14	1	8000 psi	5410739	5842106	5957734	0.93	1.00	1.02
B7	1	10000 psi	5652604	5548531	6179044	1.02	1.00	1.11
B8	1	10000 psi	5896709	6218476	6147232	0.95	1.00	0.99
B9	2	6000 psi	5920475	6054505	6243267	0.98	1.00	1.03
B10	2	6000 psi	5514727	5987163	6591322	0.92	1.00	1.10
B15	2	8000 psi	5552809	5865866	6178680	0.95	1.00	1.05
B16	2	8000 psi	5433467	5749920	5914802	0.94	1.00	1.03
B5	2	10000 psi	5742260	5742260	6101724	1.00	1.00	1.06
B6	2	10000 psi	6135538	6135538	6087874	1.00	1.00	0.99
					Precaster Average	0.95	1.00	1.02
C15	1	6000 psi	5361887	5852081	5768839	0.92	1.00	0.99
C16	1	6000 psi	5316550	5669291	5873662	0.94	1.00	1.04
C3	1	8000 psi	NR	NR	NR	N/A	N/A	N/A
C4	1	8000 psi	NR	NR	NR	N/A	N/A	N/A
C13	1	8000 psi	5467162	5703930	5256502	0.96	1.00	0.92
C14	1	8000 psi	5724921	5636111	6141728	1.02	1.00	1.09
C17	1	10000 psi	5379897	5718944	6061863	0.94	1.00	1.06
C18	1	10000 psi	5521769	5503201	6464934	1.00	1.00	1.17
C7	2	6000 psi	4918083	5578404	5541205	0.88	1.00	0.99
C8	2	6000 psi	5463248	5551066	5758729	0.98	1.00	1.04
C11	2	8000 psi	4894355	5108175	4684385	0.96	1.00	0.92
C12	2	8000 psi	5122080	5720468	5667847	0.90	1.00	0.99
C9	2	10000 psi	5569658	6029447	5794423	0.92	1.00	0.96
C10	2	10000 psi	5628182	5888487	6036981	0.96	1.00	1.03
					Precaster Average	0.95	1.00	1.02
					Overall Average	0.96	1.00	1.02

Table B.15. Ratio of Batch Average to 28-Day Batch Average for Splitting Tensile Strength.

Batch No.	Set	f'c Class	Batch Average (psi)			Ratio to 28-Day Average		
			7 Days	28 Days	56 Days	7 Days	28 Days	56 Days
A15	1	6000 psi	755	844	741	0.90	1.00	0.88
A16	1	6000 psi	834	880	748	0.95	1.00	0.85
A5	1	8000 psi	698	738	748	0.95	1.00	1.01
A6	1	8000 psi	813	597	761	1.36	1.00	1.27
A13	1	8000 psi	NT	NT	NT	N/A	N/A	N/A
A14	1	8000 psi	NT	NT	NT	N/A	N/A	N/A
A17	1	10000 psi	693	794	873	0.87	1.00	1.10
A18	1	10000 psi	748	728	808	1.03	1.00	1.11
A7	2	6000 psi	753	614	721	1.23	1.00	1.17
A8	2	6000 psi	644	688	767	0.94	1.00	1.12
A9	2	8000 psi	581	743	865	0.78	1.00	1.16
A10	2	8000 psi	613	868	908	0.71	1.00	1.05
A11	2	10000 psi	694	704	778	0.99	1.00	1.11
A12	2	10000 psi	674	788	794	0.86	1.00	1.01
					Precaster Average	0.96	1.00	1.07
B3	1	6000 psi	646	653	605	0.99	1.00	0.93
B4	1	6000 psi	544	648	649	0.84	1.00	1.00
B11	1	6000 psi	NT	NT	NT	N/A	N/A	N/A
B12	1	6000 psi	NT	NT	NT	N/A	N/A	N/A
B13	1	8000 psi	702	625	608	1.12	1.00	0.97
B14	1	8000 psi	599	756	580	0.79	1.00	0.77
B7	1	10000 psi	627	620	713	1.01	1.00	1.15
B8	1	10000 psi	661	735	560	0.90	1.00	0.76
B9	2	6000 psi	679	770	745	0.88	1.00	0.97
B10	2	6000 psi	645	579	600	1.11	1.00	1.04
B15	2	8000 psi	628	569	659	1.10	1.00	1.16
B16	2	8000 psi	587	595	687	0.99	1.00	1.15
B5	2	10000 psi	623	678	633	0.92	1.00	0.93
B6	2	10000 psi	645	707	650	0.91	1.00	0.92
					Precaster Average	0.96	1.00	0.98
C15	1	6000 psi	623	647	648	0.96	1.00	1.00
C16	1	6000 psi	605	546	637	1.11	1.00	1.17
C3	1	8000 psi	509	568	533	0.90	1.00	0.94
C4	1	8000 psi	589	590	561	1.00	1.00	0.95
C13	1	8000 psi	NT	NT	NT	N/A	N/A	N/A
C14	1	8000 psi	NT	NT	NT	N/A	N/A	N/A
C17	1	10000 psi	578	615	621	0.94	1.00	1.01
C18	1	10000 psi	645	618	630	1.04	1.00	1.02
C7	2	6000 psi	554	625	663	0.89	1.00	1.06
C8	2	6000 psi	616	628	662	0.98	1.00	1.05
C11	2	8000 psi	592	610	555	0.97	1.00	0.91
C12	2	8000 psi	574	602	635	0.95	1.00	1.05
C9	2	10000 psi	546	617	656	0.88	1.00	1.06
C10	2	10000 psi	568	656	664	0.87	1.00	1.01
					Precaster Average	0.96	1.00	1.02
					Overall Average	0.96	1.00	1.02

Table B.16. Ratio of Batch Average to 28-Day Batch Average for Modulus of Rupture.

Batch No.	Set	f'c Class	Batch Average (psi) 7 Days	Batch Average (psi) 28 Days	Batch Average (psi) 56 Days	Ratio to 28-Day Average 7 Days	Ratio to 28-Day Average 28 Days	Ratio to 28-Day Average 56 Days
A15	1	6000 psi	1024	1250	1397	0.82	1.00	1.12
A16	1	6000 psi	1092	1293	1420	0.84	1.00	1.10
A5	1	8000 psi	883	1001	1070	0.88	1.00	1.07
A6	1	8000 psi	889	1063	1099	0.84	1.00	1.03
A13	1	8000 psi	NT	NT	NT	N/A	N/A	N/A
A14	1	8000 psi	NT	NT	NT	N/A	N/A	N/A
A17	1	10000 psi	1110	1232	1277	0.90	1.00	1.04
A18	1	10000 psi	1112	1199	1291	0.93	1.00	1.08
A7	2	6000 psi	954	971	1217	0.98	1.00	1.25
A8	2	6000 psi	910	956	1147	0.95	1.00	1.20
A9	2	8000 psi	937	1050	1261	0.89	1.00	1.20
A10	2	8000 psi	974	1129	1454	0.86	1.00	1.29
A11	2	10000 psi	947	934	1072	1.01	1.00	1.15
A12	2	10000 psi	970	998	958	0.97	1.00	0.96
					Precaster Average	0.91	1.00	1.12
B3	1	6000 psi	922	930	1093	0.99	1.00	1.18
B4	1	6000 psi	937	948	1126	0.99	1.00	1.19
B11	1	6000 psi	NT	NT	NT	N/A	N/A	N/A
B12	1	6000 psi	NT	NT	NT	N/A	N/A	N/A
B13	1	8000 psi	1047	1112	1177	0.94	1.00	1.06
B14	1	8000 psi	1025	1170	1131	0.88	1.00	0.97
B7	1	10000 psi	1076	1077	1093	1.00	1.00	1.01
B8	1	10000 psi	1069	1107	1079	0.97	1.00	0.97
B9	2	6000 psi	1039	1134	1035	0.92	1.00	0.91
B10	2	6000 psi	1011	1117	1136	0.91	1.00	1.02
B15	2	8000 psi	1005	1113	1105	0.90	1.00	0.99
B16	2	8000 psi	1014	1108	1035	0.92	1.00	0.93
B5	2	10000 psi	1088	1146	1139	0.95	1.00	0.99
B6	2	10000 psi	1041	1139	1118	0.91	1.00	0.98
					Precaster Average	0.94	1.00	1.02
C15	1	6000 psi	914	1010	1089	0.90	1.00	1.08
C16	1	6000 psi	1031	1025	1055	1.01	1.00	1.03
C3	1	8000 psi	769	847	802	0.91	1.00	0.95
C4	1	8000 psi	792	908	902	0.87	1.00	0.99
C13	1	8000 psi	NT	NT	NT	N/A	N/A	N/A
C14	1	8000 psi	NT	NT	NT	N/A	N/A	N/A
C17	1	10000 psi	985	1107	1084	0.89	1.00	0.98
C18	1	10000 psi	883	1103	1022	0.80	1.00	0.93
C7	2	6000 psi	858	1009	983	0.85	1.00	0.97
C8	2	6000 psi	844	1016	1025	0.83	1.00	1.01
C11	2	8000 psi	908	953	861	0.95	1.00	0.90
C12	2	8000 psi	928	880	918	1.06	1.00	1.04
C9	2	10000 psi	842	1048	1012	0.80	1.00	0.96
C10	2	10000 psi	988	1111	1025	0.89	1.00	0.92
					Precaster Average	0.90	1.00	0.98
					Overall Average	0.91	1.00	1.04

Table B.17. Bias Factors for Compressive Strength.

Batch No.	Set	f'c Category	Compressive Strength (psi)				Bias Factor	
			Specified 28-Day	Specified Release	28-Day Batch Avg.	1-Day Batch Avg.	28-Day	1-Day
A15	1	6000 psi	6250	6250	11813	7800	1.89	1.25
A16	1	6000 psi	6250	6250	11770	7800	1.88	1.25
A5	1	8000 psi	8573	5416	11519	6960	1.34	1.29
A6	1	8000 psi	8573	5416	10965	6960	1.28	1.29
A13	1	8000 psi	8484	6324	11285	7800	1.33	1.23
A14	1	8000 psi	8484	6324	11720	7800	1.38	1.23
A17	1	10000 psi	8963	6252	11240	7020	1.25	1.12
A18	1	10000 psi	8963	6252	11976	7020	1.34	1.12
A7	2	6000 psi	5909	5284	9920	5695	1.68	1.08
A8	2	6000 psi	5909	5284	9393	5695	1.59	1.08
A9	2	8000 psi	7540	5890	11454	6370	1.52	1.08
A10	2	8000 psi	7540	5890	11561	6370	1.53	1.08
A11	2	10000 psi	9196	6919	10057	7100	1.09	1.03
A12	2	10000 psi	9196	6919	9614	7100	1.05	1.03
B3	1	6000 psi	7048	5508	9865	7192	1.40	1.31
B4	1	6000 psi	7942	6290	9438	6550	1.19	1.04
B11	1	6000 psi	6525	6525	10842	7845	1.66	1.20
B12	1	6000 psi	6525	6525	10167	7845	1.56	1.20
B13	1	8000 psi	8000	N/A	10037	6774	1.25	N/A
B14	1	8000 psi	8000	N/A	9949	5659	1.24	N/A
B7	1	10000 psi	8983	6527	9635	6537	1.07	1.00
B8	1	10000 psi	8983	6527	10145	6537	1.13	1.00
B9	2	6000 psi	6525	6525	10177	6537	1.56	1.00
B10	2	6000 psi	6525	6525	9615	6537	1.47	1.00
B15	2	8000 psi	8000	N/A	8896	6320	1.11	N/A
B16	2	8000 psi	8000	N/A	9294	6498	1.16	N/A
B5	2	10000 psi	8983	6555	9239	6293	1.03	0.96
B6	2	10000 psi	8983	6555	9278	6293	1.03	0.96
C15	1	6000 psi	6512	5816	9204	7223	1.41	1.24
C16	1	6000 psi	6512	5816	9300	7223	1.43	1.24
C3	1	8000 psi	7099	5716	8673	5730	1.22	1.00
C4	1	8000 psi	7099	5716	9156	5730	1.29	1.00
C13	1	8000 psi	7469	6048	9158	6287	1.23	1.04
C14	1	8000 psi	7469	6048	9396	6287	1.26	1.04
C17	1	10000 psi	9000	N/A	8951	7800	0.99	N/A
C18	1	10000 psi	9000	N/A	9244	7800	1.03	N/A
C7	2	6000 psi	6178	5204	9498	6450	1.54	1.24
C8	2	6000 psi	6178	5204	9513	6450	1.54	1.24
C11	2	8000 psi	8102	6590	8261	6567	1.02	1.00
C12	2	8000 psi	8102	6590	8911	6567	1.10	1.00
C9	2	10000 psi	9152	7034	9354	7092	1.02	1.01
C10	2	10000 psi	9152	7034	10115	7092	1.11	1.01

Table B.18. Bias Factors for Modulus of Elasticity.

Batch No.	Set	f'c Category	Modulus of Elasticity (psi)			Bias Factor	
			28-Day Batch Avg.	Predicted AASHTO	Predicted Best Fit	AASHTO	Best Fit
A15	1	6000 psi	7883587	4792817	4980587	1.64	1.58
A16	1	6000 psi	7742723	4792817	4980587	1.62	1.55
A5	1	8000 psi	NR	N/A	N/A	N/A	N/A
A6	1	8000 psi	NR	N/A	N/A	N/A	N/A
A13	1	8000 psi	7244789	5584074	5802844	1.30	1.25
A14	1	8000 psi	7555760	5584074	5802844	1.35	1.30
A17	1	10000 psi	7270314	5739546	5964407	1.27	1.22
A18	1	10000 psi	7583556	5739546	5964407	1.32	1.27
A7	2	6000 psi	7002962	4660235	4842811	1.50	1.45
A8	2	6000 psi	7471298	4660235	4842811	1.60	1.54
A9	2	8000 psi	7301139	5264250	5470490	1.39	1.33
A10	2	8000 psi	7358513	5264250	5470490	1.40	1.35
A11	2	10000 psi	6742949	5813669	6041434	1.16	1.12
A12	2	10000 psi	7020166	5813669	6041434	1.21	1.16
B3	1	6000 psi	NR	N/A	N/A	N/A	N/A
B4	1	6000 psi	NR	N/A	N/A	N/A	N/A
B11	1	6000 psi	6603573	4897124	5088981	1.35	1.30
B12	1	6000 psi	6763782	4897124	5088981	1.38	1.33
B13	1	8000 psi	6320265	5422453	5634891	1.17	1.12
B14	1	8000 psi	5842106	5422453	5634891	1.08	1.04
B7	1	10000 psi	5548531	5745946	5971057	0.97	0.93
B8	1	10000 psi	6218476	5745946	5971057	1.08	1.04
B9	2	6000 psi	6054505	4897124	5088981	1.24	1.19
B10	2	6000 psi	5987163	4897124	5088981	1.22	1.18
B15	2	8000 psi	5865866	5422453	5634891	1.08	1.04
B16	2	8000 psi	5749920	5422453	5634891	1.06	1.02
B5	2	10000 psi	5742260	5745946	5971057	1.00	0.96
B6	2	10000 psi	6135538	5745946	5971057	1.07	1.03
C15	1	6000 psi	5852081	4892243	5083909	1.20	1.15
C16	1	6000 psi	5669291	4892243	5083909	1.16	1.12
C3	1	8000 psi	NR	N/A	N/A	N/A	N/A
C4	1	8000 psi	NR	N/A	N/A	N/A	N/A
C13	1	8000 psi	5703930	5239406	5444673	1.09	1.05
C14	1	8000 psi	5636111	5239406	5444673	1.08	1.04
C17	1	10000 psi	5718944	5751380	5976705	0.99	0.96
C18	1	10000 psi	5503201	5751380	5976705	0.96	0.92
C7	2	6000 psi	5578404	4765130	4951816	1.17	1.13
C8	2	6000 psi	5551066	4765130	4951816	1.16	1.12
C11	2	8000 psi	5108175	5456912	5670700	0.94	0.90
C12	2	8000 psi	5720468	5456912	5670700	1.05	1.01
C9	2	10000 psi	6029447	5799744	6026963	1.04	1.00
C10	2	10000 psi	5888487	5799744	6026963	1.02	0.98

279

Table B.19. Bias Factors for Splitting Tensile Strength.

Batch No.	Set	f'c Category	Splitting Tensile Strength (psi)			Bias Factor	
			28-Day Batch Avg.	Predicted AASHTO	Predicted Best Fit	AASHTO	Best Fit
A15	1	6000 psi	844	585	522	1.44	1.62
A16	1	6000 psi	880	585	522	1.50	1.69
A5	1	8000 psi	738	685	611	1.08	1.21
A6	1	8000 psi	597	685	611	0.87	0.98
A13	1	8000 psi	NT	N/A	N/A	N/A	N/A
A14	1	8000 psi	NT	N/A	N/A	N/A	N/A
A17	1	10000 psi	794	701	625	1.13	1.27
A18	1	10000 psi	728	701	625	1.04	1.17
A7	2	6000 psi	614	569	507	1.08	1.21
A8	2	6000 psi	688	569	507	1.21	1.36
A9	2	8000 psi	743	643	573	1.16	1.30
A10	2	8000 psi	868	643	573	1.35	1.52
A11	2	10000 psi	704	710	633	0.99	1.11
A12	2	10000 psi	788	710	633	1.11	1.25
B3	1	6000 psi	653	621	554	1.05	1.18
B4	1	6000 psi	648	659	588	0.98	1.10
B11	1	6000 psi	NT	N/A	N/A	N/A	N/A
B12	1	6000 psi	NT	N/A	N/A	N/A	N/A
B13	1	8000 psi	625	662	590	0.94	1.06
B14	1	8000 psi	756	662	590	1.14	1.28
B7	1	10000 psi	620	701	626	0.88	0.99
B8	1	10000 psi	735	701	626	1.05	1.18
B9	2	6000 psi	770	598	533	1.29	1.44
B10	2	6000 psi	579	598	533	0.97	1.09
B15	2	8000 psi	569	662	590	0.86	0.96
B16	2	8000 psi	595	662	590	0.90	1.01
B5	2	10000 psi	678	701	626	0.97	1.08
B6	2	10000 psi	707	701	626	1.01	1.13
C15	1	6000 psi	647	597	533	1.08	1.22
C16	1	6000 psi	546	597	533	0.91	1.03
C3	1	8000 psi	568	623	556	0.91	1.02
C4	1	8000 psi	590	623	556	0.95	1.06
C13	1	8000 psi	NT	N/A	N/A	N/A	N/A
C14	1	8000 psi	NT	N/A	N/A	N/A	N/A
C17	1	10000 psi	615	702	626	0.88	0.98
C18	1	10000 psi	618	702	626	0.88	0.99
C7	2	6000 psi	625	582	519	1.07	1.20
C8	2	6000 psi	628	582	519	1.08	1.21
C11	2	8000 psi	610	666	594	0.92	1.03
C12	2	8000 psi	602	666	594	0.90	1.01
C9	2	10000 psi	617	708	631	0.87	0.98
C10	2	10000 psi	656	708	631	0.93	1.04

280

Table B.20. Bias Factors for Modulus of Rupture.

Batch No.	Set	f'c Category	Modulus of Rupture (psi)			Bias Factor	
			28-Day Batch Avg.	Predicted AASHTO	Predicted Best Fit	AASHTO	Best Fit
A15	1	6000 psi	1250	593	791	2.11	1.58
A16	1	6000 psi	1293	593	791	2.18	1.64
A5	1	8000 psi	1001	694	926	1.44	1.08
A6	1	8000 psi	1063	694	926	1.53	1.15
A13	1	8000 psi	NT	N/A	N/A	N/A	N/A
A14	1	8000 psi	NT	N/A	N/A	N/A	N/A
A17	1	10000 psi	1232	710	947	1.73	1.30
A18	1	10000 psi	1199	710	947	1.69	1.27
A7	2	6000 psi	971	577	769	1.68	1.26
A8	2	6000 psi	956	577	769	1.66	1.24
A9	2	8000 psi	1050	651	868	1.61	1.21
A10	2	8000 psi	1129	651	868	1.73	1.30
A11	2	10000 psi	934	719	959	1.30	0.97
A12	2	10000 psi	998	719	959	1.39	1.04
B3	1	6000 psi	930	630	840	1.48	1.11
B4	1	6000 psi	948	668	891	1.42	1.06
B11	1	6000 psi	NT	N/A	N/A	N/A	N/A
B12	1	6000 psi	NT	N/A	N/A	N/A	N/A
B13	1	8000 psi	1112	671	894	1.66	1.24
B14	1	8000 psi	1170	671	894	1.74	1.31
B7	1	10000 psi	1077	711	948	1.52	1.14
B8	1	10000 psi	1107	711	948	1.56	1.17
B9	2	6000 psi	1134	606	808	1.87	1.40
B10	2	6000 psi	1117	606	808	1.84	1.38
B15	2	8000 psi	1113	671	894	1.66	1.24
B16	2	8000 psi	1108	671	894	1.65	1.24
B5	2	10000 psi	1146	711	948	1.61	1.21
B6	2	10000 psi	1139	711	948	1.60	1.20
C15	1	6000 psi	1010	605	807	1.67	1.25
C16	1	6000 psi	1025	605	807	1.69	1.27
C3	1	8000 psi	847	632	843	1.34	1.01
C4	1	8000 psi	908	632	843	1.44	1.08
C13	1	8000 psi	NT	N/A	N/A	N/A	N/A
C14	1	8000 psi	NT	N/A	N/A	N/A	N/A
C17	1	10000 psi	1107	712	949	1.56	1.17
C18	1	10000 psi	1103	712	949	1.55	1.16
C7	2	6000 psi	1009	590	786	1.71	1.28
C8	2	6000 psi	1016	590	786	1.72	1.29
C11	2	8000 psi	953	675	900	1.41	1.06
C12	2	8000 psi	880	675	900	1.30	0.98
C9	2	10000 psi	1048	717	957	1.46	1.10
C10	2	10000 psi	1111	717	957	1.55	1.16

Table B.21. Summary of Unit Weight of Concrete.

Batch No.	Set	f'c Class	Unit Weight (pcf) Specimen A	Specimen B	Average
A15	1	6000 psi	151.1	149.0	150.1
A16	1	6000 psi	149.5	150.4	150.0
A5	1	8000 psi	151.3	NT	151.3
A6	1	8000 psi	150.6	NT	150.6
A13	1	8000 psi	149.7	NT	149.7
A14	1	8000 psi	150.6	151.3	150.9
A17	1	10000 psi	150.5	150.7	150.6
A18	1	10000 psi	152.1	151.8	151.9
A7	2	6000 psi	150.6	151.4	151.0
A8	2	6000 psi	151.2	150.2	150.7
A9	2	8000 psi	151.8	150.7	151.2
A10	2	8000 psi	151.2	151.7	151.4
A11	2	10000 psi	149.5	149.6	149.6
A12	2	10000 psi	150.4	149.0	149.7
Precaster Average					150.6
B3	1	6000 psi	149.9	NT	149.9
B4	1	6000 psi	149.9	NT	149.9
B11	1	6000 psi	148.9	148.0	148.4
B12	1	6000 psi	149.8	149.7	149.8
B13	1	8000 psi	148.5	150.2	149.3
B14	1	8000 psi	147.2	150.2	148.7
B7	1	10000 psi	148.1	148.9	148.5
B18	1	10000 psi	152.1	151.8	151.9
B9	2	6000 psi	148.7	NT	148.7
B10	2	6000 psi	149.3	148.4	148.8
B15	2	8000 psi	147.1	147.7	147.4
B16	2	8000 psi	148.8	149.2	148.9
B5	2	10000 psi	149.5	149.2	149.4
B6	2	10000 psi	149.3	149.0	149.1
Precaster Average					149.1
C15	1	6000 psi	146.6	147.5	147.1
C16	1	6000 psi	146.8	148.4	147.6
C3	1	8000 psi	145.7	NT	145.7
C4	1	8000 psi	147.7	NT	147.7
C13	1	8000 psi	147.3	146.9	147.1
C14	1	8000 psi	147.4	146.4	146.9
C17	1	10000 psi	145.9	146.3	146.1
C18	1	10000 psi	146.6	146.1	146.4
C7	2	6000 psi	148.3	147.5	147.9
C8	2	6000 psi	147.6	148.2	147.9
C11	2	8000 psi	NT	NT	N/A
C12	2	8000 psi	NT	NT	N/A
C9	2	10000 psi	147.4	148.1	147.7
C10	2	10000 psi	148.2	149.2	148.7
Precaster Average					147.2
Overall Average					149.1

282

Individual creep and shrinkage strain measurements for each specimen obtained from electrical strain gages during the creep test are provided in Figure B.19 to Figure B.27. The plots are arranged by precaster name and batch number. Each frame includes samples collected from two batches of the same concrete mixture on the same day. For each creep frame, there are four creep cylinders (two from each batch) and two shrinkage cylinders (one from each batch). Note that the creep measurements (shown as black lines) are the total measured strain (including shrinkage) for a creep specimen. The shrinkage measurements are shown as dark gray lines.

For all samples except A7-A8, every strain gage channel was connected with strain gages on a steel block for the purpose of temperature compensation. For the samples from batches A7-A8, each of the creep specimens and the first shrinkage specimen have two strain gages attached laterally on the side of the specimen. As a result of this setup, the effect of lateral shrinkage was included in the reading. In order to obtain the creep strain reported in Chapter 4, the strain from the first shrinkage specimens was subtracted from the total strain of a creep specimen in the same batch. The second shrinkage specimen had two strain gages on a steel block. Therefore, the strain measured was only due to longitudinal shrinkage, similar to the other sets of tests.

A few strain gages did not function for total duration of the creep and shrinkage testing. The main cause was insecure solder connections between strain gages and lead wires. It was not possible to solder the wire back on the strain gage because the system was very sensitive to small changes in resistance. Replacing gages is problematic because new gages would have their own resistance values that vary within a certain range from the nominal value. New solder connections would also have a different resistance and result in a change in output. Also, the strain gages and wire were coated with protective coating that obstructed re-soldering.

There was one channel of data for a batch A9 creep sample, for which the reading was not stable. It was not clear what the problem was in this case. Therefore, the measured strain for this specimen was not included.

Shrinkage strain measurements for each shrinkage prism specimen are provided in Figure B.28 to Figure B.43. Again, plots are arranged by precaster name and batch number.
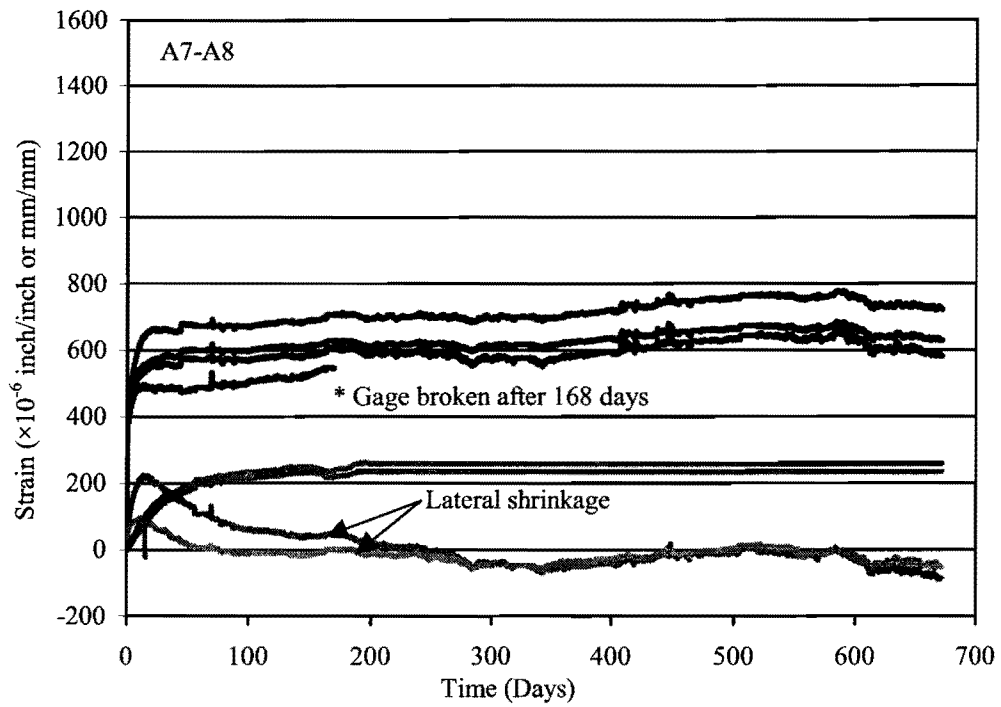
**Figure B.19. Creep Test for Batches A7-A8.**
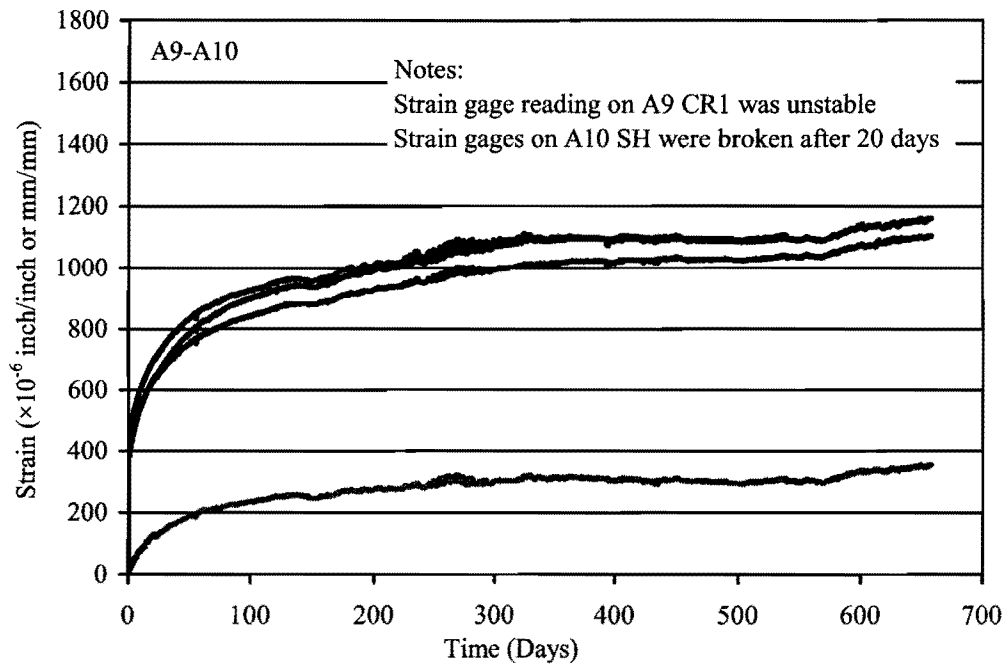

Figure B.20. Creep Test for Batches A9-A10.

284
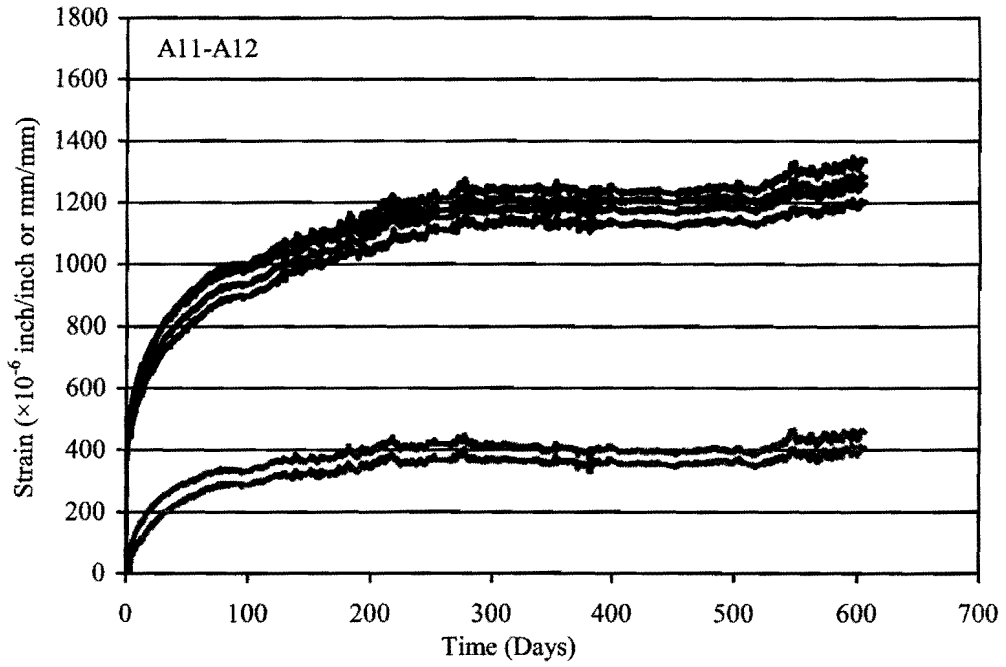
**Figure B.21. Creep Test for Batches A11-A12.**
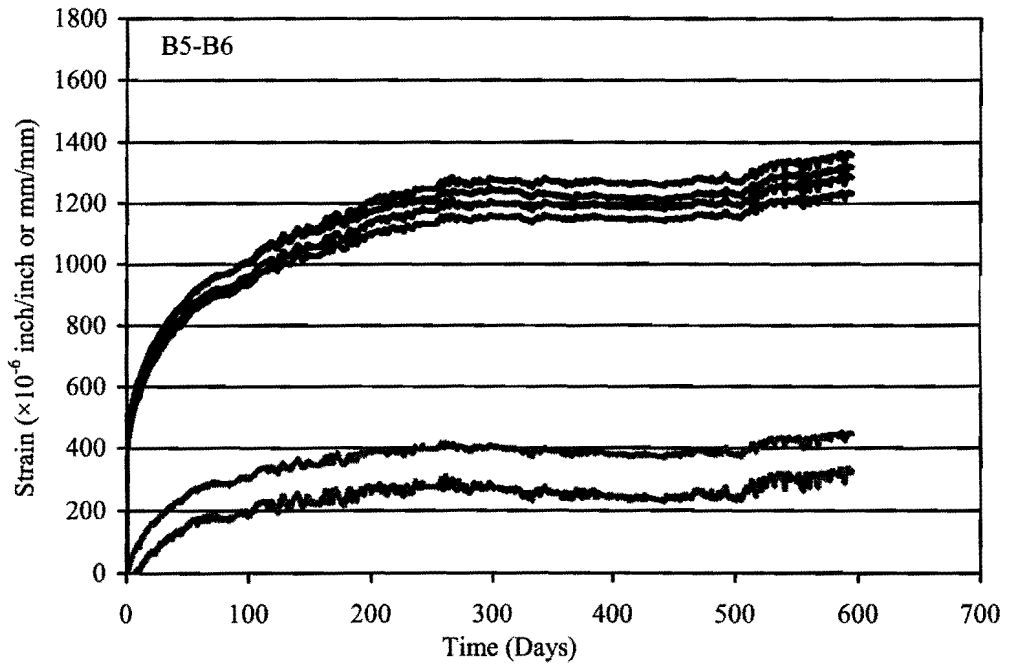

Figure B.22. Creep Test for Batches B5-B6.
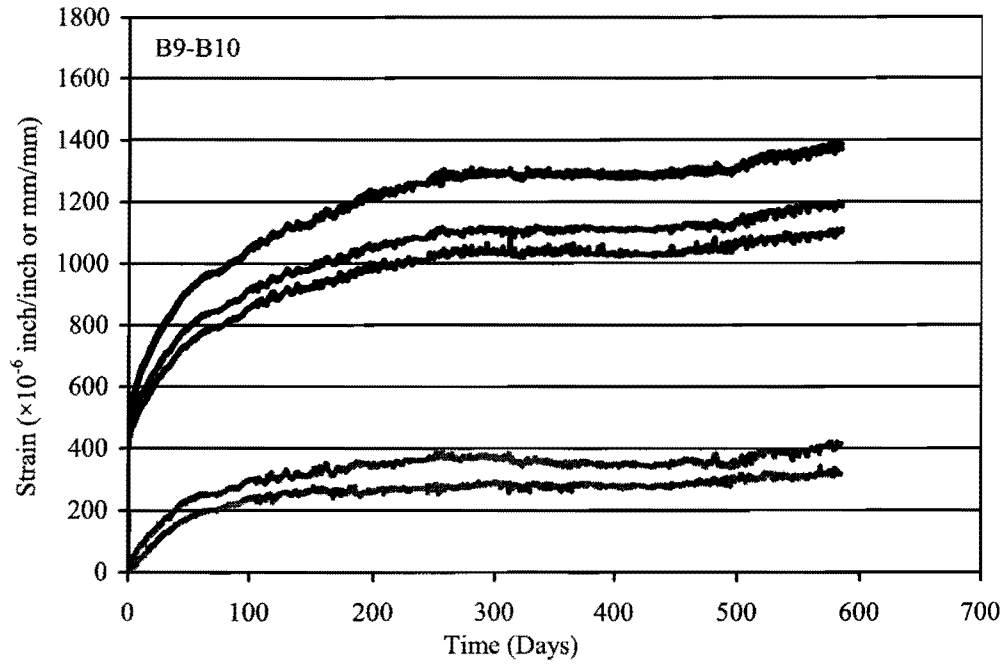
**Figure B.23. Creep Test for Batches B9-B10.**
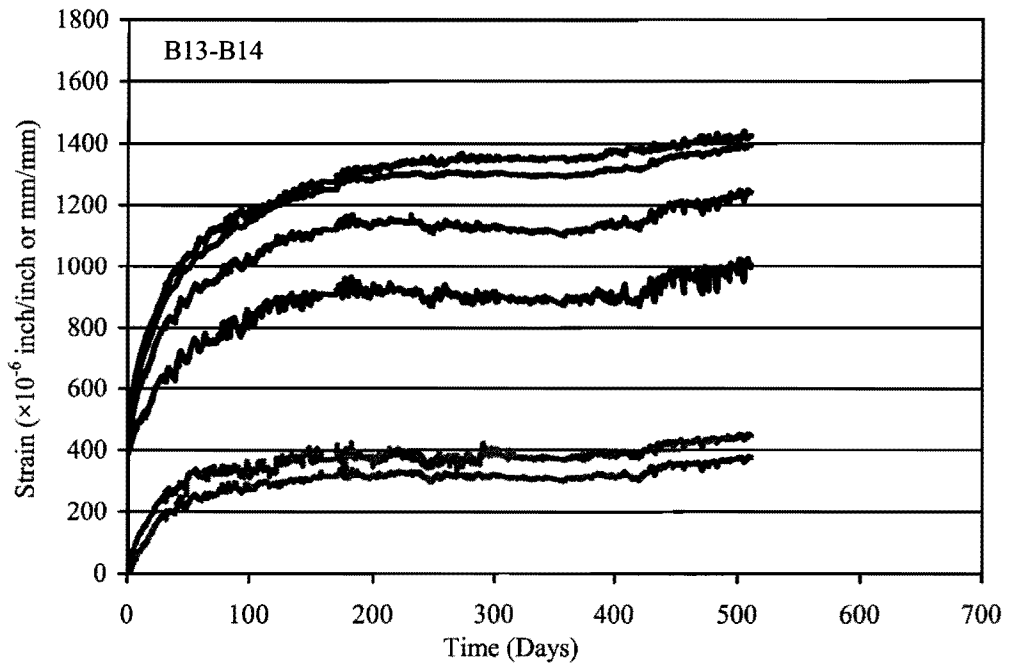

Figure B.24. Creep Test for Batches B13-B14.

286
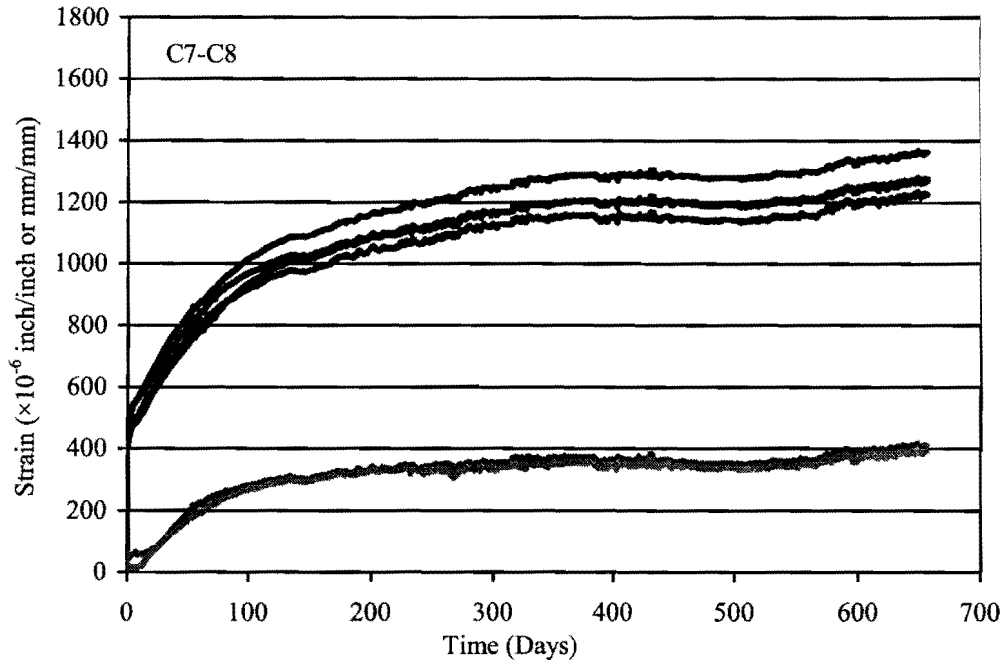
Figure B.25. Creep Test for Batches C7-C8.
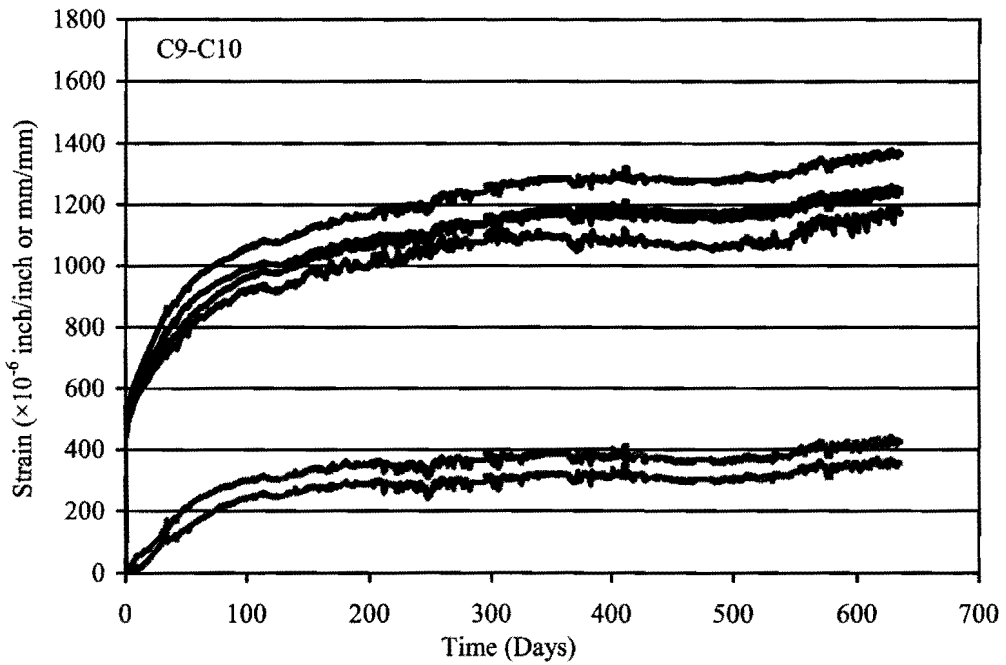

Figure B.26. Creep Test for Batches C9-C10.

287
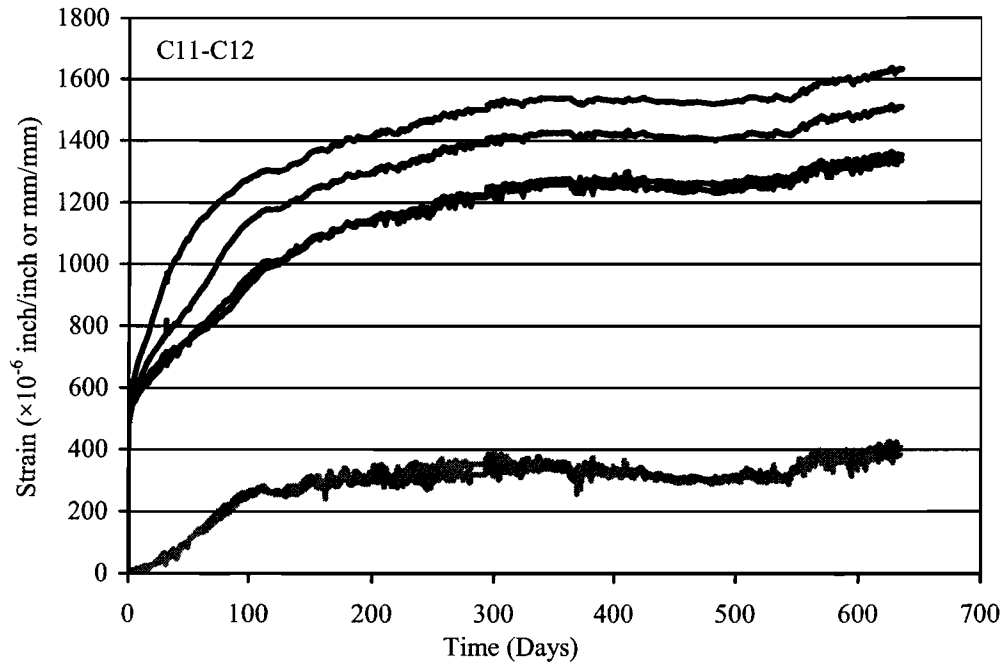
Figure B.27. Creep Test for Batches C11-C12.
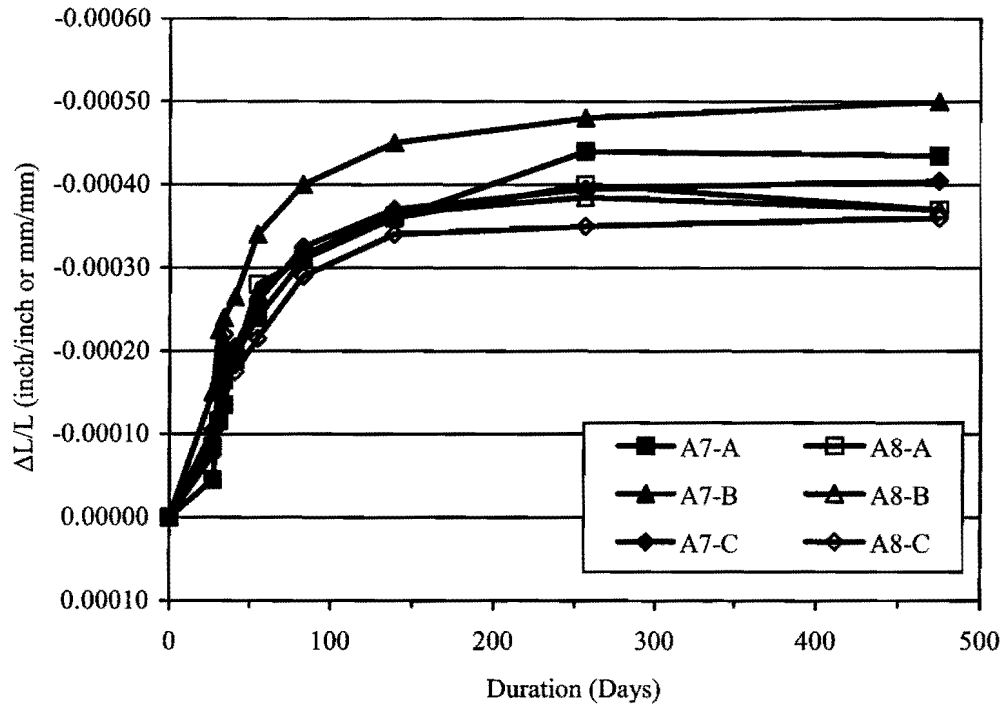
Figure B.28. Shrinkage Test for Batches A7-A8.
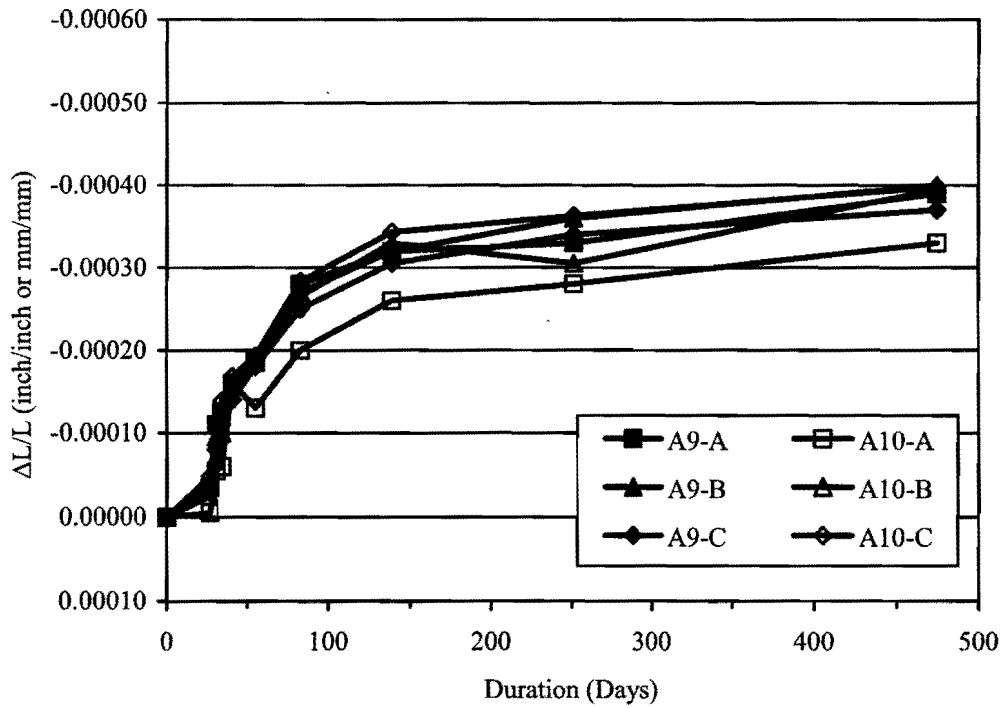
Figure B.29. Shrinkage Test for Batches A9-A10.

289
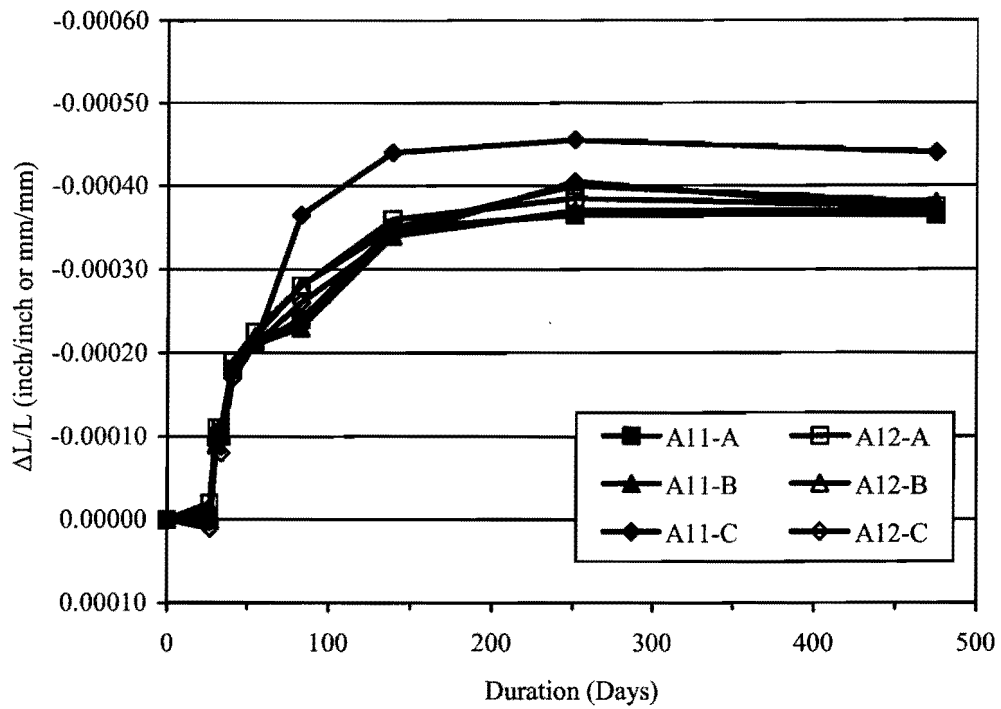
Figure B.30. Shrinkage Test for Batches A11–A12.
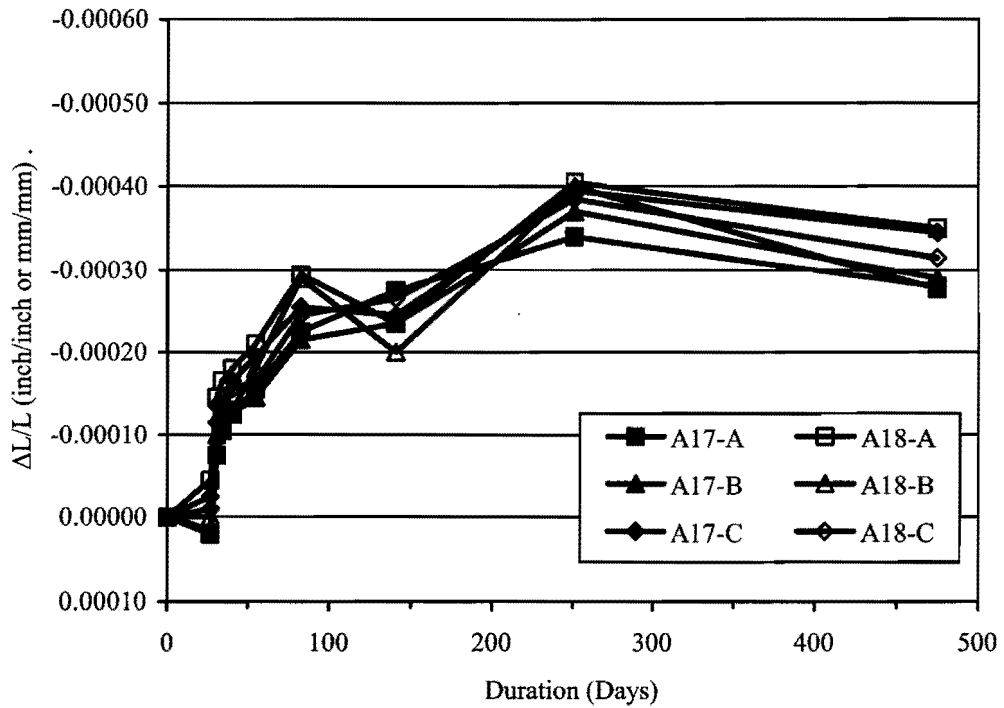
**Figure B.31. Shrinkage Test for Batches A17–A18.**

290
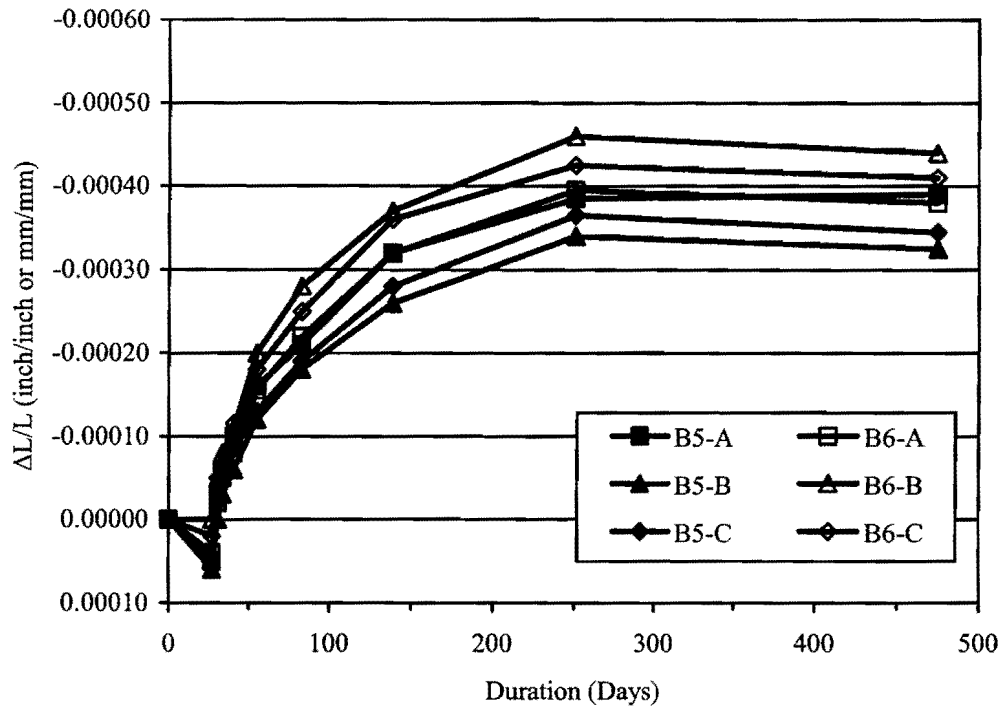
Figure B.32. Shrinkage Test for Batches B5-B6.
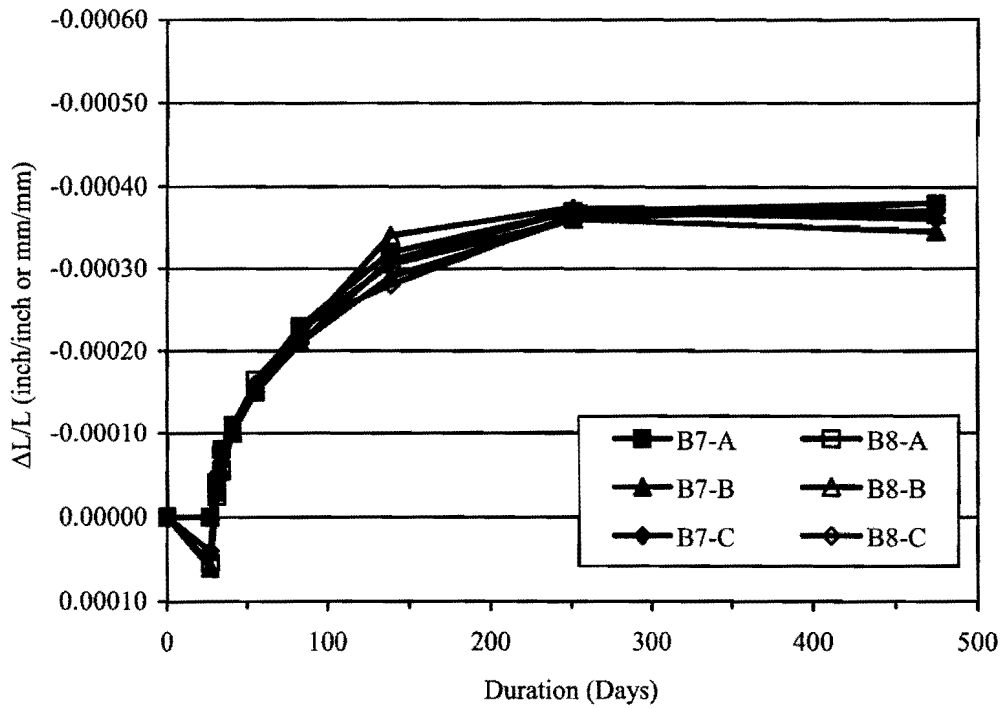
**Figure B.33. Shrinkage Test for Batches B7-B8.**

291
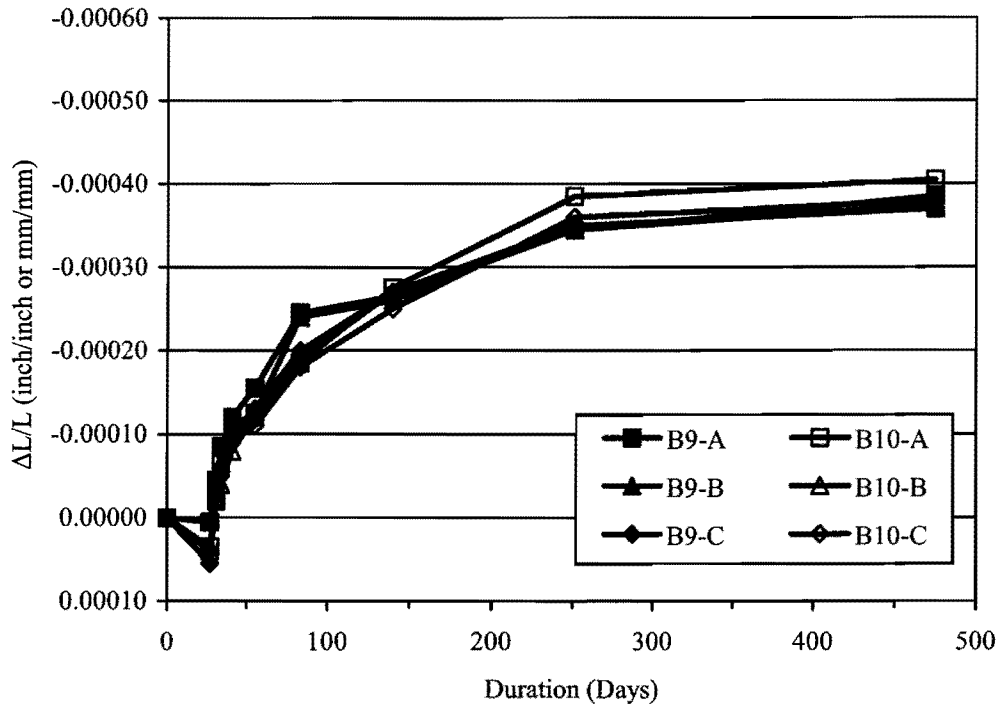
Figure B.34. Shrinkage Test for Batches B9-B10.

Note: The readings from B11-A were inconsistent due to a damaged contact point. Therefore, the readings were rejected.
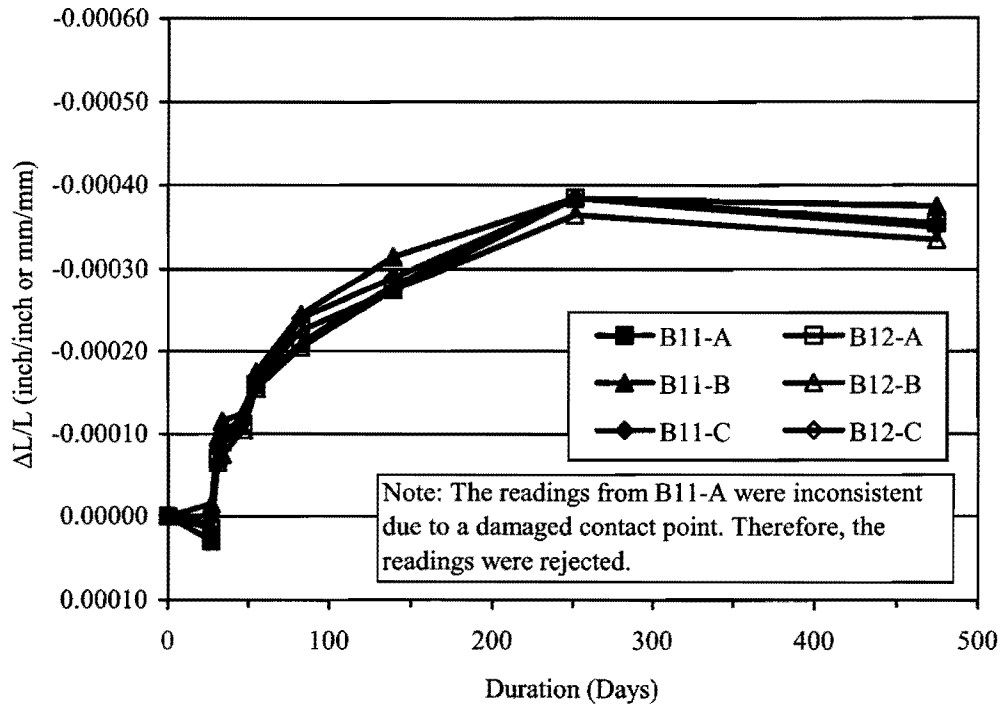
**Figure B.35. Shrinkage Test for Batches B11-B12.**

292
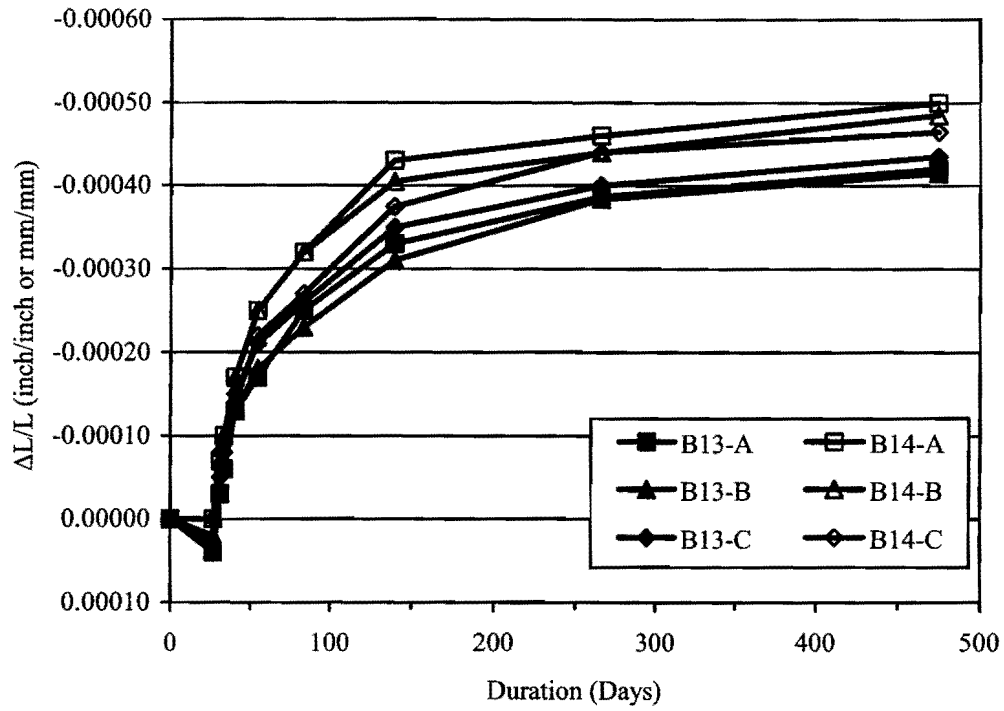
**Figure B.36. Shrinkage Test for Batches B13-B14.**
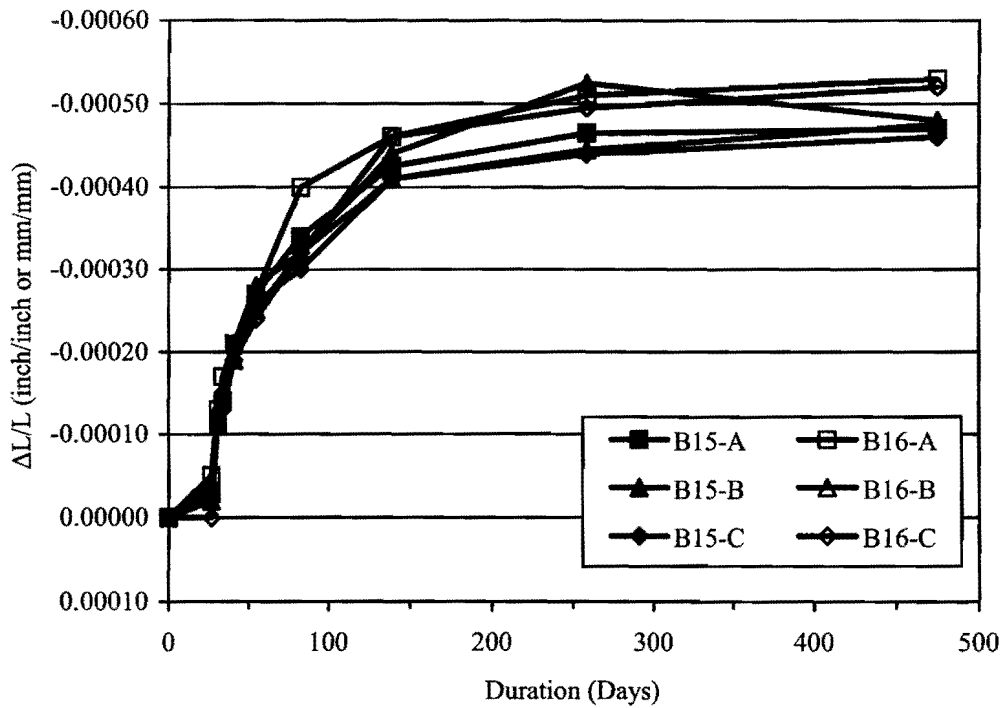
Figure B.37. Shrinkage Test for Batches B15-B16.

293
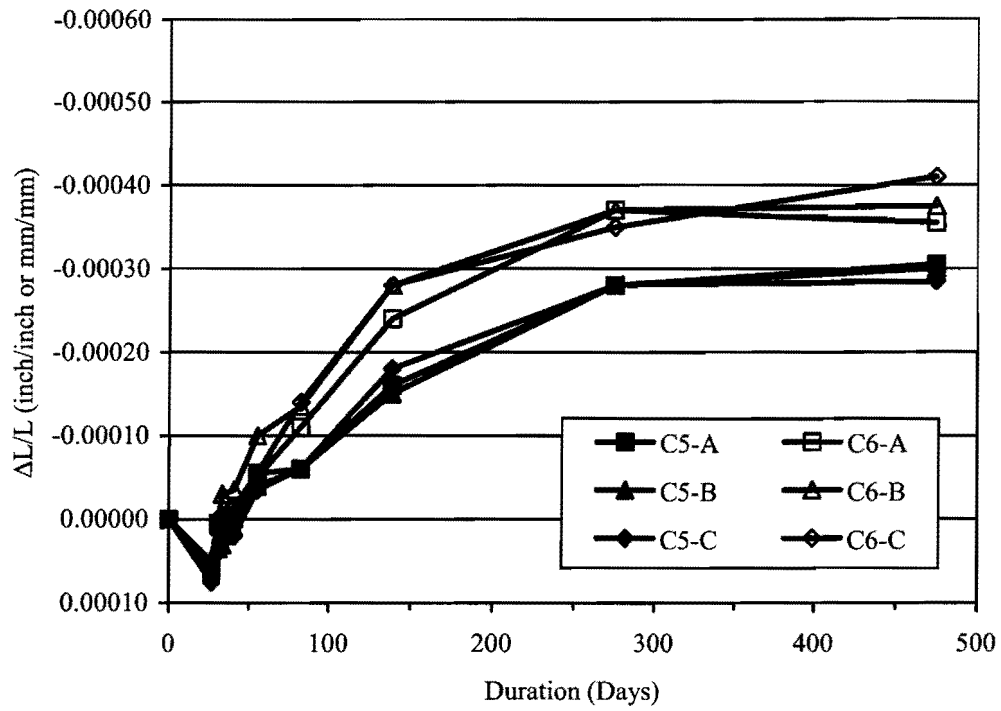
Figure B.38. Shrinkage Test for Batches C5-C6.
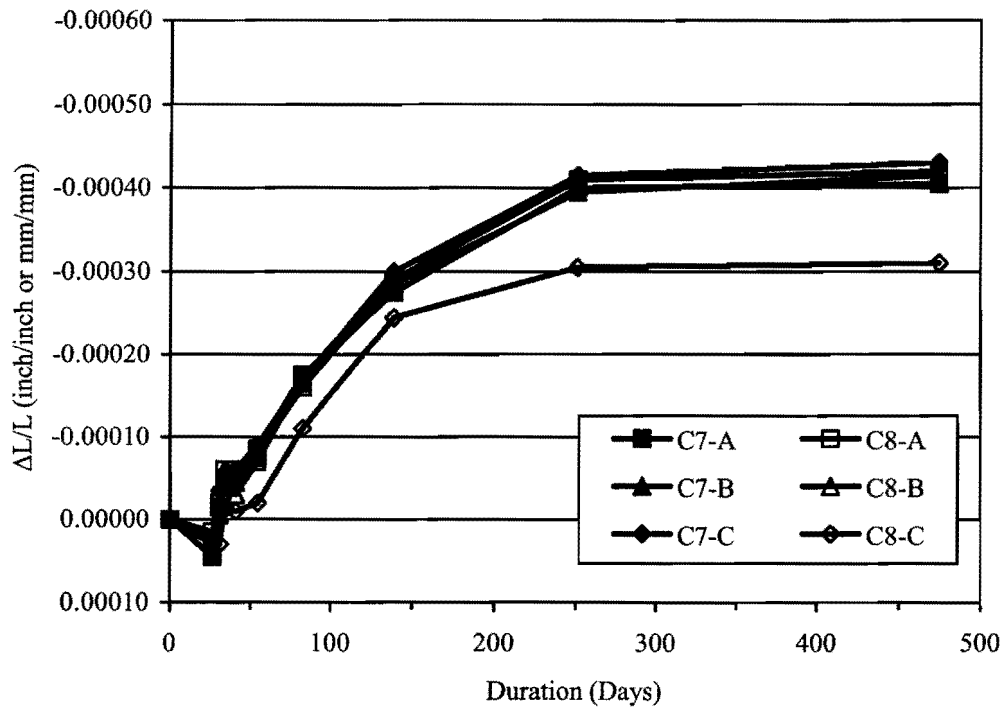

Figure B.39. Shrinkage Test for Batches C7-C8.

294
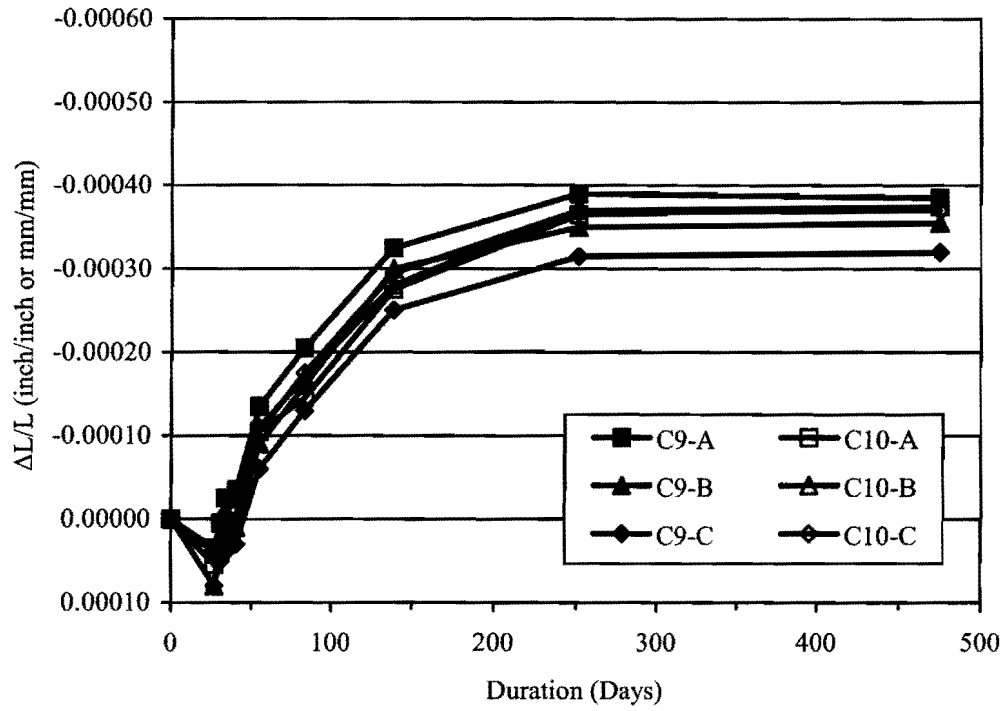
**Figure B.40. Shrinkage Test for Batches C9-C10.**
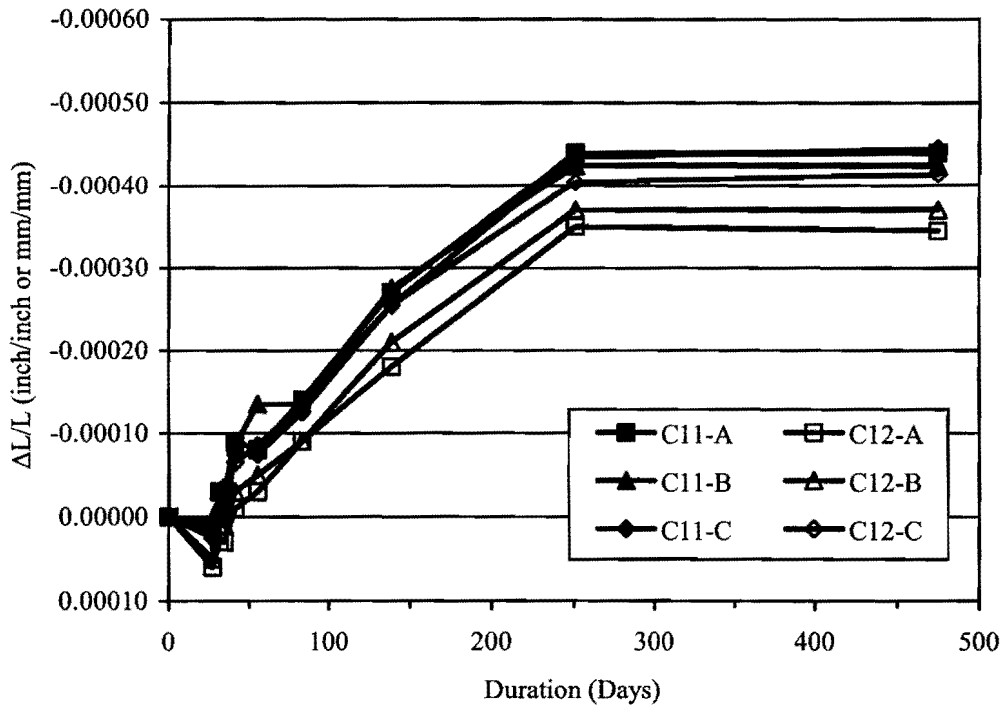
**Figure B.41. Shrinkage Test for Batches C11-C12.**

295
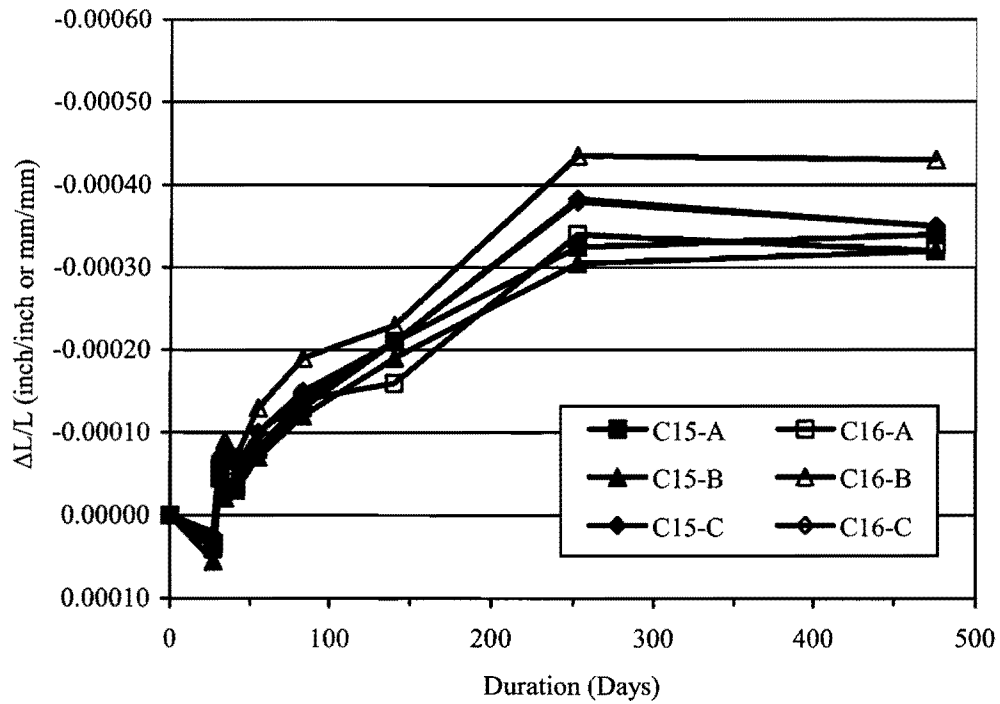
**Figure B.42. Shrinkage Test for Batches C15-C16.**
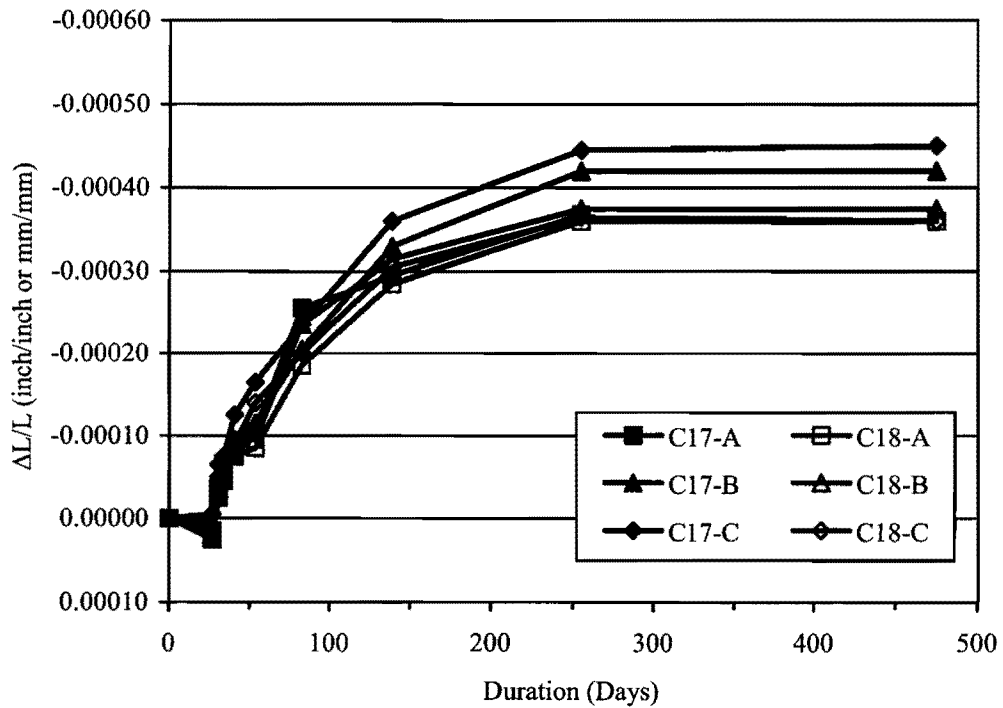
Figure B.43. Shrinkage Test for Batches C17-C18.

296

APPENDIX C

EFFECTS OF CAPPING ON THE MODULUS OF ELASTICITY

Because limited data were available regarding the difference between the modulus of elasticity of HSC tested using sulfur caps and neoprene caps, the comparison study was conducted to assure that both cap types yield the same value.

A compressometer was used to measure the deformation of 4×8 inch (100×200 mm) cylindrical specimens for both cases. The test procedures followed ASTM C 469 (1994b). Two specimens for each batch were randomly selected for the test using each type of cap. A paired T test was used to determine whether the difference between the mean modulus of elasticity from both cap types is significant or not. The detail of the analysis can be found in many statistical textbooks, such as that by Milton and Arnold (1995). Briefly, the following hypothesis is tested:

$$H_0 : \mu_{sulfur} = \mu_{neoprene}$$

$$H_1 : \mu_{sulfur} \neq \mu_{neoprene}$$

The above hypothesis is equivalent to the following:

$$H_0 : \mu_D = 0$$

$$H_1 : \mu_D \neq 0$$

where D is the difference between the moduli of elasticity from two cap types. The test statistic for this hypothesis is:

$$t = \frac{\bar{D} - 0}{S_D / \sqrt{n}} \qquad (C.1)$$

where $\bar{D}$ and S_D are sample mean and sample standard deviation of D, respectively, and n is the number of paired samples. The statistic t has a student-t distribution with the degree of freedom (n-1). A large value of t or smaller probability of having greater value of t (p-value) indicate that the difference is too large to occur by chance; therefore, the null hypothesis H$_0$ is rejected.

The test data from 10 pairs of moduli of elasticity are presented in Table C.1.

Table C.1. Comparison between Moduli of Elasticity Tested Using Sulfur Caps and Neoprene Caps.

Precaster	Batch No.	Age Tested	Sulfur Cap			Neoprene Cap			Difference in Avg. (D) (psi)
			A (psi)	B (psi)	Avg. (psi)	A (psi)	B (psi)	Avg. (psi)	
A	7	7 days	6560343	6304127	6432235	7316343	6790461	7053402	621167
A	8	7 days	7042854	6934612	6988733	7127744	6588802	6858273	-130460
A	7	28 days	7710970	7321415	7516192	7075511	6930413	7002962	-513230
A	8	28 days	7240732	7317921	7279327	7472863	7469732	7471298	191971
A	9	7 days	6506859	6795129	6650994	6790834	7104502	6947668	296674
A	10	7 days	6644670	6792723	6718697	7131932	7595465	7363699	645002
A	9	28 days	7011619	6941314	6976466	7473746	7128533	7301139	324673
A	10	28 days	7073242	7274443	7173843	7442584	7274443	7358513	184671
C	7	7 days	5611283	4843511	5227397	4978966	4857199	4918083	-309314
C	8	7 days	5217289	5312438	5264864	5638183	5288313	5463248	198385
								Mean	150954
								Standard Deviation	373251

From Table C.1,

$$t = \frac{150954 - 0}{373251 / \sqrt{10}} = 1.279$$

The p-value for this test (having nine degrees of freedom) is equal to 0.233, which is larger than 0.05. Because the p-value is large, the null hypothesis cannot be rejected. Therefore, the moduli of elasticity tested using sulfur caps and neoprene caps are not significantly different at 0.05 level.

As a result of this study, only the neoprene caps were used for the rest of the tests.

APPENDIX D

WHEATSTONE BRIDGE CIRCUIT FOR STRAIN GAGES

The principal of a strain gage is that the change in strain causes the change in the electrical resistance of the gage. By measuring the resistance of the gage, the strain can be determined. However, because the change in strain is usually small, it is not practical to measure the resistance directly using an ohmmeter. As a result, the resistance is typically measured using a Wheatstone bridge circuit. The circuit consists of four resistances, a DC voltage source, and a detector. The basic Wheatstone bridge is shown in Figure D.1. A constant excitation voltage (E) is connected to the bridge at node A and C. The output voltage (e_0) is measured at node D and B and is recorded by the data acquisition system.
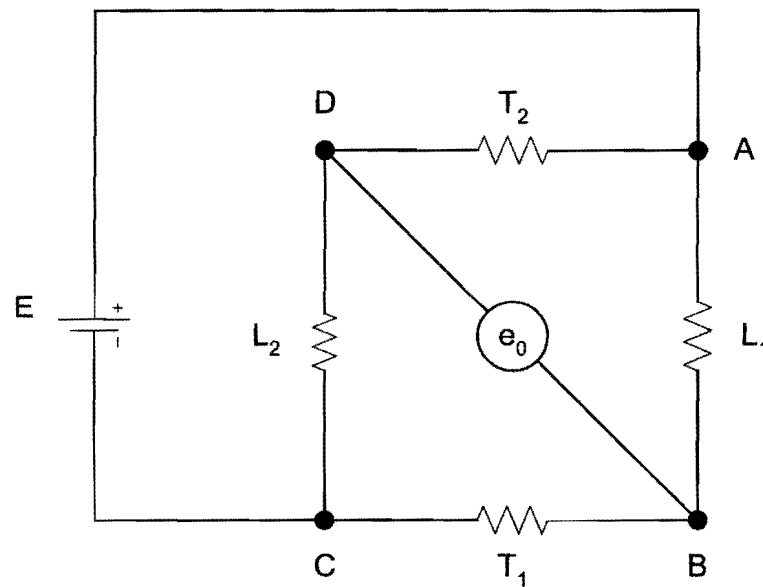

Figure D.1. Wheatstone Bridge Circuit.

Often, only one resistance in the circuit is a strain gage; the rest are dummy resistances in the measuring instrument. This arrangement is called a quarter-bridge circuit. However, for the

measurement of creep and shrinkage in this project, a full bridge circuit is used. The benefits of using a full bridge circuit for the strain gages are:

- increased sensitivity of the measurement because several strain gages are used,

- savings in data logging channels because only one output is measured for four gages, and

- the effect of temperature can be eliminated.

For this project, the resistances L and T shown in Figure D.1 are longitudinal and temperature compensation strain gages, respectively. Normally, all gages used have the same resistance.

At the initial stage when there is no strain, the resistance of all strain gages is the same and the output voltage reading is zero. The bridge circuit is now said to be balanced.

When there is a change in the length of the strain gages, their resistances change proportionally. The unit change in the resistance of each strain gage is related to the strain using the following equation:

$$\frac{\Delta R}{R_G} = F_G \varepsilon \qquad (D.1)$$

where ΔR is the change in the resistance, ε is the strain, F_G and R_G are the gage factor and nominal resistance of the strain gage (provided by the strain gage manufacturer), respectively.

As the resistances of the strain gages in the circuit change, the bridge circuit will no longer be balanced. The following equation shows that the measured output voltage depends on the resistance of the gages in the circuit:

$$\frac{e_0}{E} = \frac{L_1/T_1}{L_1/T_1 + 1} - \frac{T_2/L_2}{T_2/L_2 + 1} \qquad (D.2)$$

By comparing the measured output voltage with the known output voltage when a known strain is applied, it is possible to determine the strain in the specimen.

The use of the Wheatstone bridge circuit is best demonstrated numerically. All of the strain gages used in this project have a nominal resistance of 350 ohms and have a gage factor of 2.07. The excitation voltage used is constant at 6.0 V.

Table D.1 shows the state when there is no strain in any strain gages. The change in the resistance calculated using Equation D.1 is zero, and the value $\frac{e_0}{E}$ calculated using Equation D.2 is also zero.

Table D.1. Condition 1: No Strain.

Straingage	Gage Resistance (Ω)	Strain ($\times 10^{-6}$)	Gage Factor	ΔR (Ω)	Resistance (Ω)	e_0/E
L_1	350	0	2.07	0.0000	350.00	0
T_1	350	0	2.07	0.0000	350.00	
L_2	350	0	2.07	0.0000	350.00	
T_2	350	0	2.07	0.0000	350.00	

Assuming that, at one point, there is a creep strain of 600 $\mu\varepsilon$ on the specimen (compressive strain) and a strain due to temperature increase of 100 $\mu\varepsilon$. Therefore, the strain in the longitudinal gage is -600 + 100 = -500 $\mu\varepsilon$. As seen in Table D.2, these strains cause the change in the resistance of each strain gage and the change in the output voltage.

Table D.2. Condition 2: 600 με Creep Strain and 100 με Temperature Strain.

Straingage	Gage Resistance (Ω)	Strain ($\times 10^{-6}$)	Gage Factor	ΔR (Ω)	Resistance (Ω)	e_0/E
L_1	350	-500	2.07	-0.3623	349.64	-0.00062
T_1	350	100	2.07	0.0725	350.07	
L_2	350	-500	2.07	-0.3623	349.64	
T_2	350	100	2.07	0.0725	350.07	

Tables D.3 and D.4 show the state of the circuit when there are further increases of creep strain for 500 με and 1000 με, respectively, while the temperature remains the same. Figure D.2 provides the plot of the voltage output from the conditions in Table D.2 to Table D.4. It is clear that the output voltage changes proportionally to the change in the resistance of the longitudinal gages.

Table D.3. Condition 3: 1100 με Creep Strain and 100 με Temperature Strain.

Straingage	Gage Resistance (Ω)	Strain ($\times 10^{-6}$)	Gage Factor	ΔR (Ω)	Resistance (Ω)	e_0/E
L_1	350	-1000	2.07	-0.7245	349.28	-0.00114
T_1	350	100	2.07	0.0725	350.07	
L_2	350	-1000	2.07	-0.7245	349.28	
T_2	350	100	2.07	0.0725	350.07	

Table D.4. Condition 4: 1600 με Creep Strain and 100 με Temperature Strain.

| Straingage	Gage Resistance (Ω)	Strain ($\times 10^{-6}$)	Gage Factor	ΔR (Ω)	Resistance (Ω)	e_0/E
L_1	350	-1500	2.07	-1.0868	348.91	-0.00166
T_1	350	100	2.07	0.0725	350.07	
L_2	350	-1500	2.07	-1.0868	348.91	
T_2	350	100	2.07	0.0725	350.07	
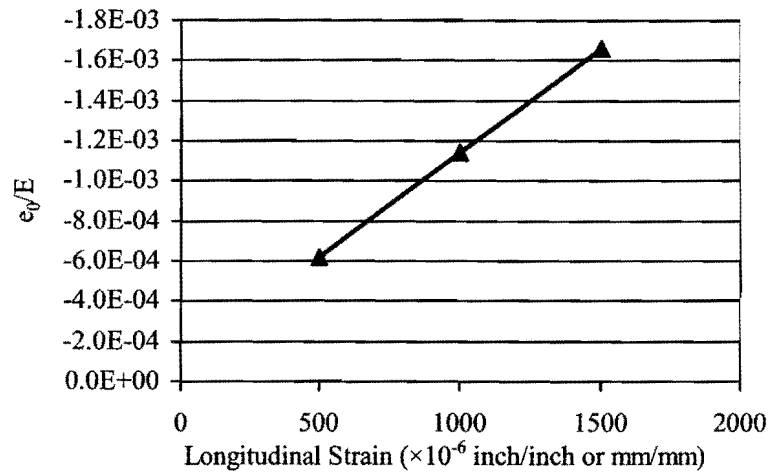
Figure D.2. Output Voltage versus Longitudinal Strain.

Table D.5 shows the effect of an additional 200 µε in all strain gages due to further increase of temperature from the case in Table D.3. The voltage output is still the same. Therefore, the effect of strain change due to temperature is eliminated.

Table D.5. Condition 5: 1100 µε Creep Strain and 300 µε Temperature Strain.

Straingage	Gage Resistance (Ω)	Strain (×10⁻⁶)	Gage Factor	ΔR (Ω)	Resistance (Ω)	e₀/E
L₁	350	-800	2.07	-0.5796	349.42	-0.00114
T₁	350	300	2.07	0.2174	350.22	
L₂	350	-800	2.07	-0.5796	349.42	
T₂	350	300	2.07	0.2174	350.22	

In order to exclude the temperature effect using a full bridge circuit, the temperature compensation strain gages should be placed on the same material as the longitudinal strain gages so that all of the gages will have the same change in strain due to temperature. However, it is not feasible to put the temperature compensation strain gages on concrete because there will also be an effect from the shrinkage of concrete. Therefore, the temperature compensation strain gages

303

should be placed on a material that has the same coefficient of thermal expansion as concrete but does not shrink. Steel was chosen because:

- it has the coefficient of thermal expansion of $6.5 \times 10\text{-}6/$ °F, which is close to that of concrete ($6.0 \times 10\text{-}6/$ °F) (although the effect of temperature is not completely eliminated, it should be very small);

- it is inexpensive; and

- it can be easily found in any desired shape and size.

Because the effect of temperature is volumetric (the change in strain is the same in all directions), it is unnecessary for the steel piece to have the same shape and size as the cylinder specimen. Therefore, the temperature compensation strain gages are placed on a small steel block.

Measurements Group, Inc. manufactured the strain gages used in this project. The model number for the strain gages used for concrete specimens and steel block are N2A-05-20CBW-350 and CEA-06-125UT-350, respectively.

APPENDIX E

SAS SOURCE CODE

The command code for the analysis of the data using SAS statistical analysis software (1999) is provided below. The same commands were used for compressive strength, modulus of elasticity, splitting tensile strength, and modulus of rupture. Therefore, only that for the compressive strength is shown here. To use this code with other properties, simply substitute the compressive strength test results under the "cards" command with appropriate values. It must also be noted that only part of the full data are listed under the "cards" command for illustration purposes. In addition, only important results generated by this command code were presented in this appendix.

```
data Batches; * summaries for each batch;
input Precaster $ Batch $ Age $ Set $ Class Cyl1-Cyl4 Design;
Mix=compress(Precaster||"-"||Age||"-"||Set||"-"||Class); * compute batch stats;
NoCyl=n(of Cyl1-Cyl4); BAvg=mean(of Cyl1-Cyl4);
CVBatch=std(of Cyl1-Cyl4)/BAvg; LogBAvg=log10(BAvg);
LogDsgn = Log10(Design);
cards;

A 5    07    Set1    8    9831.606714    9894.732992    9539.656916    .    8573
A 6    07    Set1    8    9214.857369    9864.210725    9626.145973    .    8573
A 5    28    Set1    8    11489.99365    11601.20034    11465.77321    .    8573
A 6    28    Set1    8    10778.78359    10943.6012     11173.47476    .    8573
A 5    56    Set1    8    12144.8432     12219.96073    12150.88466    .    8573
A 6    56    Set1    8    11769.05648    12195.67865    11559.6339     .    8573
B 3    07    Set1    6    8437.113598    8303.048311    8897.078105    .    7048
B 4    07    Set1    6    8629.401768    8130.231789    8437.113598    .    7942
B 3    28    Set1    6    9737.548989    10243.30653    9613.493996    .    7048
B 4    28    Set1    6    9392.950103    9482.906802    .         .    7942
B 3    56    Set1    6    9978.282531    9379.223919    10753.90079    .    7048
B 4    56    Set1    6    9616.579618    9949.747393    .         .    7942

;;;
run;
proc print data=Batches;
run;
data Distr;
set Batches;
LCyl1=Log10(Cyl1);
LCyl2=Log10(Cyl2);
LCyl3=Log10(Cyl3);
LCyl4=Log10(Cyl4);
AveofLog=mean(of LCyl1-LCyl4);
E=Cyl1-BAvg;
EL=LCyl1-AveofLog; output;
```

```
E=Cyl2-BAvg;
EL=LCyl2-AveofLog; output;
E=Cyl3-BAvg;
EL=LCyl3-AveofLog; output;
E=Cyl4-BAvg;
EL=LCyl4-AveofLog; output;
drop Cyl1-Cyl4;
run;

proc insight data=Distr; dist E;
run;
proc insight data=Distr; dist EL;
run;

proc insight data=Batches; * diagnostic plots;
scatter BAvg CVBatch * Design Age Precaster;  * CV looks constant;
scatter LogBAvg * LogDsgn;
run;

proc glm data=Batches; * test equality of cv's;
class Precaster Age Class;
model CVBatch = Precaster|Age|Class/ss1;
means Precaster Age Class/tukey; means Precaster|Age|Class/tukey;
run;

data Mixes; * summaries for each mix (weights due to NoCyl ignored);
array B B1-B2; array L L1-L2;
do i=1,2; set Batches; B(i)=BAvg; L(i)=LogBAvg; end;
MAvg=(B1+B2)/2; CVMix=sqrt(2)*abs(B1-B2)/(B1+B2);
MLogBAvg=(L1+L2)/2;
drop i NoCyl Batch BAvg CVBatch LogBAvg B1-B2 L1-L2;
run;

proc print data=Mixes;
run;

proc insight data=Mixes; * diagnostic plots;
scatter MAvg CVMix * Design Age Precaster Class;
scatter MLogBAvg * LogDsgn;
run;

proc glm data=Mixes; * test equality of cv's;
class Precaster Age Class;
model CVMix = Precaster|Age|Class/ss1;
means Precaster Age Class/tukey; means Precaster|Age|Class/tukey;
run;

proc glm data=Mixes; * basic check of relationship;
class Precaster Age;
model MAvg = Design Precaster|Age Design*Precaster Design*Age Design*Precaster*Age/ss3;
run;
proc glm data=Mixes; * basic check of relationship;
class Precaster Age;
model MLogBAvg = Design Precaster|Age Design*Precaster Design*Age Design*Precaster*Age/ss3;
run;
proc glm data=Mixes; * basic check of relationship;
class Precaster Age;
model MLogBAvg = Design Precaster Design*Precaster/ss3 solution;
run;

proc sort data=Mixes; by Precaster;
proc reg data=Mixes; by Precaster;
model MAvg = Design;
proc reg data=Mixes; by Precaster;
model MLogBAvg = Design;
run;
```

306

```
proc sort data=Mixes; by Age Precaster;
proc reg data=Mixes; by Age Precaster;
model MAvg = Design;
run;
proc reg data=Mixes; by Age Precaster;
model MLogBAvg = Design;
run;
proc means n mean cv; var MAvg;
class Precaster Age; ways 2;
run;
proc means n mean std; var MLogBAvg;
class Precaster Age; ways 2;
run;
proc means n mean cv; var MAvg;
class Age; ways 2;
run;

* Restrict to 7 day data.;
data Avg7Day; set Mixes; if Age=7;
run;
proc print data=Avg7Day;
run;
proc insight data=Avg7Day; Class Precaster;
fit MAvg = Design Precaster Design*Precaster;
fit MLogBAvg = LogDsgn  Precaster LogDsgn*Precaster;
by Precaster;
scatter MAvg MLogBAvg * Design;
fit MAvg = Design;
fit MLogBAvg = LogDsgn;
run;

* Restrict to 28 day data.;
data Avg28Day; set Mixes; if Age=28;
run;
proc print data=Avg28Day;
run;
proc insight data=Avg28Day; Class Precaster;
fit MAvg = Design Precaster Design*Precaster;
fit MLogBAvg = LogDsgn  Precaster LogDsgn*Precaster;
by Precaster;
scatter MAvg MLogBAvg * Design;
fit MAvg = Design;
fit MLogBAvg = LogDsgn;
run;

* Restrict to 56 day data.;
data Avg56Day; set Mixes; if Age=56;
run;
proc print data=Avg56Day;
run;
proc insight data=Avg56Day; Class Precaster;
fit MAvg = Design Precaster Design*Precaster;
fit MLogBAvg = LogDsgn  Precaster LogDsgn*Precaster;
by Precaster;
scatter MAvg MLogBAvg * Design;
fit MAvg = Design;
fit MLogBAvg = LogDsgn;
run;
```

APPENDIX F

TESTING NOTES

During the project, there were some changes in the way the experiments were done. All the changes are summarized chronologically in Table F.1.

Table F.1. Summary of Changes in Testing.

Precaster	Batch No.	Age	Loading Type for Compressive Strength	Hydraulic Valve on 500 kips MTS Machine	Use Aligning Jig for Splitting Tensile Test	Testing Machine for Modulus of Rupture
A	5,6	7 days	Stroke Control	Small	N	100 kips
B	3,4	7 days	Stroke Control	Small	N	100 kips
C	3,4	7 days	Stroke Control	Small	N	25 kips
A	5,6	28 days	Stroke Control	Big	N	25 kips
B	3,4	28 days	Stroke Control	Big	N	25 kips
C	3,4	28 days	Stress Control	Big	N	100 kips
A	5,6	56 days	Stress Control	Big	Y	100 kips
B	3,4	56 days	Stress Control	Big	Y	100 kips
C	3,4	56 days	Stress Control	Big	Y	100 kips
All Other Tests			Stress Control	Big	Y	25 kips

The stroke control mode was used for some of the compressive strength tests and was later changed to the stress control mode because it is more appropriate to use a stress control mode for a hydraulically operated machine. In both cases, the standard rate of loading was used. The hydraulic valve on the 500 kips machine affects the rate of loading. When a small valve was used, the load rate near failure deviated slightly from the standard rate because the machine could not keep up with the rate. As a result, the compressive strength measurement may be affected. Therefore, the measured compressive strengths from the samples tested with the stroke control mode or with a small valve were not used in the analysis of the compressive strength data. However, they were used in the evaluation of prediction formulas for splitting tensile

strength and modulus of rupture. The errors due to the different load rate when testing the compressive strength were considered to be small relative to the errors inherit in the predictions.

An aligning jig was not used in early tests of the splitting tensile strength. Specimens were loaded between the bearing blocks of the testing machine. Plywood strips were used in all tests to help distribute the load. Both the bearing blocks of the testing machine and the bearing strip of the aligning jig were rigid. Therefore, it was not expected that the test result would be affected whether the aligning jig was used or not.

Two testing machines were used for the modulus of rupture tests. Both of the testing machines were programmed to load at the standard load rate. It was also expected that the testing machines would not significantly affect the test results.